DANMARKS OG GRØNLANDS GEOLOGISKE UNDERSØGELSE **RAPPORT 2024/25**

# CCS2022-2024 WP1: The Gassum structure

## Seismic data and interpretation to mature potential geological storage of CO2

Marie Keiding, Henrik Vosgerau, Ulrik Gregersen, Erik Skovbjerg Rasmussen, Florian W.H. Smit, Morten Bjerager, Anders Mathiesen, Finn Mørk, Michael B.W. Fyhn, Tomi Adriansyah Jusri, Shahjahan Laghari, Niels H. Schovsbo, Henrik I. Petersen, Lars Henrik Nielsen, Emma Sheldon, Karen Dybkjær, Bodil W. Lauridsen, Rasmus Rasmussen, Tanni Abramovitz & Lasse M. Rasmussen

GEOLOGICAL SURVEY OF DENMARK AND GREENLAND
DANISH MINISTRY OF CLIMATE, ENERGY AND UTILITIES

G E U S

# CCS2022-2024 WP1: The Gassum structure

## Seismic data and interpretation to mature potential geological storage of CO2

Marie Keiding, Henrik Vosgerau, Ulrik Gregersen, Erik Skovbjerg Rasmussen, Florian W.H. Smit, Morten Bjerager, Anders Mathiesen, Finn Mørk, Michael B.W. Fyhn, Tomi Adriansyah Jusri, Shahjahan Laghari, Niels H. Schovsbo, Henrik I. Petersen, Lars Henrik Nielsen, Emma Sheldon, Karen Dybkjær, Bodil W. Lauridsen, Rasmus Rasmussen, Tanni Abramovitz & Lasse M. Rasmussen

GEOLOGICAL SURVEY OF DENMARK AND GREENLAND
DANISH MINISTRY OF CLIMATE, ENERGY AND UTILITIES

G E U S

# Preface

A new Danish Climate Act was decided by the Danish Government and a large majority of the Danish Parliament on June 26th, 2020. It includes the aim of reducing the Danish greenhouse gas emissions with 70% by 2030 compared to the level of emissions in 1990. The first part of a new Danish CCS Strategy of June 30th, 2021 includes a decision to continue the initial investigations of sites for potential geological storage of $CO_2$ in Denmark. GEUS has therefore from 2022 commenced seismic acquisition and investigations of potential sites for geological storage of $CO_2$ in Denmark.

The structures decided for maturation by the authorities are some of the largest structures onshore Zealand, Jutland and Lolland and in the eastern North Sea (Fig. 1.1). The onshore structures include the Havnsø, Gassum, Thorning, and Rødby structures, and in addition the small Stenlille structure as a demonstration site. The offshore structures include the Inez, Lisa and Jammerbugt structures. A GEUS Report is produced for each of the structures to mature the structure as part of the CCS2022–2024 project towards potential geological storage of $CO_2$.

The intension with the project reporting for each structure is to provide a knowledge-based maturation with improved database and solid basic descriptions to improve the understanding of the formation, composition, and geometry of the structure. Each report includes a description overview and mapping of the reservoir and seal formations, the largest faults, the lowermost closure (spill-point) and structural top point of the reservoir, estimations of the overall closure area and gross-rock volume. In addition, the database will be updated, where needed with rescanning of some of the old seismic data, and acquisition of new seismic data in a grid over the structures, except for the Inez and Lisa structures, which have sufficient seismic data for this initial maturation.

The reports will provide an updated overview of the database, geology, and seismic interpretation for all with interests in the structures and will become public available. Each reporting is a first step toward geological maturation and site characterization of the structures. A full technical evaluation of the structures to cover all site characterization aspects related to $CO_2$ storage including risk assessment is recommended for the further process.

# Content

# Dansk sammendrag

Regeringen og et bredt flertal i Folketinget vedtog i juni 2021 en køreplan for lagring af $CO_2$, der inkluderer undersøgelser af potentielle lagringslokaliteter i den danske undergrund. Der er derfor udvalgt fire store strukturer på land med dataindsamling og kortlægning til videre modning: Havnsø, Gassum, Rødby og Thorning, samt den mindre Stenlille struktur til demonstrationslagring (Fig. 1.1). Derudover indsamles nye data til kortlægning og modning for den kystnære Jammerbugt struktur, mens de to strukturer Inez og Lisa, længere mod vest i Nordsøen, kortlægges og modnes baseret på eksisterende data.

Gassum strukturen er en stor struktur, der ligger i det østlige Midtjylland, mellem Hobro, Mariager og Randers. Tidligere og nye seismiske data viser strukturens form, og de nye seismiske data viser desuden tilstedeværelsen af flere større forkastninger omkring toppen af strukturen. Korrelation af de seismiske data til Gassum-1 boringen centralt i strukturen og andre nærtliggende boringer giver vigtig information om geologien af reservoir og segl.

Dette sammendrag opsummerer forundersøgelsen og den initiale vurdering af lagringsmuligheden i Gassum strukturen. Vurderingen bygger på tolkning af eksisterende samt nye geologiske og geofysiske data og viden (Kapitel 3−5) og belyser undergrundens geologiske opbygning i og omkring Gassum strukturen (Kapitel 6–7). Vurderingen har fokus på strukturens form, størrelse, overordnede opdeling inklusive reservoir- og seglforhold, geologiske risikofaktorer, især større forkastninger og segl, og der foretages en vurdering af statisk lagringskapacitet for det primære reservoir (Kapitel 8). Desuden opsummeres anbefalinger til yderligere modning af strukturen hen imod en mulig $CO_2$-lagring (Kapitel 9, 10).

### Datagrundlag

Gassum strukturen er dækket af ældre refleksionsseismiske data med 2D profiler af sparsom tæthed og kvalitet indsamlet i 1960'erne, 1970'erne og 1980'erne, samt et tættere netværk af nye refleksionsseismiske data indsamlet i 2023 for dette projekt (Fig. 4.1.1). De ældre datasæt er generelt af dårlig kvalitet med meget støj. Derfor blev der i februar til maj 2023 indsamlet ti nye 2D refleksionsseismiske profiler på i alt 221 km ved hjælp af vibroseis-lastbiler som seismisk kilde og et dobbelt optagesystem bestående af en landstreamer med geofoner trukket bag lastbilerne og trådløse geofoner i vejsiden. Disse data har markant forbedret dækning og kvaliteten af data samt tolkningsmulighederne over strukturen og flankerne. Uppsala Universitet gennemførte indsamlingen og processeringen på vegne af GEUS, med vibroseis-lastbiler fra polske Geopartner Geofizyka og med feltassistance fra universitetsstuderende fra Københavns og Uppsala universiteter. COWI varetog ansøgninger om tilladelser, logistik, dele af kommunikationen og den løbende borgerkontakt. Der blev i forbindelse med indsamlingen informeret på tre informationsmøder for borgere, via projektwebside, informationsbreve og flyers, samt på to besøgsdage.

Det nye 2D seismiske indsamling (GEUS2023-GASSUM) har forbedret datagrundlaget over toppen og flankerne af Gassum strukturen og muliggør en væsentlig forbedret kortlægning, særligt af forkastninger i toppen af reservoir og segl.

## Tolkning

Gassum strukturen er en geologisk fire-vejs-lukning, som er opstået som følge af dannelsen af en dybtliggende saltpude i det underliggende Zechstein salt. Saltpudens vækst hævede de overliggende lag, herunder reservoir og segl, op gennem millioner af år gennem Trias og Jura til ind i Kridt tid, hvorved der blev dannet en stor lukket antiklinal. Det primære reservoir-segl par i Gassum strukturen er Gassum-Fjerritslev formationerne (Kapitel 6, 7). Beskrivelser fra boringer viser, at Gassum Formationen og store dele af Fjerritslev Formationen indeholder henholdsvis gode reservoir og segl intervaller. Derudover er der et sekundært, højereliggende reservoir-segl par i Frederikshavn-Vedsted formationerne samt et dybereliggende reservoir-segl par i form af Skagerrak Formationen og de overliggende Ørslev–Falster–Tønder formationer. Som omtalt i rapporten danner Haldager Sand og Flyvbjerg formationerne sandsynligvis yderligere reservoirer i strukturen.

Strukturen lukker på flere stratigrafiske niveauer fra Trias til Jura. Særligt vigtigt er lukningen på toppen af Gassum Formation (tidlig Jura alder) med det primære reservoir, som har fokus i denne vurdering. Gassum Formationen har en tykkelse på ca. 130 m i Gassum-1 boringen, som ligger tæt på toppen af strukturen, og har en god lateral kontinuitet baseret på korrelation med de nærtliggende boringer Hobro-1, Kvols-1 and Voldum-1. Gassum Formationen består i Gassum-1 og de nærtliggende boringer af sandsten med lerstenslag.

I Gassum-1 boringen har Gassum Formationen en netto tykkelse af reservoirsandsten på 56,7 m. Et reservoir i Gassum Formationen defineres som en sandsten, der har et ler-indhold <0.5% og porøsitet >10%. Gassum Formation sandstenen i Gassum-1 boringen har en gennemsnitlig porøsitet på 28,5% og en gennemsnitlig permeabilitet på 1500 mD (midlet over kernemålingerne), hvilket giver gode reservoiregenskaber (Kapitel 7).

Der er gennemført en opdateret tolkning af Gassum strukturen på baggrund af eksisterende data kombineret med de nye seismiske data (Kapitel 6). Der anvendes boringskorrelation og seismiske profiler for at identificere seismiske refleksioner og intervaller, der kan korreleres med de geologiske formationer. Tolkningen viser, at toppen af reservoiret, som er kortlagt ved Top Gassum Formationen i Gassum strukturen, er veldefineret og lukker med et areal på 280 $km^2$ i 2300 m dybde.

De nye data viser desuden en markant, ca. 15 km lang øst-vest gående forkastningszone nær toppen af strukturen, nord for Gassum-1 boringen. De største forkastninger er normalforkastninger og er givetvis dannet ved strækning af lagene forårsaget af bevægelserne i den dybe saltpude. Forkastningerne er identificeret på flere af de seismiske profiler og strækker sig fra Ørslev Formationen op til Kridt pakken (Chalk Group), med den største tæthed i Gassum, Fjerritslev og Frederikshavn Formationerne. Forskydningerne i toppen af Gassum Formationen og i seglet (bl.a. Fjerritslev Formationen) er op til ca. 40–60 ms, svarende til op til omkring 100 m. Tilstedeværelsen af en forkastning nord for Gassum-1 boringen var kendt fra de få ældre seismiske linjer, men de nye data viser, at forkastningszonen er betydeligt længere og har større forsætning end hidtil antaget. Derudover ses mindre forkastninger i den sydlige del af strukturen, som også kan have en betydning for lagring af $CO_2$.

På grund af forkastningernes betydelige forsætninger og laterale udstrækning i Gassum Formationen (primære reservoir) og Fjerritslev Formationen (primære segl) i og omkring toppen af strukturen bør der foretages en nærmere undersøgelse af forkastningerne i forbindelse med yderligere modning af strukturen. Grundet afstanden mellem de 2D seismiske profiler er det nuværende datagrundlag stadigvæk ikke tilstrækkeligt til en fyldestgørende undersøgelse af segl-integriteten og eventuel risiko for lækage af $CO_2$, samt hvorvidt nogle

forkastninger kan danne barrierer (compartments) ifm. $CO_2$-lagring. En yderligere modning af strukturen bør derfor baseres på nye tætliggende seismiske (3D) data og yderligere tekniske vurderinger.

# 1. Summary

The subsurface in Denmark has many deep structures offshore and onshore, and some of these are suited for $CO_2$ storage. Eight structures named in Fig. 1.1 were selected for initial investigation and maturation through seismic acquisition, geological analyses, and renewed mapping during 2022–2024 by GEUS, with cooperating partners on acquisition and processing (see chapter 4).

New 2D seismic data were acquired across the Gassum structure to improve the database with more dense, good quality seismic data. The improved seismic database is used in this report – together with well logs from the Gassum-1 well near the top of the structure and with ties to other nearby wells – to improve the understanding of the structure in terms of its geological development, the lowermost closure (spill-point) and top point at the top of the reservoir, the overall closure area and potential static storage capacity, the largest faults, and details of reservoir and seal successions for this initial maturation. The new seismic data and grids in two-way time of key seismic horizons are available at the GEUS CCS data webpage.

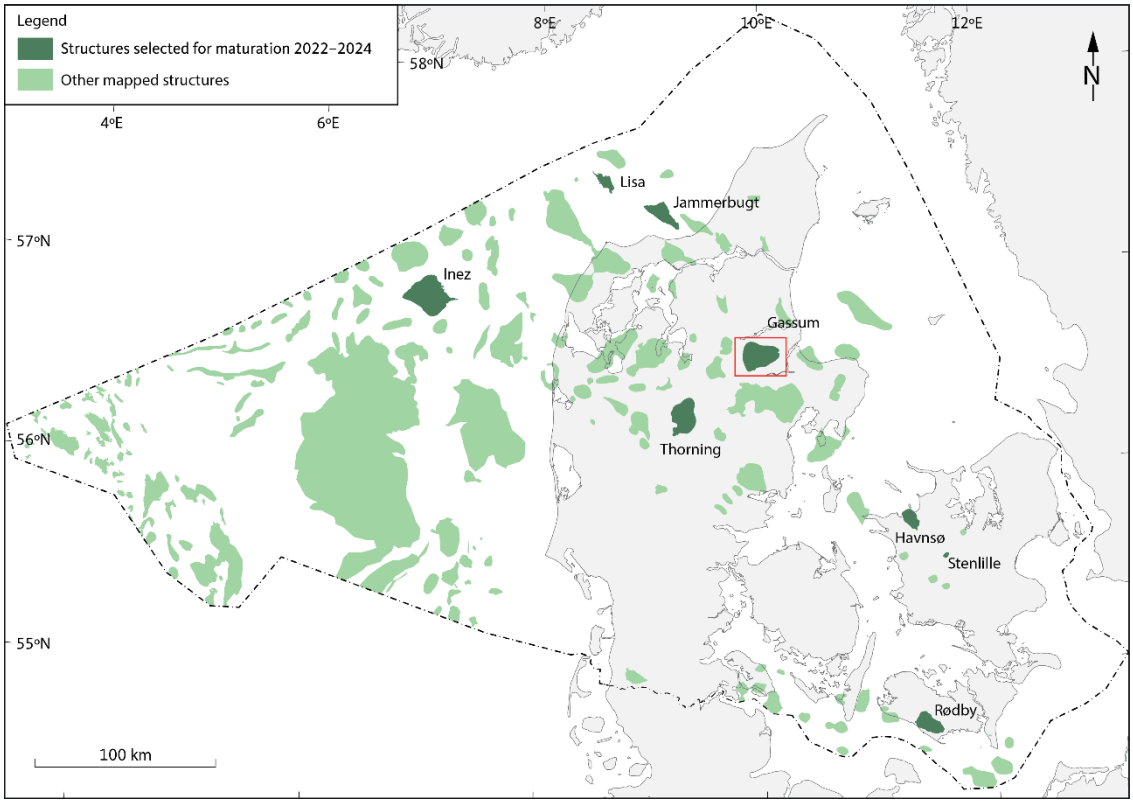


**Figure 1.1**. *Map of Danish structures with potential for geological storage of $CO_2$. The named dark green structures (Stenlille, Havnsø, Rødby, Gassum, Thorning, Jammerbugt, Lisa and Inez) are currently investigated with acquisition of new data and updated mapping in GEUS' CCS project during 2022–2024. This reporting is for the Gassum structure, and the study area is marked with a red rectangle.*

The new 2D seismic survey (GEUS2023-GASSUM) included in the present reporting was acquired in the spring 2023 and consists of ten seismic lines with a total line length of c. 221 km across the structure (Chapter 4).

The Gassum structure is a geological four-way dip structure with an areal extent of around 280 $km^2$ (Fig. 1.2). The main reservoir-seal couples of the Gassum structure are the Gassum Formation and Fjerritslev Formation, which are shown in Figure 1.3. Descriptions of well logs show that the Gassum Formation and large parts of the Fjerritslev Formation contain suitable reservoir and seal intervals, respectively. In addition, a secondary, shallower reservoir-seal couple is provided by the Frederikshavn Formation and the Vedsted Formation, and a deeper situated reservoir-seal couple of the Skagerrak Formation and the Ørslev–Falster–Tønder formations. As discussed in the report, the Haldager Sand and Flyvbjerg formations possibly form additional reservoirs in the structure. See Chapter 7.1 for more details on the reservoirs.

The Gassum Formation is c. 130 m thick in the Gassum-1 well located near the centre of the structure (Figs. 1.2, 1.3). There is a large lateral continuity based on mapping with seismic correlation from the nearby Hobro-1, Kvols-1 and Voldum-1 wells. The Gassum Formation consists in the Gassum-1 and nearby wells of sandstones with interbedded claystones. The net sand thickness in the Gassum-1 well is 56.7 m providing a net to gross ratio of 0.46.

A reservoir is defined as a sandstone containing a volume of shale <0.5% and with porosities >10%. The Gassum Formation sandstones in the Gassum-1 well have average porosity of 28.5% and average permeability of 1500 mD (mean value of core measurements), providing good reservoir properties.

The primary seal for the Gassum Formation in the structure is the Fjerritslev Formation, which is several hundred-meter-thick mudstone successions of Early Jurassic age, and it includes generally good to very good sealing mudstones. The lowermost part of the formation (F-Ia Mb) includes a number of thin siltstone and sandstone beds, which probably to some extent reduce the seal quality, whereas the upper and thickest part of the formation (F-Ib to F-IV Mb) is a good quality seal. Above this formation are the secondary seals, which includes the Vedsted Formation mudstones and Rødby Formation marl and chalk of Early Cretaceous ages. Above these follows the km-thick Upper Cretaceous Chalk Group, which is overlain by thinner younger deposits. Safe storage in the Gassum Formation of natural gas and monitoring for potential leakage through many years has proven that primary Fjerritslev Formation seal is efficient in the Stenlille structure. The same stratigraphic seal formation is also expected in the Gassum structure. See also Section 7.2 for more details on the seals.

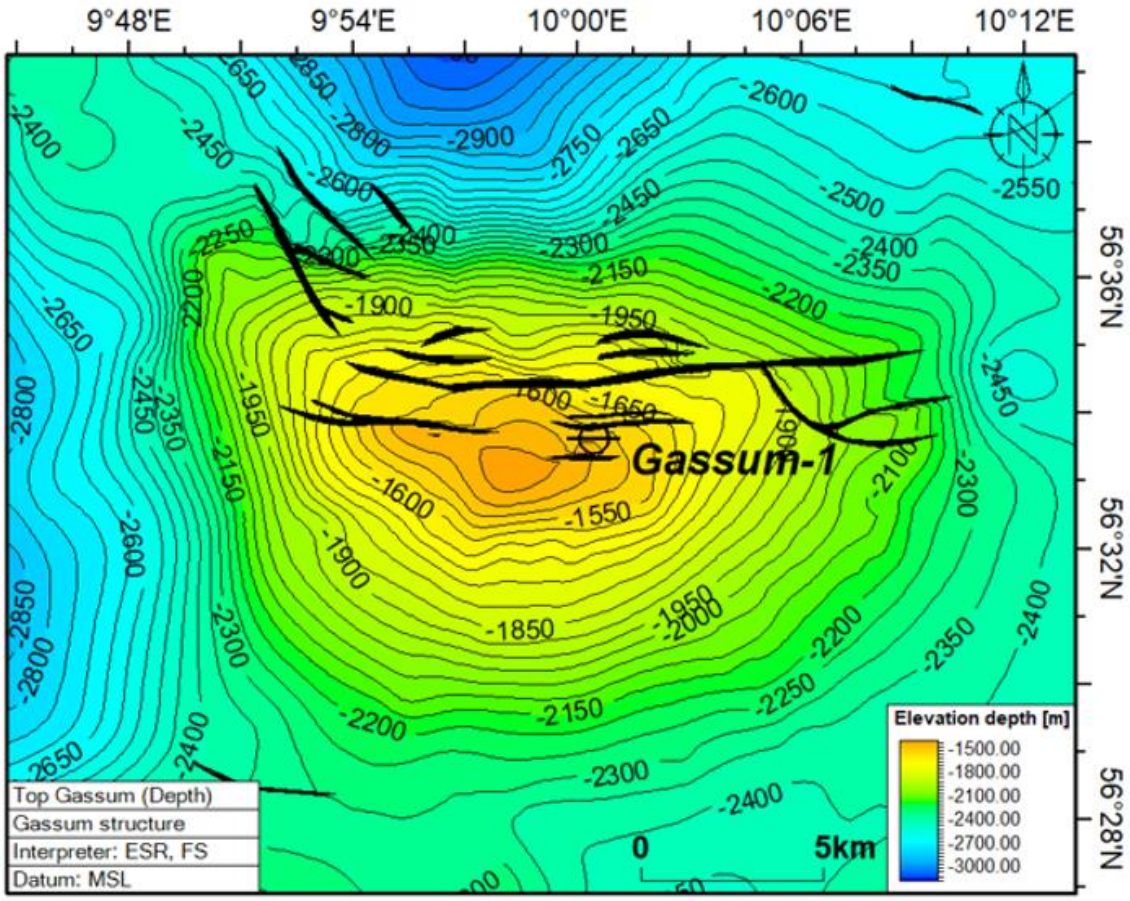


**Figure 1.2.** *Depth-structure map of the Top Gasssum in meters (m) below mean sea level (b.msl) shown with the largest faults as black, filled polygons and the location of the Gassum-1 well. The map is produced with a 250x250 m grid and mildly smoothed. Note that the lowest closing contour is 2300 m.*

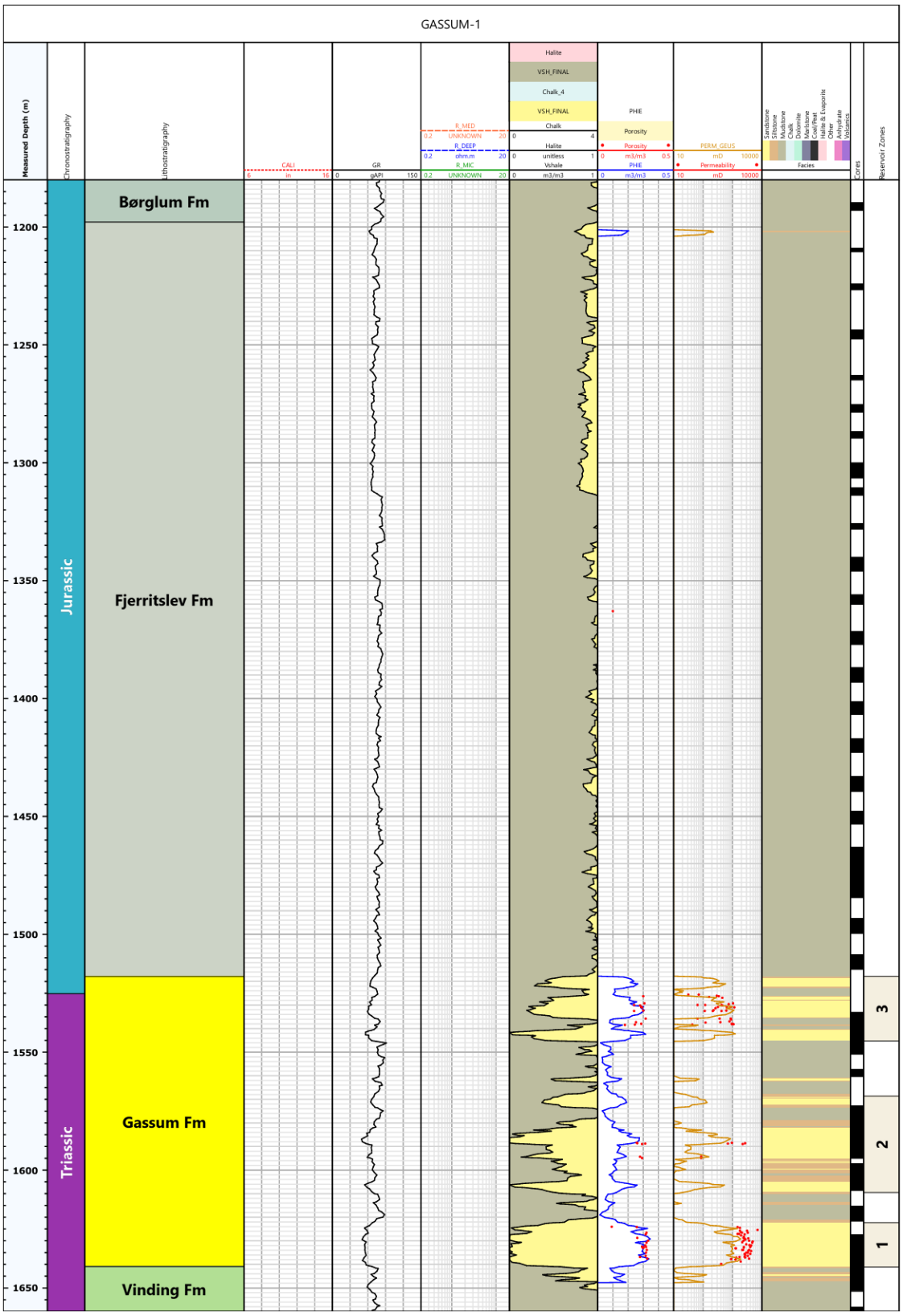


**Figure 1.3.** *Interpreted lithology of the Gassum and Fjerritslev Fms in the Gassum-1 well based on petrophysical log interpretation and information from core data, cutting samples etc. Columns to the right mark three potential reservoir subunits (1–3) in the Gassum Fm and cored parts of the formations (black columns).*

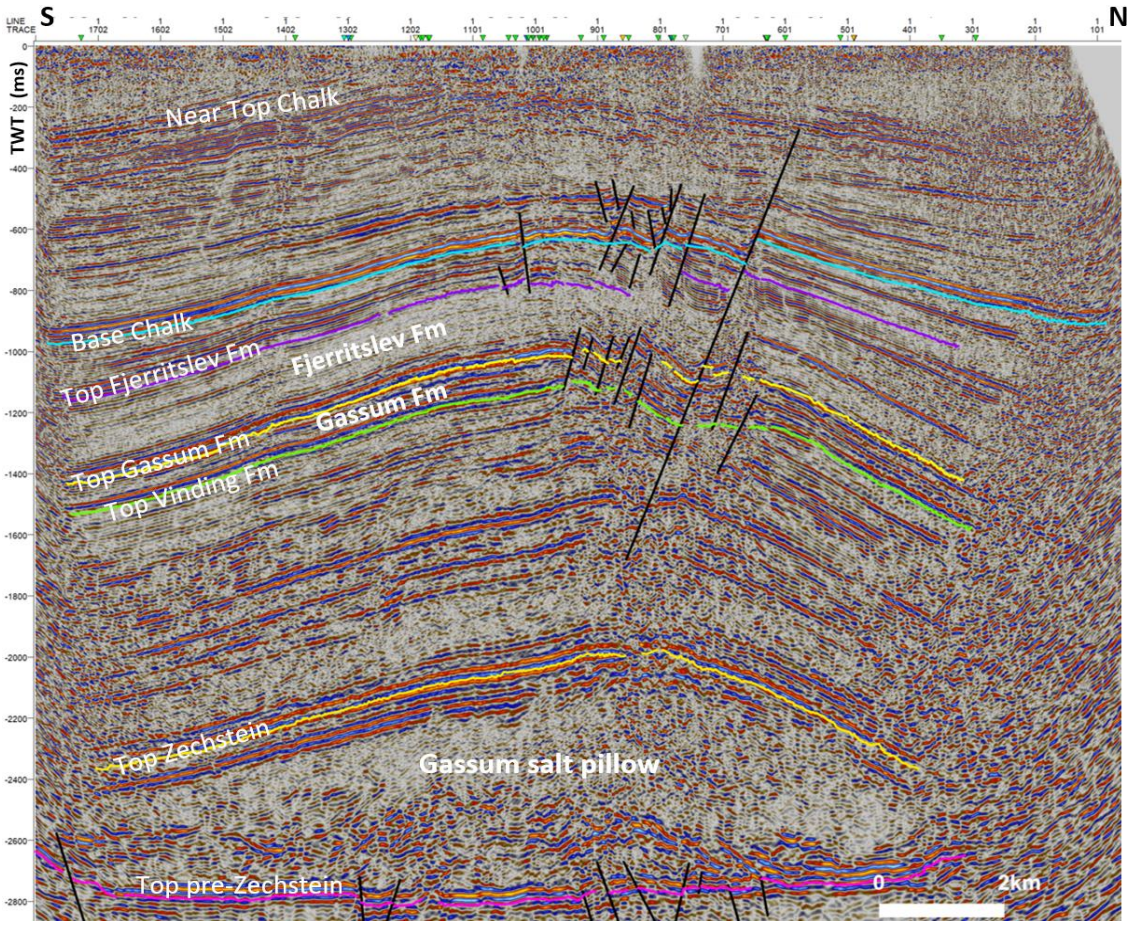


**Figure 1.4.** *2D seismic line P5 from GEUS2023_GASSUM-RE2023 showing the Gassum structure from Top-Zechstein level, with the salt pillow and overlying stratigraphic units incl. Gassum Fm and Fjerritslev Fm near the Gassum-1 well. The interpreted faults are shown with black lines*.

The new data and mapping confirm that the Gassum structure has closures at the Top Gassum Formation and also at shallower levels including the top of the secondary reservoir of the thick sandstone intervals of the Frederikshavn Formation. The area of the lowermost closure on the Top Gassum depth-structure map is c. 280 km$^2$ at the closing contour of c. 2300 m depth below mean sea level (Fig. 1.2). The top of the structure at the Top Gassum map is at c. 1375 m depth, and the relief of the structure at Top Gassum is thus c. 975 m The calculations in this study show a significant static storage capacity of the Gassum Formation of 498 Mt $CO_2$ (Chapter 8).

A major fault zone is present near the top of the structure (Figs. 1.3, 1.4) causing offsets in top Gassum Formation as well as the seal (e.g., Fjerritslev Formation) of up to 40–60 milliseconds, corresponding to c. 100 m offset. The fault zone can be identified at multiple seismic profiles. It trends east-west and extends for c. 15 km along the top of the structure, near and north of the Gassum-1 well. The presence of a fault north of the Gassum-1 well was known based on the old seismic data, however, the new data show that the fault is both much longer

and has a larger offset that previously known. The faults near the top of the structure should be further evaluated to identify possible risks such as leakage along the fault planes and the possible compartmentalization of the reservoir. Other smaller faults are present at other parts of the structure, which may also affect the possibilities for $CO_2$ storage.

The new 2D seismic data has significantly improved the seismic database with more dense, good quality seismic data. However, additional seismic acquisition, in particular of 3D data over the Gassum structure and the potential injection and storage areas is recommended, for more detailed interpretation prior to $CO_2$ injection, as there is still some distance between the line data coverage. This can improve site-specific knowledge with more details on the faults, reservoir and seal and provide input to modelling of $CO_2$ migration and analyses of geological and other technical uncertainties and risks. Repeated seismic surveys in same place can subsequently contribute to monitor the extent of the $CO_2$ migration, together with other monitoring techniques (e.g., well logging, downhole seismics, micro seismicity, surface deformation, etc). The knowledge from the investigated structures will be included in the further work of the authorities to reveal opportunities and requirements towards further maturation for potential geological $CO_2$ storage.

# 2. Introduction

Carbon capture and storage (CCS) is an important instrument for considerably lowering atmospheric $CO_2$ emissions (IPCC 2022). Geological storage of $CO_2$ is known from more than 30 sites situated in many countries, including Norway (Sleipner), Canada (Weyburn) and Germany (Ketzin), since the first started more than 25 years ago (e.g., Chadwick et al. 2004) and more than 190 facilities are in the project pipeline (Global CCS Institute 2022).

The Danish subsurface is highly suited for $CO_2$ storage, and screening studies document an enormous geological storage potential that is widely distributed below the country and adjacent sea areas (Larsen et al. 2003; Anthonsen et al. 2014; Hjelm et al. 2022; Mathiesen et al. 2022). The significant Danish storage potential is based on the favorable geology that includes excellent and regionally distributed reservoirs, tight seals, large structures, and a relatively quiescent tectonic environment. The largest storage potential is contained within saline aquifers, and the Danish onshore and nearshore areas contain a number of these structures with a potentially significant $CO_2$ storage potential (Hjelm et al. 2022).

The Gassum structure is one of these structures and is a relatively large structure geographically located in eastern part of Jutland (Fig. 1.1), and geologically in the central part of the Danish Basin (Fig. 3.1). The structure was only covered by a limited number of old, poor quality 2D seismic lines, acquired in the 1960s, 1970s and 1980s. However, in 2023 new seismic data for this project was acquired (see Chapter 4). The seismic lines can be tied to the Gassum-1 well located near the centre of the Gassum structure as well as other nearby wells, which document the geology. The Gassum structure is expected to have storage potential for resources such as $CO_2$, and this structure with the Gassum Formation is the focus of this study, but also a shallower and a deeper reservoir-seal couple of the structure is described.

Earlier screening projects by GEUS for structures relevant for CCS have also evaluated the Gassum structure for potential $CO_2$ storage. A comprehensive summary with an evaluation of the $CO_2$ storage potential in Denmark, including an initial evaluation of the Gassum structure, was provided by Hjelm et al. (2022).

In this study, the Gassum structure is investigated further based on evaluation of the integrated database of old and new seismic data, with correlation to wells, to characterize its tectonic and depositional evolution, composition with reservoir-seal couples, faults and geometry towards maturation for potentially geological storage of $CO_2$.

# 3. Geological setting

The Gassum structure is located in the Danish Basin which forms the eastern part of the WNW−ESE trending Norwegian–Danish Basin (Vejbæk 1997, Nielsen 2003). To the south the Danish Basin is separated from the North German Basin by the Ringkøbing-Fyn High, and to the north and northeast by the Sorgenfrei-Tornquist Zone which further north is limited by the Skagerrak-Kattegat Platform (Figs. 3.1, 3.2). Both the Norwegian–Danish Basin and the North German Basin are intracratonic basins formed by stretching of the lithosphere which caused Carboniferous−Permian rifting with extension and normal faulting followed by basin subsidence. The Ringkøbing-Fyn High probably formed at the same time due to less stretch than the basin areas (Vejbæk 1997). The tectonism led to large, rotated fault blocks, intrusive volcanism, extensive erosion, and mostly coarse siliciclastic deposition (Rotliegende) affecting large parts of the basin (Vejbæk 1997; Michelsen & Nielsen 1991, 1993; Nielsen 2003).

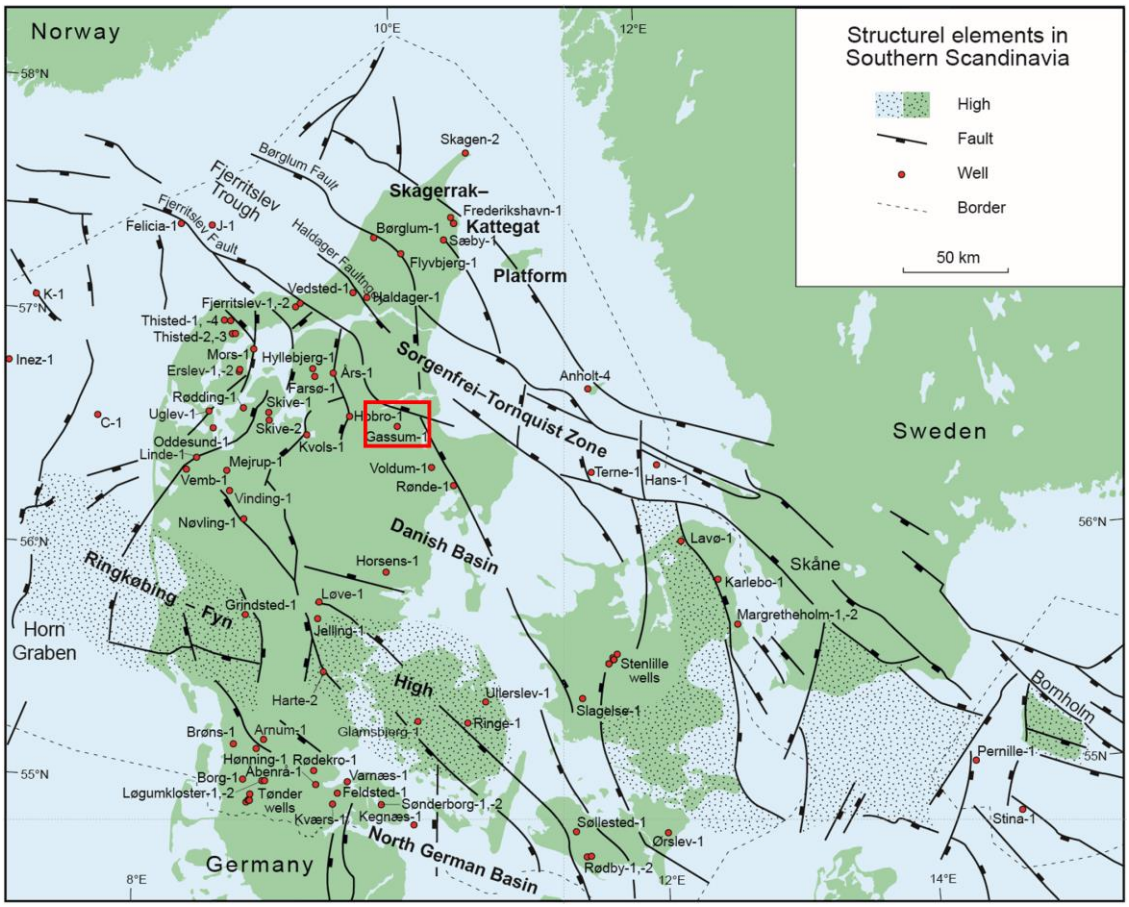


**Figure 3.1.** *Map of the main structural elements including highs, basins, and main faults onshore and offshore Denmark. The elements include the Danish Basin, the Sorgenfrei-Tornquist Zone, the Skagerrak-Kattegat Platform, the Ringkøbing-Fyn High, and the northern part of the North German Basin. The study area is indicated with the red square. Positions of deep wells are also marked. Modified from Nielsen (2003).*

After mainly evaporites (Zechstein Group) developed in shallow basin areas during late Permian time, the region subsided and thick Triassic clay and mud-dominated successions formed with a few sandstones and minor carbonate and salt deposits (Bunter Shale, Bunter Sandstone, Ørslev, Falster, Tønder, Oddesund, Vinding formations; Figs. 3.3, 3.4, 3.5A,B). Sandstones are in particular known from the Bunter Sandstone Formation but are also present along the northern basin margin in the Skagerrak Formation (Bertelsen 1978, 1980). During latest Triassic (Rhaetian) and into the earliest Jurassic (Hettangian–early Sinemurian) times the coastal to continental areas were repeatedly overstepped by the sea depositing the Gassum Formation (Fig. 3.6). The relative sea-level rise resulted during the Early Jurassic in the deposition of thick claystone-dominated successions with some silty and sandy layers (Fjerritslev Formation), which have been correlated basin wide in several depositional sequences and members (Nielsen 2003; Michelsen et al. 2003).

Mainly Middle−Late Jurassic regional uplift and salt mobilization led to formation of structures, associated faults, and major erosion in large parts of the basins, with a hiatus expanding towards the Ringkøbing-Fyn High (Fig. 3.3) (Nielsen 2003). However, fault-related subsidence continued in the Sorgenfrei-Tornquist Zone, where sand and mud were deposited (Middle Jurassic Haldager Sand Formation). Regional subsidence occurred again during the late Middle Jurassic and generally continued until Late Cretaceous–Paleogene time, when subsidence was replaced by uplift and erosion related to the Alpine deformation and the opening of the North Atlantic. The deposits from the last period of subsidence consist of Upper Jurassic–Lower Cretaceous mudstones and sandstones (Flyvbjerg, Børglum, Frederikshavn, Vedsted and Rødby formations) followed by thick Upper Cretaceous carbonate and calcareous deposits (Chalk Group), which were formed throughout the Danish Basin. Finally, Cenozoic including Quaternary successions were deposited in the Danish Basin, with episodic uplift (Japsen & Bidstrup 1999; Japsen et al. 2007). Deposits of sandstone in the Late Jurassic–Early Cretaceous interval are mainly known from the Flyvbjerg and Frederikshavn formations.

The significant amounts of sediments deposited throughout the Mesozoic period caused underlying deposits of Zechstein salt to be plastically deformed and in some places to move upwards along zones of weakness. This resulted in uplift of the underlying layers in some places (salt pillows) or breaching by the rising salt (salt diapirs). Above the salt structures, the layers may be absent or partly absent due to non-deposition or erosion, whereas increased subsidence along/in the flanks of the salt structures (in the edge depressions) may have led to corresponding layers being extra thick in these areas.

The Bunter Sandstone, Gassum and Frederikshavn formations all contain potential sandstone reservoirs in the Gassum structure. However, in this study the Gassum Formation is considered the prime reservoir for $CO_2$ storage as it is overlain by a several hundred meters thick mudstone-dominated succession of the Fjerritslev Formation, which in general is considered as having good seal properties.

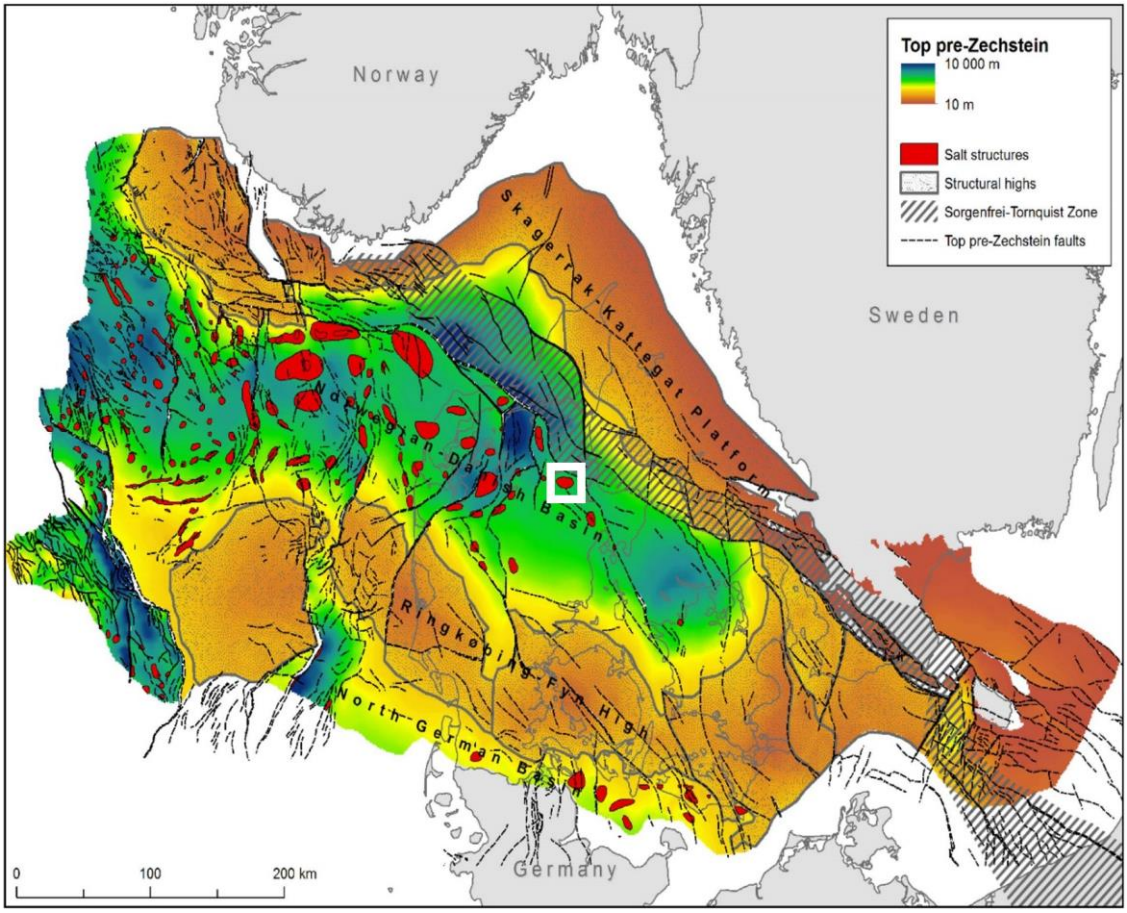


**Figure 3.2.** *Map of the main structural elements onshore and offshore Denmark, including highs, basins, and main faults. The location of the study area around the Gassum structure is marked with a white square. The elements include the Norwegian–Danish Basin (of which the eastern part in Denmark is the Danish Basin), the Sorgenfrei-Tornquist Zone, the Skagerrak-Kattegat Platform, the Ringkøbing-Fyn High, and the northern part of the North German Basin. Modified from Vejbæk & Britze (1994).*

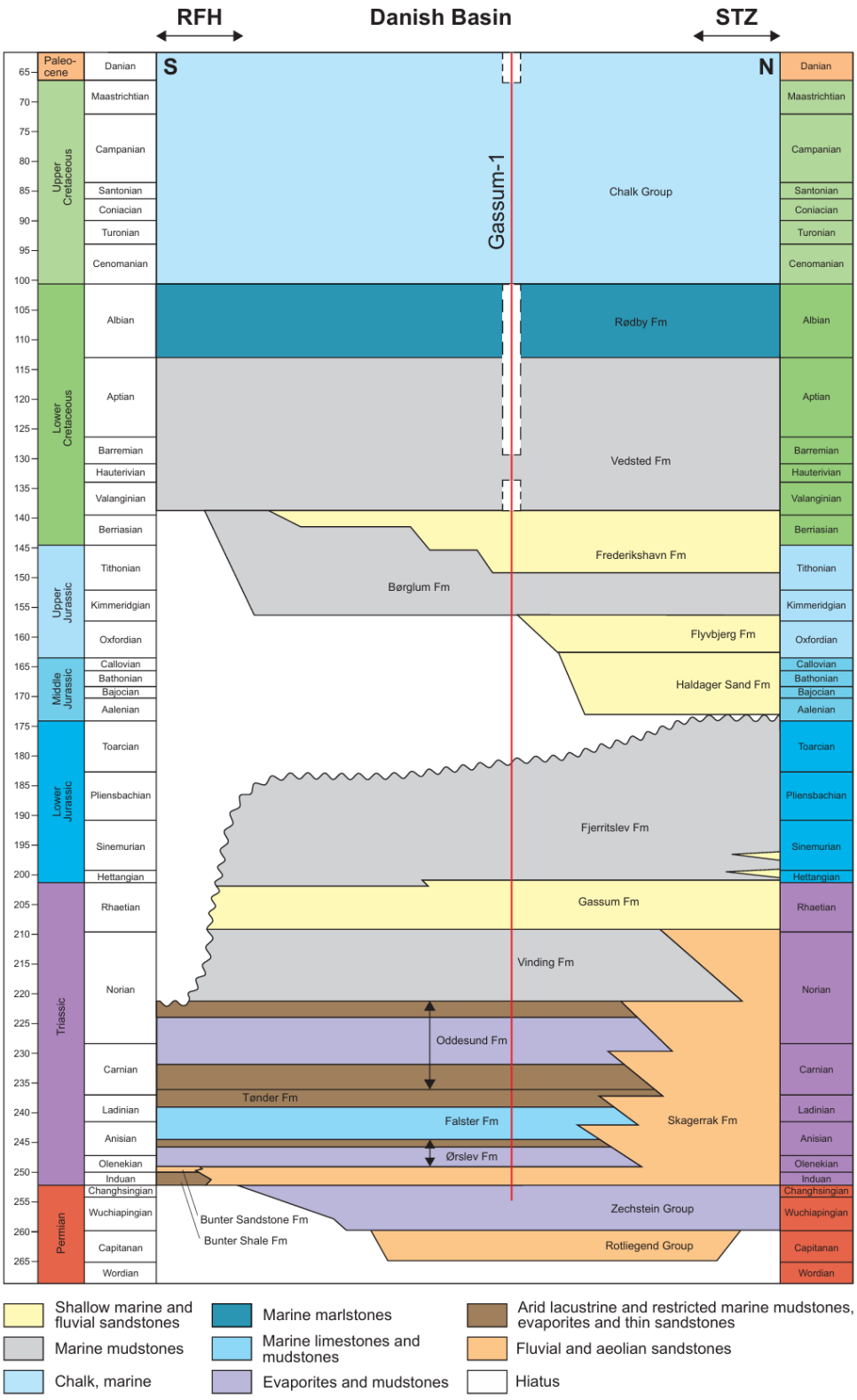


**Figure 3.3**. *Generalized stratigraphy from south to north in the Danish Basin in which the Gassum-1 well is located. To the south the basin is limited by the Ringkøbing-Fyn High (RFH) and to the north by the Sorgenfrei-Tornquist Zone (STZ) (Fig. 3.2). Bunter Shale, Skagerrak and Haldager Sand Fms are not identified in the Gassum-1 well. Based on Bertelsen (1980) and Nielsen (2003).*

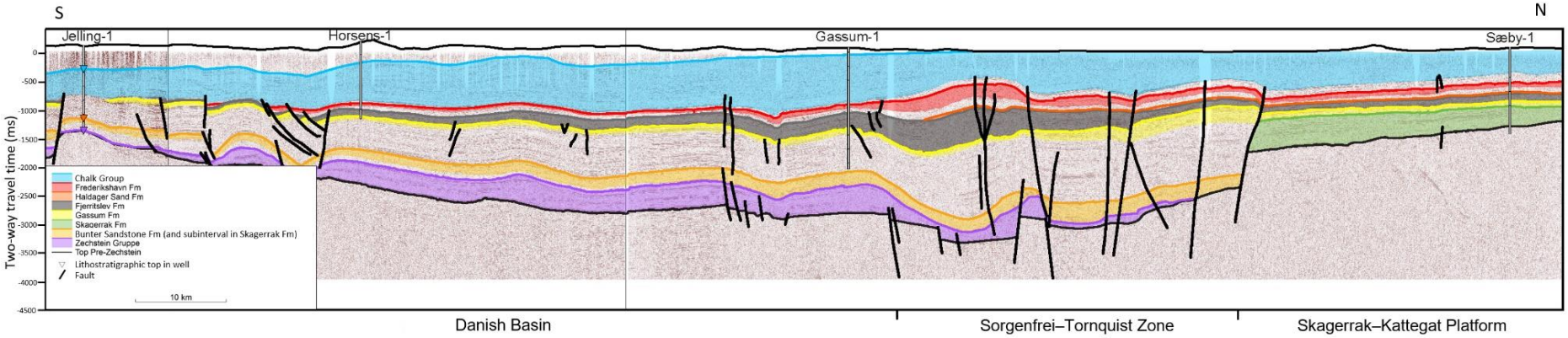


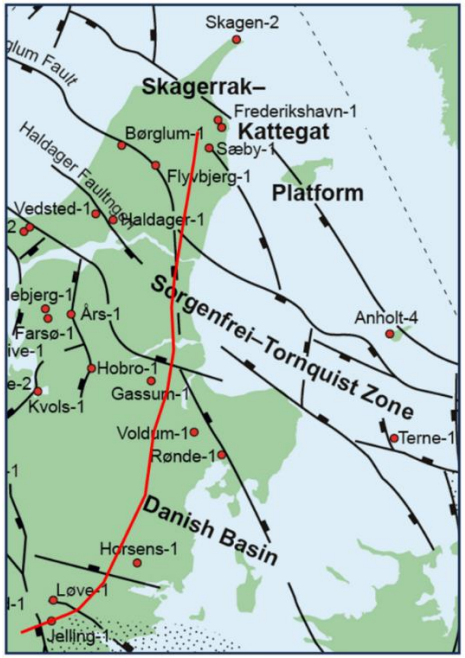


**Figure 3.4**. *Regional S–N profile through eastern Jylland, extending over the Danish Basin, Sorgenfrei–Tornquist Zone and the Skagerrak–Kattegat Platform (approximate location of profile is shown with red line on map). Interpreted lithostratigraphy: purple indicates the deep Zechstein salt, orange the Bunter Sandstone Fm, green the Skagerrak Fm, yellow the Gassum Fm, dark grey the Fjerritslev Fm, pink the Haldager Sand Fm, red the Frederikshavn Fm and blue the Chalk Group. Triangle positions mark lithostratigraphic well-top ties only shown for Jelling-1). All wells are projected onto the profiles. The composite seismic profiles are modified from https://dybgeotermi.geus.dk*

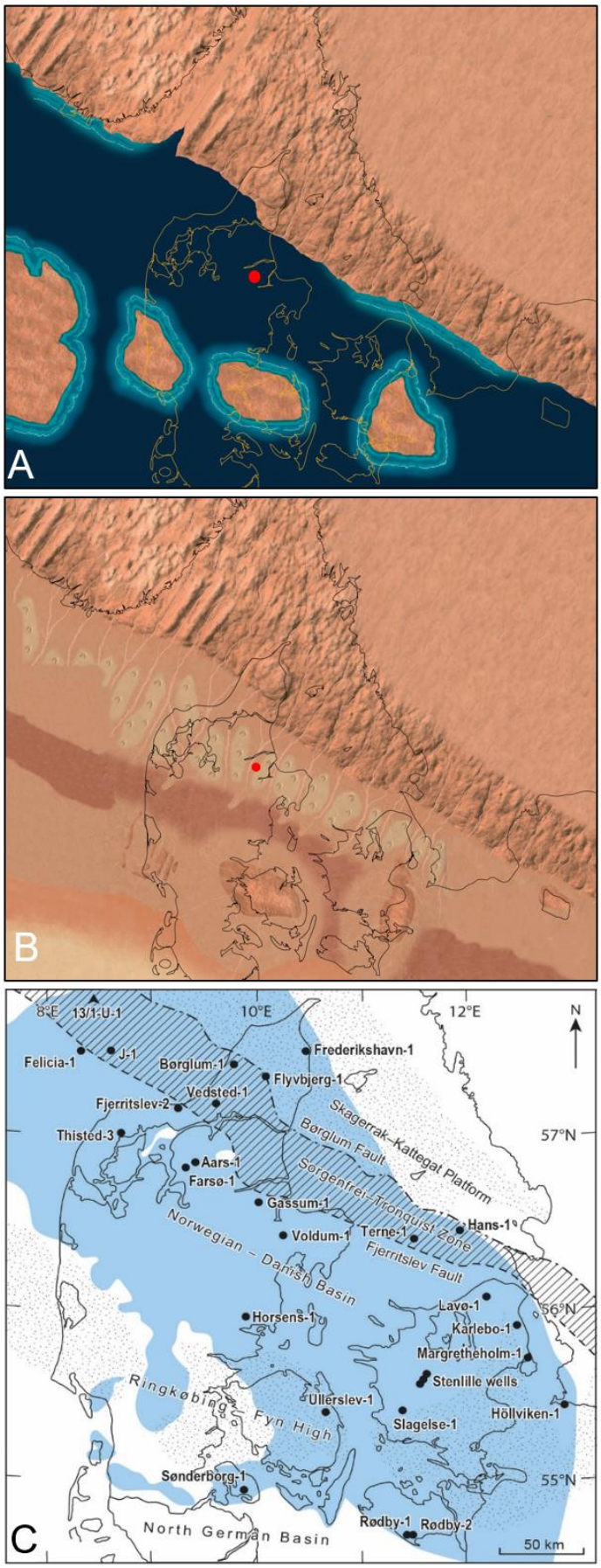


**Figure 3.5.** *Paleogeographic maps of Denmark and southern Scandinavia illustrating the possible distribution of general depositional environments. The Gassum structure area is marked with a small red circle.*

*(A) Late Permian (Zechstein) sea (dark blue), coastal near areas (light blue) and onshore areas (orange red). From Rasmussen & Nielsen (2020).*

*(B) Early–Middle Triassic (incl. the Bunter Sandstone Fm) dominated by desert with local sand dunes, lakes and sabkhas. From Rasmussen & Nielsen (2020).*

*(C) Late Triassic (Rhaetian) to earliest Jurassic (Hettangian–early Sinemurian) Gassum Fm distribution in Denmark. From Olivarius et al. (2022). Earlier work (e.g., Nielsen 2003, Vosgerau et al. 2020, see also Section 7.1) show that the Gassum Fm is composed of several depositional sequences with regressions–transgression cycles and deposition in onshore, nearshore, and shallow marine environments.*

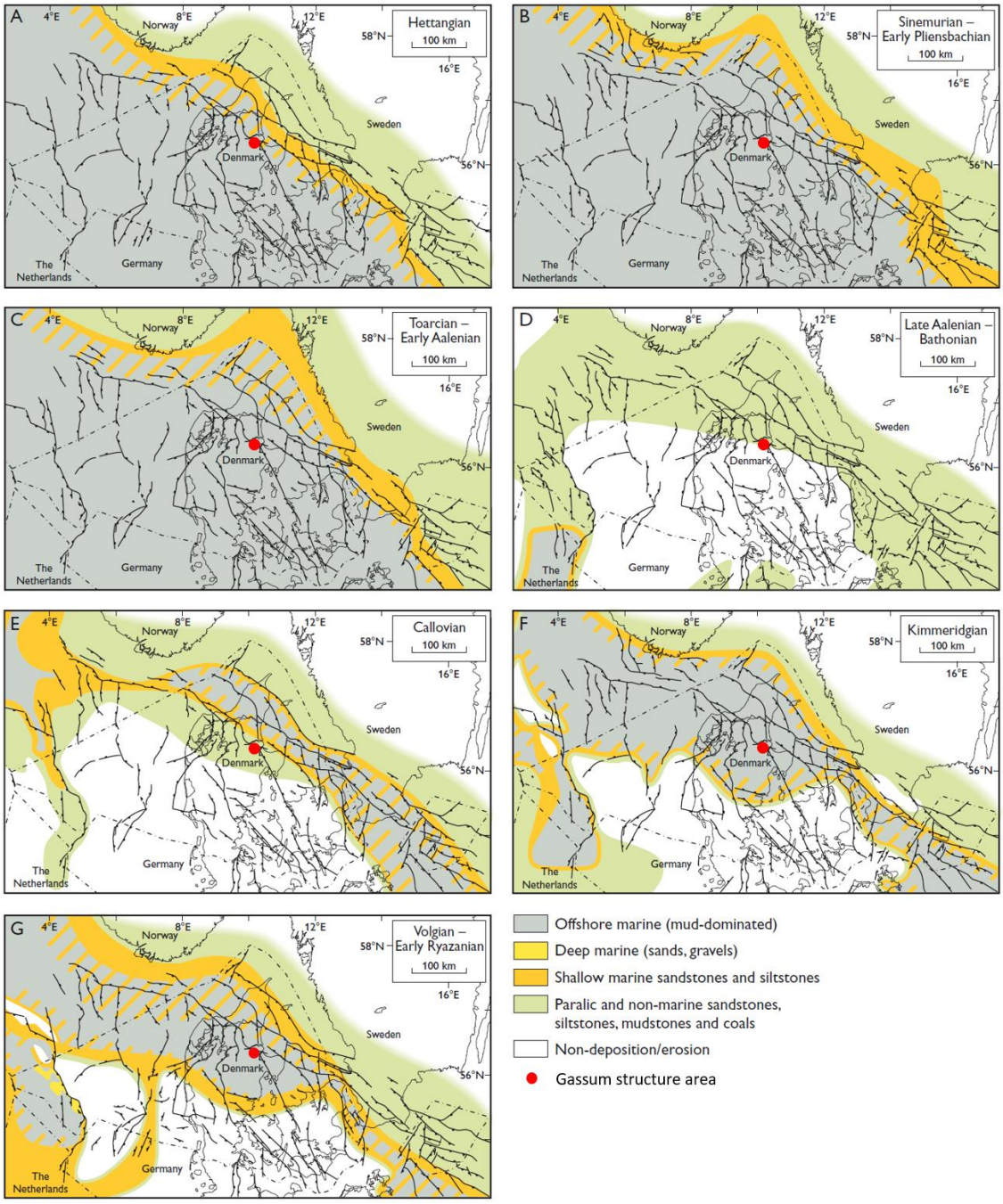


**Figure 3.6.** *Paleogeographic maps of Denmark showing the inferred distribution of general depositional environments during the Jurassic time. From Hettangian to Toarcian or Aalenian (A–C), the Danish area was characterized by deposition of marine clays with some layers and beds of siltstone and sandstone, forming the present-day Fjerritslev Formation which is the primary seal of the Gassum Formation. During the Aalenian–Callovian (D–E) regional uplift took place and large areas, including the Gassum structure area (red circle), was characterized by erosion and/or non-deposition. In the Late Jurassic (F–G), renewed subsidence in the central part of the Danish Basin led to redeposition of marine mud (Børglum Fm) and in more proximal areas also marine sand (Frederikshavn Fm). From Petersen et al. (2008) modified from Michelsen et al. (2003).*

# 4. Database

## 4.1 Seismic data

The new seismic survey of GEUS2023-GASSUM (including the original processing and the reprocessed GEUS2023-GASSUM-RE2023) and scattered lines of DNJ8183D, SSL6267 and PRKL7374A provide data for the interpretation of the Gassum area (Fig. 4.1.1). There is a high variation in density of seismic lines from up to 4 to 5 km south and east of the Gassum-1 well to c. 2 km adjacent and to the northwest of the Gassum-1 well. The quality varies from excellent of the GEUS2023-GASSUM survey, to moderate of the DNJ8183D survey, and poor to very poor of the remaining data (Fig. 4.1.2). The high quality GEUS2023-GASSUM survey, however, is challenged by dimming of the signals at road bends and at the end of each line (Fig. 4.1.3).

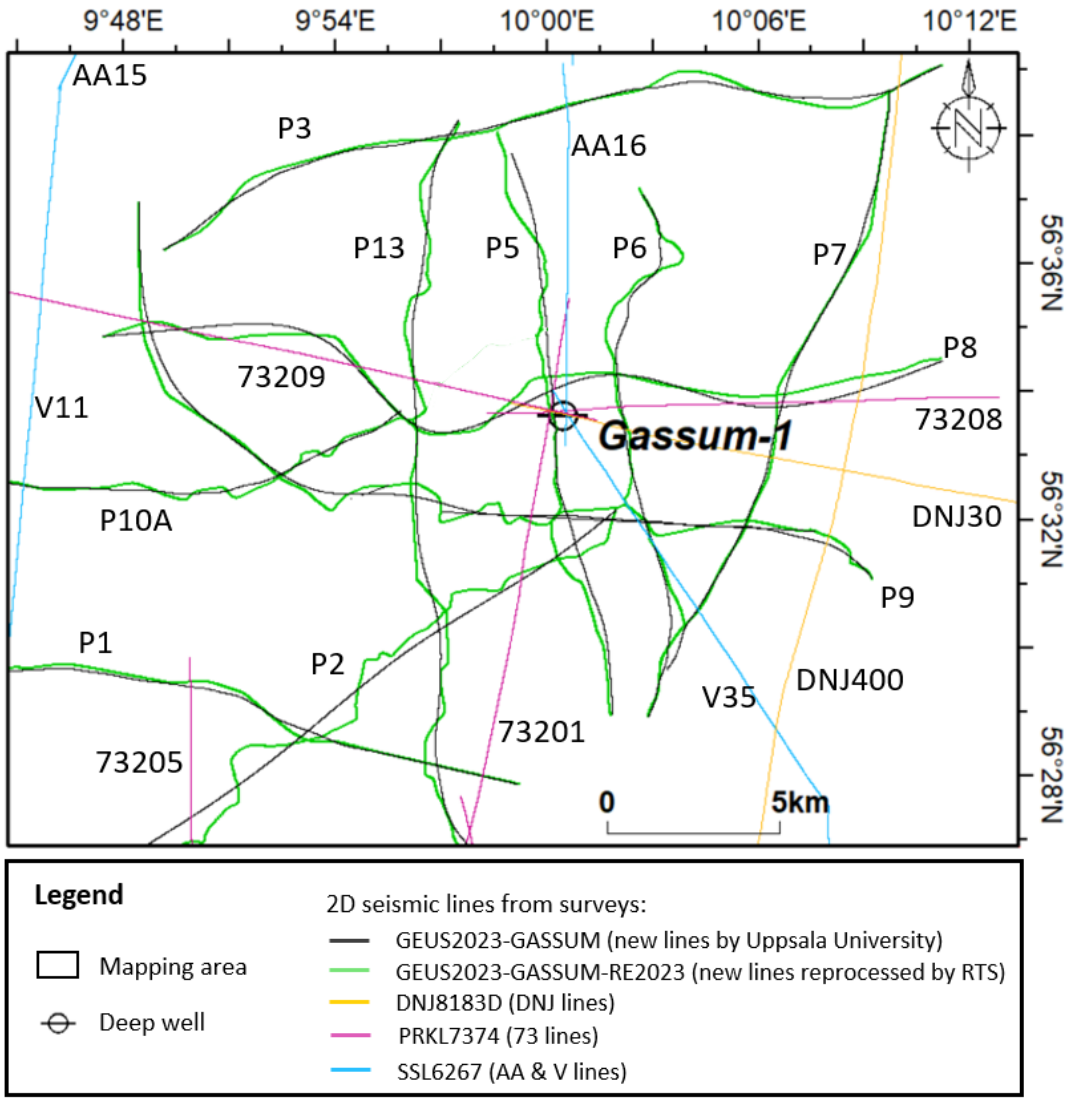


**Fig. 4.1.1**. *Database map with publicly available seismic surveys and deep well (Gassum-1) from the study with line names (new lines are abbreviated ex. 'P1' from 'GEUS23_GSM_P1').*

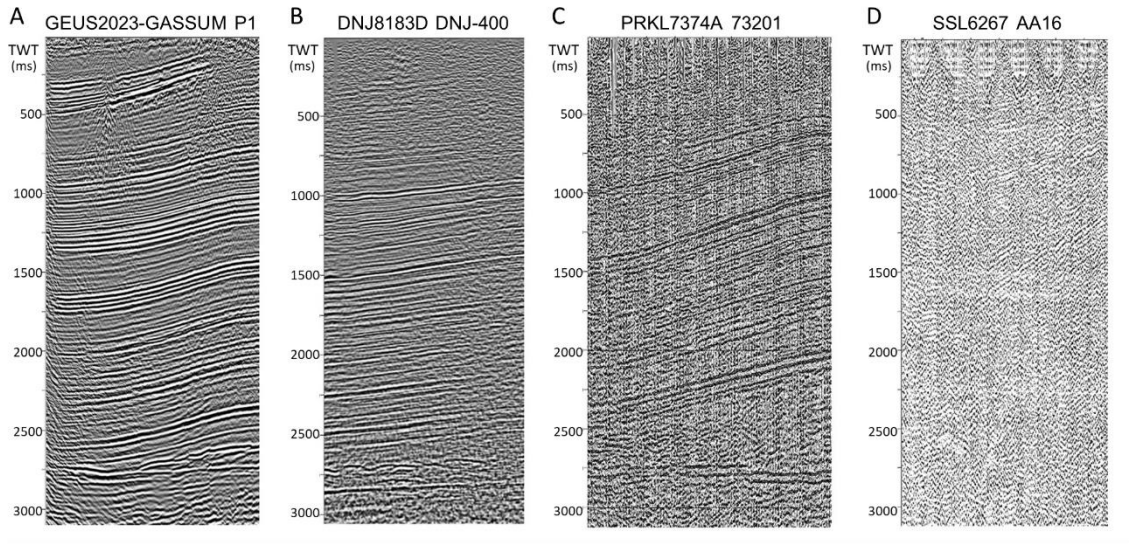


**Fig. 4.1.2.** *Four examples of seismic data quality in the study area. A) The new GEUS2023-GASSUM survey with excellent quality. B to D) The older surveys shows a quality variation from good to very poor.*

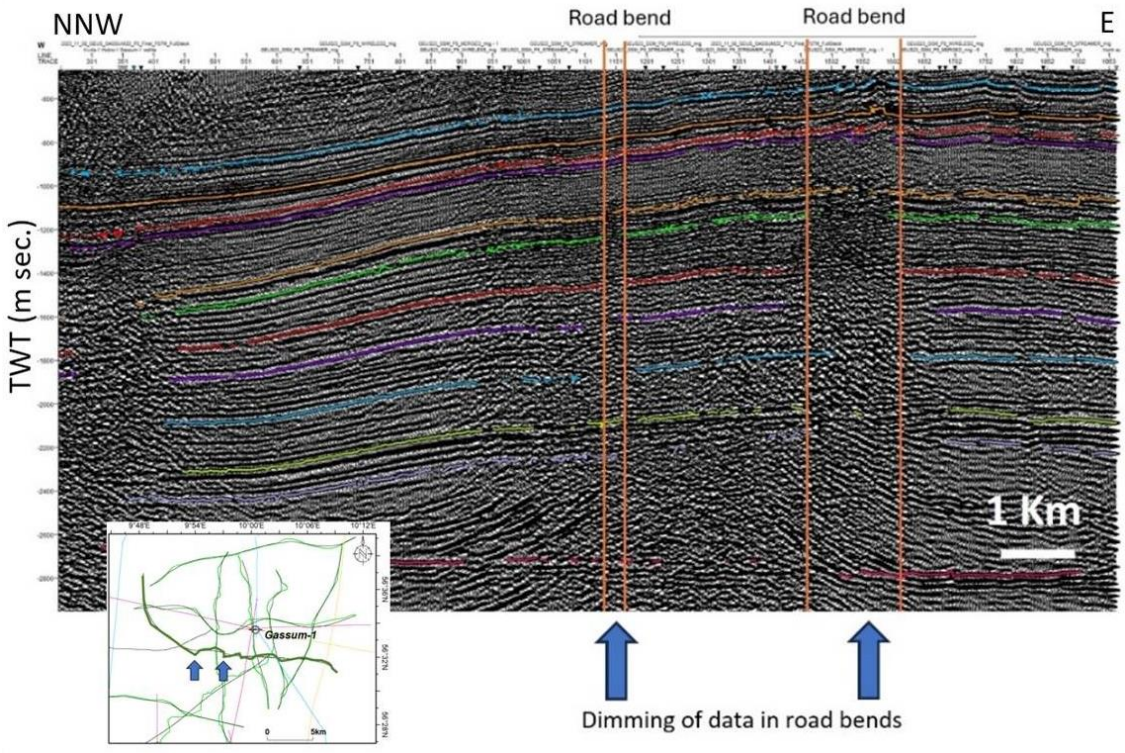


**Fig. 4.1.3**. *Example of strong dimming of signals at road bends in the new GEUS2023-GASSUM-RE2023 seismic data. The road bends are marked with arrows on both seismic section (line P9) and shotpoint map.*

### Seismic data mis-ties

All new seismic lines and vintage regional seismic lines for the Gassum structure (tie near at Gassum-1 well) to coastal areas are examined for mis-ties. As the interpretation in Petrel is performed with data at mean sea level lines are adjusted to fit this level. Time-shifts are required for lines of the GEUS2023-GASSUM-RE2023 survey and for line DNJ-30 (Table 4.1.2). We use constant time shifts.

**Table 4.1.1**. *Seismic surveys and lines used in the mapped Gassum area with time shifts*

| Survey | Line: Vertical, constant time-shift (millisecond TWT) |
|---|---|
| **GEUS2023-GASSUM** | GEUS23-GSM_P1, P2, P3, P5, P6, P7, P8, P9, P10A, P13: 0 ms |
| **GEUS2023-GASSUM-RE2023** | GEUS23-GSM_P1: -20 ms, P2: -20 ms, P3: -30 ms, P5: -20 ms, P6: -30 ms, P7: -10 ms, P8: -10 ms, P9: -15 ms, P10A: -20 ms, P13: -30 ms |
| **DNJ8183D** | DNJ-30: 20 ms, DNJ-400: 0 ms |
| **PRKL7374A** | 73201, 73205, 73208, 73209: 0 ms |
| **SSL6267** | AA15, AA16, V11, V35: 0 ms |

## 4.2 Seismic data acquisition and processing by Uppsala University

The new GEUS2023-GASSUM 2D seismic survey acquired over the Gassum structure in 2023 was organized by GEUS for the initial maturation described in this report, and with Uppsala University in charge of acquisition and first processing. Each of the survey profiles are named: GEUS23_GSN_P1, -P2, -P3, -P5, -P6, -P7, -P8, -P9, P10A, and P13 with a total line length of c. 221 km. The positions of the profiles are shown in Fig. 4.2.1, where they are abbreviated P1–P13. Line extensions include a reference to the type of the geophone recording: streamer, wireless and merged (streamer & wireless together), and if the version is stacked (stk), or stacked and migrated (mig) – e.g., GEUS23_GSN_P1_merged_stk. Link to survey processing summary sheet: GEUS2023-GASSUM (geus.dk).

In addition, GEUS issued a company reprocessing in 2023 of the survey: GEUS2023-GASSUM-RE2023 (see chapter 4.3).

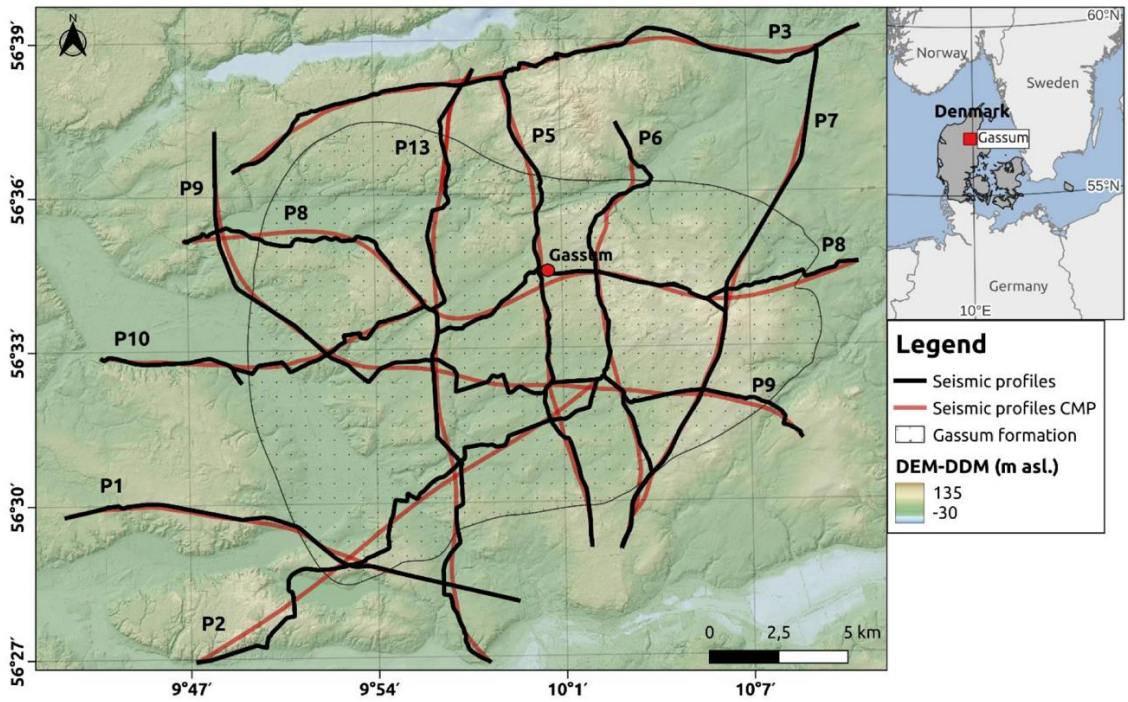


**Figure 4.2.1.** *Map with locations of the seismic profiles from the acquisition and processing report (Malehmir & Westgate 2023). Red lines are locations of the final migrated seismic profiles (here the profiles of wireless and merged files). Black lines are locations at the roads, where the seismic data were acquired.*

## Acquisition of the seismic survey

Uppsala University was contracted to acquire and process a new seismic survey with the ten reflection seismic profiles of the survey GEUS2023-GASSUM, in a research and development cooperation. The survey was conducted from February 2nd to May 30st 2023 (Figs. 4.2.1–4.2.3) and was delivered and reported in the acquisition and processing report of December 2023 by Malehmir & Westgate (2023) (Fig. 4.2.4).

The purposes of this cooperation acquisition project are mainly:

1. to improve the database at the data-poor area around Gassum to mature the Gassum structure towards potential storage of $CO_2$;
2. to acquire new seismic lines to improve the data coverage with modern data;
3. to acquire modern high fold data for imaging and interpretation of the shallow and deeper subsurface, in particular the key reservoir (mainly Gassum Formation), seal (mainly Fjerritslev Formation), faults and the geometry of the Gassum structure.
4. to expand knowledge of CCS operations through research and education, here in cooperation with universities.

*Collaboration partners*

Uppsala University contracted the Polish company Geopartner Geofizyka with two small trucks equipped with vibration hydraulic pistons as source for the vibro-seismic data. Students in geophysics and geoscience from University of Copenhagen and University of Aarhus were hired as field assistants to conduct field support, including deploying the wireless

geophones and surveying their positions with Differential GPS, adjusting the landstreamer and distributing information folders and flyers to citizens. COWI was contracted for acquiring permits, logistical planning, assessments in relation to landowners and support on external contacts to authorities and citizens.

*Communication & meetings*

Communication with the local community was provided through three public information meetings on January 10th, 2023 (Hotel Amerika, Hobro), on January 17th, 2023 (Netværk-shuset N1, Randers), and on June 6th, 2023 (Hotel Amerika, Hobro). A public visit day was held on March 25th, 2023. Information flyers and folders were provided to landowners in the vicinity of the acquisition, and information mainly on the website of project. In addition, local medias made interviews and articles on the acquisition (e.g., DR Østjylland on April 4th, 2023: "Danmarks undergrund bliver scannet for lagerplads til $CO_2$"), TV2 NORD on March 13th, 2023: "Lokale om muligt $CO_2$-lager: - Det er en udfordring, vi må stå sammen om at få løst", and TV2 19 News reportage on March 5th, 2023).

*Survey design*

The acquisition took place from February 2nd to May 30th, 2023, and the seismic data were recorded along the ten lines shown in Figure 4.1.1.

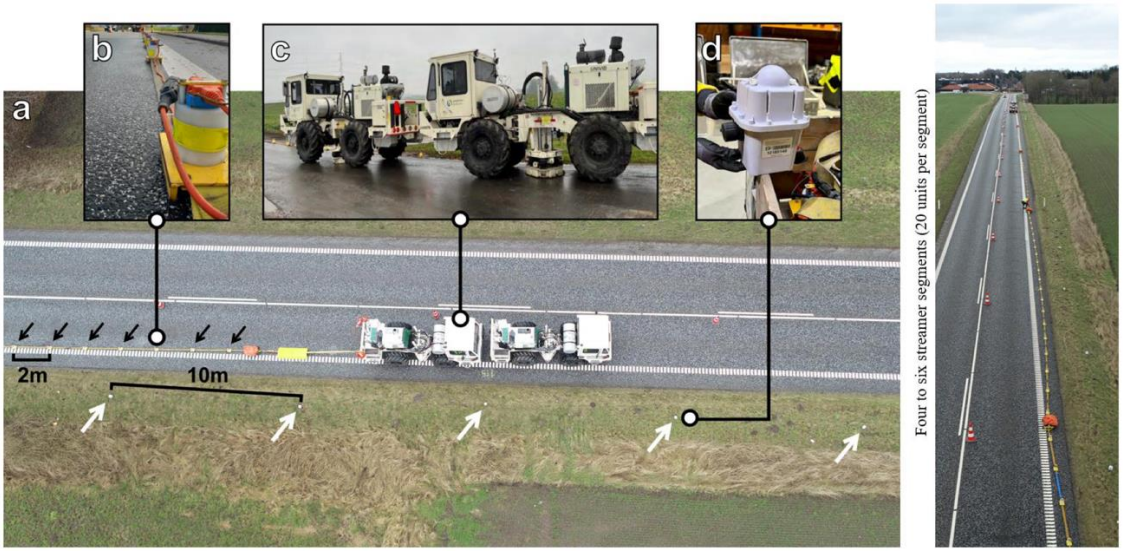


**Figure 4.2.2**. *(a) Operational setup of field equipment. (b) Micro-electromechanical systems (MEMS) sensors mounted at 2 m intervals on a landstreamer towed behind the rear vibroseis truck. (c) Two vibroseis trucks are operated with syncronised vibrations. (d) Wireless geophones are planted every 10 m along the profile. Figure from Malehmir and Westgate (2023).*

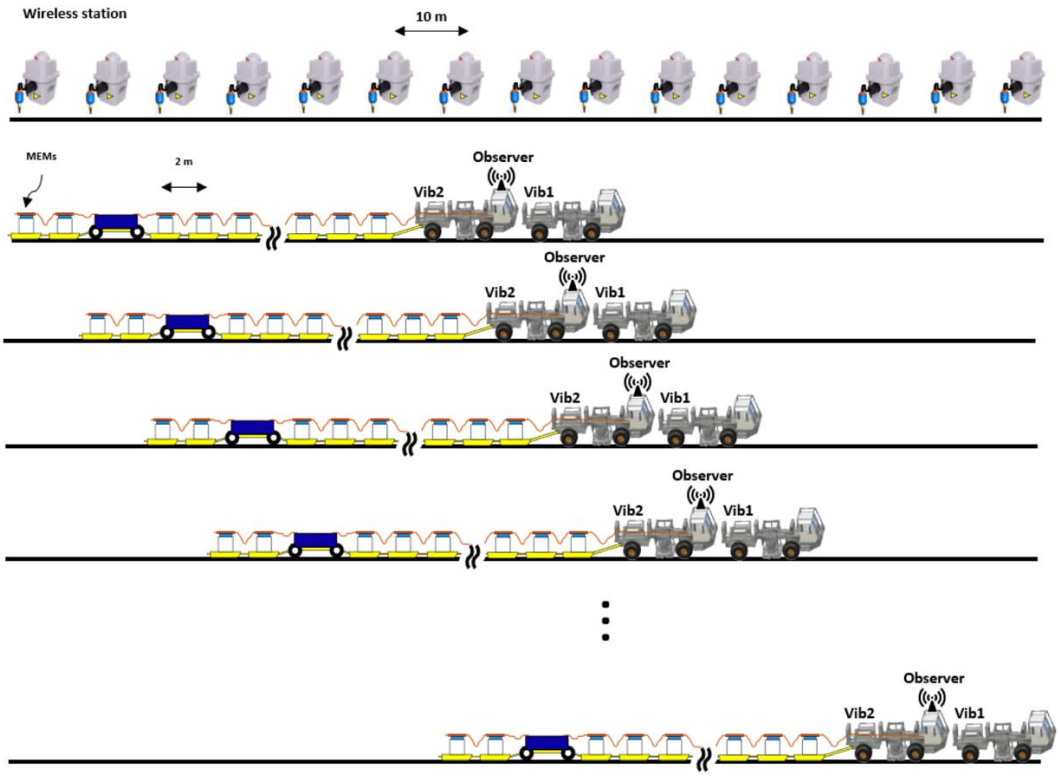


**Figure 4.2.3.** *Diagram of the data collection procedure. Figure from Malehmir and Westgate (2023).*

As seismic source, two small 12 tonnes vibroseis trucks (INOVA UNIVIB-326) were used with synchronized vibrating hydraulic pistons lowered in firm contact with the road (Fig. 4.2.2, Table 4.2.1). The vibroseis trucks operated at a peak force of 95 kN and generated syncronised seismic sweeps every 10 m along the profile. The seismic sweeps had a linear increase in bandwidth from 10 Hz to 140 Hz over 18 seconds. At every shot-point location, this sweep was repeated three times to improve signal-to-noise ratio in the subsequent processing.

When passing close to buildings, control measurements with a vibration monitor were carried out near the foundation of the buildings to secure that vibrations stay below a threshold, as defined by the German norm DIN 4150-3. If the vibrations approached the threshold, the vibrations were done with a smaller force or in some case shot points were skipped.

Before the acquisition, the field personnel followed a road-safety course, and were equipped with safety clothing during fieldwork. Every day started with a meeting for all field personnel with a briefing of the day's plan and any safety concerns.

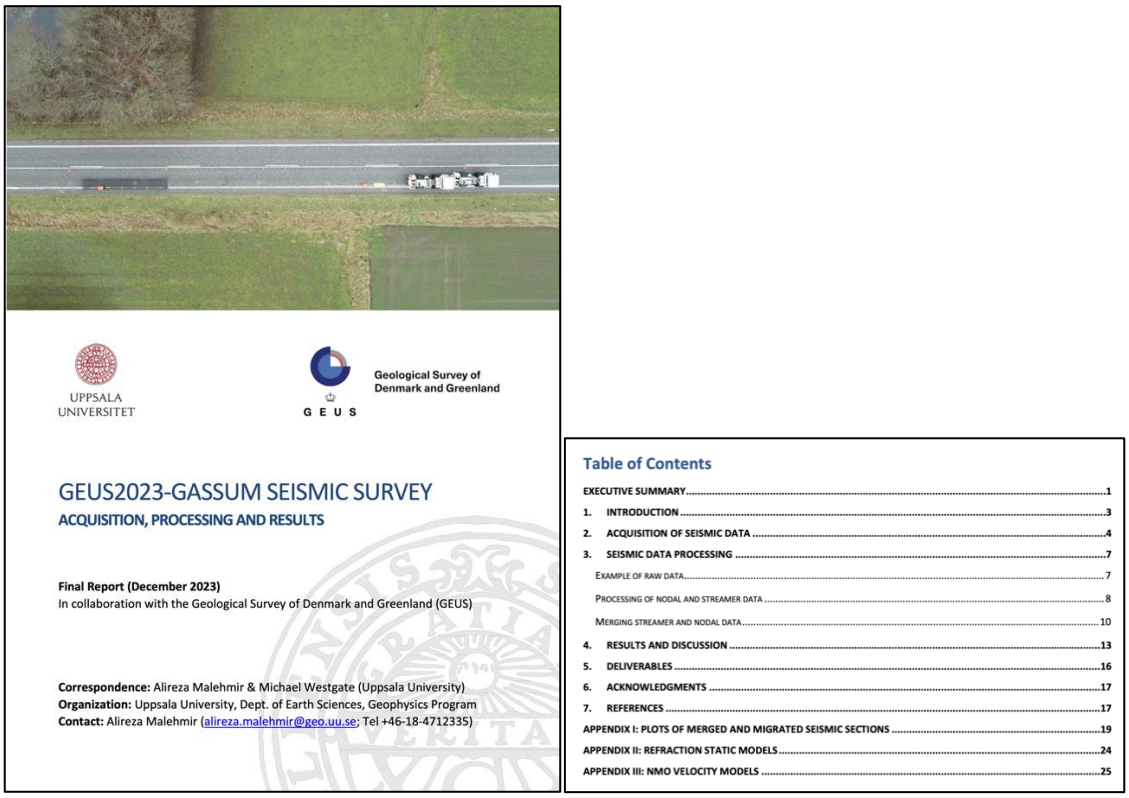

UPPSALA UNIVERSITET

Geological Survey of Denmark and Greenland

GEUS

GEUS2023-GASSUM SEISMIC SURVEY

ACQUISITION, PROCESSING AND RESULTS

**Final Report (December 2023)**
In collaboration with the Geological Survey of Denmark and Greenland (GEUS)

**Correspondence:** Alireza Malehmir & Michael Westgate (Uppsala University)
**Organization:** Uppsala University, Dept. of Earth Sciences, Geophysics Program
**Contact:** Alireza Malehmir (alireza.malehmir@geo.uu.se; Tel +46-18-4712335)

Table of Contents



**Figure 4.2.4**. *The front page and table of contents of the GEUS2023-GASSUM seismic survey: Acquisition and processing report (Malehmir & Westgate 2023), which can be accessed at the survey processing summary sheet: GEUS2023-GASSUM (geus.dk).*

The reflected seismic signals were recorded using a dual sensor system consisting of a land-streamer and wireless geophones (Fig. 4.2.2). The recording time was 25 seconds for each sweep. The landstreamer was mounted with micro-electromechanical systems (MEMS) sensors at 2 m interval with a sampling interval of 1 ms. The SeisMove landstreamer is developed by Uppsala University and consists of one to six 40 m long segments that were attached end-to-end and dragged behind the tailing vibroseis truck. The number of attached segments depended on logistical viability of any given day's traverse. Less segments were used where the day's zone had multiple sharp bends or passed through towns, while straight, flat stretches permitted the use of more segments. The wireless geophones were placed in the roadside with 10 m interval and used a frequency of 10 Hz and a 2 ms sampling interval (Table 4.2.1). Differential GPS measurements were taken to retrieve precise (within 10–30 cm) positions of the geophones. Both the operational zone and the active spread for each recording system changed per day, with an average of 200 m spread length for the land-streamer, and 7 km spread length for the geophones.

Papers, reporting and abstracts from Uppsala University present the results of the acquisition and processing of the GEUS2023-GASSUM survey, including: Malehmir & Westgate (2023), Konstantinidis et al. (2023), Westgate et al. (2023), Westgate et al. (2024), Westgate et al (submitted).

**Table 4.2.1.** *Table showing the main onshore seismic data acquisition parameters from the 2D GEUS2023-GASSUM seismic survey: Acquisition and processing report (Table 1; Malehmir & Westgate 2023).*

| **Survey Parameters** | | |
|---|---|---|
| Recording system | Sercel Lite | |
| Source | INOVA UNIVIB-326<br>(2 x 12t, 95 kN per truck) | |
| Source sweep | 10 Hz to 140 Hz linear sweep over 18 s<br>3 sweeps per shotpoint | |
| Shotpoint spacing | 10 m | |
| Geodetic surveying | Reach RX RTK DGPS | |
| **Recording Parameters** | *Landstreamer* | *Nodal recorders* |
| Receiver spacing | 2 m | 10 m |
| Spread type | End-on spread | Split spread |
| Offset (near, far) (average) | (12 m, 240 m) | (0 m, 3500 m) |
| Geophone | 10 Hz spike | MEMs 3C |
| Sampling interval | 1 ms | 2 ms |
| Record length | 25 s | 25 s |
| (before; after cross-correlation) | 6 s | 6 s |

### Seismic data processing by Uppsala University

Each seismic profile was independently processed; however, the overall processing flow was kept consistent, with only minor variations in the input parameters per profile. Streamer data and wireless geophone data were independently processed, yielding a final stacked and migrated section each. Additionally, each dataset was merged in the prestack domain, uniformalised, and jointly stacked and migrated to produce a third section per profile.

Table 4.2.2 lists the processing steps used for both datasets. The 25 second seismic records were correlated with the theoretical 10–140 Hz linear sweep and data length after vibroseis cross correlation is 7 seconds. After correlation, shot gathers were inspected for abnormalities, such as noisy traces to be discarded or correction of polarity reversals from individual geophones.

**Table 4.2.2**. *Processing sequence for the landstreamer and wireless nodal recorders. Table from the Final Acquisition and Processing Report of the GEUS2023-GASSUM survey (Malehmir & Westgate 2023).*

| | Processing step | Details | |
|---|---|---|---|
| | | *Landstreamer* | *Nodal recorders* |
| 1. | Import SEGD data | ✓ | ✓ |
| 2. | Cross-correlation with theoretical sweep | ✓ | ✓ |
| 3. | Vertical stack of repeat shots | ✓ | ✓ |
| 4. | Automatic gain control (AGC) | 200 ms | 300 ms |
| 5. | Conversion to minimum phase | ✓ | ✓ |
| 6. | Import geometry and CMP binning | 2 m CMP spacing | 5 m CMP spacing |
| 7. | First arrival picking and computation of refraction statics | | ✓ |
| 8. | Muting of noisy traces | ✓ | ✓ |
| 9. | Elevation statics | Toporaphic statics using replacement velocity of 2500 m/s and reference elevation of 106 m | |
| 10. | Bandpass filter | (10 – 30 – 130 – 140) Hz | (10 – 35 – 130 – 140) Hz |
| 11. | Airwave attenuation (330 m/s) | ✓ | ✓ |
| 12. | Sloped median filter | 500 m/s<br>800 m/s | 1000 m/s<br>2000 m/s |
| 13. | Refraction static corrections | | ✓ |
| 14. | Constant velocity analysis | ✓ | ✓ |
| 15. | Reflection-based residual statics | One round | One round |
| 16. | First break top mute | ✓ | ✓ |
| 17. | NMO correction | 50 % stretch mute | 50 % stretch mute |
| 18. | Stack | ✓ | ✓ |
| 19. | Datum reduction | Traces shifted to fixed datum at 106 m | |
| 20. | Bandpass filter | (10 – 30 – 120 – 140) Hz | (10 – 30 – 120 – 140) Hz |
| 21. | F-X deconvolution coherency filter | ✓ | ✓ |
| 22. | Amplitude balance | ✓ | ✓ |
| 23. | Finite Difference migration | ✓ | ✓ |

The data were converted to minimum phase using a statistical approach in which the characteristic wavelet was empirically determined directly from the trace records and used to design a matching filter that maps the wavelet to its minimum phase equivalent. The match filter was then convolved with each trace to approximate the minimum-phase data.

The Differential GPS data were used to set the geometry information of shot and receiver locations. The traces were then binned into common midpoint (CMP) bins, each centrally located along a spline curve that traversed the points of highest CMP density based on the nodal sensor locations. The CMP spacing was set to 5 m for the nodal data and 2 m for the streamer data to optimize horizontal resolution. For consistency, the same crooked processing line was used to bin the streamer data.

Static corrections, consisting of both floating datum and refraction static corrections, were calculated. The first arrival of every trace was picked and used for inverse modelling of the near-surface velocity variations of the weathered layer along each profile to retrieve the refraction static shifts.

A combination of bandpass filters and median filters were used to remove both coherent noise sources, such as traffic noise and groundroll, and random noise such as weather-related or electrical noise. A predictive deconvolution filter was designed to compress the

minimum phase wavelet and attenuate multiples. Gap and operator lengths were chosen from computing autocorrelogram windows over portions of the data that exhibited high-quality reflections and strong multiples.

After the prestack processing flow, velocity analysis was performed using localised constant velocity stacks (CVSs) over a gradient of velocities. This analysis was systematically performed across each profile along reflection horizons at their respective arrival times, thus producing an RMS velocity model for normal moveout (NMO) corrections. An NMO stretch mute was applied where wavelengths were stretched beyond 50%.

Residual statics were calculated from the reflection events and applied to the data for improved reflection coherency. The velocity model was updated with a second round of CVS analysis. The traces were then sorted into CMP bins and stacked to unity using a diversity stacking algorithm. The stacked section was then reduced to a fixed datum of 106 m above sea level (the highest point of the survey area) and passed through a bandpass filter to attenuate any introduced noise, followed by a coherency filter (f-x deconvolution) and an amplitude gain to recover deeper and subtle reflectors. Finally, the stacked section was migrated using a finite-difference migration algorithm based on the velocity models created by the CVS analysis.

Merging the prestack data of the wireless geophones and the landstreamer unites the benefits of each dataset configuration and optimizes the signal-to-noise ratio of both datasets. The dense spacing and high resolution of the streamer sensors improves the shallow reflection signals, while the larger spread of the wireless geophone data allows for detection of deeper reflectors that will have signals at larger offsets.

**Table 4.2.3.** *Steps taken to merge the landstreamer and wireless geophone data. Table from the Final Acquisition and Processing Report of the GEUS2023-GASSUM survey (Malehmir & Westgate 2023).*

| | Processing step | Details |
|---|---|---|
| 1. | Import streamer and wireless datasets | Each dataset has been processed prestack. Streamer data resampled to 2 ms to match wireless data. |
| 2. | Update geometry with new CMP line | Re-bin merged CMP gathers with 5 m bin spacing. |
| 3. | Automatic gain control | Window length: 300 ms. |
| 4. | Elevation static correction | Static shifts based on elevation: new reference elevation 106 m and replacement velocity 2500 m/s. (premerged datasets had respective elevation statics reversed prior to merging). |
| 5. | Bandpass filter | (10 – 35 – 120 – 140) Hz |
| 6. | Alignment of datasets | Bulkshift of streamer traces by 10 ms.<br>One round of reflection-based residual static corrections. |
| 7. | Constant velocity analysis | Velocity model based on wireless dataset with minor updates. |
| 8. | NMO correction | 50 % stretch mute. |
| 9. | Stack | |
| 10. | Datum reduction | Traces shifted to fixed datum at 106 m |
| 11. | Bandpass filter | (10 – 30 – 120 – 140) Hz |
| 12. | F-X deconvolution coherency filter | |
| 13. | Amplitude balance | |
| 14. | Finite Difference migration | |

Table 4.2.3 summarizes the steps taken to merge the two datasets. The processed prestack data, up to and including residual static corrections, of both datasets were streamed

into the processing scheme. The first step was to update the geometry: traces were re-sorted into shot gathers of increasing offset and then binned into CMP gathers using an updated CMP line that traversed the same path as the initial datasets. After testing different bin sizes and spacing, a 5 m spacing between bin centres was chosen based on the quality of the stack.

A comparison between stacks from landstreamer, wireless, and merged data is shown in Figure 4.2.5. Due to the higher frequency content of the streamer data for shallow depth, the reflections of the merged section appear sharper than those of the wireless data, which is able to image deeper reflections. The noise that is more prevalent in the landstreamer data comes through in the deeper part of the merged gather and the wireless appears less noisy, but the reflection signals are preserved with a good signal-to-noise ratio and the overall effect of merging the data appears to be nett positive for the quality of the data.

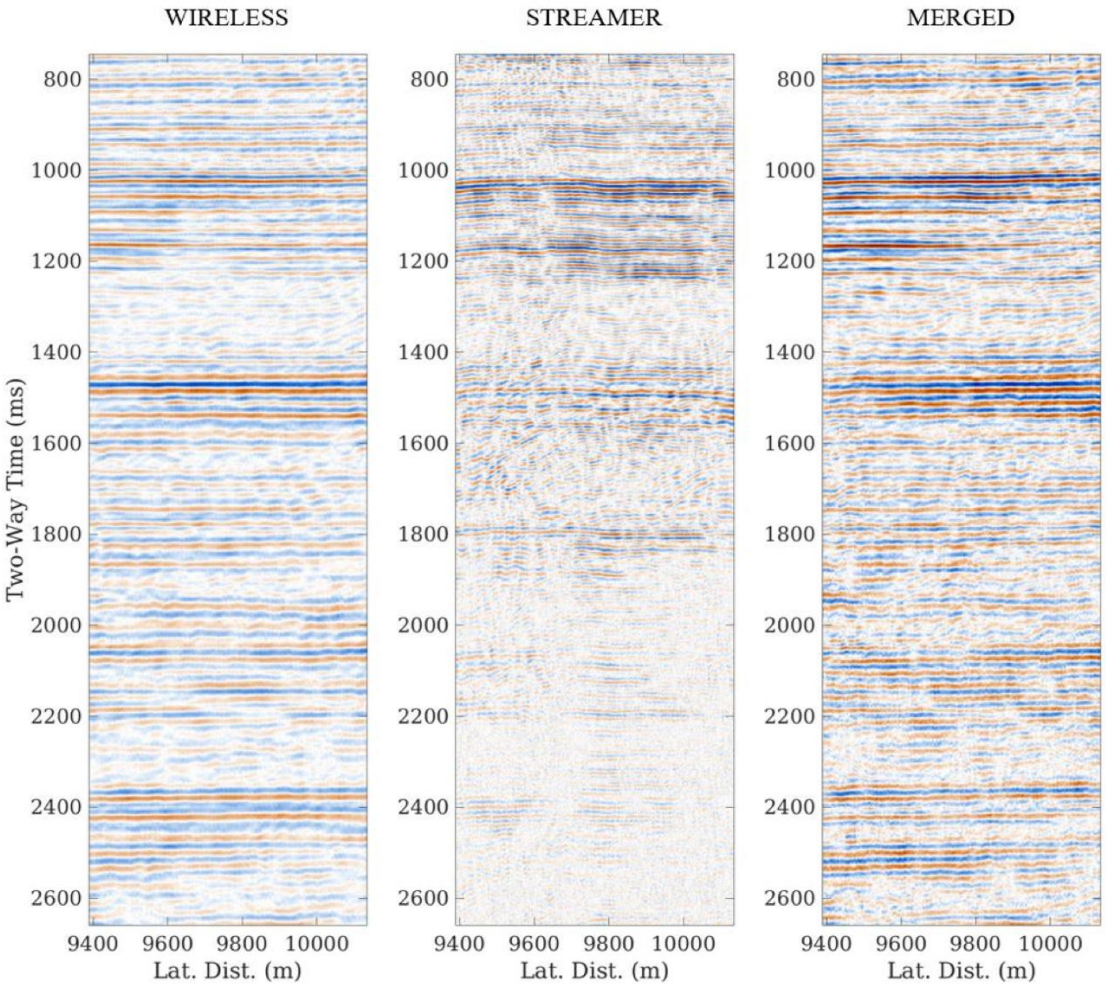


**Figure 4.2.5.** *A zoomed portion of one of the stacked profiles, comparing wireless, landstreamer, and merged datasets. Figure from Malehmir and Westgate (2023).*

### Deliverables from Uppsala University

The deliverables from the GEUS2023-GASSUM seismic survey are listed in Table 4.2.3.

**Table 4.2.3**. *List of deliverables. Table from the Final Acquisition and Processing Report of the GEUS2023-GASSUM survey (Malehmir & Westgate 2023).*

| Profile N | Description | Wireless | Streamer | Merged |
|---|---|---|---|---|
| GEUS23_GSM_P<N>_<TYPE>_raw.segy | Seismic SEGY files of data at different processing steps: raw; processed; brutestack; stack; mirgated | ✓ | ✓ | |
| GEUS23_GSM_P<N>_<TYPE>_proc.segy | | ✓ | ✓ | ✓ |
| GEUS23_GSM_P<N>_<TYPE>_brtstk.segy | | ✓ | ✓ | |
| GEUS23_GSM_P<N>_<TYPE>_stk.segy | | ✓ | ✓ | ✓ |
| GEUS23_GSM_P<N>_<TYPE>_mig.segy | | ✓ | ✓ | ✓ |
| **Textual_Headers** | | | | |
| GEUS23_GSM_P<N>_<TYPE>_raw.rch | Files containing text that was used for textual header in corresponding SEGY files. | ✓ | ✓ | |
| GEUS23_GSM_P<N>_<TYPE>_proc.rch | | ✓ | ✓ | ✓ |
| GEUS23_GSM_P<N>_<TYPE>_brtstk.rch | | ✓ | ✓ | |
| GEUS23_GSM_P<N>_<TYPE>_stk.rch | | ✓ | ✓ | ✓ |
| GEUS23_GSM_P<N>_<TYPE>_mig.rch | | ✓ | ✓ | ✓ |
| **Refraction_Model** | | | | |
| GEUS23_GSM_P<N>_<TYPE>_refstat_model.segy | Near surface velocity model. | ✓ | | |
| **Static_Corrections** | | | | |
| GEUS23_GSM_P<N>_<TYPE>_cdpfltstatic.txt | Elevation static shifts. | ✓ | ✓ | ✓ |
| GEUS23_GSM_P<N>_<TYPE>_refstat.txt | Refraction static shifts. | ✓ | | |
| GEUS23_GSM_P<N>_<TYPE>_resstat.txt | Residual static shifts. | ✓ | ✓ | ✓ |
| **Geometries** | | | | |
| GEUS23_GSM_P<N>_<TYPE>_coords_cmp.txt | CMP coordinates. | ✓ | ✓ | ✓ |
| GEUS23_GSM_P<N>_<TYPE>_coords_shot.txt | Shot coordinates. | ✓ | | |
| GEUS23_GSM_P<N>_<TYPE>_coords_rec.txt | Receiver coordinates. | ✓ | ✓ | ✓ |
| **Velocities** | | | | |
| GEUS23_GSM_P<N>_<TYPE>_nmo.txt | NMO velocity model. | ✓ | ✓ | ✓ |
| GEUS23_GSM_P<N>_<TYPE>_mig.txt | FD migration velocity model. | ✓ | ✓ | ✓ |
| **PFT Files** | | | | |
| GEUS23_GSM_P<N>_pft_<DATA>.txt | Pairs of profile peg numbers and wireless serial numbers. | ✓ | | |
| GEUS23_GSM_P<N>_active_spread.txt | Active spread for each day during acquisition of profile. | ✓ | | |

## 4.3 Seismic data reprocessing

Realtimeseismic (RTS) reprocessed the wireless seismic data from the GEUS2023-GAS-SUM survey with the following objectives:

1. Obtaining optimal resolution for identifying key geologic formations and features in the study area.
2. Understanding and suppressing the crooked line artefacts.
3. Ensuring optimal ties between the seismic lines.

The reprocessing project, GEUS2023-GASSUM-RE2023, lasted around ten weeks, from September 29th to December 11th, 2023. It aimed to improve the migrated stack profiles from the original processing to assist the geological interpretation of the Gassum structure. The reprocessed seismic data and the comprehensive reprocessing report are available on the survey processing summary sheet: GEUS2023-GASSUM-RE2023 (geus.dk). The general processing sequence implemented in the reprocessing is shown in Table 4.3.1.

**Table 4.3.1.** *Processing sequence for the reprocessing of wireless data from the GEUS2023-GASSUM survey.*

| | **Processing steps** |
|---|---|
| 1. | Input analysis |
| 2. | Geometry QC |
| 3. | Firstbreak picking |
| 4. | 3D diving wave tomography |
| 5. | Refraction statics |
| 6. | Residual refraction statics |
| 7. | Stacking velocity picking |
| 8. | Reflection statics |
| 9. | Surface wave attenuation |
| 10. | High amplitude noise attenuation |
| 11. | Surface-consistent amplitude correction |
| 12. | Surface-consistent deconvolution |
| 13. | Time-variant filtering |
| 14. | 3D regularization |
| 15. | Prestack time migration |
| 16. | Migration velocity updating |
| 17. | Residual moveout correction |
| 18. | Spectral shaping |
| 19. | Time-variant filtering |
| 20. | Trim statics |
| 21. | Outside mute |
| 22. | Dip estimate |
| 23. | Structure-oriented denoising |
| 24. | PSTM common image gather stacking |
| 25. | Post-stack enhancement |

### Static effects

Processing onshore seismic data is usually challenged by static effects due to factors such as dynamic topography and near-surface velocity heterogeneities. A common practice of static correction involves first arrival modelling using refracted ray theory (Palmer 1980). This theory assumes that the modelled interval velocities always increase with depth and that there are no vertical velocity changes within subsurface intervals. However, those assumptions are often violated in reality, leading to failure in removing persistent static effects. To anticipate such issues, the reprocessing utilized tomostatics – an advanced static correction technique based on a velocity model generated using turning ray tomography (Zhu et al. 1992; Zhang & Toksöz 1998). Using a turning ray forward model, tomostatics can accommodate a vertical velocity gradient within defined velocity intervals by implementing first arrival inversion. Tomostatics can also tolerate velocity decrease with depth, given that the overall velocity gradients still enable the rays to return to the surface within the recording offset. Using tomostatics, the reprocessing anticipated potential static-related artefacts due to complex near-surface geology and missing near-surface refractors (Zhu et al. 1992; Zhang & Toksöz 1998).

Besides the static correction, the implemented migration technique also plays a crucial role in the reprocessing. The reprocessing utilized a Kirchhoff prestack time migration (PSTM) technique to anticipate conflicting dips with different stacking velocities and complex non-hyperbolic moveouts (Yilmaz 2001).

### Crooked line artefacts

Due to the logistic setup of the seismic field campaign, the seismic data could only be acquired along roads. This limitation causes significant challenges with artefacts in the new GEUS2023-GASSUM stack seismic data due to crookedness, i.e., road bending and irregular acquisition geometry.

Crooked lines cause irregular source-receiver offsets along the lines and shift reflection points away from the lines, producing midpoint dispersion and uneven subsurface wavefield illumination, as illustrated in Fig. 4.3.1.

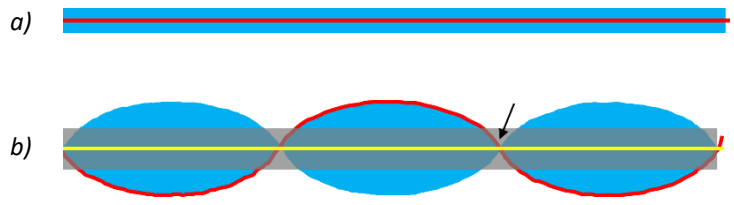


**Figure 4.3.1.** *Illustration of the effects of seismic line shapes on midpoint locations. Red: seismic lines; blue: midpoint locations (midpoint dispersion in the case of the crooked line); yellow: a smoothed binning line from the crooked line; grey: a binning area for the smoothed line; the arrow highlights an example of binned areas with potentially missing traces in the offset classes. (a) A straight seismic line produces midpoints exactly below the line. The blue area highlights the midpoints below the line; the crossline binning is unnecessary because all the reflections are in-plane. (b) A crooked line produces midpoint dispersion away from exactly below the line.*

Crooked lines can also cause uneven fold coverage due to irregular trace distribution and missing traces in the offset classes. The low fold coverage at the crooked areas produces migration artefacts, known as migration smiles, as the migration smears the amplitudes along the wavefield isochron. This phenomenon is similar to the migration effect at the ends of a seismic profile. Therefore, the crooked line artefacts found on a stack profile are arguably made up, at least part of it, by migration smiles.

To suppress the crooked line artefacts, GEUS preferred the reprocessing to implement binning line smoothing followed by 3D regularization (Schonewille et al. 2009). The binning line smoothing aimed to achieve even fold coverage. On the other hand, the 3D regularization ensured even fold coverage by filling the missing traces in the bins and offset classes.

### Reprocessing test to suppress crooked line artefacts

GEUS and RTS did a test to understand the crooked line artefacts and to assess the binning line smoothing approach. The test had been carried out prior to the reprocessing of the Gassum project and implemented on a line (the test line P4) from GEUS2023-RØDBY 2D survey (Abramovitz et al. 2024), which also produced crooked lines. Figure 4.3.2a shows the final PSTM stack profile from the test line obtained without binning line smoothing[1] and 3D regularization, and we can see prominent crooked line artefacts on the profile. The intermediate processing output before the final PSTM stack is the raw PSTM stack, shown in Fig. 4.3.2b, and the same crooked line artefacts as in the final PSTM stack are also noticeable in the raw PSTM stack. Since the final PSTM stack is made of the raw PSTM profile after residual moveout correction, demultiple, spectral shaping, time-variant filtering, trim statics, structure-oriented denoising, and poststack enhancement (Table 4.3.1), it is confirmed that the artefacts are unlikely caused by any or the combination of those processes.

The effects of binning line smoothing and 3D regularization on the stack profile were then tested. Figure 4.3.3 shows a stack profile from the test line before the migration, with binning line smoothing and with (Fig. 4.3.3a) and without (Fig. 4.3.3b) 3D regularization. Both profiles in Fig. 4.3.3 show that the crooked line artefacts are barely noticeable before the migration, indicating that the artefacts are likely and mainly caused by the migration as migration smiles.

[1] The reprocessing, in all cases, necessitated the use of subtle binning line smoothing for all lines, without altering the main crookedness trends. The term 'without line smoothing ' in this context is synonymous with subtle binning line smoothing.

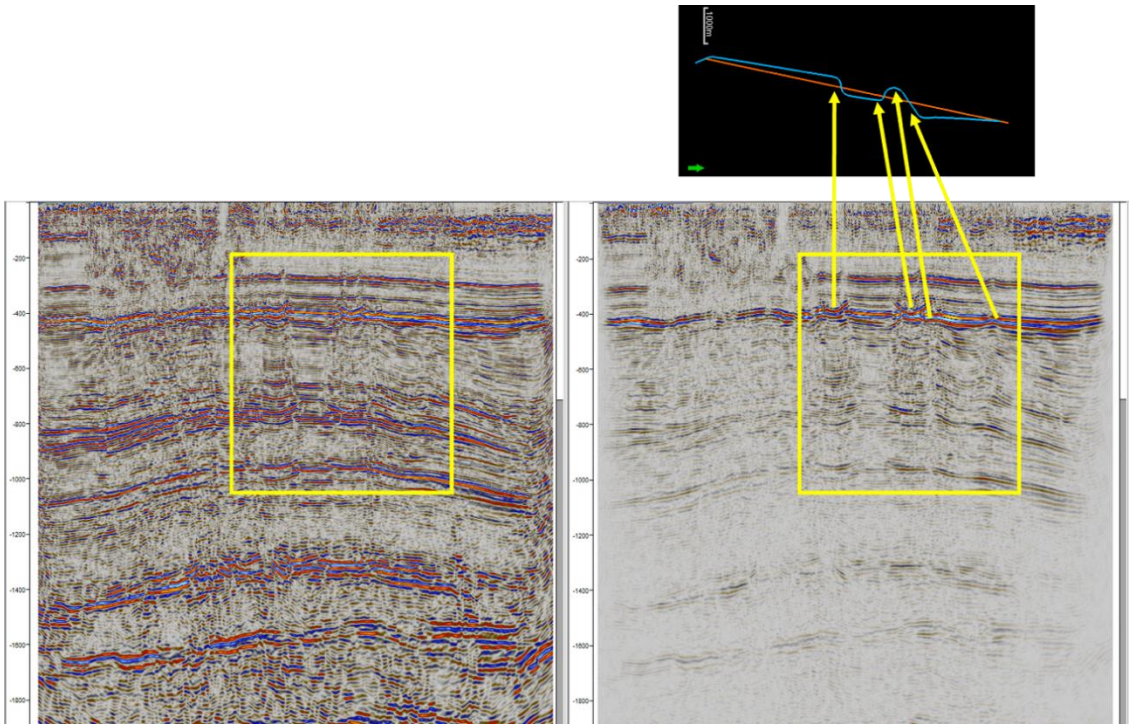

*a)* *b)*

**Figure 4.3.2.** *Prestack time migration (PSTM) stack profiles from the test line, i.e., line P4 of the GEUS2023-RØDBY survey (Abramovitz et al. 2024) without smoothing. (a) Final. (b) Raw. The yellow boxes highlight the crooked line artefacts (migration smiles). The map shows the seismic line before (blue) and after (orange) smoothing. The yellow arrows show that the artefacts on the profile coincide with the crooked areas on the map.*

The effects of 3D regularization on the test line independently from the binning line smoothing were also tested. Figure 4.3.4 shows the raw PSTM stack profiles (after migration) from the test line with binning line smoothing and with and without the 3D regularization. The figure shows that the migration smiles are not completely suppressed on the profile without the 3D regularization but mostly removed on the profile with the 3D regularization.

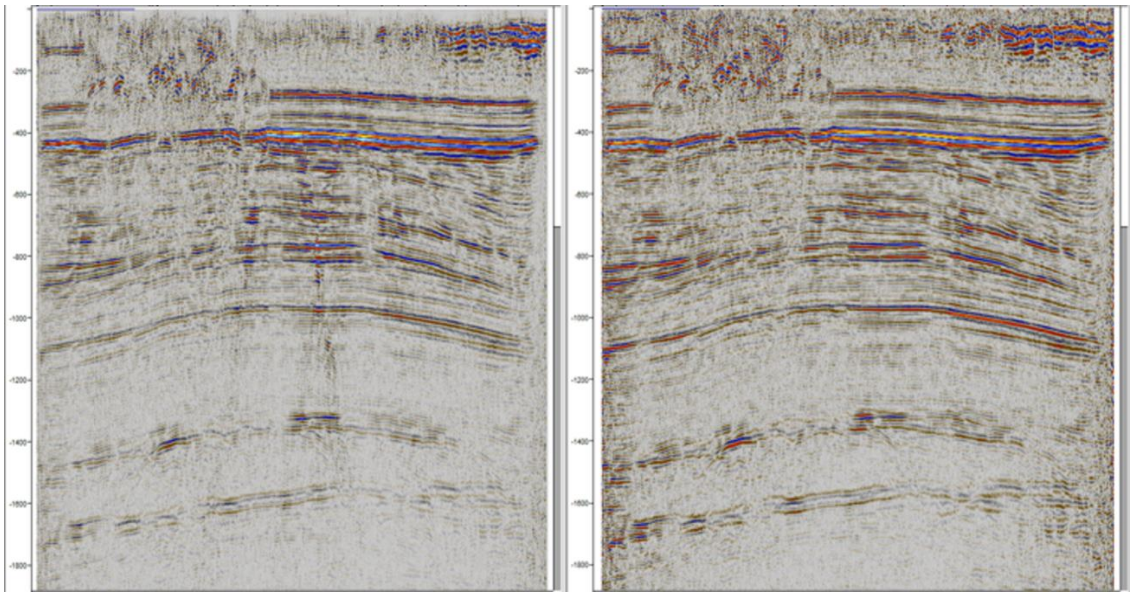

*a)* *b)*

**Figure 4.3.3.** *Stack profiles from line P4 of the GEUS2023-RØDBY survey (Abramovitz et al. 2024) before the migration and with binning line smoothing. (a) Without 3D regularization. (b) With 3D regularization.*

Overall, the test results confirm that the migration smiles make up the crooked line artefacts and that they can be suppressed by binning line smoothing followed by 3D regularization.

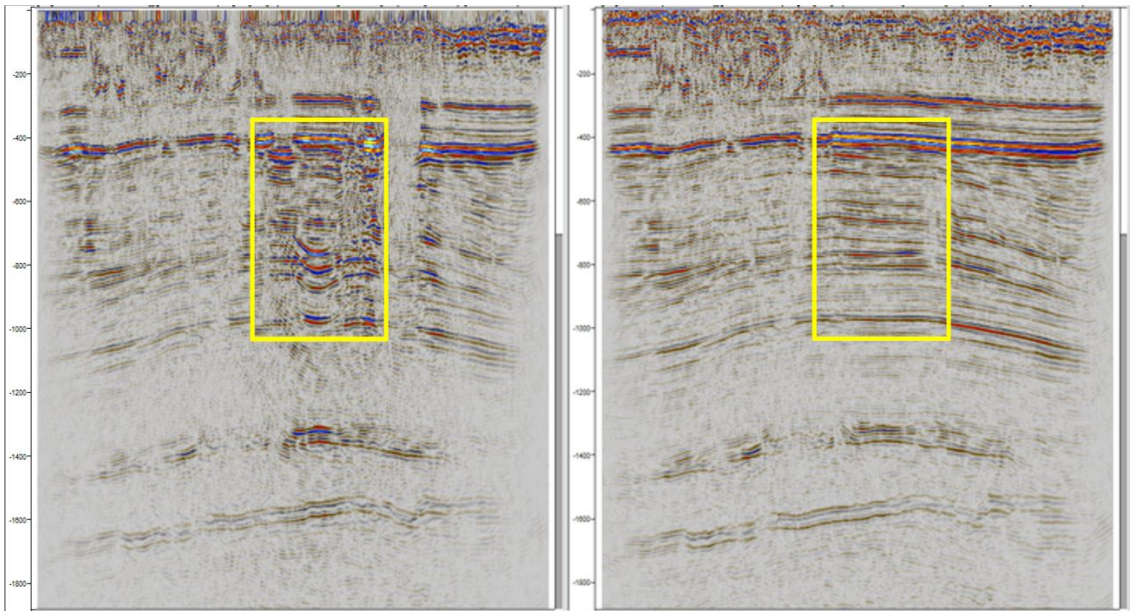

*a)* *b)*

**Figure 4.3.4.** *Raw PSTM stack profiles (after migration) from the test line, i.e., line P4 of the GEUS2023-RØDBY survey (Abramovitz et al. 2024), with line smoothing. (a) Without 3D regularization. (b) With 3D regularization. The yellow boxes highlight the migration smiles that are not entirely suppressed on the profile without the 3D regularization but mostly removed on the profile with the 3D regularization.*

### Reprocessing results

The reprocessing final results in terms of PSTM stack profiles show remarkable improvement from the poststack time migration (POSTM) stack profiles produced by the original processing.

As an example, Fig. 4.3.5 shows the comparison of the original and reprocessed migrated stack profiles from profile P2 of the GEUS2023-GASSUM survey (see map in Fig. 4.2.1). The comparison indicates that the reprocessing provides much more coherent reflections than the original profile, and such improvement has allowed us to interpret geologic features and key reflections associated with more confidence.

### Discussion

The binning line smoothing followed by the 3D regularization is probably the quickest solution to deal with the crooked line artefacts – yet there are likely better approaches that can lead to more accurate seismic interpretation. Binning line smoothing of a crooked line means projecting the complex midpoint dispersion due to the line crookedness into a smooth binning line traverse. This approach basically shifts the seismic interpretation from the original line geometry onto another binning line traverse and likely includes unintended out-of-plane reflections from the dispersed midpoints. Nevertheless, although the approach of the binning line smoothing followed by the 3D regularization might not be the best to deal with the crooked line artefacts, it is considered the most reasonable approach that could still assist the seismic interpretation within a relatively short time.

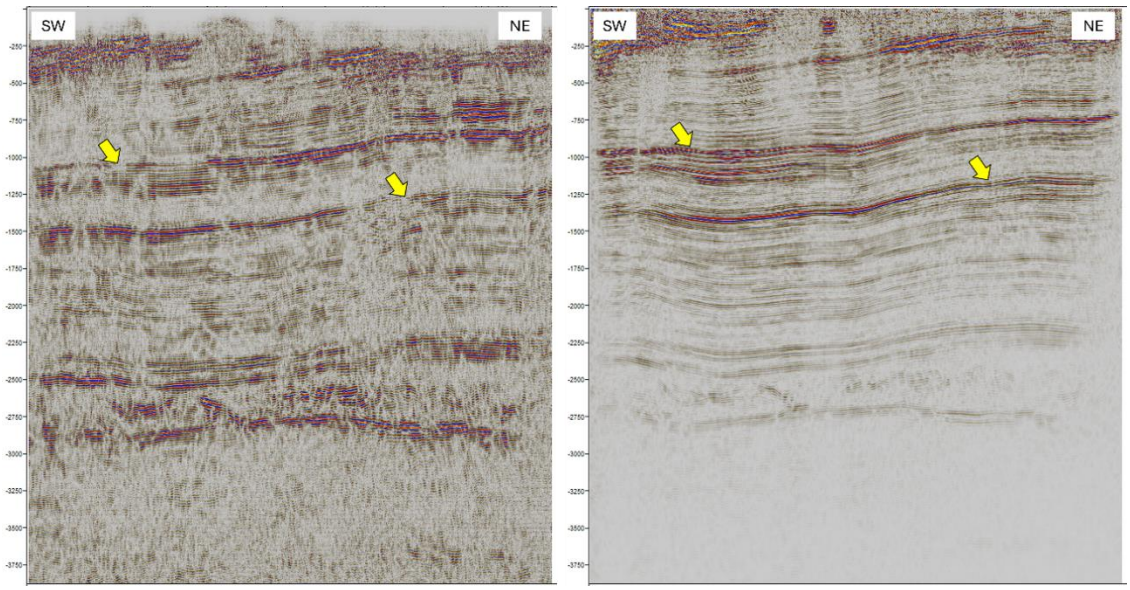


*a)* *b)*

**Figure 4.3.5.** *The comparison of (a) the original processing and (b) the reprocessing of final migrated stack profiles for line P2 of the GEUS2023-GASSUM survey. The yellow arrows highlight examples where reflections are much more coherent in the reprocessed profile than in the original processing profile.*

In principle, crooked lines violate a fundamental assumption in 2D seismic imaging, i.e., a straight-line geometry with a regular offset pattern and an even fold coverage. Therefore,

problems related to the midpoint dispersion and the uneven fold coverage caused by crooked lines can hardly be resolved only by conventional 2D seismic imaging (Wu 1996). Conventional 2D seismic processing includes normal moveout (NMO) and dip moveout (DMO) corrections, which affect only the inline reflections. In addition to the NMO and DMO corrections, 2D crooked line seismic processing requires a correction also for the out-of-plane reflections in the presence of dip through so-called cross-dip moveout (CDMO) correction (Nedimović & West 2003).

Instead of simply projecting the midpoint dispersion onto a smooth binning line traverse, studies show that more appropriate ways to deal with a crooked line can generally grouped into two categories: 1) correcting for the cross-dip reflections and 2) processing the crooked line as 3D.

Some cross-dip analysis techniques have been developed with time, including constant shift (Larner et al. 1979), cross-dip moveout (CDMO) correction (Nedimović & West 2003), iterative cross-dip moveout correction (Beckel & Juhlin 2019), generalized cross-dip moveout (GCDMO) correction (Mancuso & Naghizadeh 2021), and 2.5D multifocusing imaging (Fam et al. 2023). Nevertheless, all these techniques have considerable limitations, including laborious computation and limited accuracy for far-offset data acquired from a severely crooked line.

On the other hand, processing a crooked line in 3D is relatively more straightforward than a cross-dip correction-based approach. Processing a crooked line as 3D takes the advantage of having the midpoint dispersion by using it as pseudo-3D or 2.5D reflection points (Schmelzbach et al. 2007; Wu 1996). The pseudo-3D nature of midpoint dispersion from crooked lines allows us to image complex 3D structures around the crooked areas by simply binning and processing the data from the crooked lines in 3D. The main limitation of this approach is that it can produce low-resolution images due to low fold coverage in areas not well illuminated by the recorded wavefield.

Looking to the future, we propose further studies to implement seismic processing techniques for overcoming crooked line artefacts, particularly 2.5D multifocusing imaging (Fam et al. 2023) and crooked line processing as 3D. These innovative approaches hold great promise, as they have the potential to bring more accurate subsurface seismic images, thereby enhancing the reliability of subsurface geologic interpretation.

## 4.4 Well data

The Gassum structure is drilled by the Gassum-1 well. The well was finalised in 1951 and has TD in a depth of 3462 m (below Kelly Bushing). For this study, the nearest wells to the Gassum structure have been included and tabulated in Table 4.4.1.

Well logs are used here for interpretation, in particular of lithology, and selected logs are used for well log-based sequence stratigraphy, seismic to well ties and for seismic reservoir characterization and interpretation. See Chapters 5–7 for the specific used well logs.

Original logs: Caliper (CAL), Gamma-Ray (GR), Spontaneous Potential (SP), compressional Sonic (DT), Resistivity (R_deep mostly used), Neutron Porosity (NPHI) and Density (RHOB) logs.

Derived (interpreted) logs: Shale volume ($V_{shale}$), Effective porosity (PHIE), and Permeability estimates. The latter were derived from porosity-permeability relationships, established based on an analysis of core analysis data.

**Table 4.4.1**. *List of the wells utilized in this study, with information on the year of drilling completed, operator, Kelly Bushing (KB, m above mean seal level), Total Depth (TD, m below Kelly Bushing, measured drilled depth), deviation and Chronostratigraphy of the TD units.*

| Well | Year | Operator | KB a.msl (m) | TD b. KB (m) | Deviated | TD |
|---|---|---|---|---|---|---|
| **Kvols-1** | 1976 | DUC | 19.2 | 2641 | No | Triassic |
| **Hobro-1** | 1974 | Gulf | 32.3 | 2610 | No | Triassic |
| **Gassum-1** | 1951 | DAPCO | 58 | 3462 | No | Permian |
| **Voldum-1** | 1974 | Gulf | 34.7 | 2312 | No | Triassic |

### Well samples: Cores, SWC and ditch cutting samples

A number of cores exists from the Gassum well whereas only sidewall cores (SWC) and ditch cutting samples exist from the nearest wells to the Gassum (Table 4.4.2). The used samples and results are further discussed in Chapter 7.

**Table 4.4.2**. *Overview of the different cores, SWC and cuttings related to formation and well site. Lithostratigraphic subdivision of wells according to Nielsen and Japsen (1991).*

| Cores | Kvols-1 | Hobro-1 | Gassum-1 | Voldum-1 |
|---|---|---|---|---|
| **Chalk Group (>750 m MD)** | SWC | - | Cores 11-16 | - |
| **Lower Cret. units** | - | SWC | Cores 17-18 | SWC |
| **Frederikshavn Fm** | SWC | - | Cores 19-30 | - |
| **Børglum Fm** | SWC | SWC | Core 31 | SWC |
| **Flyvbjerg Fm** | formation not present | SWC | formation not present | formation not present |
| **Haldager Sand Fm** | - | SWC | formation not present | SWC |
| **Fjerritslev Fm** | SWC | SWC | Cores 32-52 | SWC |
| **Gassum Fm** | - | SWC | Cores 53-73 | SWC |
| **Vinding Fm** | - | SWC | Cores 74-80 | SWC |
| **Oddesund Fm** | - | - | Cores 81-88 | SWC |
| **Tønder Fm** | - | below TD | Cores 89-97 | below TD |
| **Falster Fm** | - | below TD | Cores 98-99 | below TD |
| **Ørslev Fm** | - | below TD | Cores 100-111 | below TD |
| **Skagerrak Fm** | - | below TD | Cores 112-126 | below TD |
| **Cuttings** | Yes | Yes | Yes | Yes |

# 5. Methods

## 5.1 Seismic interpretation and well-ties (Chapter 6)

The correlation of seismic surfaces is based on the well velocity survey of the Gassum-1 well and well-ties (Nielsen & Japsen 1991). Below the Skagerrak Formation, within which the well terminates, the identification of surfaces (Top Zechstein and Top pre-Zechstein) is based on seismic characteristics, e.g. the amplitude of reflectors, reflection patterns of underlaying and overlaying strata, and internal reflections patterns. It is assumed that the upperpart of the Zechstein succession is composed of alternating evaporitic deposits of, e.g., carbonates and anhydrite. A confident correlation to nearby wells, Voldum-1 and Hobro-1 is uncertain due to poor seismic data between the Gassum area and the two wells in question.

In total 12 surfaces have been mapped and they are from the oldest to youngest: (1) Top pre-Zechstein, (2) Top Zechstein, (3) Top Skagerrak, (4) Top Ørslev, (5) Top Tønder, (6) Top Vinding, (7) Top Gassum, (8) Top Fjerritslev, (9) Top Frederikshavn, (10) Base Chalk, (11) Intra Chalk and (12) Top Chalk (Fig. 5.1.1; Table 5.1.1).

The seismic follows normal polarity, with a positive reflection (boundary to higher acoustic impedance) placed in a peak (black) and a negative reflection (boundary to lower acoustic impedance) in a trough (white) on the seismic displays of the new seismic data.

**Table 5.1.1**. *Seismic horizons interpreted and the polarity picked*.

| Surface | Polarity |
|---|---|
| Top Chalk | Peak |
| Intra Chalk | Trough |
| Base Chalk | Trough |
| Top Frederikshavn | Peak |
| Top Fjerritslev | Trough |
| Top Gassum | Peak |
| Top Vinding | Peak |
| Top Tønder | Peak |
| Top Ørslev | Peak |
| Top Skagerrak | Peak |
| Top Zechstein | Peak |
| Top pre-Zechstein | Peak |

A few key lines were selected to form the basis for a more detailed seismic facies analysis of the Gassum Formation and Frederikshavn Formation (see Chapter 7).

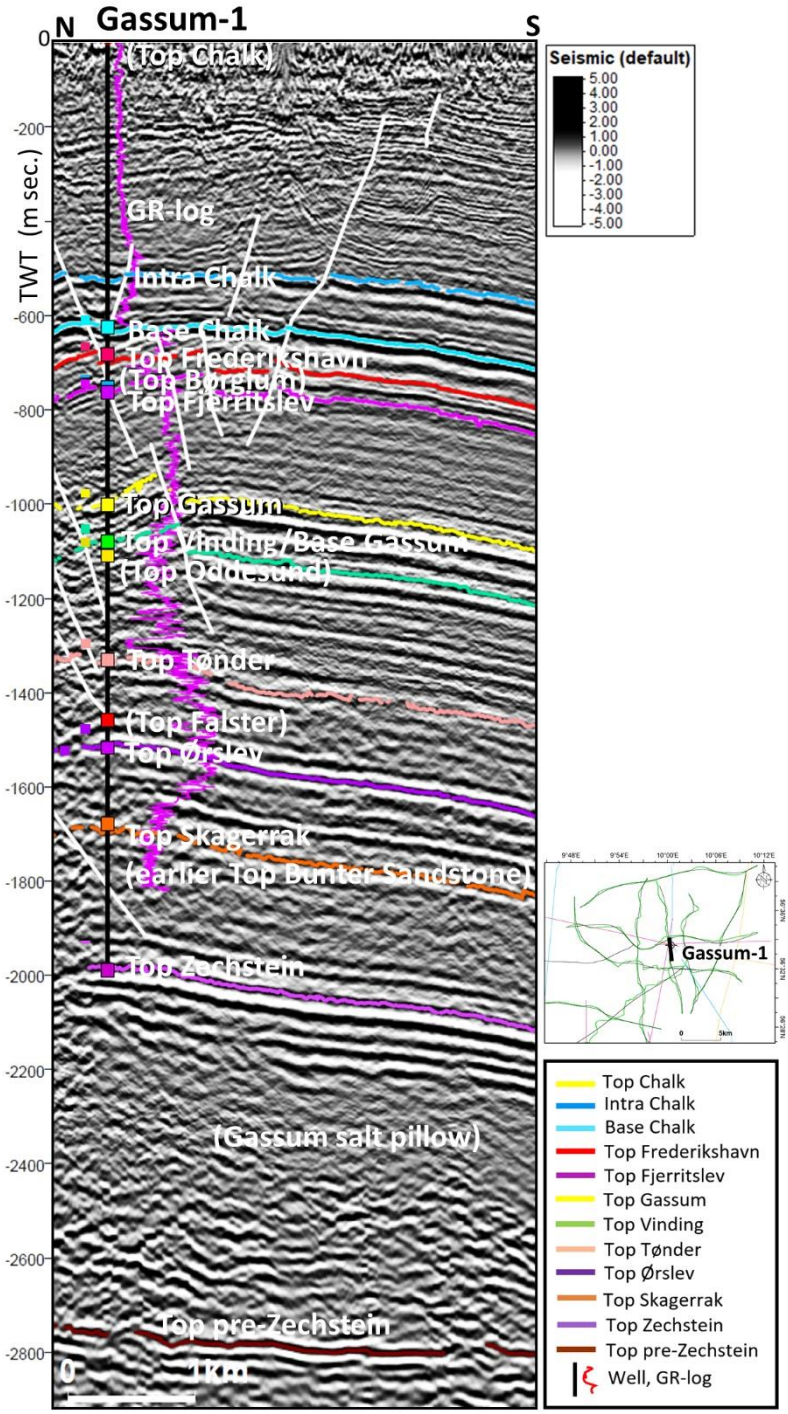


**Fig. 5.1.1**. *Well tie correlation with the Gassum-1 well (gamma log displayed in purple) and the new GEUS23-GSM-P5 reprocessed seismic line. Small coloured boxes are well-tops at lithostratigraphic boundaries in the well. Top Chalk is elevated above mean seal level and not shown in the seismic data but is indicated in a bracket. The well has TD in the top of the Gassum salt pillow.*

## 5.2 Well-to-seismic tie and synthetic seismogram (Chapter 6)

In the study area, only the Gassum-1 well is located and was drilled during 1948–1951 by the Danish American Prospecting Co. The wireline logging program included electrical log, micro-resistivity, calliper, and gamma-ray log, but no sonic nor check shots were acquired. Therefore, manually picked MD-TWT pairs from Nielsen and Japsen (1991) were used, which based TWT picks for each main stratigraphic unit on recognizable seismic markers at the Gassum-1 location. Resulting interval velocities were evaluated to be geologically realistic. Fortunately, in the nearest well (25 km) Voldum-1, a density and sonic log were available covering the Lower Cretaceous to Triassic strata. Therefore, a well-to-seismic tie was possible by using a standard Ricker wavelet (25 Hz) with positive polarity, and a tie to seismic line 73207. While seismic data quality of that line is poor, a confident tie was possible based on the main reflections (Fig. 5.2.1). Therefore, a seismic correlation could be made towards Gassum-1 well adding confidence to the picked TWT-MD picks in Gassum-1 well from Nielsen and Japsen (1991) (see Fig. 5.2.2).

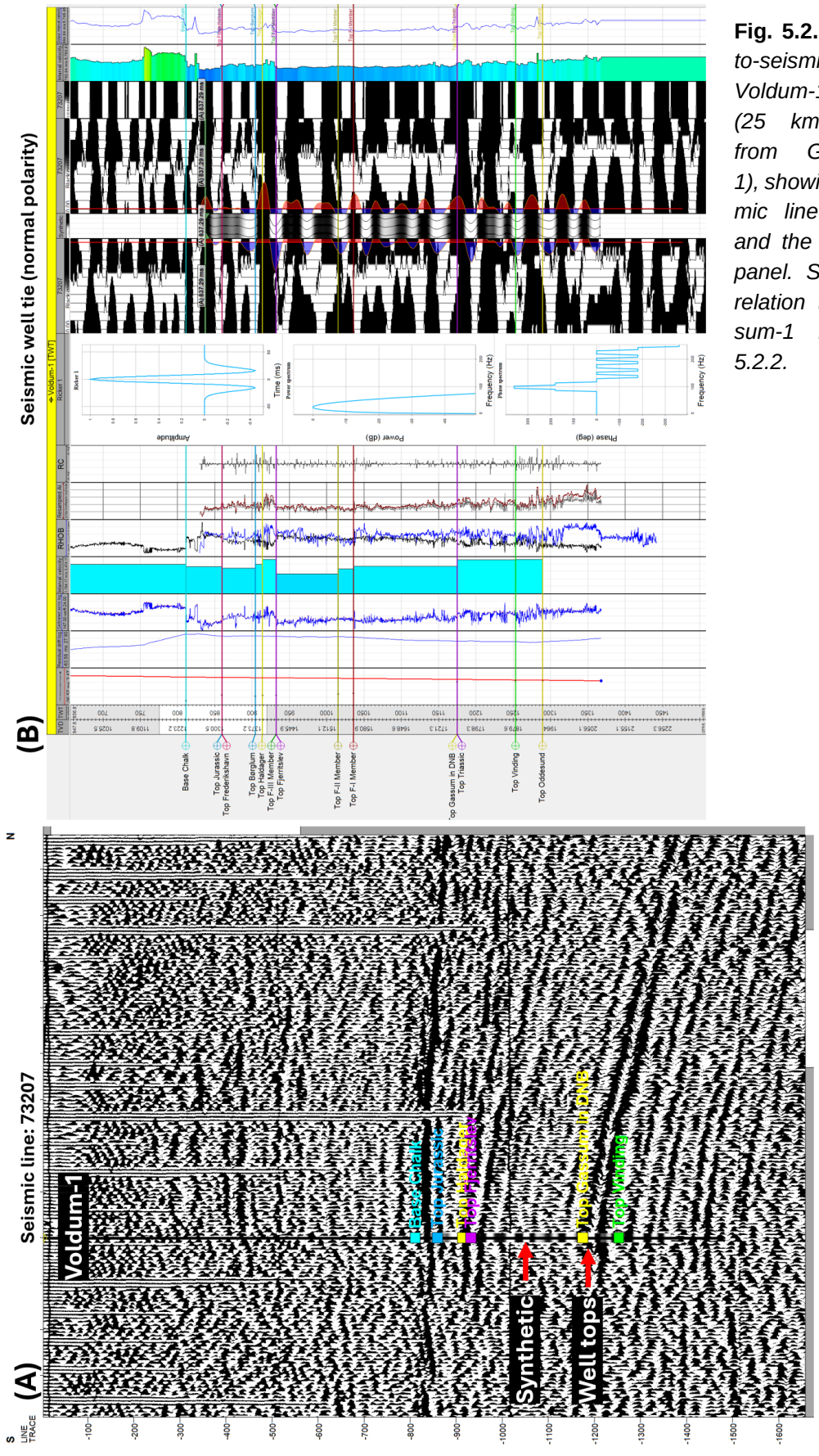


**Fig. 5.2.1.** *Well-to-seismic tie for Voldum-1 well (25 km away from Gassum-1), showing seismic line 73207 and the well tie panel. See correlation to Gassum-1 in Fig. 5.2.2.*

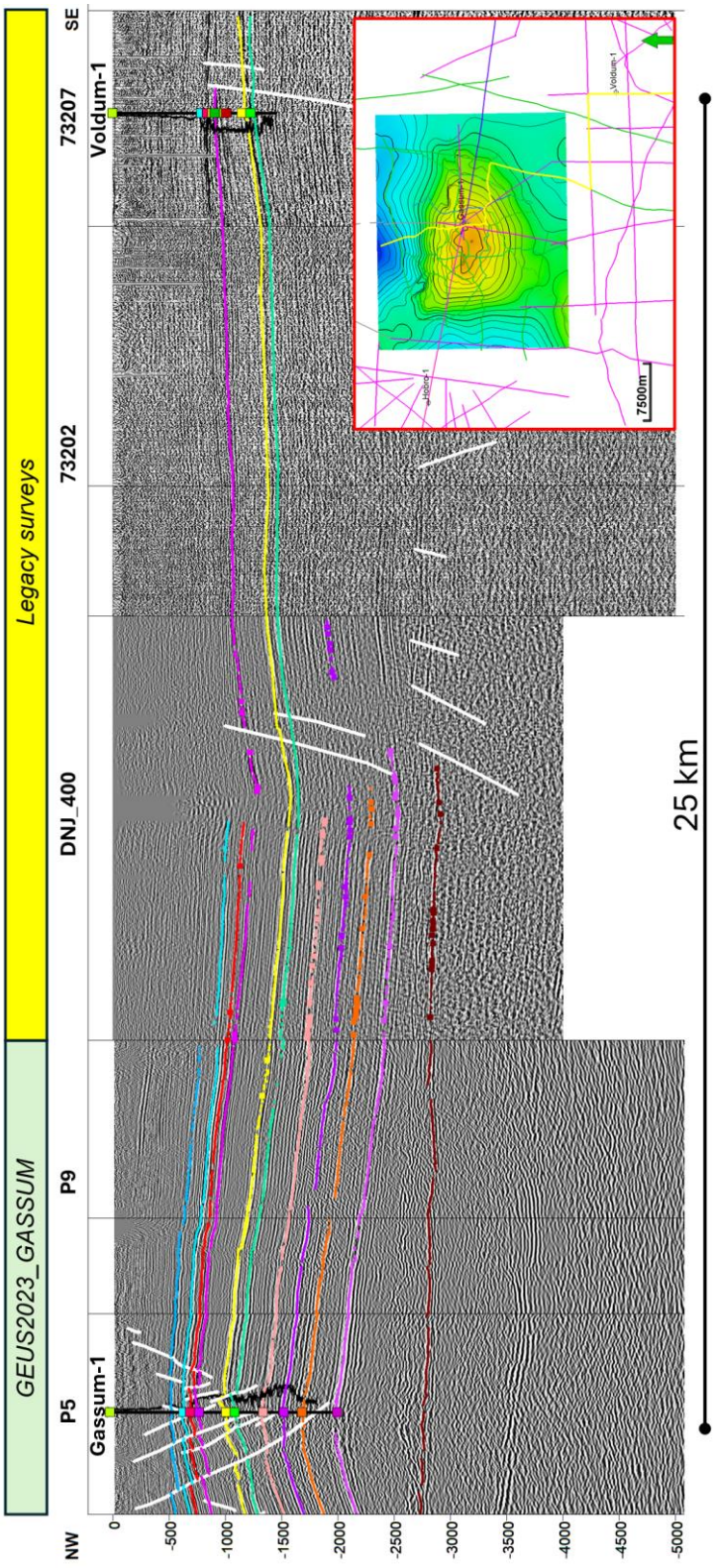


**Fig. 5.2.2.** *Seismic correlation to nearest well Voldum-1 using legacy seismic data. In Voldum-1 density and sonic logs were available so that a well-to-seismic tie could be made (see Fig. 5.2.1)*

## 5.3 Seismic time to depth conversion (Chapter 6)

A regional velocity model was constructed to convert the interpreted horizons from the time domain to the depth domain. The general idea of velocity modelling and depth-conversion is to have in 3D space an idea of the average velocities in the subsurface. With these data, the corresponding depth of a Two-Way-Time horizon can be obtained since Depth = One-Way-Time * Average Velocity; or (Time-Way-Time)/2 * Average Velocity. The model area was defined so that the velocity model includes the entire Gassum structure and the spill points, defining a total model area of 30 by 25 km (750 km$^2$) (Fig. 5.3.1).

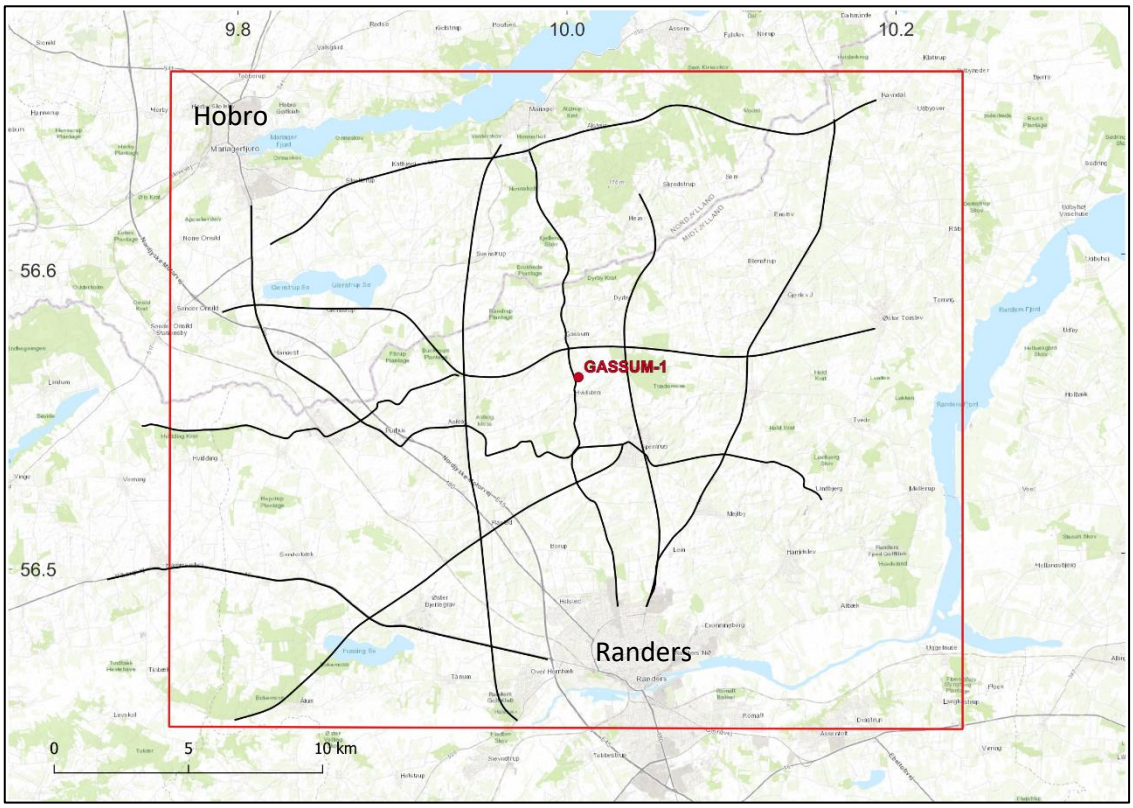


**Figure 5.3.1.** *Area (30 by 25 km) of the regional velocity model, showing the used Gassum-1 well, and the seismic lines of the new GEUS2023-GASSUM-RE2023 survey (black lines).*

The data available include:

1) Digital Elevation Model from FOHM (100x100 m), marking the top of the model;
2) Top Chalk Group depth map from the FOHM hydrogeological model based on Jupiter boreholes and shallow geophysics[2], since this level is at a too shallow depth to be picked confidently in the seismic data east of the diagonal line from Hobro to Randers due to uplift and erosion. A merging workflow will be described;
3) Well top markers for each corresponding mapped horizon;
4) Manually picked TWT-MD pairs at the Gassum-1 well from Nielsen and Japsen (1991)
5) 11 Two-Way-Time (TWT) seismic horizons of the main stratigraphic units, utilizing the legacy 2D lines (listed in Table 4.1.1) and including the new GEUS2023-GAS-SUM-RE2023 lines):
    a. Gridded to 250x250 m,
    b. Taking into fault polygons for the top of the surfaces,
    c. Horizon adjusted in TWT to match the TWT depth of the corresponding well top using the Time Depth Relationship in the Gassum-1 well;
    d. Smoothing of 1 iteration and a filter width of 5
6) Seismic migration (RMS) velocities from the 2D lines (GEUS2023-GASSUM-RE2023).

The general workflow was to establish a 3D structural model first in TWT, reflecting the geometric architecture of the study area, and model the available average velocity sources within this model using geostatistical methods and having the subsurface architecture steer the propagation of the average velocities within each zone. This 3D average velocity function is then used to find the depth of each mapped horizon.

Since Top Chalk Group marks the boundary between Tertiary and Quaternary sediments with significant lower velocities than the Chalk Group below, it was key to include this into the model. However, due to erosion and uplift approximately east of a diagonal line between Hobro and Randers and limited Tertiary/Quaternary, and deep incisions in the fjords, a seismic pick of Top Chalk Group is not possible (see Fig. 5.3.2a,b,c). To overcome this problem, a Top Chalk Group surface was obtained that is based on borehole and shallow geophysics from the Fælles Offentlig Hydrologisk Model (FOHM), corresponding to surface 8000_Paleogen_ler_bund (Fig. 5.3.2d). Since this data is in depth, a time-conversion was made using the average velocities found in seismic profiles in the post-Chalk package of 2100 m/s (Fig. 5.3.2a). It was decided to keep the part of the seismically mapped Top Chalk Group west of the diagonal line, since here it is clearly observed in seismic data, while east of the line the FOHM model provides the TWT depths. Then a merging procedure was undertaken to merge the two horizons, keeping each sector, and lastly making sure the incisions seen at the land elevation surface are reflected. The final result is seen in Fig. 5.3.2e.

[2] https://data.geus.dk/geusmap/?mapname=fohm#baslay=baseMapDa&optlay=&extent=186514.4032921811,6057103.9094650205,855485.5967078189,6392896.0905349795

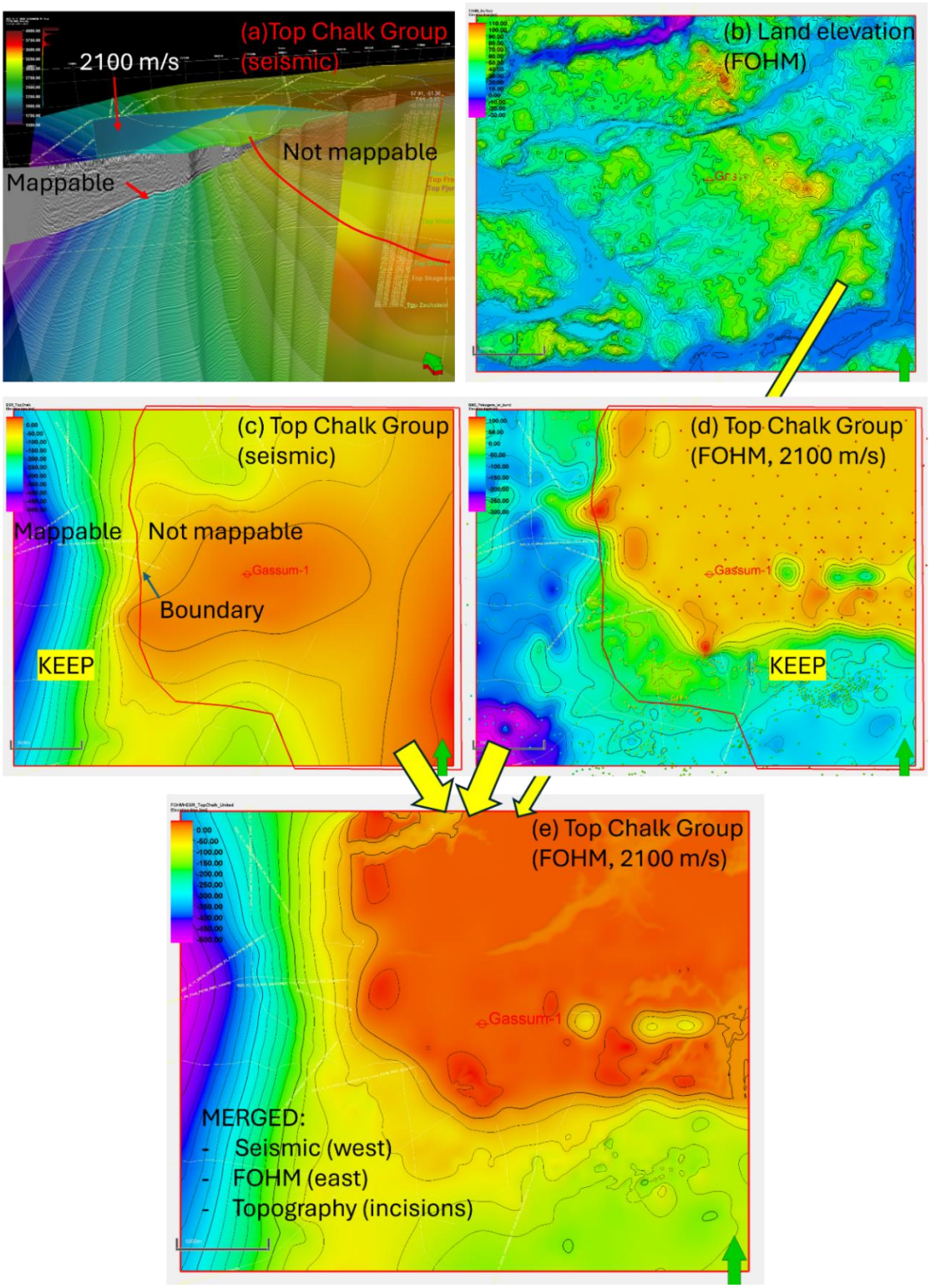


**Figure 5.3.2.** *Top Chalk Group (TWT ms); (a) western part of study it is possible to pick Top Chalk from seismic, east not due to erosion; (b) land elevation data from FOHM model. (c) Seismic mapped Top Chalk Group with boundary indicating where it can be mapped. (d) Top Chalk Group from FOHM model, time-converted using 2100 m/s. Dots are interpretation points (boreholes, shallow geophysics); (e) final Top Chalk Group surface reflecting a merge between the seismic, FOHM and elevation data.*

Practically, to account for vertical and lateral variations in average velocities found within the stratigraphic units as seen in the well TDRs and the seismic migration velocities, the velocity model was constructed in two steps, followed by depth-conversion of the TWT seismic horizons (Fig. 5.3.3):

1. *First*, a 3D average velocity cube was constructed using kriging with 3D trend (same methodology as used in the Stenlille study (Gregersen et al. 2022)):
    a. A structural model was constructed based on the TWT gridded surfaces, and layered such that average a cell was 250 m x 250 m and on average 10 ms TWT thick
    b. The average velocities from the well time-depth relationship in the Gassum-1 well formed the primary data.
    c. Seismic migration velocities from the 2D lines were upscaled into the established structural 3D grid (using arithmetic mean), and subsequently extrapolated within each zone using full tension option in Petrel (Spline in Tension algorithm). This formed the 3D trend for the kriging operation.
2. *Second*, a multi-layer velocity model was created using the modelled 3D average velocities as velocity input, and 3D horizons and well tops to correct the velocity values to achieve a match between depth-converted horizon and well top.
3. *Finally*, TWT seismic horizons were depth-converted using the created velocity model.

The workflow was performed within Petrel® (2022) by the following steps:

- QC of the input data:
    - Checking time-depth relationship from Gassum-1 TWT-MD pairs, slight manual adjustments to match main markers (such as Base Chalk Group) with new seismic data;
    - Creating an average velocity log from the average velocity point set in the Time-Depth Relationship file;
    - Adjusting the TWT seismic horizons to well markers since seismic peaks or troughs not necessarily coincide with the well tops, in order to get a good TWT to TVD (True Vertical Depth) fit of main stratigraphic units; checking TWT thicknesses for bullseyes originating from horizon mis-picks or extrapolation, smoothening anomalies.
    - Time-convert the Top Chalk Group depth map from the hydrological model using an average velocity of 2100 m/s for the overlying succession. Merging this with the seismically picked Top Chalk Group, and incorporating the incisions;
- Defining a 3D modelling grid (250x250 m) based on the QC-ed TWT horizons using the Petrel structural modelling tool:
    - Model zonation according to the following horizons: Surface, Top Chalk Gr, Base Chalk Gr, Top Fjerritslev Formation, Top Gassum Formation, Top Vinding Formation, Top Tønder Formation, Top Ørslev Formation, Top Skaggerak, Top Zechstein Gr, Top Pre-Zechstein (Fig. 5.3.3a).
    - Vertical layering was defined such that layer thickness is between 10–20 ms, with higher resolutions where large velocity changes occur (e.g., between Base Chalk Gp and the Lower Cretaceous strata).

- Defining a 3D average velocity property using kriging with the Petrel Petrophysical Modelling tool:
    - Average velocities from the Time-Depth Relationships in the Gassum-1 well was upscaled into the 3D grid, which were used as primary data for kriging.
    - With a Petrel workflow the 2D seismic migration velocities from all profiles in the GEUS2023-GASSUM-RE2023 dataset were sampled as a point cloud, which then were upscaled into the 3D grid. Data analysis on these upscaled cells helped to find azimuth and variogram ranges within the data, to steer the kriging operation.
    - These seismic derived upscaled cells were then extrapolated into the entire 3D grid using the full tension option in the property operations (Spline in Tension) (Fig. 5.3.3b, inset). Previous experience with the minimum curvature method showed that that method is not suitable, since it maintains a gradient over long distances and can lead to geologically unrealistic low or high velocity values. This is especially the case with sparse data points as we have in our dataset. In contrast, full tension extrapolation tends to flatten values and appears more realistic. This extrapolated volume forms the 3D trend for the kriging operation.
    - Kriging with 3D trend, using average velocity in the borehole as primary data and seismic-derived 3D average velocity property as 3D trend (Fig. 5.3.3c). Azimuth and variogram ranges for each zone came from Data Analysis.
- Create an “advanced velocity model” using the same 3D seismic horizons (tied in TWT to boreholes from seismic-well-tie Time-Depth Relationship), well tops for calibration, and 3D average velocity grid from previous step as velocity model (Fig. 5.3.3d).
    - Without applied correction, the average depth residual was in the order of 10–40 m, since velocities at the boreholes are steered by the TDRs which are included in the 3D property. Away from the structures, the velocities are much more uncertain, and thus a 10% depth error is a conservative estimate.
    - The final velocity model used the well tops (“global correction”) to improve to depth-converted horizons by adjusting the velocities (Fig. 5.3.3e).
- Depth-convert the TWT horizons using the constructed velocity model (Fig. 5.3.3f).
- The velocity model is called: VM_TDR+3DAvgVel_Property_corrected.

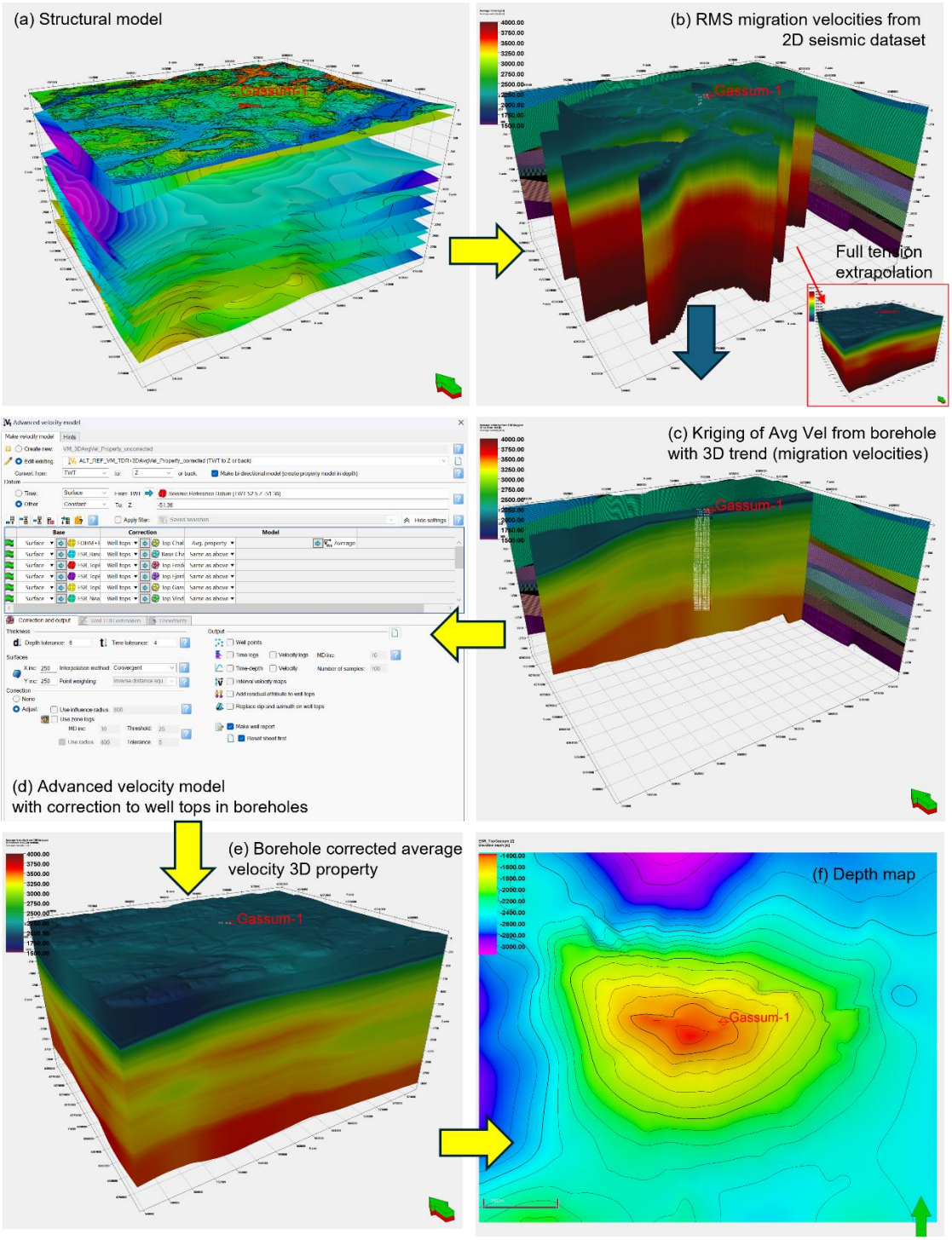


**Figure 5.3.3.** *(a) 3D perspective of the 11 horizons considered in the velocity model, which define the structural grid (250x250 m x c.10 ms). The Gassum structure is penetrated by the Gassum-1 well, which provides the time-depth relationship. (b) The structural grid is indicated by the sections (0–3000 ms TWT), and the upscaled 2D average seismic migration velocities are shown (purple: 1500 m/s to red: 4000 m/s). (c) The data are interpolated within the grid using a full tension algorithm (Spline in Tension) and smoothened 10x to remove outliers where the 2D intersect. (d) An advanced velocity model is set up using the 11 horizons and associated well tops for correction. (e) Velocities are adjusted to find a match between depth-converted horizon and well tops. (f) This cube is then used to depth-convert the TWT horizons. (depth=average velocity*(surface TWT)/2).*

## 5.4 Investigation of reservoir and seal (Chapter 7)

The geology of the reservoir and seal successions are described using well completion reports, publications, and in-house studies of well-logs and geological well samples mainly from cores. In addition, a limited number of studies focusing on lithology and biostratigraphy are available. The aim of these studies is to provide a more detailed understanding of reservoir and seal characteristics (see Chapter 7).

The reservoir characteristics presented and discussed in Chapter 7 are derived mainly from the acquired gamma ray log that is calibrated against conventional core analysis and descriptions, descriptions of cuttings and sidewall cores. Potential main reservoir units were identified from core descriptions and verified by the gamma ray log. Reservoir parameters were evaluated based on well data with emphasis on data from the Gassum-1 well (which penetrates the Gassum structure) and the nearest wells to the structure, Kvovls-1, Hobro-1 and Voldum-1. In petrophysical terms, a sandstone reservoir is herein defined as a rock having <50% volume of shale ($V_{shale}$), and an effective porosity (PHIE) of >10%. The permeability is estimated using in-house relationships between porosity and permeability, which is based on conventional core measurements. Seal lithology, thickness and grain-sizes were similarly evaluated based on petrophysical logs, ditch cuttings samples and cores, as well as regional geological development of these units known from seismic and well data.

## 5.5 Storage capacity assessment (Chapter 8)

To compare the potential $CO_2$ storage structures GEUS uses a simple widely accepted equation for saline aquifers, where static theoretical storage capacity of reservoir units with buoyant trapping is estimated from (e.g., Goodman et al. 2011):

$$SC = GRV * N/G * \varphi * \rho_{CO2R} * S_{Eff} \quad (1)$$

*where:*

- ***SC*** Storage Capacity or Mass of $CO_2$ (MT).
- ***GRV*** Gross Rock Volume (GRV) is confined within the upper and lower boundary of the gross reservoir interval (t) and above of the deepest closing contour from where spillage from the trap will occur. To get a representative GRV the lower boundary may be moved to a position closer to the upper boundary so expected the gross reservoir interval in the structure represents the surrounding wells. This will give a more correct estimation of the GRV.
- ***N/G*** Average net to gross reservoir ratio of aquifer across the entire trap (GRV).
- $\boldsymbol{\phi}$ Average effective reservoir porosity of aquifer within trap (GRV).
- $\boldsymbol{\rho_{CO2R}}$ Average $CO_2$ density at reservoir conditions across all of trap.
- $\boldsymbol{S_{Eff}}$ Storage efficiency factor relates to the fraction of the available pore volume that will store $CO_2$ within the trap (GRV). This fraction depends on the size of storage domain, heterogeneity of formation, compartmentalization, permeability, porosity, and compressibility, but is also strongly influenced by different well designs and injection schemes (e.g., Wang et al. 2013).

Evaluation and estimation of the $CO_2$ storage capacity (SC) in deep saline aquifers is complex and accurate estimations of storage capacity are only practical at local site-specific scales. In open aquifers, as assumed here, the reservoir pressure is expected to stay constant during $CO_2$ injection, as the water will be pushed beyond the boundaries. The calculated stored $CO_2$ is the maximum amount that theoretical can be injected until it reaches the boundaries (i.e., 'lowermost closed contour').

Static $CO_2$ storage capacity (Eq. 1) estimations is difficult due to lack of knowledge on the storage efficiency factor ($S_{Eff}$) that reduce the storage capacity to a more realistic estimation. The $CO_2$ storage efficiency factor was first introduced in 2007 in regional-scale assessments of storage capacity in the United States and Europe. The efficiency of $CO_2$ storage is regarded as a combination of various factors combined into one efficiency factor, and many published papers show factors values from <1% to more than 20%, emphasizing that no single factor value or set of values can universally be used. Regional storage efficiency factors are estimated to be 1–4% (e.g., $CO_2$ Storage Atlas of the US and Canada 2008), while trap specific storage efficiency have values around c. 4–18% for clastic sediments (Gorecki et al. 2009); c. 3–10% (Goodman et al. 2011) and c. 5–20% for traps in German North Sea area (BGR 2023, on-going project).

The Stenlille is the best-known case in the Danish onshore area. A maximum storage efficiency factor of 0.4 (or 40%) for a four-way dip-closure has previously been estimated and was used for the geologically excellent and well described Gassum Formation sandstone reservoir. Furthermore, the Stenlille structure has been used for natural gas storage for many years and consists of high-permeable sandstone layers with no faults offsetting the reservoir and overlying seal. Thus, for comparison reasons GEUS uses a storage efficiencies factor of 40% in the Stenlille structure and 10% in all other potential structures, and structures where the primary reservoir is not the Gassum Formation but e.g. the deeper situated Bunter Sandstone Formation. Thus, lower storage efficiency values reaching more realistic values from 5–10% are used in structures with no well data and only minor faults offsetting the reservoirs/seals.

The storage efficiency represents the fraction of the total available pore volume of the saline aquifer that will be occupied by the injected $CO_2$ in the trap volume (i.e., the Gross Rock Volume (GRV)) and is regarded as the fraction of stored $CO_2$ relative to the pore volume, - and has both a space and time dependency. It depends primarily on the relationship between the vertical and horizontal permeability, where a low vertical to horizontal permeability ratio will lateral distribute the $CO_2$ better over the reservoir than a high ratio, why an internally layered reservoir with alternating sandstones and impermeable or poorly permeable claystones acting as seals may have an advance. The storage efficiency to also depends on the size of the storage domain, heterogeneity of the formation, compartmentalization, porosity, permeability, pressure, temperature, salinity, and compressibility, all parameters that are influenced by number of injection wells, design and injection strategy.

More precise $CO_2$ storage capacity estimations are related to communication of fluids within the reservoir and the degree of pressurization during injection. Pressurization must not induce fracturing and depends on relation between pore pressure and volume increase, and compressibility of the rock and the fluids in the reservoir. Furthermore, injection and storage of $CO_2$ in deep saline formations requires estimates of fluid pressures that will not induce fracturing or create fault permeability that can lead the $CO_2$ to escape from the reservoir. To ensure this, identification of faults and analyses of fault stability are necessary and requires precise evaluation of, e.g., fault orientations, pore fluid pressure distribution and in-situ

stresses in and around the storage site. Changes in injection rates induce stress can changes formation pressures and $CO_2$ storage volumes, why determination of in situ stresses and modelling of fault stability are essential for the safe $CO_2$ injection and detailed modelling of storage capacity.

The estimations of storage capacity in Eq. (1) assume a static approach where the pores in the trap is expected to be 100% connected. However, it does not include dynamic pressure build-up and movement of $CO_2$ and in-place brine (water) in the saline aquifer, neither inside nor out-side the trap. Furthermore, it does not regard the solubility of $CO_2$ in water, where more than 10% can normally be dissolved in the water, and the presence of salt causing scales inside the storage reservoir reducing the efficiency of $CO_2$ injection. A dynamic reservoir simulation will take these factors into account and will obviously produce different storage capacity results, depending on the selected parameters. A more realistic dynamic reservoir simulation of the potential storage capacity is normally carried out by the awarded license holders and operators and should be used for local-scale $CO_2$ storage reserves estimates and should also consider operational and regulatory factors.

In this study estimation of storage capacity follows Eq. (1) and are furthermore biased by imperfect seismic and reservoir data, depth conversion, reservoir thickness estimates and $CO_2$ density. To address this uncertainty ranges have been chosen to reflect each parameter uncertainty, and the distribution has been modelled utilizing a simple Monte Carlo simulation in-house tool. To achieve stable and adequate statistical representation of both input distribution and result output, 10.000 trials are calculated for each simulation. This methodology is simplistic and does not incorporate e.g. correlations of input parameters. However, for the purpose of initial estimation of volumes, $CO_2$ storage capacities and for comparison of potential structures for $CO_2$ storage, the methodology is considered relevant and adequate. The method is used for the estimations in Chapter 8.

# 6. Results of seismic and well-tie interpretation

## 6.1 Stratigraphy of the structure

In total 12 regional seismic stratigraphic horizons were interpreted in the study area. These are from the deepest to the shallowest: (1) Top pre-Zechstein (Base Zechstein or Top Rotliegend), (2) Top Zechstein, (3) Top Skagerrak, (4) Top Ørslev, (5) Top Tønder, (6) Top Vinding (Base Gassum), (7) Top Gassum, (8) Top Fjerritslev, (9) Top Frederikshavn, (10) Base Chalk, (11) Intra Chalk, and (12) Top Chalk.

The Top Zechstein and shallower horizons are tied to nearest wells, in particular to the Gassum-1 well (Figs. 5.1.1, 6.1.1). The seismic horizons were picked near to the top or base of a formation or a group and are named after the nearest top or base (e.g., 'Top Gassum' horizon is near to the top of the Gassum Formation).

The deepest horizons, Top Pre-Zechstein and Top Zechstein were included mainly to constrain the structural evolution and the Top Chalk mainly to provide a thickness of the Chalk Group for the depth conversion, and also for the late structural evolution.

The seismic tie to the Gassum-1 well (Fig. 5.1.1 – new data of the GEUS2023-GASSUM 2D seismic survey) shows the interpreted seismic horizons and the picked peak or trough reflections as described in Table 5.1.1, e.g. with a significant white ("soft-kick") trough seismic reflection (normal polarity) at the Base Chalk. The seismic stratigraphic horizons tied to Gassum-1 and correlated with the lithostratigraphy at well-tops from Nielsen & Japsen (1991) are shown in Figure 6.1.1. The lithostratigraphic formations and groups with focus on the reservoirs and seals are described in Chapter 7. The mapped seismic stratigraphic horizons correlated to the Gassum-1 are briefly described here.

The Gassum structure is cored by a salt pillow, the top of which is drilled 3383 m below mean sea level near TD in the Gassum-1 well (Fig. 6.1.1). The salt pillow is composed by Zechstein Group evaporites and is overlain by sandstone and mudstone of the Skagerrak Formation. The Skagerrak Formation was previously attributed to the Bunter Sandstone Formation (e.g., Nielsen & Japsen 1991) (se also Chapter 7). The Skagerrak Formation has a certain reservoir potential and is a secondary reservoir and is overlain by mudstone (seal) of the Ørslev Formation (see Chapter 7). The Falster Formation is not mapped. Above the Ørslev Formation, the Tønder Formation (to Top Tønder), and the Oddesund Formation + Vinding Formation (to Top Vinding or Base Gassum) are mapped. The Gassum Formation (from Top Vinding to Top Gassum) denotes the primary reservoir succession. The Gassum Formation is overlain by the Fjerritslev Formation forming a primary sealing unit (see also Chapter 7). There is a major gap in stratigraphy interpreted from well data near the Top Fjerritslev horizon (Fig. 6.1.1). The succeeding Børglum Formation is very thin in Gassum-1 and its top is not mapped here. Middle to Upper Jurassic formations (Haldager Sand Formation and Flyvbjerg Formation) may occur between the Fjerritslev and Børglum formations over most of the Gassum structure, but only thin parts may be present in the Gassum-1 well (see also next section and Chapter 7). The overlying mapped horizon is Top Frederikshavn. The Frederikshavn Formation contains a reservoir potential and forms a secondary reservoir within the Gassum structure overlain by mudstone (seal) of the Vedsted Formation (see Chapter 7), underneath the mapped Base Chalk horizon. The shallowest part mapped is the Chalk Group, situated

between Base and Top Chalk horizons. In addition, an internal horizon (Intra Chalk) was interpreted in the lower part of the Chalk Group, possible forming the top of a secondary seal (see Chapter 7).

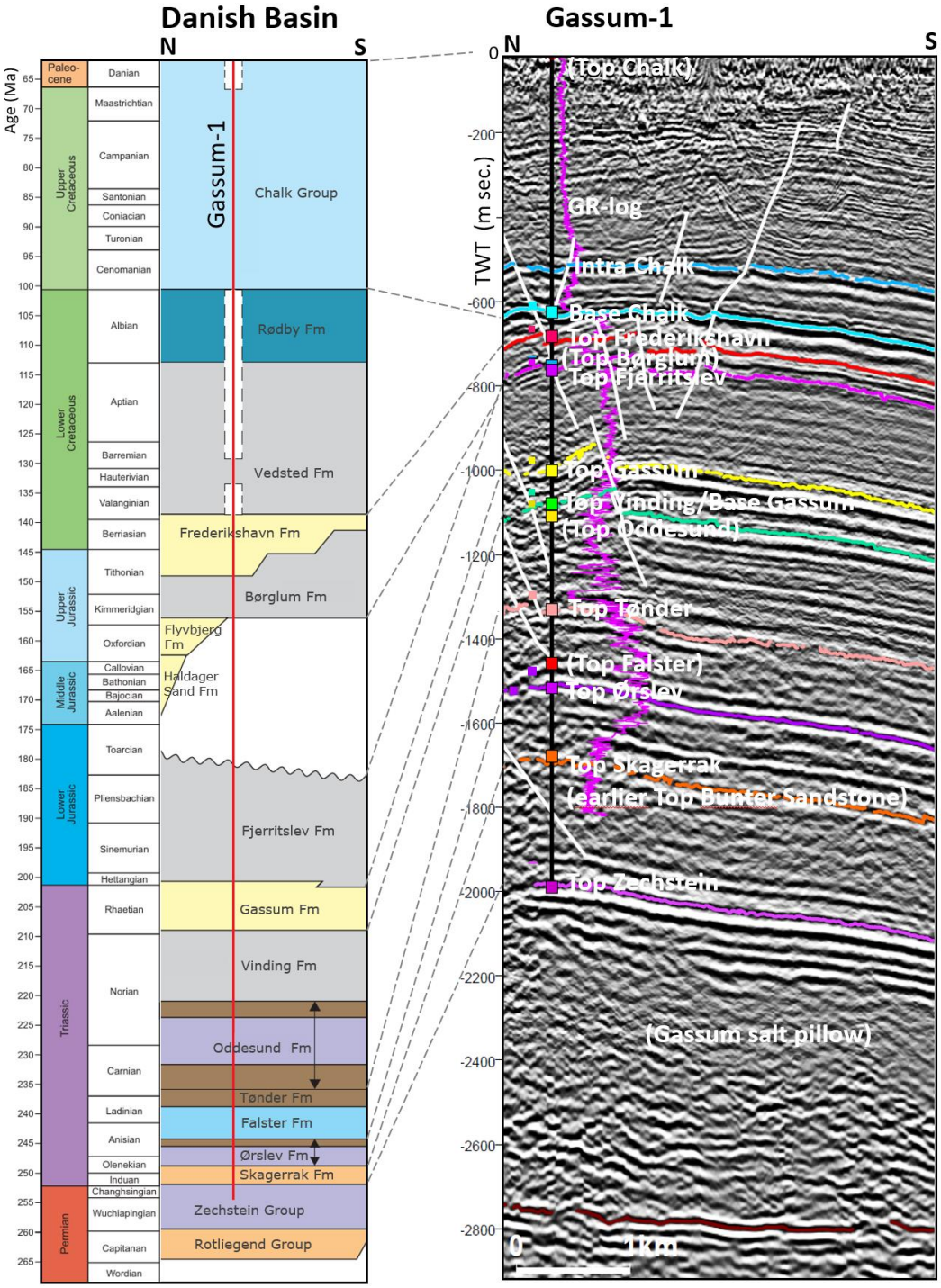


**Figure 6.1.1.** Lithostratigraphy *with well-tie correlation of the Gassum-1 well and the new GEUS23-GSM-P5 reprocessed seismic line (larger line section is shown in Fig. 6.2.4). Seismic horizons are interpreted from correlation with well-tops (small coloured squares along the well in the seismic section), marking the positions of interpreted lithostratigraphic boundaries in the well (Nielsen and Japsen 1991). The well is floored (TD) in the upper part of the Gassum salt pillow. The lowermost dark red horizon (at c. 2800 ms TWT) is the Top pre-Zechstein. The lithostratigraphy is a (flipped) part of Fig. 3.3.*

## 6.2 Structure description and tectonostratigraphic evolution

The structural development of the Gassum structure, is interpreted based on the relative geometry of the mapped seismic surfaces (Figs. 6.2.1–6.2.3), thicknesses of the stratigraphic units bracketed between the surfaces, the fault configuration as well as lapping pattern along the surfaces and their variations through time constrained by correlation with well stratigraphy–especially the Gassum-1 well (Figs. 6.2.4–6.2.7).

### Structure description from mapped surfaces and units

*Top pre-Zechstein*

The Top pre-Zechstein surface is outlined by a strong "hard-kick" (peak) reflector denoting the top of a well-reflected, parallel reflector set (Fig. 6.2.4). The surface denotes a distinct upwards change in seismic facies. The Top pre-Zechstein surface forms an overall low relief eastward dipping monocline forming the base of the Zechstein evaporites (Figs. 6.2.1A, 6.2.2A). The northeastern corner is cut by two, NW–SE and NNW–SSE trending extensional faults down-faulting the area towards the northeast. A relay ramp occurs NE of the Gasssum-1 well. The depth variation is from c. 4650 m to c. 5250 m (b.msl). The displacement of the large faults is c. 200–300 m (NW–SE striking large faults), but up to c. 600 m in the NE area at the NNW–SSE striking fault. The central and southwestern areas contain minor faults striking N–S and E–W.

*Top Zechstein*

The Top Zechstein surface is outlined by a strong "hard-kick" reflector (Fig. 6.2.4). The surface marks the upper boundary of a c. 100 ms (millisecond) thick, strongly reflected, parallel-bedded interval. The Top pre-Zechstein surface is overlain by not as strongly reflected interval and thus denotes a general upwards decrease in reflection amplitude.

The Top Zechstein surface denotes a dome (four-way dip closure) with the crest located near the Gassum-1 well (Figs. 6.2.1B, 6.2.4). The closure has a relief of c. 800 m with an apex located at c. 3300 m depth (b.msl) (Figs. 6.2.1B, 6.2.2B). Two saddle structures situated near closures at c. 3900 m and c. 4100 m depth (b.msl), characterize the structure towards the northwest and south, respectively. The northwestern saddle structure is relatively narrow, while the southern is broader. The Zechstein Group forms a well-defined salt pillow structure – the Gassum salt pillow – with a thickness of up to c. 1300 m at the apex of the Gassum structure (Fig. 6.2.3A).

*Top Skagerrak*

The Top Skagerrak surface is characterized by mostly a strong "hard-kick" reflector (Fig. 6.2.4). The seismic reflections below (in the Skagerrak Formation) is semi-parallel to chaotic and locally troughs are observed, e.g., towards south, whereas overlying reflections are strong and more parallel (Fig. 6.2.4). However, details are disturbed by noise. The surface forms a dome (four-way dip closure) with the crest located near the Gassum-1 well and having a closure relief of c. 550 m towards NW and more (950 m) towards south (Figs. 6.2.1C, 6.2.2C). The apex is situated at c. 2600 m depth (b.msl). A minor horst structure bounded by two E–W striking faults intersect the surface over the central part of the dome (Figs. 6.2.2C,

6.2.5). An E–W trending fault also cuts the surface just east of the Gassum-1 well. The displacements at the faults are up to c. 50 m. The closure of the structure at the top Skagerrak level is controlled by a narrow saddle structure in the northwest having a lowermost closure and saddle structure near 3150 m (b.msl). A second, broader saddle structure with a saddle structure near the lowermost closure at c. 3550 m depth (b.msl) characterizes the Gassum structures at Top Skagerrak level to the south. The Skagerrak Formation thickness map (Fig. 6.2.3B) from the Top Zechstein to the Top Skagerrak surfaces shows a thick unit of c. 550–750 m across the Gassum structure.

*Top Ørslev*

The Top Ørslev surface is characterized by a strong, continuous "hard-kick" reflector between parallel to semi-parallel reflections (Fig. 6.2.4). The surface forms a dome (four-way dip closure) with an apex located just west of the Gassum-1 well at c. 2250 m depth (b.msl) (Figs. 6.2.1D, 6.2.2D). The relief of the structure at this level is c. 700 m from top to the lower closure towards NW. A minor horst structure bounded by two E–W striking faults characterize the central part of the dome (Figs. 6.2.2D, 6.2.5). A narrow half-graben structure characterizes the area around the Gassum-1 well and the area to the east of it. The half-graben is bounded by a southward dipping master fault with a displacement of c. 50 m north of the Gassum-1 well. The surface is confined by a narrow saddle structure towards the northwest with a saddle structure near the lower closure at c. 2950 m depth (b.msl). The structure at Top Ørslev level heads into a broader saddle structure in the south near a closure at 3250 m depth (b.msl). The southern saddle structure is intersected by two E–W trending faults. The thickness of the Ørslev Formation (Fig. 6.2.3C) from the Top Skagerrak to the Top Ørslev across the Gassum structure measuring around c. 300–450 m.

*Top Tønder*

The Top Tønder surface is characterized by a strong, continuous "hard-kick" reflector between parallel to semi-parallel reflections (Figs. 6.2.4, 6.2.5). The top Tønder surface forms a dome (four-way dip closure) in the central part of the mapped area, where the crest of the dome is at c. 1950 m b.msl (Figs. 6.2.1E, 6.2.2E). The surface is dissected by dominantly E–W striking normal faults that defines a c. 1 km wide graben structure on the dome crest at Top Tønder level. The northern master fault is situated north of the Gassum-1 well, strikes E–W but is slightly sinuous. It has a maximum displacement of c. 150 m at the Top Tønder level. At the northwestern flank of the dome, a narrow saddle near the closure at c. 2850 m characterizes the surface. A minor, E–W striking fault is interpreted at the slightly deeper saddle structure (near a closure at c. 2900 m b.msl) in the south.

*Top Vinding*

The Top Skagerrak surface is characterized by a strong, continuous "hard-kick" reflector between few parallel to semi-parallel, strong reflections (Figs. 6.2.4, 6.2.5). The top Vinding surface outlines a dome (four-way dip closure) in the central part of the mapped area (Figs. 6.2.1F, 6.2.2F). The crest of the closure is located at c. 1550 m depth (b.msl). The saddle structure towards south is near the closure at c. 2500 m (b.msl), whereas the NW saddle structure is near the closure at c. 2550 m (b.msl) (Fig. 6.2.2F). The surface is intersected by dominantly E–W striking normal faults that delineates a 1 km wide graben structure over the

dome crest. The long E–W striking northern master fault located north of the Gassum-1 well is slightly sinuous. The maximum displacement over the master fault at Top Vinding level is c. 50–100 m. A narrow saddle structure borders the dome towards the northwest at Top Vinding level. The northeastern side of this saddle structure is offset by a number of NNW–SSE striking faults. The saddle structure in the south is broader and is offset by a minor E - W striking fault.

The combined thickness map of the Oddesund and Vinding formations (Fig. 6.2.3E) shows thicknesses from c. 200 m and up to c. 500 m in the structure, with significant fault-related thickness variations (Figs. 6.2.4, 6.2.5).

*Top Gassum*

The Top Gassum surface is characterized by distinct "hard-kick" (peak) reflector forming the top of a strongly reflected, parallel to semi-bedded unit with typically low reflection amplitudes that correlates with the Gassum Formation in the Gassum-1 well. It is overlain by another parallel bedded unit characterized by generally lower reflection amplitudes and higher reflection frequencies (the Fjerritslev Formation), and thus denotes a distinct upwards change in seismic facies. The top Gassum surface forms a dome (four-way dip closure) in the central part of the mapped area (Figs. 6.2.1G, 6.2.2G). The relief of structure at the Top Gassum surface is c. 925 m with the apex at c. 1375 m (b.msl) just west of the Gassum-1 well (Fig. 6.2.2G). The spill point is near the closure at c. 2300 m (b.msl) defined by the saddle structure in the south, whereas a deeper saddle structure occurs at the 2400 m (b.msl) closure to NW. The surface is dissected by dominantly E–W striking normal faults that form a narrow graben structure over the dome crest. The northern, E–W striking master fault north of the Gassum-1 well is slightly sinuous and has a maximum displacement at Top Gassum level of c. 50 m, but larger displacement of more than 100 m occur west of the Gassum-1 well. Slightly west of the master fault, an opposite dipping fault is observed (Fig. 6.2.5). At the northwestern flank of the structure, a number of NNW–SSE striking faults occur. The southern saddle structure is intersected by a minor, E–W striking fault.

Previous mapping work of the Gassum structure (e.g., Hjelm et al. 2022) relied on four old (1960s and 1970s) seismic lines of poor quality available at the time. Only two north-dipping faults were detected at the time, interpreted to be striking NW–SE due to the insufficient data being available (Hjelm et al. 2022: p. 105–106). The interpretation presented here based on a denser line coverage including new and better seismic data shows a general E–W fault trend (Fig. 6.2.2G) and a south dipping master fault (Fig. 6.2.4).

The Gassum Formation thickness map (Fig. 6.2.3E) defined between the Top Vinding and Top Gassum surfaces suggest a relatively uniform thickness of c. 100–200 m, but mostly over 150 m across the Gassum structure, with a mean of c. 180 m (see Chapter 8). However, only 130 m of the Gassum Formation is drilled in the Gassum-1 well (Chapter 7). Thickness variations over faults are mostly subtle and throws are larger in younger succession (incl. Top Fjerritslev to Intra Chalk), suggesting that significant faulting commenced after deposition of the Gassum Formation (Figs. 6.2.4, 6.2.5).

*Top Fjerritslev*

The Top Fjerritslev surface is characterized by a strong, continuous "soft-kick" (trough) reflector between few parallel to semi-parallel, strong reflections and is outlined by a subtle angular unconformity (Figs. 6.2.4, 6.2.5). The surface outlines a dome (four-way dip closure)

in the central part of the mapped area centered over the crest of the underlying Zechstein salt pillow (Figs. 6.2.1H, 6.2.2H). Truncation occurs bi-directionally towards the crest of the structure from both the south and north. The crest of the closure is located at c. 1030 m depth (b.msl) and the structure at the Top Fjerritslev surface is apparently not closed by contours in the mapped area, as it seems have some open contours towards NE, but are partly cut by faults (Fig. 6.2.2H). The lowermost closure at the two saddle structures towards south and NW is c. 1900 m (b.msl) at the saddle structures. The surface is intersected by dominantly E–W striking normal faults that forms an app. 3 km graben structure over the dome crest. The E–W striking master fault dips to the south. The maximum displacement over the master fault is c. 50–100 m, which together with small conjugate faults defines an app. 3 km wide graben near the Gassum-1 well. The southern saddle structure is offset by a few E–W striking extensional faults with modest offset.

The Fjerritslev Formation thickness (Fig. 6.2.3F) defined by the difference in depth between the Top Gassum and Top Fjerritslev surfaces is significant and varies between c. 300 and c. 700 m in the mapped area. The thickness is affected by truncation along the Top Fjerritslev surface. Truncation depth generally increases towards the apex of the Gassum structure (Figs. 6.2.4, 6.2.5).

In the northern part of the structure it seems as the Fjerritslev Formation significant increases in thickness (Fig. 6.2.5). In this upper succession wedges and unconformable reflections are observed (N–S) up-dip towards the Gassum structure at an unconformity. It may be that the uppermost part of the succession here (or lowermost succeeding succession) alternatively to the Fjerritslev Formation could include younger Middle to Upper Jurassic Haldager Sand Formation and (or) Flyvbjerg Formation (Fig. 6.1.1) over most of the Gassum structure. Only thin parts may be present in the Gassum-1 well (see Chapter 7), as parts of the successions may presumably have been cut out by a fault at the Gassum-1 well or may have been partly eroded due to uplift of the structure due to salt movements. If these formations occur in parts of the structure, they may include sandstones as secondary reservoirs. Implications of such an interpretation is also, that the seal succession (e.g., Fjerritslev Formation) may be thinner, although it still remains quite thick.

*Top Frederikshavn*

The Top Gassum surface is characterized by a “hard-kick” (peak) reflector and the surface delineates a dome (four-way dip closure; Figs. 6.2.1I, 6.2.2I). The top point is located in c. 925 m depth (b.msl) and the shallowest saddle structure is near a closure at c. 1375 m (b.msl), partly fault-displaced at two faults with NW–SE and W–E trends, respectively (Fig. 6.2.2I). The 1400 m contours shown on the map does not seem to close. Top Frederikshavn is dissected by dominantly E–W striking normal faults that outline a c. 3 km wide graben structure over the dome crest. The maximum displacement over the master fault that confines the northern graben flank is c. 100–200 m at the Top Frederikshavn level. Scattered minor E–W and NW–SE to N–S trending faults are interpreted over the northern, eastern and southern flanks of the structure. Towards the NE, NW and south, three saddle structures characterize Top Frederikshavn surface. The shallowest northeastern saddle structure (1375 m b.msl) defines the spill point at Top Frederikshavn level. The southern saddle structure near a closure at 1800 m (b.msl) is broad, while the northwestern (at 1700 m b.msl) is narrower.

The Børglum Formation to Frederikshavn Formation succession seems to wedge towards the crest of the Gassum structure (Figs. 6.2.4, 6.2.5), but the formations have not been mapped separately. The succession increases in thickness at the flanks of the structure from less than 100 m at the top of the structure to more than 200 m at the flank (Fig. 6.2.3H), in particular towards north (Fig. 6.2.5) and east (Fig. 6.2.6). Thickness variations may indicate salt pillow growth.

*Base Chalk*

The Base Chalk surface is characterized by a strong, continuous "soft-kick" (trough) reflector between few parallel to semi-parallel, strong reflections (Figs. 6.2.4, 6.2.5). The surface forms a dome (four-way dip closure; Figs. 6.2.1J, 6.2.2J). Top elevation is at c. 875 m (b.msl) and spill point at the shallowest saddle structure is at c. 1200 m (b.msl) (Fig. 6.2.2J). The surface is dissected by dominantly E–W striking normal faults that forms a graben structure on the dome crest. The maximum displacement of the master fault is up to c. 100–200 m at the Base Chalk level. The width of the graben is app. 3.5 km, widest near the Gassum-1 well. A W–E trending fault, and a NW–SE trending fault dipping towards the south are seen in the northeastern part of the study area at the saddle structure (c. 1200 m depth b.msl).

The interval between the Base Chalk and the Top Frederikshavn surfaces correlates with the Vedsted Formation in the Gassum-1 well. The thickness of the Vedsted Formation (Fig. 6.2.3I) varies from c. 50 m in the top of the structure to more than c. 150 m towards the flanks of the Gassum structure. As below, the formation is faulted and most identified larger faults continue up into the Chalk Group (Figs. 6.2.4, 6.2.5). This formation also shows slightly more thickening towards the north and east.

*Intra Chalk*

The Intra Chalk surface is characterized by a strong, continuous "soft-kick" (trough) reflector between few parallel to semi-parallel, strong reflections (Figs. 6.2.4, 6.2.5). The Intra Chalk surface within the Chalk Group is not included as map but interpreted to show a possible secondary seal level (see Chapter 7) and to show faults within the Chalk Group. The Intra Chalk surface is dissected by normal faults that form a c. 3.5 km wide graben structure on the dome crest (Fig. 6.2.5). The maximum displacement of the master fault is 100–200 m.

*Top Chalk*

The Top Chalk surface is affected by Neogene uplift and erosion over most of the mapped area (Figs. 6.2.1K, 6.2.2K; see also Vejbæk 2007) and the uppermost Chalk Group (Upper Maastrichtian to Danian) has been erosionally removed over the eastern and central part of the Gassum structure (Fig. 6.1.1). Here, the Chalk Group floors Quaternary deposits typically measuring a few meters in thickness. In the western portion of the area and farthest to the south, the surface is conformable with the overlying Paleogene stratigraphy, e.g. including the Ølst Formation (Fig. 6.2.7). The Chalk Group is covered by mainly Paleogene deposits thickest developed in the western part of the the mapped area. The post Chalk succession is 25 m thick in the Gassum-1 well.

The Chalk Group is thickly developed over the Gassum area, but with thicknesses varying greatly due especially to differential erosion (Fig. 6.2.3J). The greatest thicknesses of more

than c. 1500 m occurs in the west, whereas thickness of c. 900–1000 m occur over the crestal part of the Gassum structure in the area with the deepest erosion (Figs. 6.1.1, 6.2.3J, 6.2.4).

Many faults continue up into the Chalk Group. A few of the identified faults can be traced to the very shallow part of the Chalk Group, and some may even intersect the entire chalk package (Figs. 6.2.4, 6.2.5).

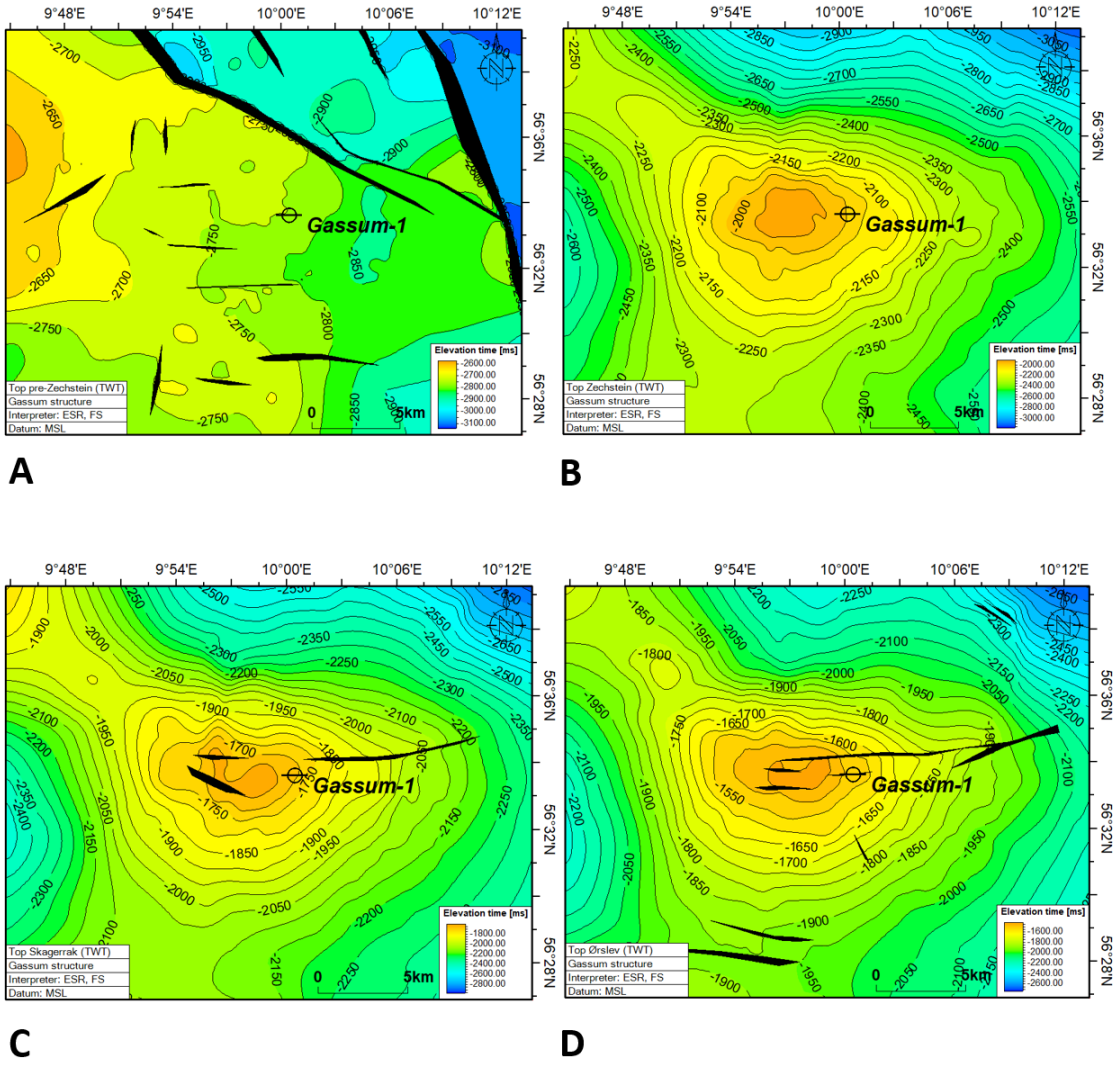


**Figure 6.2.1.** *Depth-structure maps in millisecond two-way-time (TWT) below mean sea level (b.msl) shown with the largest faults as black, filled polygons and the location of the Gassum-1 well. (A) Top pre-Zechstein; (B) Top Zechstein; (C) Top Skagerrak; (D) Top Ørslev. The maps are produced with a 250x250 m grid and mildly smoothed (1x iteration, filter width 5).*

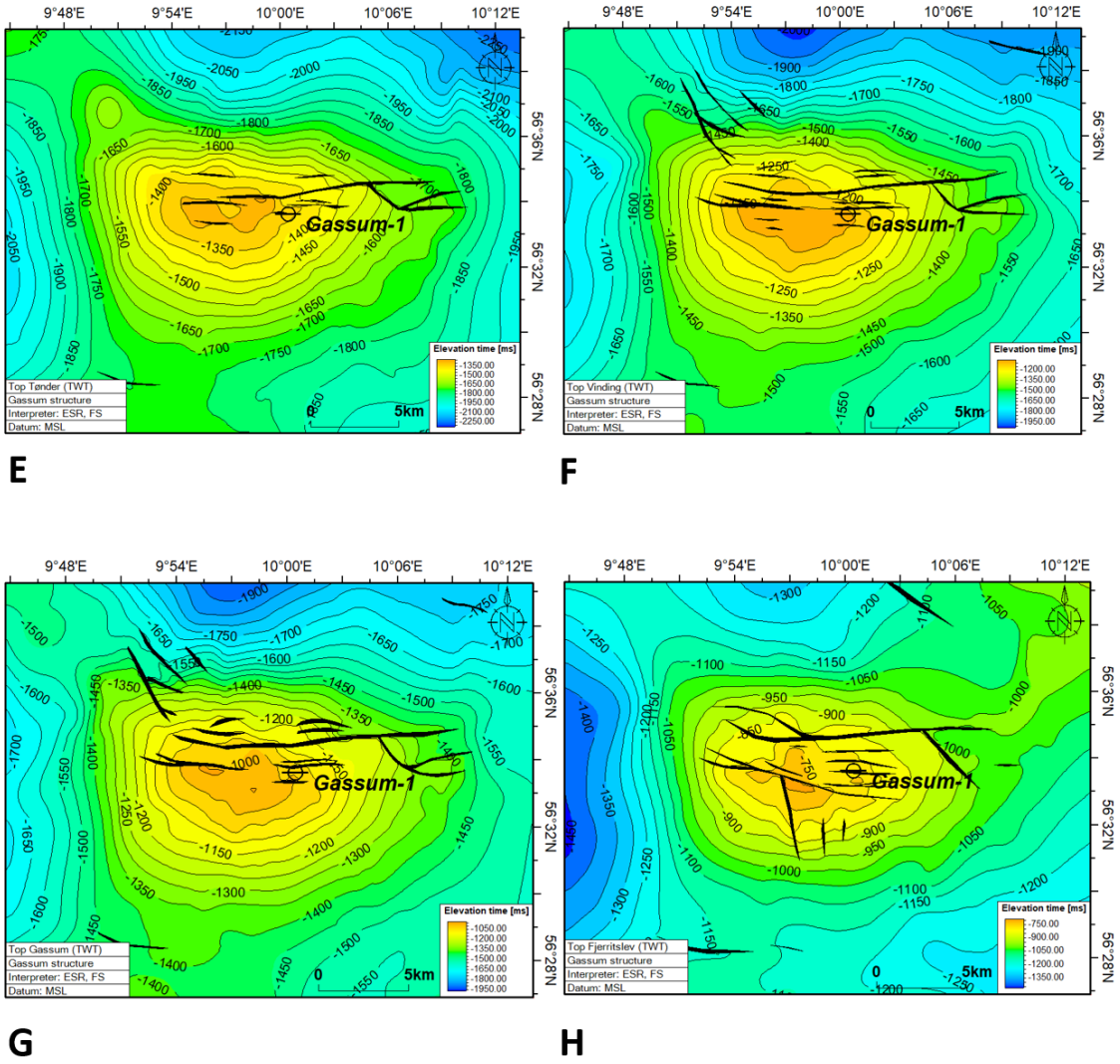


**Figure 6.2.1 (continued)**. *Depth-structure maps in millisecond two-way-time (TWT) below mean sea level (b.msl) shown with the largest faults as black, filled polygons and the location of the Gassum-1 well. (E) Top Tønder; (F) Top Vinding (Base Gassum); (G) Top Gassum; (H) Top Fjerritslev. The maps are produced with a 250x250 m grid and mildly smoothed.*

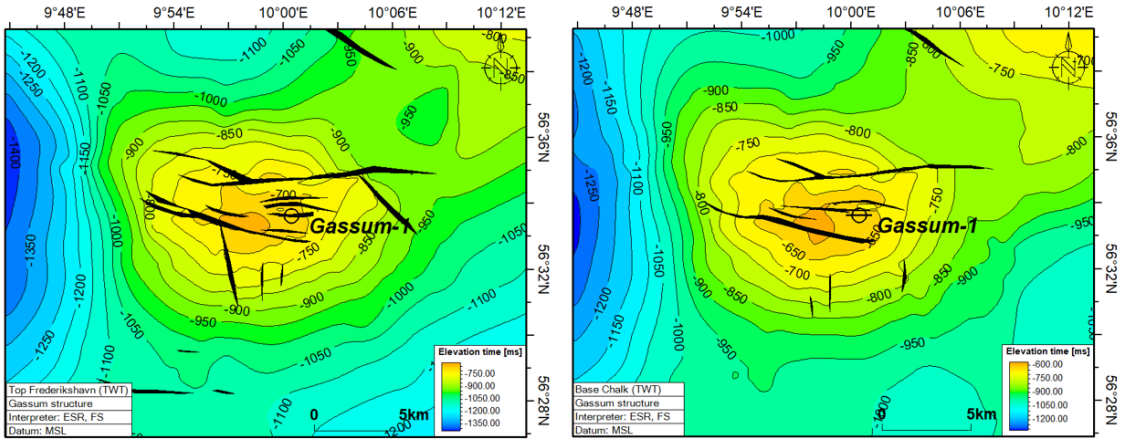


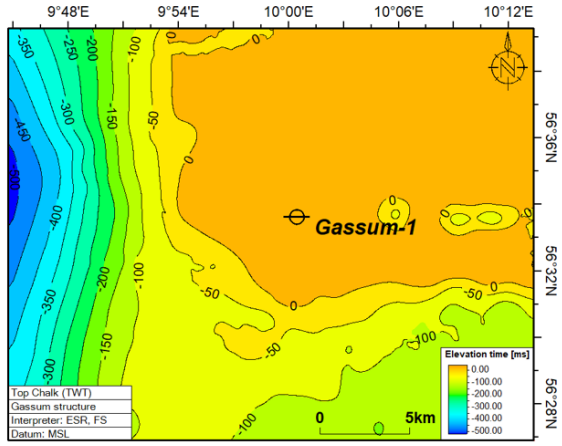


**Figure 6.2.1 (continued)**. *Depth-structure maps in millisecond two-way-time (TWT) below mean sea level (b.msl) shown with the largest faults as black, filled polygons and the location of the Gassum-1 well. (I) Top Frederikshavn; (J) Base Chalk; (K) Top Chalk (combined surface from GEUS & FOHM hydrogeological model – see Chapter 5) shown without faults. The maps are produced with a 250x250 m grid and mildly smoothed.*

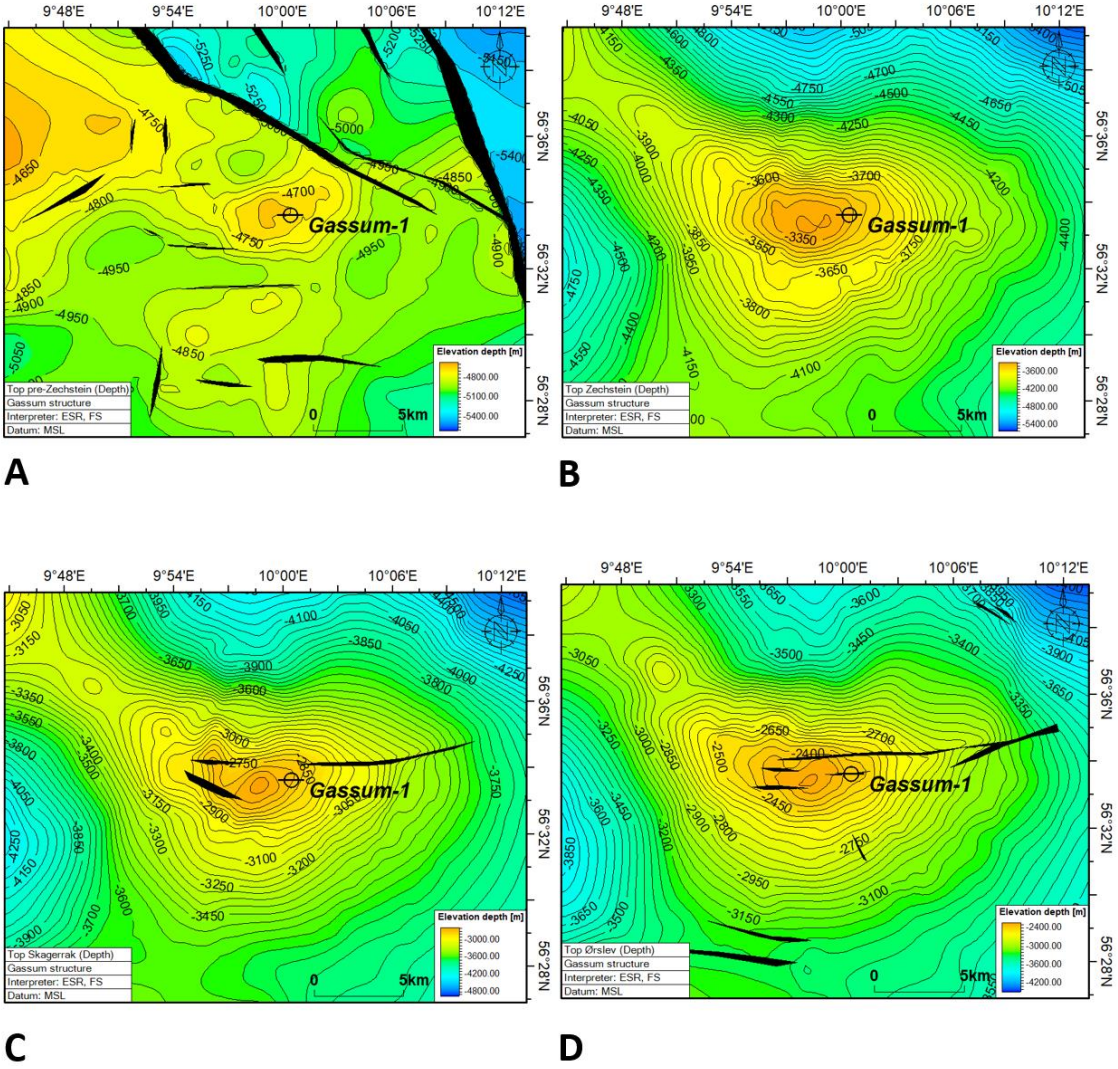


**Figure 6.2.2.** *Depth-structure maps in meter (m) below mean sea level (b.msl) shown with the largest faults as black, filled polygons and the location of the Gassum-1 well. (A) Top pre-Zechstein; (B) Top Zechstein; (C) Top Skagerrak; (D) Top Ørslev. The maps are produced with a 250x250 m grid and mildly smoothed.*

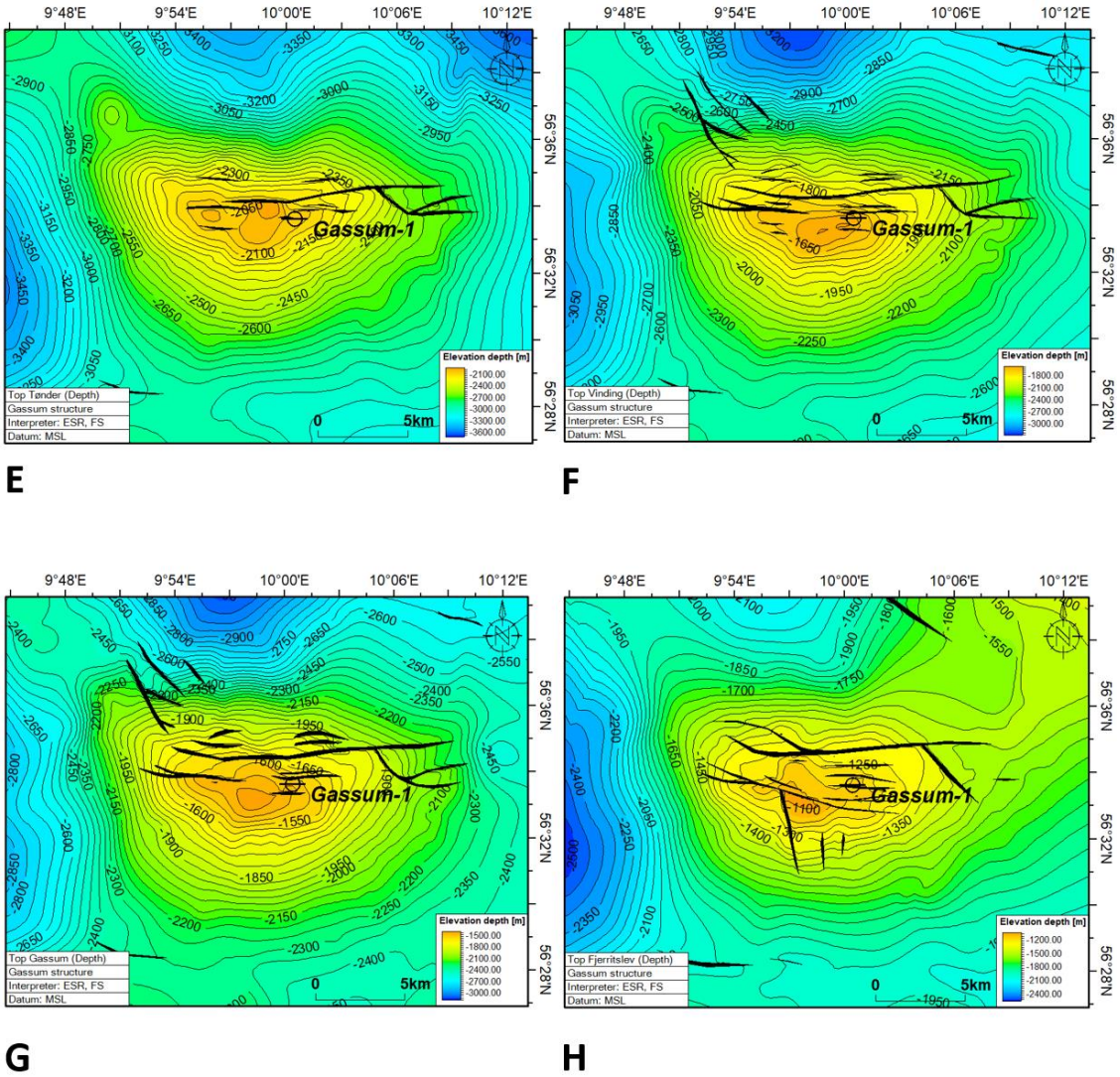


**Figure 6.2.2 (continued)**. *Depth-structure maps in meter (m) below mean sea level (b.msl) shown with the largest faults as black, filled polygons and the location of the Gassum-1 well. (E) Top Tønder; (F) Top Vinding (Base Gassum); (G) Top Gassum; (H) Top Fjerritslev. The maps are produced with a 250x250 m grid and mildly smoothed.*

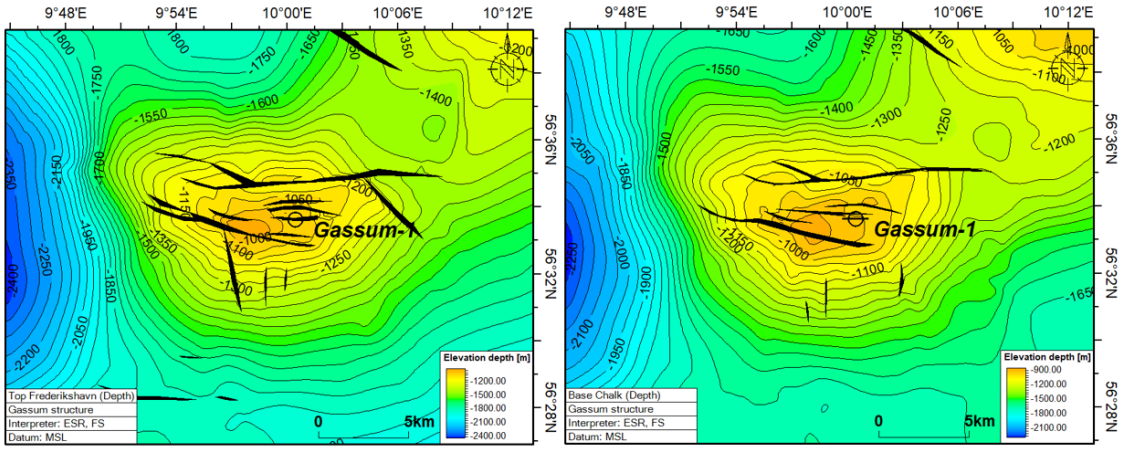


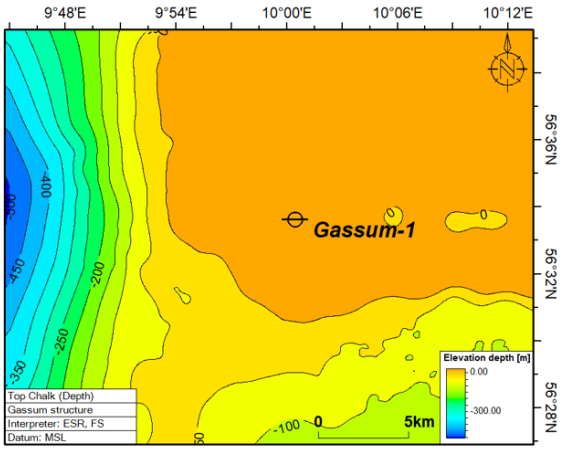


**Figure 6.2.2 (continued).** *Depth-structure maps in meter (m) below mean sea level (b.msl) shown with the largest faults as black, filled polygons and the location of the Gassum-1 well. (I) Top Frederikshavn; (J) Base Chalk; (K) Top Chalk (combined surface from GEUS & FOHM hydrogeological model – see Chapter 5), shown without faults. The maps are produced with a 250x250 m grid and mildly smoothed.*

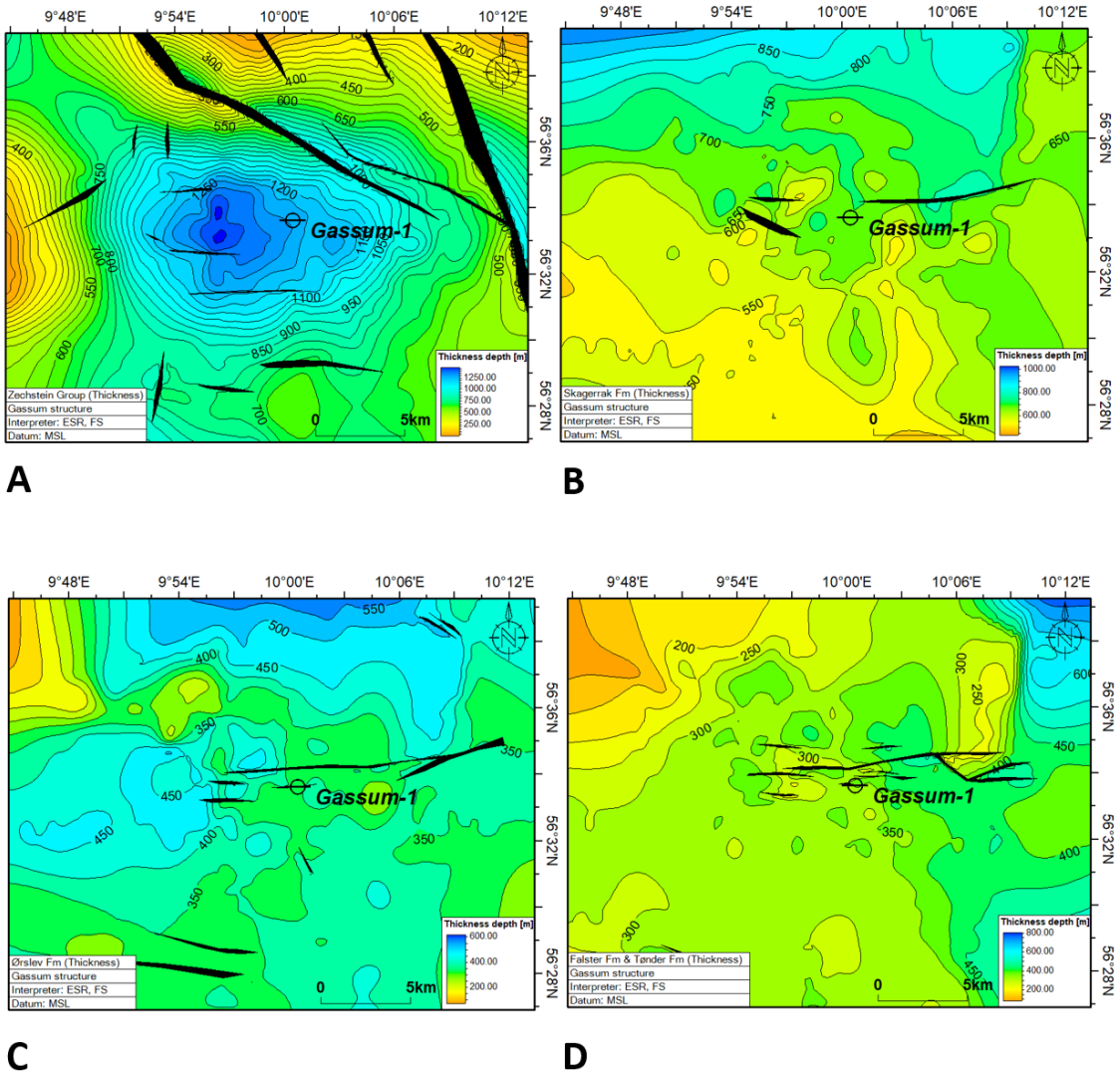


**Figure 6.2.3.** *Thickness map in meter (m) shown with the largest faults as black, filled polygons near succession top, and the location of the Gassum-1 well. (A) Zechstein Group (faults near base of succession at Top pre-Zechstein); (B) Skagerrak Fm; (C) Ørslev Fm; (D) Falster Fm and Tønder Fm. The maps are produced with a 250x250 m grid and mildly smoothed.*

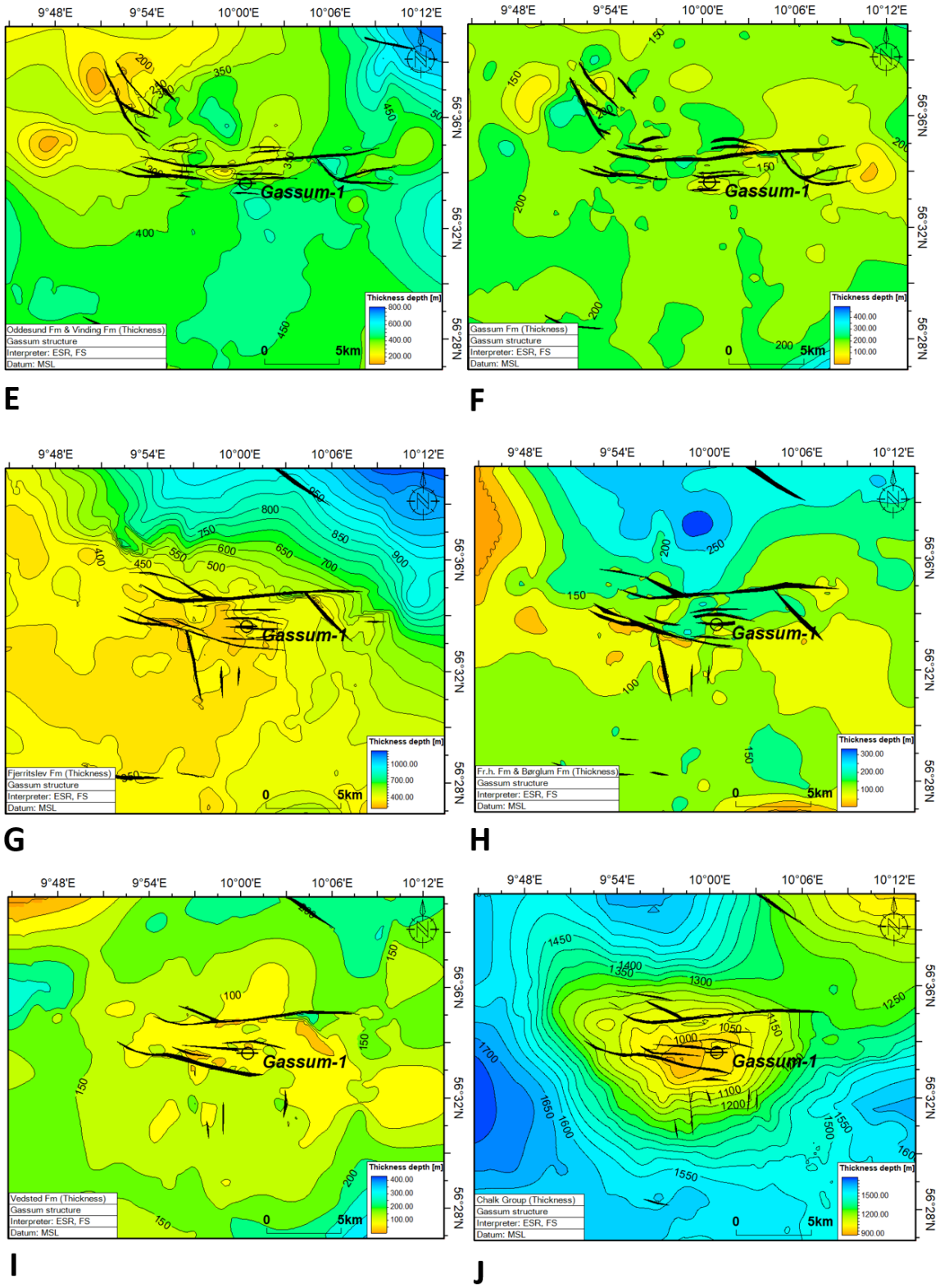


**Figure 6.2.3 (continued).** *Thickness map in meter (m) shown with the largest faults as black, filled polygons near succession top, and the location of the Gassum-1 well. (E) Oddesund Fm & Vinding Fm; (F) Gassum Fm; (G) Fjerritslev Fm; (H) Frederikshavn Fm and Børglum Fm; (I) Vedsted Fm; (J) Chalk Group (faults in the lower part of the succession at the Intra Chalk horizon, see e.g. Fig. 6.1.1). The maps are produced with a 250x250 m grid and mildly smoothed.*

### Tectonostratigraphic evolution of the Gassum structure

The surfaces including the Top Skagerrak to the Base Chalk are penetrated in the Gassum-1 well (Fig. 6.2.4) and the nearby Voldum-1 and Hobro-1 wells. All mapped surfaces, in the Gassum area, are penetrated in the Rønde-1 well located 40 km towards southeast. However, there is no confident tie via seismic data to the mentioned wells, although these wells contribute to the overall knowledge of the geology in eastern Jutland. Moreover, the Gassum-1 well drilled through a normal fault, that cuts out part of the Jurassic section in the well (uppermost Fjerritslev Formation to upper part of Børglum Formation). This stratigraphic interval is likely more completely developed over the Gassum structure in general than indicated by the Gassum-1 stratigraphy.

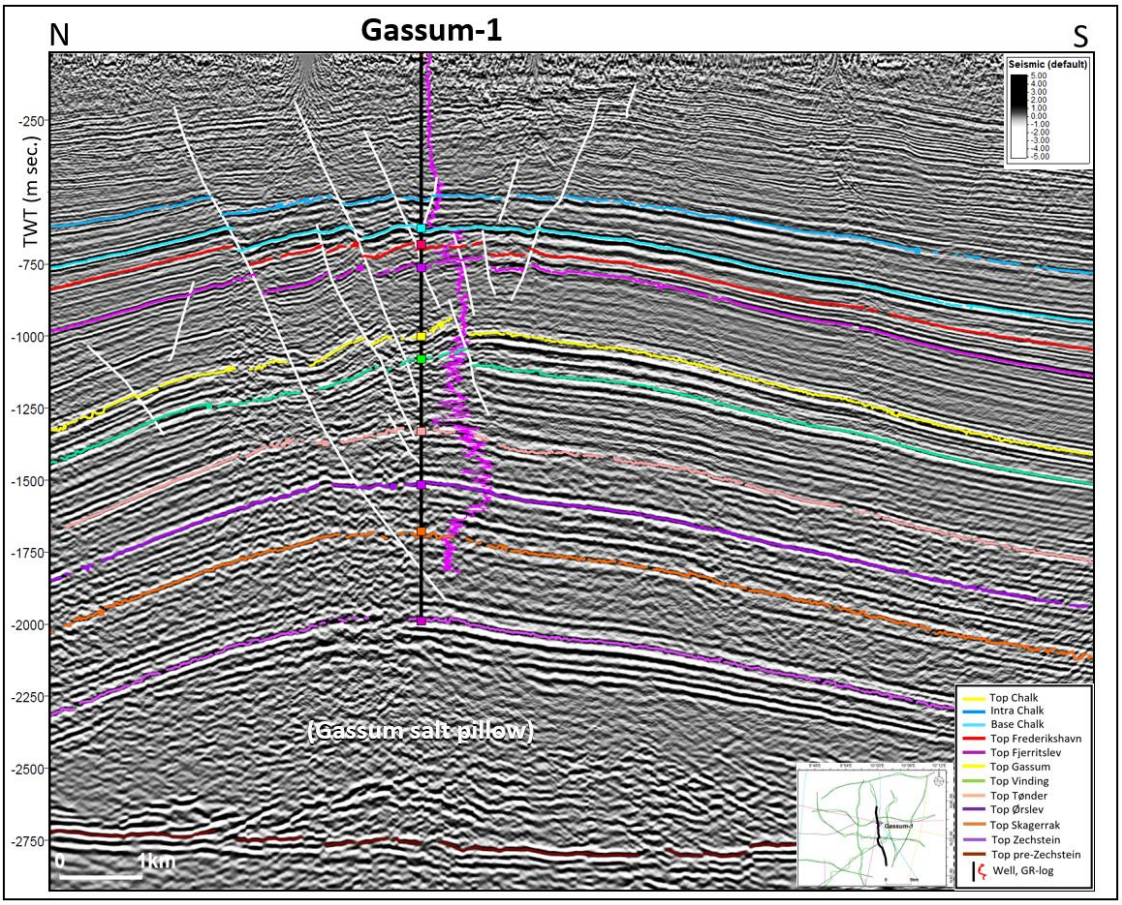


**Figure 6.2.4**. *N–S striking seismic section (GEUS23-GSM-P5, reprosessed) tying the Gassum-1 well. Note the half-graben structure above the Gassum salt pillow, where the master fault sole out near the base of the salt pillow and crosses the lower part of the well. This structure can be recognised in the Chalk Group, and to the Top Chalk surface, which is elevated above mean seal level. A significant hiatus at Top Chalk (missing upper Maastrichtian and Danian) at its top in the well (Fig. 6.1.1) indicates post-Cretaceous uplift and erosion. The line location is shown in the small map.*

*The Triassic to Jurassic evolution*

The uniform thickness of the Skagerrak Formation (Figs. 6.2.1B, 6.2.2B, 6.2.3B) records little, if any signs of syn-depositional faulting and salt tectonism. The same applies for the overlying Triassic succession. Most of this Triassic succession is intersected by E–W trending faults including the Gassum Formation, but faulting does not affect internal thicknesses, and faulting is interpreted to have occurred mainly in the Cretaceous and Cenozoic (see below). The first significant sign of pillow formation is recognized in the change in thickness induced by differential erosion along the Top Fjerritslev (Fig. 6.2.3F). However, it cannot be ruled out that a part of the extra thickness of the Fjerritslev Formation in the northern part of the structure may belong to the southernmost Haldager Sand Formation and Flyvbjerg Formation, as indicated in the stratigraphic scheme (Fig. 6.1.1). Seismic data (Figs. 6.2.5, 6.2.6) shows units, which wedge from north towards south at the flank of the structure in the uppermost part of the present interpreted Fjerritslev Formation, just below the Top Fjerritslev horizon (e.g., Fig. 6.2.5 at c. 1250–1400 ms TWT towards north). Thin parts of the successions may be present in the Gassum-1 well - See Chapter 7.

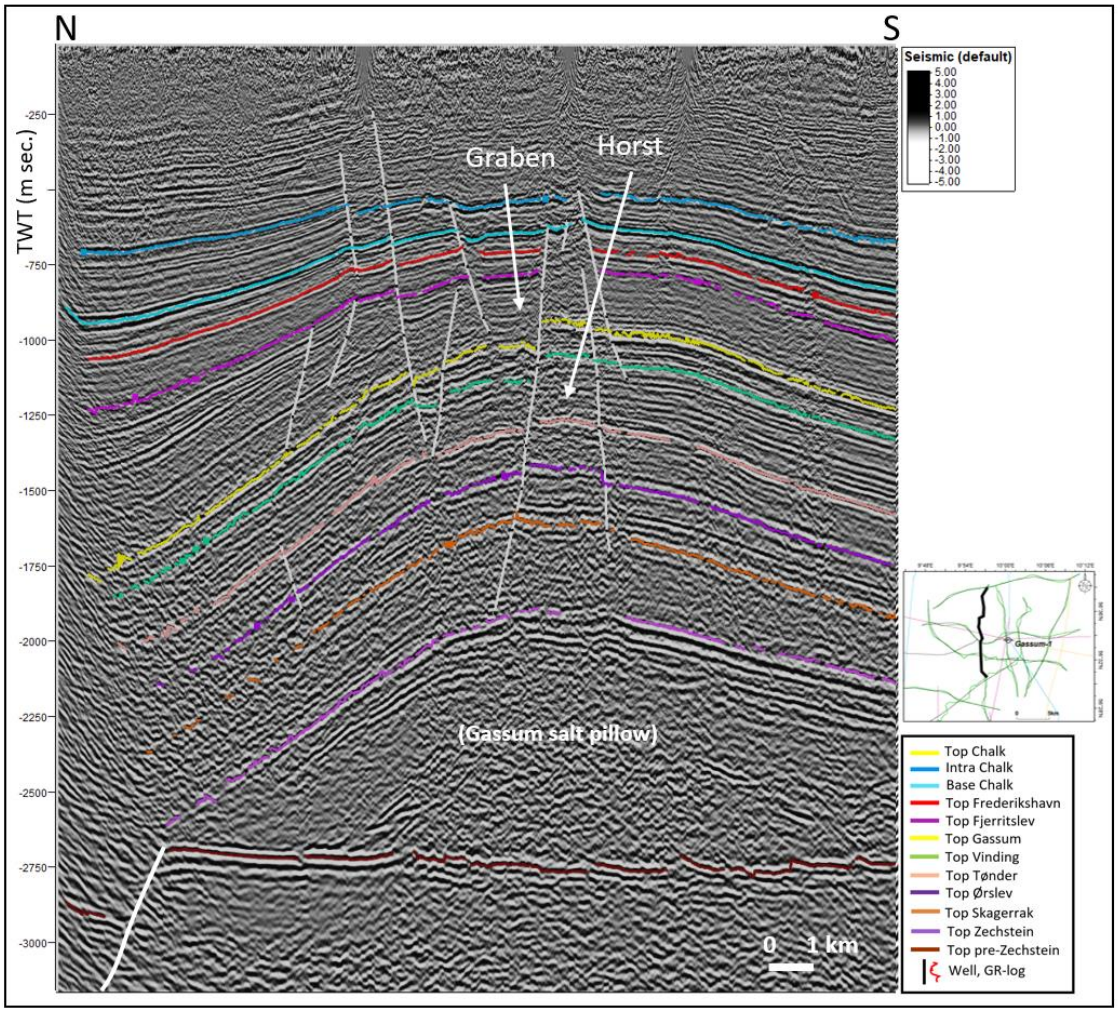


**Figure 6.2.5**. *N–S striking seismic section west of the Gassum-1 well. Note the horst and graben structures formed associated with salt movements in the Gassum salt pillow. Upper parts of the Fjerritslev Fm show internal truncation surfaces and is thickening towards the north (see discussion in the text). Also note the distinct fault at the Top pre-Zechstein level.*

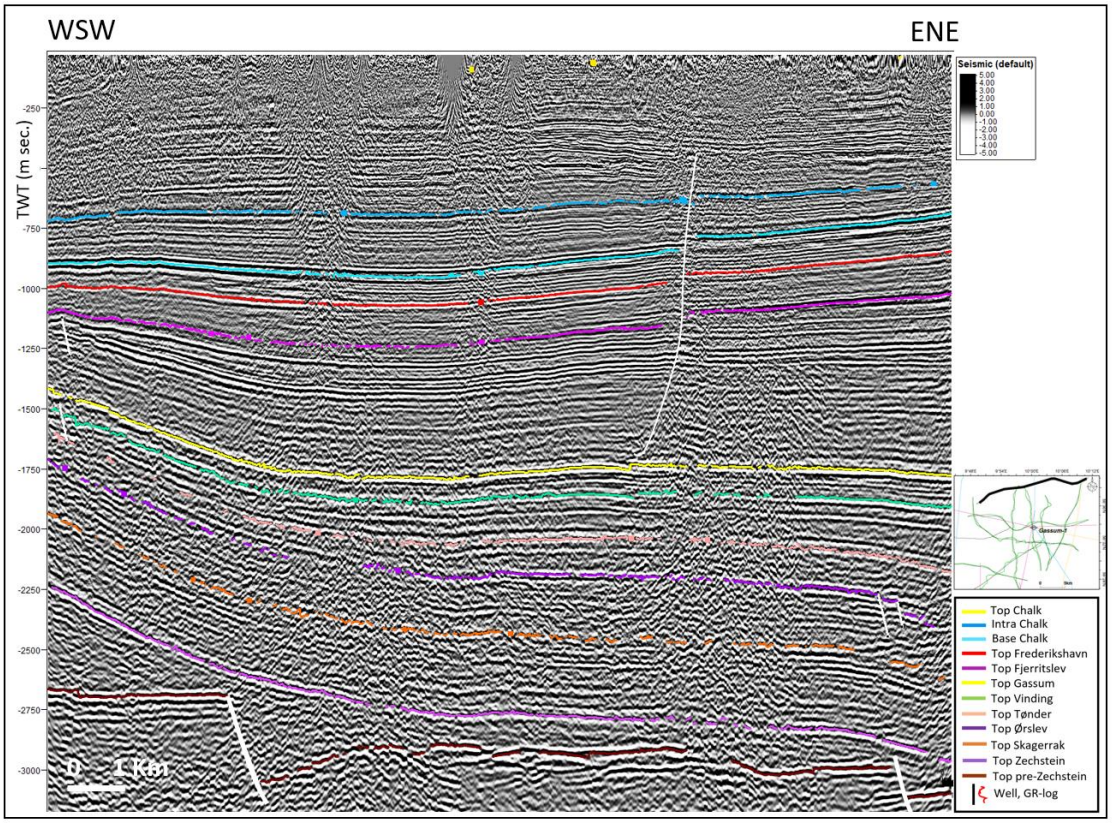


**Figure 6.2.6**. *WSE–ENE striking seismic section from the northern part of the study area. The salt structure seen in the lower left side of the section is the easternmost part of the Hobro salt pillow.*

The Top Fjerritslev may thus alternatively be placed below this wedge if these formations are included in the interpretation here. The lower part of the wedge succession partly onlap the flank of the structure and updip parts seem to be partly truncated. If these formations occur here, they may contain some sandstone, instead of the mudstone dominated Fjerritslev Formation, and thus enhancing the overall cumulative reservoir thickness. Regardless of whether the wedge belongs to the Lower Jurassic Fjerritslev Formation or the Middle–Upper Jurassic Haldager Sand and Flyvbjerg formations, there is a significant unconformity and hiatus, which seems related to uplift of the Gassum structure due to salt pillow growth. Thin parts of the succession may occur in the Gassum-1 well (see Chapter 7). Wedging of the overlying Børglum and Frederikshavn formations thinning over the crest of the Gassum structure document continued salt pillow inflation in the latest Jurassic.

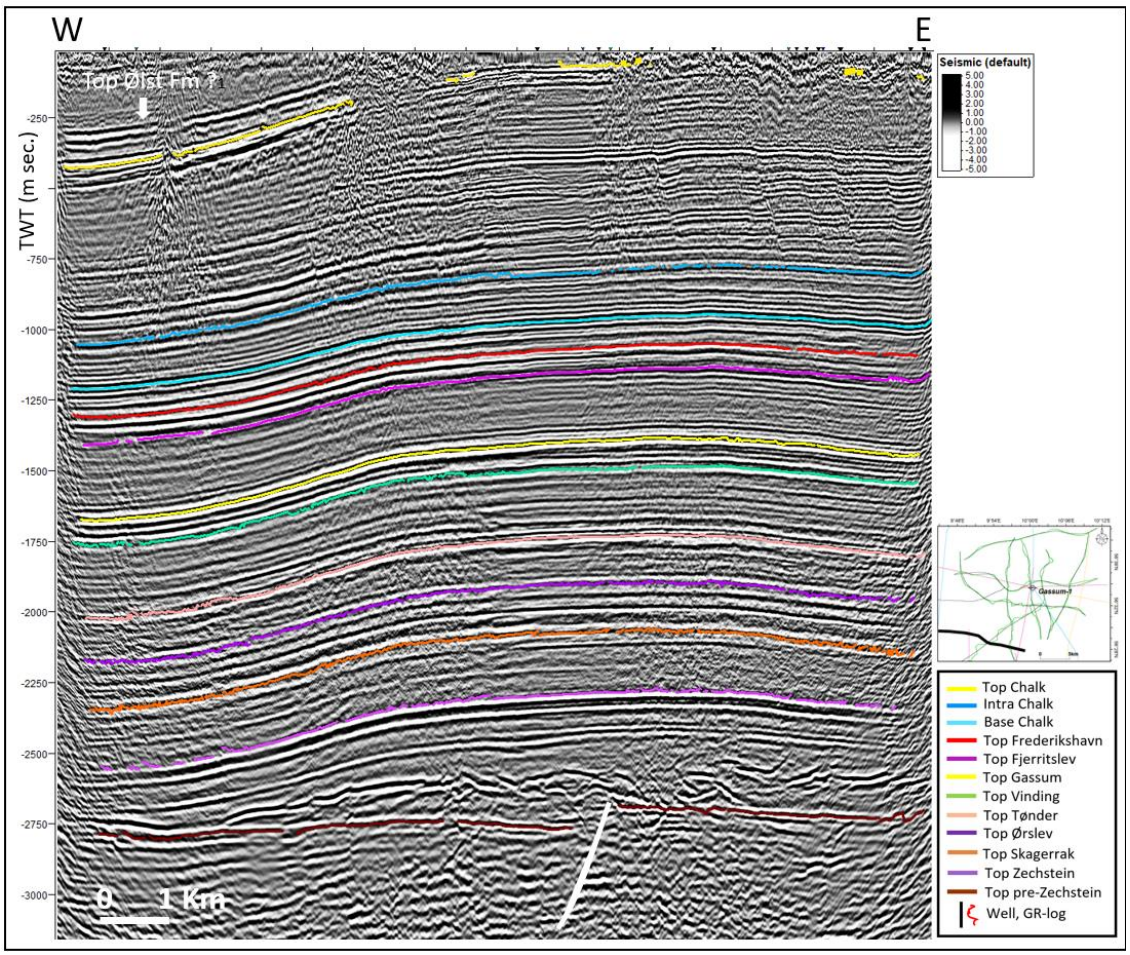


**Figure 6.2.7**. *W–E striking seismic section from the southern part of the study area, Note that the Top Chalk group can be mapped here, but otherwise, the chalk Group is strongly eroded in the area and actually outcrop just north of the study area, east of the town of Assens.*

*The Cretaceous to Cenozoic evolution*

During the Lower Cretaceous, the sand-rich Frederikshavn Formation (Fig. 6.1.1) became deposited over the area forming a secondary reservoir, which is overlain by the Vedsted Formation mudstones (seal) (Chapter 7). Parts of the Vedsted Formation stratigraphy and the overlying Rødby Formation known from other wells (e.g., Hobro-1) seem to be missing here (Fig. 6.1.1), also probably due to uplift related to salt pillow growth.

The prevailing E–W striking fault pattern (Figs. 6.2.4, 6.2.5), can be recognized on all maps between the Top Ørslev and Intra Chalk horizons with offsetting the Jurassic to latest Cretaceous succession (Figs. 6.2.1–6.2.3). The faulting is interpreted to have been associated with salt motion, and consequently, the youngest salt movements must be Late Cretaceous and/or Cenozoic in age. This is confirmed by the decreasing chalk thickness over the crest of the Gassum structure controlled by erosion after Cenozoic salt pillow growth.

The Gassum area is located adjacent to the Sorgenfrei-Tornquist Zone at which major inversion tectonism occurred during the Late Cretaceous and early Cenozoic (Liboriussen et al. 1987; Mogensen & Korstgaard 1993). Cenozoic salt motion in the Danish area is well known too (Clausen 2012; Rasmussen 2009). At the Eocene–Oligocene transition, salt movements took place near the Thorning Structure (Japsen et al. 2007). In the Gassum area, the truncation pattern of the Paleogene succession towards the base of the Quaternary suggests a

coeval phase of salt pillow growth; in fact, the Gassum structure was initially discovered due to the near-surface subcrop pattern (Fig. 6.2.8).

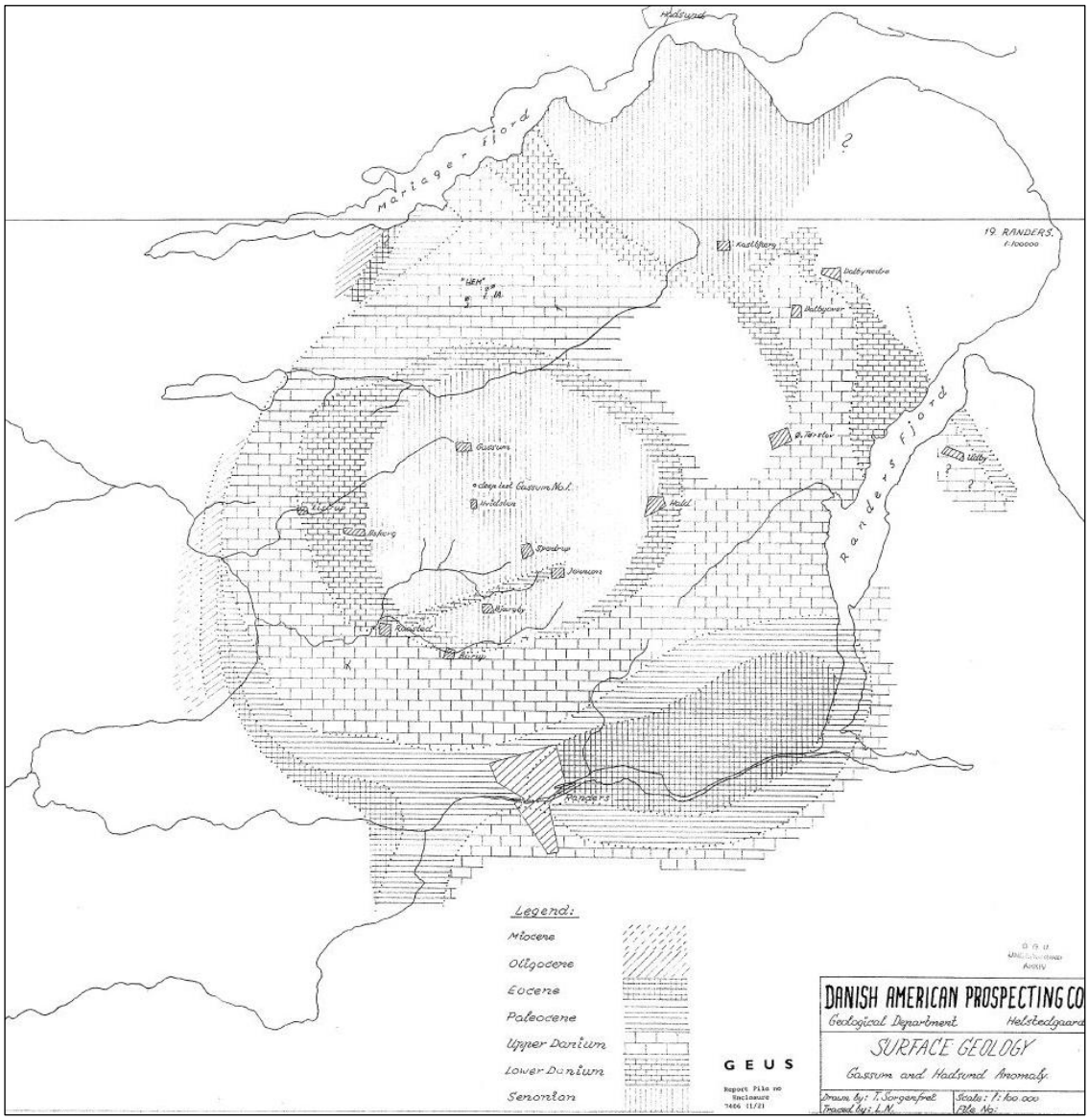


**Figure 6.2.8**. *Concentric subcrop pattern of Cenozoic and Upper Cretaceous strata at the Gassum structure documenting Cenozoic salt pillow growth (from Gassum-1 final well report, 1951).*

Neogene to even Quaternary salt motion is documented elsewhere in Denmark (Rasmussen & Dybkjær 2005; Hansen & Rasmussen 2008; Rasmussen 2004; Sirocko et al. 2008). The very shallow seismic sections are disturbed by noise but may be better resolved with additional data. Shallow faults, as well as the deeper faults and the nature of the shallow section, should be closely mapped and investigated for the integrity of seals and other risks.

In summary, the Gassum structure has developed during different geological phases including uplift and salt pillow growth in Middle–Late Jurassic, Lower Cretaceous, and Cenozoic times. Faults associated with salt movements developed mostly during the Jurassic and Cretaceous. The largest faults sole out on or near the Top Zechstein, and some can be traced at least up in the Chalk Group.

# 7. Geology and parameters of the reservoirs and seals

In this study the Upper Triassic–Lower Jurassic Gassum Formation is considered the primary reservoir for $CO_2$ storage in the Gassum structure. This is because it generally has good reservoir properties and not least because it is overlain by a several hundred meters thick mudstone-dominated succession of the Lower Jurassic Fjerritslev Formation which is known to have good seal properties (Figs. 7.1.1, 7.1.2). Hence, the Gassum-Fjerritslev formations are considered as the primary reservoir–seal pair in the structure. Secondary reservoirs include the deeper situated Triassic Skagerrak Formation and the shallower Upper Jurassic–Lower Cretaceous Frederikshavn Formation. The review of these, and their associated seals, is done more briefly compared to the primary reservoir-seal pair. The Middle Jurassic Haldager Sand Formation is not included in the review of potential reservoirs for $CO_2$ storage as it has generally been considered not present in the Gassum-1 well which penetrates the Gassum structure. However, the boundary between the Fjerritslev Formation and the Børglum Formation in the Gassum-1 well reflects a hiatus. Samples closely above the top of the Fjerritslev Formation (from core 32) show fragments of coalified wood, spores and pollen, and no marine palynomorphs – unlike the typical marine mudstones of the Børglum Fomation (Karen Dybkjær, pers com). In addition, the well site report (Danish American Prospecting Co 1951) indicates the presence of varicoloured mudstones (core 31) suggesting subaerial exposure. It is thus possible that thin beds of the Middle Jurassic Haldager Sand Formation and/or lower Upper Jurassic Flyvbjerg Formation are present in the well overlying the Middle Jurassic unconformity. Also, the seismic interpretation leave room for the Haldager Sand and Flyvbjerg formations to be present down-flank the structure. The Haldager Sand and Flyvbjerg formations may therefore form additional sandstone reservoirs in the Gassum structure. More conclusive data are needed to deduce this, which is why a detailed description of the Haldager Sand and Flyvbjerg formations are not included in this report. In general, it should be emphasized that these secondary reservoirs likewise may constitute excellent sandstone reservoirs for the storage of $CO_2$ within the Gassum structure.

The key well is Gassum-1 since it is the only well that penetrates the Gassum structure. The well has its TD in the uppermost Zechstein Group at a depth of 3462 m MD (Fig. 7.1.1). The quality of the petrophysical log data of the well is limited and do not cover the lowermost approximately 400 m of the well, hence data from the nearest wells to the Gassum structure (Kvols-1, Hobro-1 and Voldum-1) are included in the estimation of reservoir properties. However, the sandstone intervals in the Gassum-1 well are largely cored (Fig. 7.1.1) and analysis of the cores contributes to the estimation of the sandstone's reservoir properties. Interpreted well logs for the included wells, are shown in Appendix A. A direct tie of the Gassum-1 well to seismic horizons is associated with uncertainty as seismic signals in the vicinity of the well is blurred due to the presence of faults (see Chapter 6).

The Gassum Formation is subdivided into depositional sequences that are correlated between the wells to outline possible reservoir subunits in the formation. Likewise, is the Fjerritslev Formation subdivided into its informal members which have variable seal properties. The subdivision of the formations is based on integration of sedimentological interpretations of cores, petrophysical log patterns and palynological data (Nielsen 2003 and present study). The biostratigraphic zonations used include the ostracod zonation of Michelsen (1975), the dinocyst zonation of Poulsen 1996 and Poulsen & Riding (2003) and a combination of the spore-pollen zonations of Dybkjær (1991) and Lindström et al. (2023). The biostratigraphic

database varies from well to well. Thus, from some wells a solid biostratigraphic framework exists while the database is more sporadic from others. In Appendix B, the available biostratigraphy is summarized for each well based on data from reports and publications combined with new data from some of the wells. In addition, links are given to stratigraphic summary charts for each well. The charts combine the chronostratigraphy, lithostratigraphy, biostratigraphy and sequence stratigraphy and further include the bio-events and biozonations.

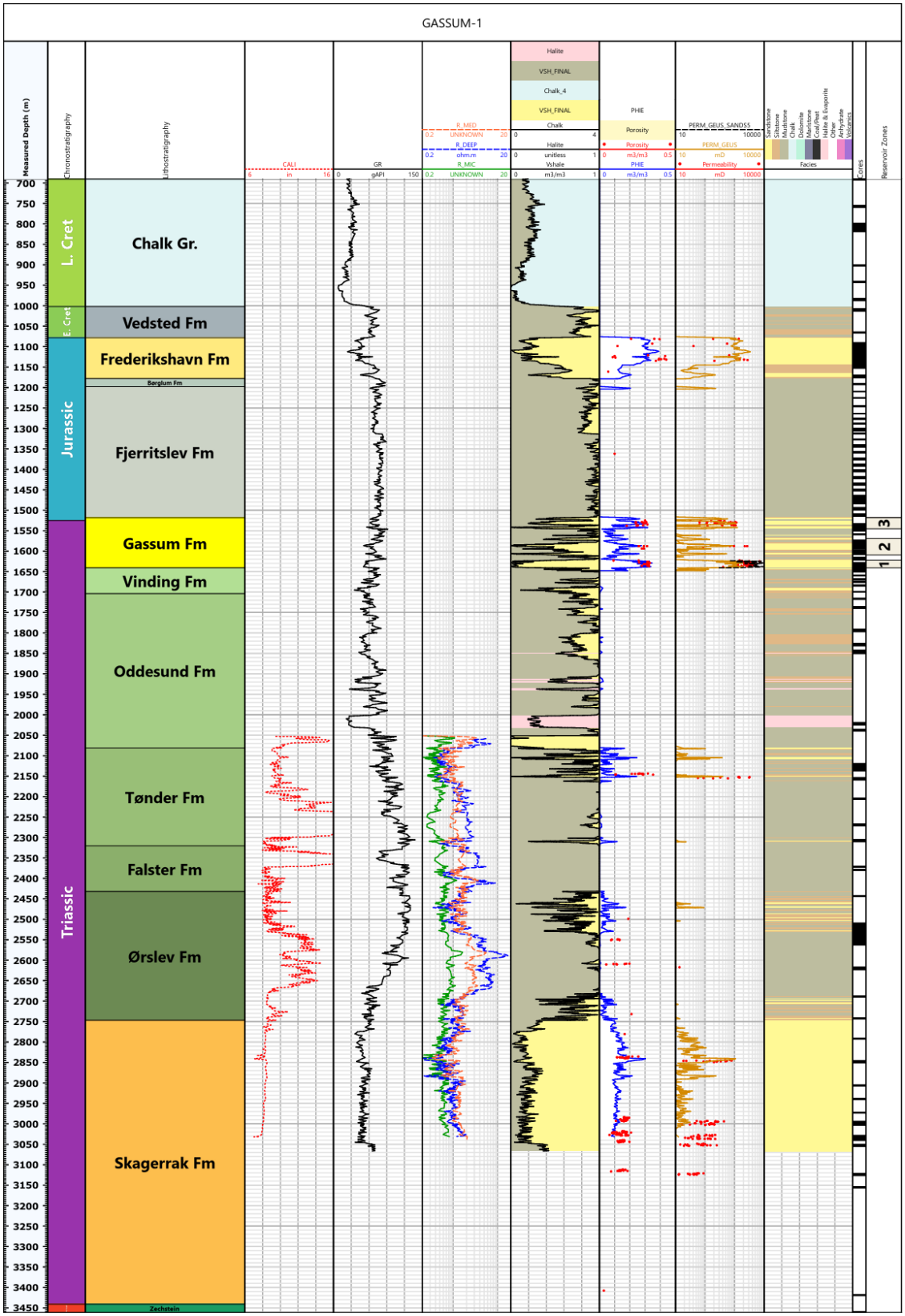


**Figure 7.1.1.** *Lithostratigraphic subdivision of the Gassum-1 well with interpreted lithology and formations based on petrophysical log interpretation and information from core data, cutting samples etc. Sandstones of the Gassum Fm are the primary reservoir with mudstones of the overlying Fjerritslev Fm being the main seal. Sandstones of the Frederikshavn and Skagerrak formations form secondary reservoirs.*

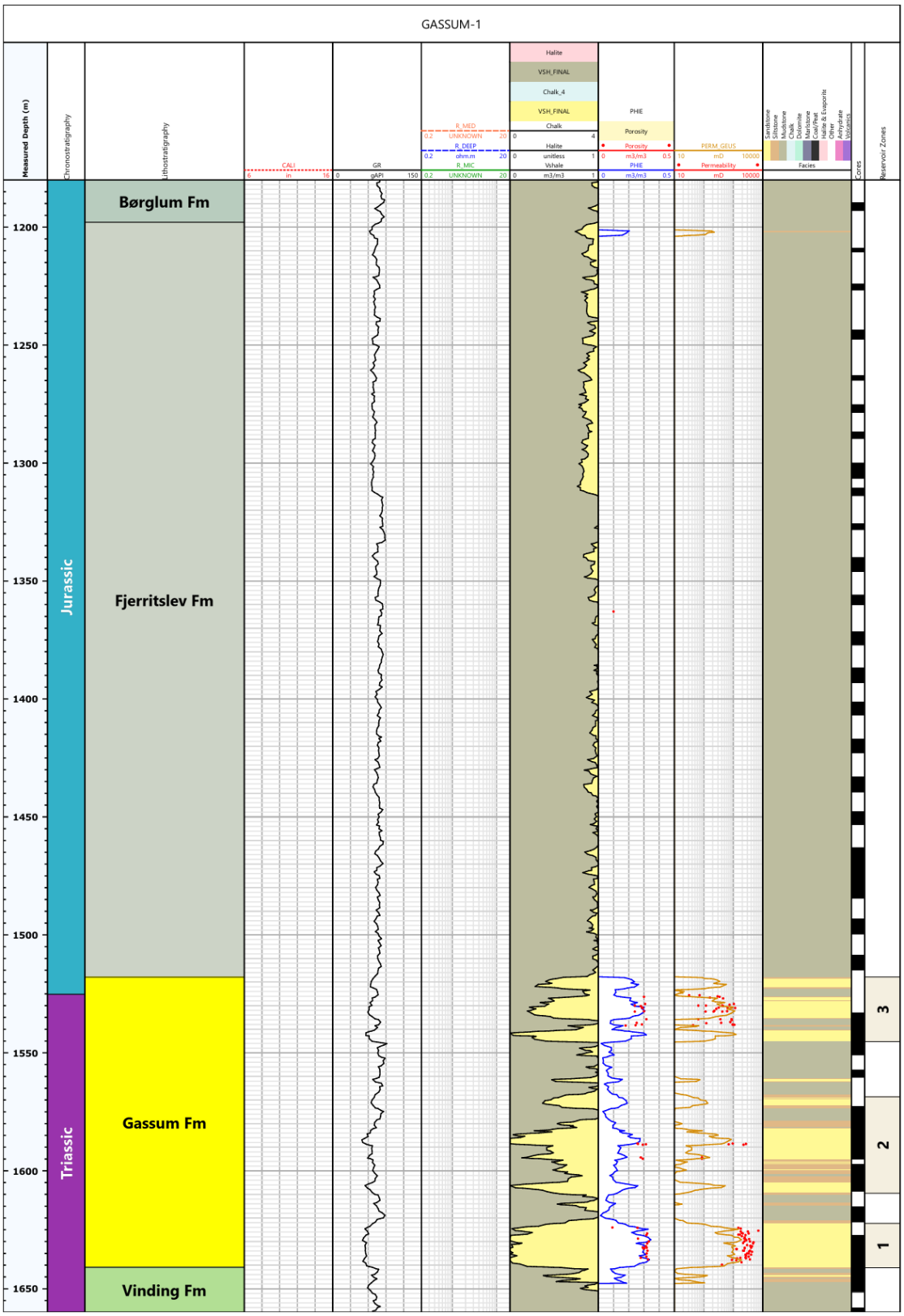


**Figure 7.1.2.** *The Gassum-1 well with interpreted lithology based on petrophysical log interpretation and information from core data, cutting samples etc. Zoom section of the Gassum Fm and its primary seal (Fjerritslev Fm) in Figure 7.1.1. Columns to the right mark three potential reservoir subunits (1–3) in the Gassum Fm and cored parts of the Gassum and Fjerritslev Fms (black columns). The cores are here marked at the depth positions that are indicated on the core boxes. However, core depths need to be reduced approximately 20-25 ft. (see Fig. 7.1.9).*

## 7.1 Reservoirs – Summary of geology and parameters

In the following description of reservoirs, emphasis is on the Gassum Formation whereas the secondary reservoirs, Frederikshavn and Skagerrak formations, are described more briefly.

### The primary reservoir: The Gassum Formation

The Gassum Formation is the best-known sandstone reservoir in the Danish onshore subsurface. It is used for geothermal energy in Thisted and Sønderborg and has also been used for seasonal storage of natural gas for more than 30 years in the Stenlille structure. The good reservoir properties of the formation have thus been proven at several places in Denmark. The formation is widespread in the Danish Basin and locally in the Danish part of the North German Basin (Fig. 7.1.3). It has a general thickness of 30–160 m (Nielsen & Japsen 1991; Nielsen 2003). Locally it is missing due to uplift and erosion related to regional uplift in the Middle Jurassic, at the 'Base Middle Jurassic unconformity' or the 'Mid-Cimmerian Unconformity' *sensu* Nielsen (2003), and above structures formed by vertical salt movements. The Gassum Formation is of Late Triassic–Early Jurassic age with the upper boundary showing a significant younging towards the northern, north-eastern, and eastern basin margins (Fig. 7.1.3B) (Bertelsen 1978, 1980; Michelsen et al. 2003; Nielsen 2003). The upper formation boundary is thus of latest Rhaetian age in the central parts of the basin whereas it is of Early Sinemurian age along the basin rims (Nielsen 2003 and references therein). This diachronic development of the boundary reflects an overall backstepping of the general coastline toward the basin margins during latest Triassic–Early Jurassic time owing to an overall rise in relative sea-level, interpreted as caused by a combination of regional basin subsidence and a eustatic sea-level rise (Nielsen 2003).

In general, the Gassum Formation is dominated by fine to medium-grained, in places coarse-grained, light grey sandstones, alternating with darker coloured clay- and siltstones and locally thin coal layers (Bertelsen 1978; Michelsen et al. 2003; Nielsen 2003). The sandstones are classified as subarkoses and arkoses following the classification of McBride (1963) (Weibel et al. 2020). The sediments were deposited during repeated sea-level fluctuations in Late Triassic–Early Jurassic times when the Danish Basin was mainly a shallow marine to coastal area. Large quantities of sand were transported into the basin by rivers which were sourced by erosion of the Fennoscandian Shield and, to a lesser degree, locally from the Ringkøbing-Fyn High in periods when this was exposed (Nielsen 2003 and references herein).

.

Recent provenance studies suggest that the basin was sourced also with sand from southerly Variscan source areas (Olivarius et al. 2020, 2022) (Fig. 7.1.4), perhaps transported into the basin through grabens intersecting the Ringkøbing-Fyn High such as the Øresund Basin and the "Storebælt trough".

The high influxes of sediment almost balanced subsidence implying that the intracratonic basin largely remained shallow and almost flat-based, but with its deepest part located near its center (Hamberg & Nielsen 2000). Due to the flat, low-gradient basin floor and overall shallow water conditions, sediment accumulation was very sensitive to Late Triassic and Early Jurassic fluctuations in relative sea level which resulted in repeated long-distance progradation or retrogradation of the coastline. A large part of the sandstones in the formation therefore represents shoreface deposits, but significant amounts are also fluvial or estuarine in origin. This is especially the case for the lower part of the formation where pronounced high-order relative sea level falls led to the progradation of rivers into the central part of the basin and the establishment of estuaries during succeeding rise in relative sea level.

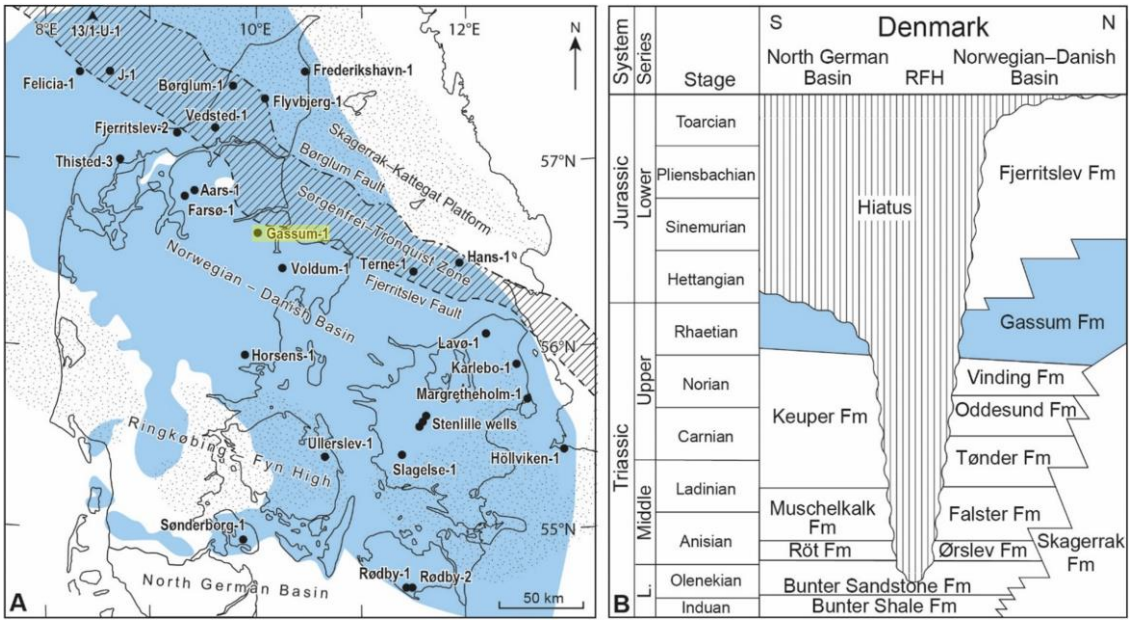


**Figure 7.1.3.** (*A) Estimated distribution of the Gassum Formation in the Danish onshore and nearshore area shown in blue. Also shown is selected wells and main structural elements including the Norwegian–Danish Basin and the North German Basin which are separated by the Ringkøbing-Fyn High (RFH). The Gassum-1 well which penetrates the Gassum structure is emphazied. (B) Stratigraphic scheme of the Lower Triassic–Lower Jurassic succession onshore Denmark revealing among others the time-transgressive nature of the of the top of the Gassum Formation. The hiatus relates to uplift and erosion in Middle Jurassic time. For the RFH, maximum age of the hiatus is shown but in some areas younger strata may be preserved on the high as also suggested for the Gassum Fm on the map to the left. However, over the central parts of Fyn the distribution of the Gassum Fm is difficult to map due to limited seismic data coverage. The formation is present in the Ullerslev-1 well but missing in the Ringe-1 and Glamsbjerg-1 wells located in this area (well location shown in Fig. 3.1). From Olivarius et al. (2022).*

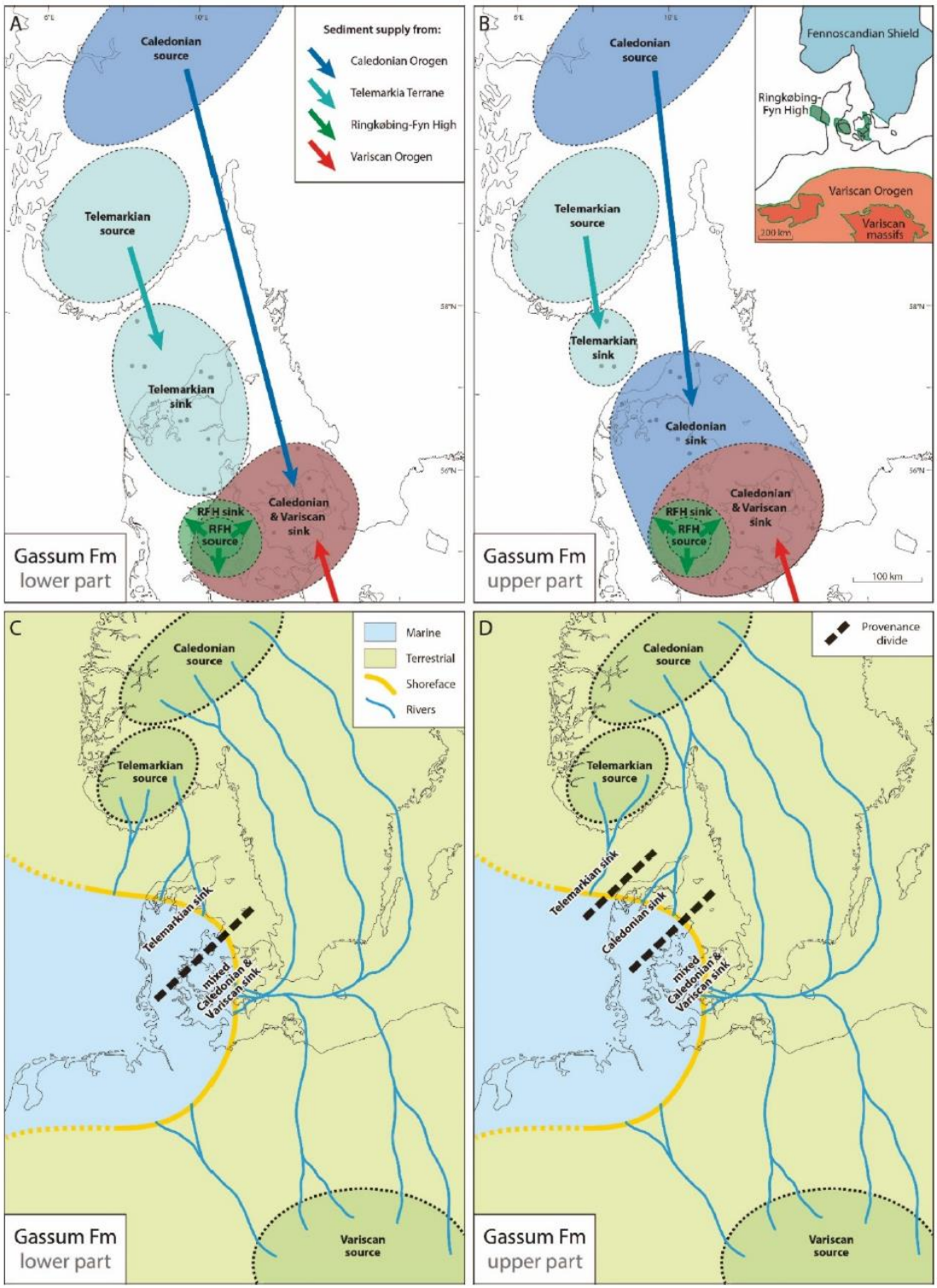


**Figure 7.1.4.** *Provenance of the lower (A) and upper (B) parts of the Gassum Formation showing the location of the primary source areas (Caledonian, Sveconorwegian, and Variscan) and the minimum extend of their sinks as evident from zircon U-Pb data from wells in the Danish Basin and the northern North German Basin. Sediments were locally supplied from exposed parts of the Ringkøbing-Fyn High . Tentative and generalized paleogeographic reconstructions for the lower (C) and upper (D) parts of the formation, where the primary difference is which of the Fennoscandian source areas that supplied most sediments to the basin. The maps represent snapshots since the coastline moved back and forth due to repeated transgressions and regressions in time. From Olivarius et al. (2022).*

## The Gassum Formation in the Gassum structure

*Depth, thickness, and extent*

The Gassum Formation has a mean thickness across the structure of 180 m, however the Gassum-1 well shows a thickness of the Gassum Formation of 130 m and a vertical depth to the top of the formation of c. 1518 m MD (Table 7.1.1). The present depth corresponds roughly to a maximum burial depth of around 2100 m prior to exhumation events (Japsen et al. 2007). The seismic mapping and interpretation indicate that the formation is present in the entire structure, with a thickness mostly of approximately 100–200 m (Fig. 6.2.3F).

**Table 7.1.1**. *Approximately depths to the Top and Base of the Gassum Fm and its thickness in Gassum-1 and the nearest wells (given in Nielsen & Japsen 1991). See Fig. 3.1 for location of wells.*

| Well | Rotary Table – m above terrain | Measured/True vertical depth (meter below Rotary Table) | | Thickness (m) |
|---|---|---|---|---|
| | | Top Gassum Fm | Base Gassum Fm | |
| Gassum-1 | 4.6 | 1518 | 1648 | 130 |
| Kvols-1 | 6.8 | 2424 | 2533 | 109 |
| Hobro-1 | 5.0 | 2376 | 2521 | 145 |
| Voldum-1 | 4.8 | 1757 | 1885 | 128 |

*Subdivision*

The Gassum Formation is subdivided into eight depositional sequences, SQ 2–SQ 9, based on integration of sedimentological interpretations of cores, petrophysical log patterns and biostratigraphic data (Nielsen 2003 and present study) (Fig. 7.1.5). However, for SQ 2 and SQ 9 it is only the sandstone-dominated highstand and lowstand system tracts, respectively, that form part of the formation. The numbering of sequences and their associated surfaces follows the sequence stratigraphic nomenclature in Nielsen (2003). This was developed for the Upper Triassic–Jurassic sedimentary succession in the Danish Basin and showed that individual sequences in most cases can be correlated basin-wide from well to well.

Each sequence is based by a sequence boundary (SB) formed at the time of maximum fall in relative sea level. Lowstand systems tracts (LST) formed between sequence boundaries (SB) and the first transgressive surface (TS). Transgressive systems tracts (TST) formed between the TS and the maximum flooding surface (MFS). Highstand systems tracts (HST) formed between the MFS and the SB of the next sequence. This simple sequence stratigraphic approach (e.g., Payton 1977) is following the divisions of Nielsen (2003). There are also other concepts (e.g., Catuneanu 2019), but these are not discussed further here. Figure 7.1.5 shows how the depositional sequences link to interpreted depositional facies and environments, and that the sequences can be corelated from well to well.

In general, the LST and HST deposits of the sequences are dominated by shoreface sandstones whereas the MFS occurs in intervals of offshore mudstones. The sequences reflect

an overall aggradational to progradational stacking pattern from the base of the Gassum Formation and up to SB 5. This surface is interpreted to have formed by fluvial erosion and bypass followed by the deposition of fluvial or estuarine sand during relative sea-level rise. From SB 5 and upwards to MFS 7 the overall stacking pattern is retrogradational with the shoreface sandstone intervals of the sequences becoming thinner on behalf of thicker offshore mudstone intervals. After a shorter progradational event the overall transgression culminated in Early Jurassic times with deposition of the overlying Fjerritslev Formation which is more than 300 m thick and consists almost entirely of offshore mudstones. However, relative thick sandstone intervals are present above SB 7 in Gassum-1 compared to the other wells (Fig. 7.1.5).

High order sea-level variations formed the individual sequences and generated the complex internal reservoir architecture of the Gassum Formation with mainly lowstand and highstand intervals forming internal sandstone reservoirs that are separated by transgressive intervals of mudstone and heteroliths (Fig. 7.1.5). The logpanel of Gassum-1 and the nearest wells, indicates that the internal sandstone and mudstone units have regional extent. However, it is possible that the mudstone units locally are truncated due to erosion related to fall in relative sea level and the associated formation of sequence boundaries. If so, this implies that sandstone intervals from different sequences locally are connected. This seems to be the case for the lower part of the Gassum Formation in the Hobro-1 well whereas well-defined mudstone intervals separate the sandstone reservoirs in the other wells (Fig. 7.1.5). The resolution of the seismic data is not high enough to deduce if some of the internal seals in places are truncated away from the Gassum-1 well within the Gassum structure. However, locally low relief erosional surfaces occur as well as areas showing accretion from east to the west and south to north, respectively (Fig. 7.1.6). Considering the overall coastal environment, outlined by the interpreted cores (Fig. 7.1.9), leaves several possible interpretations of these seismic features, e.g. estuarine incision, longshore accretion of spits, and flood tidal deltas.

The mudstone units possibly form internal seals in the Gassum Formation. In the Gassum-1 well, these potential seals are up to 24 m thick. This is partly considered in the outlining of the reservoir properties of the Gassum Formation by providing details not only on the Gassum Formation as one single reservoir, but also characterizing three reservoir subunits in the section dealing with the reservoir quality of the Gassum Formation (see below). Each of the reservoir subunits extends over more than one depositional sequence (Fig. 7.1.5). The lowermost one, named unit 1, consists entirely of sandstone whereas the two upper ones (units 2 and 3) each consist of three sandstone intervals separated by mudstone intervals.

*Lithology, provenance, and depositional environment*

In the Gassum-1 well, the sandstones of the Gassum Formation are mainly fine or fine to medium grained (Danish American Prospecting Co 1951, Nielsen 2003, Fig. 7.1.9). The mineralogical maturity is relatively low revealed by a high feldspar content (Fig. 7.1.7). This is assigned to a direct sediment supply from Fennoscandia and limit distance of transport from the source areas (Fig. 7.1.4). Fennoscandia being the source area is supported by zircon dating of samples from SQ´s 2 and 7. These suggest that the area of the Gassum structure received sediments from northern source areas (Telemarkian and Caledonian in Fig. 7.1.4) as is also the picture for zircon dating of the Gassum Formation from other wells in Northern Jutland (Olivarius et al. 2022).

Nielsen (2003) interpreted the depositional environments of the Gassum Formation in the Gassum-1 well based on an interpretation of its cores (Fig. 7.1.8) supplemented with palynological data and interpretation of the vertical gamma-ray motif (Fig. 7.1.9). The results of these core interpretations are transferred to the well in the log panel where also the sequence stratigraphic subdivision of the well is shown (Fig. 7.1.5). As mentioned, the formation is interpreted as mainly reflecting alternating shoreface and offshore deposition under the influence of relative sea-level variations. The exception is the presence of estuarine and lacustrine deposits above SB 5 and SB 7, respectively (Figs. 7.1.5, 7.1.9).

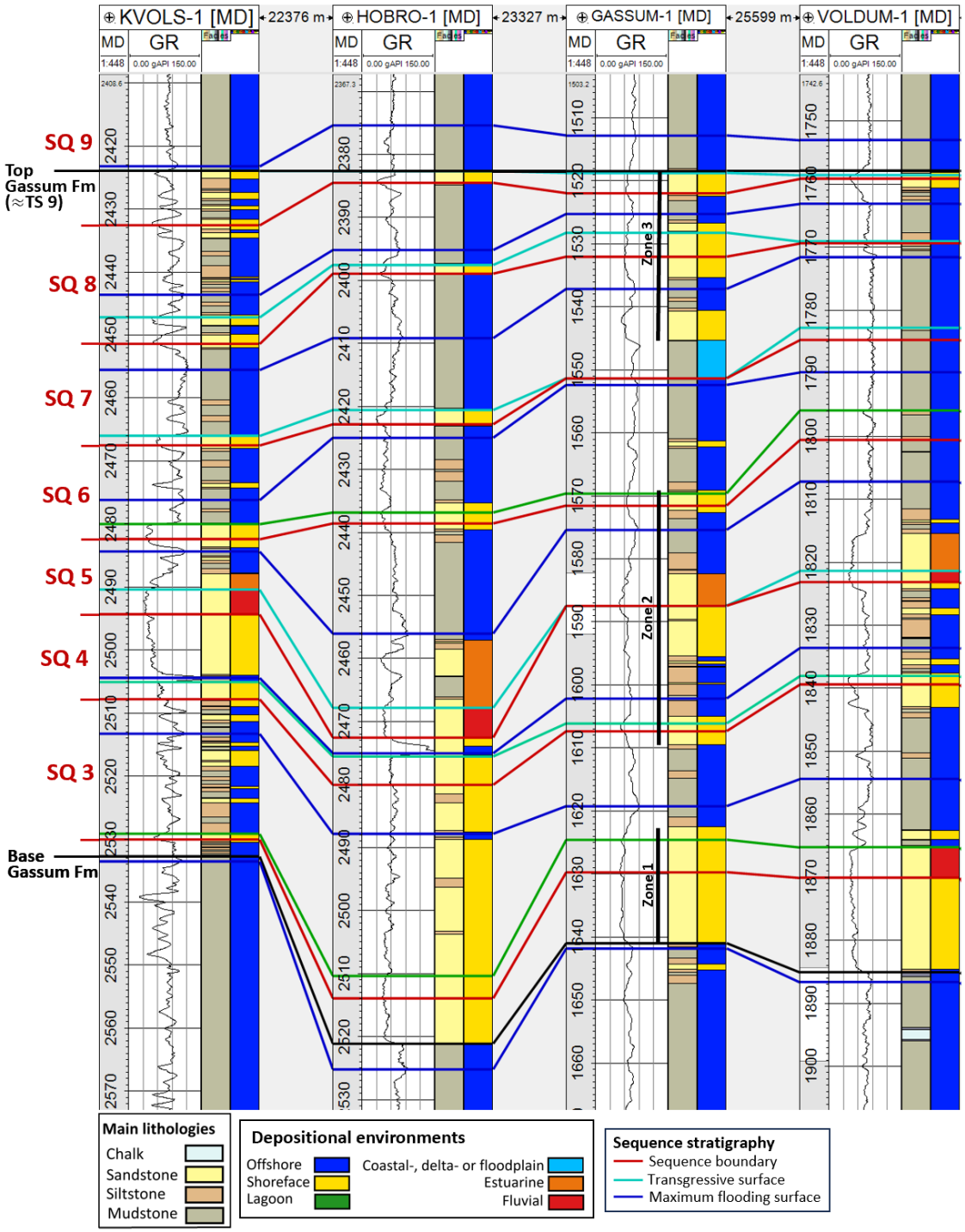


**Figure 7.1.5.** *Correlation panel focusing on the Gassum Formation in the nearest wells to the Gassum structure. Placement of sequence stratigraphic surfaces and interpretation of depositional environments is tentative and would benefit from supplementary palynological data. However, for the Gassum-1 well the interpretation of the Gassum Formation relies on extensive core interpretations given in Nielsen (2003) (Fig. 7.1.9). The transgressive surface TS 9 represents the top of the Gassum Formation in the wells and is used as datum line. Reservoir zones 1–3, dealt with in the estimation of reservoir quality below, is marked for the Gassum-1 well. Location of wells relative to the Gassum structure is seen in Figures 3.1 and 7.1.3.*

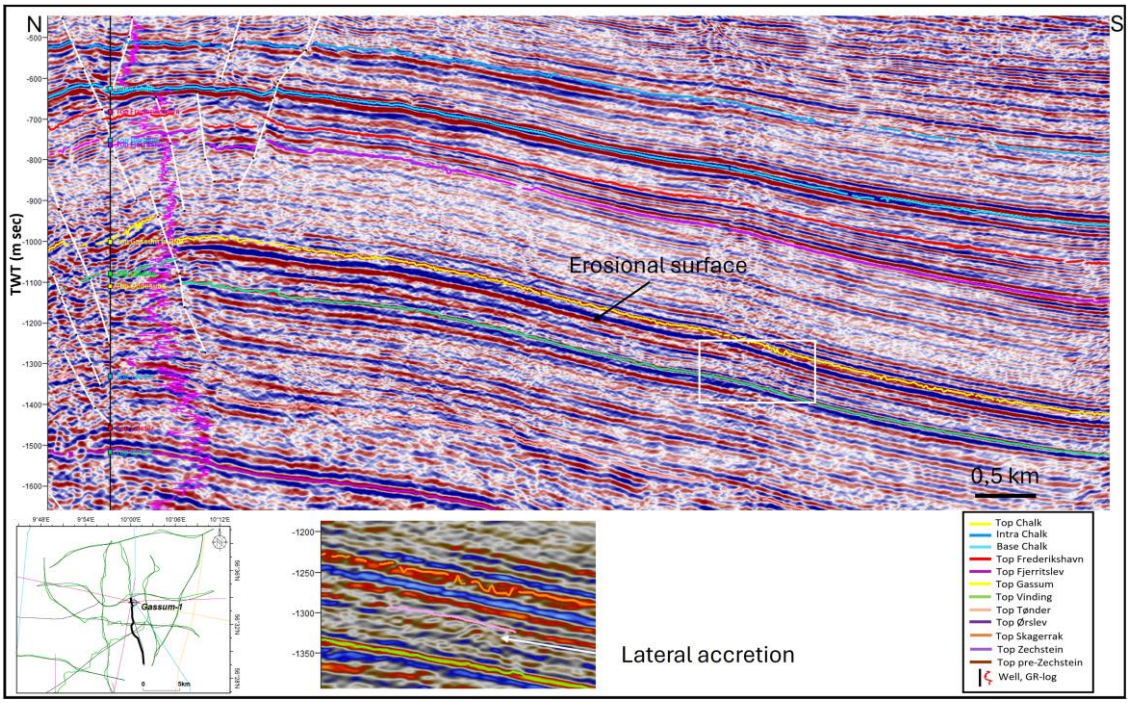


**Figure 7.1.6.** *Mapping of the Gassum Fm along the reprocessed seismic line GEUS23_GSM_P5 (location shown as black line on inserted figure in lower left corner). The seismic section is in two-way time. The overall seismic reflection pattern in the Gassum Fm is characterized by a parallel to sub parallel, high amplitude reflection pattern. The highest amplitudes are found in the north-western portion of the study area. Lower relief erosional surfaces occur sporadically as well as local areas with local accretion (see zoom-in the lower middle part of the figure which is a of white rectangle. The accretion occurs in the middle part of the Gassum Fm and show accretion from east to the west and south to north, respectively (see zoom-in figure of the part of the seismic section marked with a white rectangle). Direct correlation with the Gassum-1 well (shown to the left with its lithostratigraphic surfaces and gamma-ray motif) is not possible as this well is in a fault zone.*

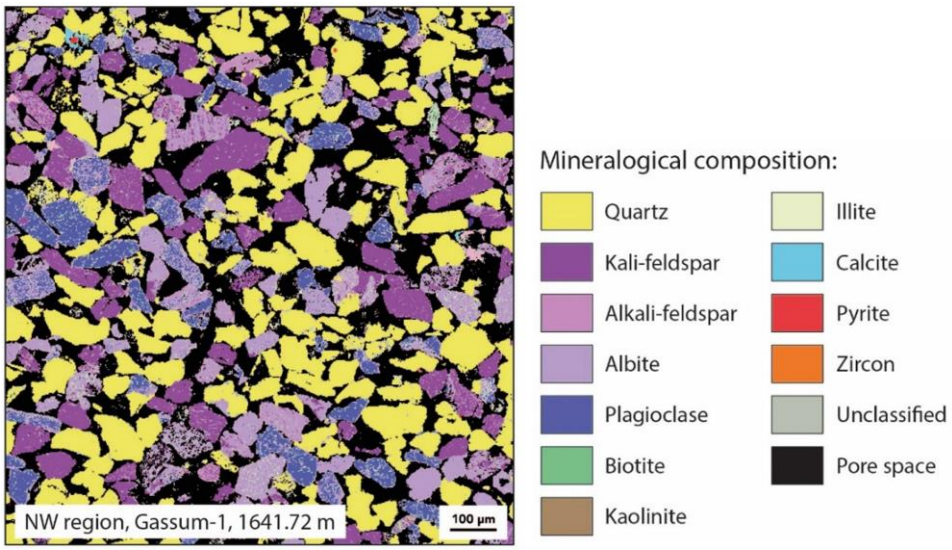


**Figure 7.1.7.** *Mineral map of a sample from SQ 2 in the Gassum-1 well constructed by the automated quantitative mineralogy method (AQM). A low mineralogical maturity is revealed by the high feldspar content. Also notice the abundant pore space. From Olivarius et al. (2022).*


**Figure 7.1.8.** *Cores of the Gassum Fm in the Gassum-1 well showing mainly fine- and medium-grained shoreface sandstones. Core diameter is c. 8.5 cm. Cored intervals are marked on the petrophysical log of the well in Figure 7.1.2. Photos by Emil Fønss Jensen (Jensen 2023).*

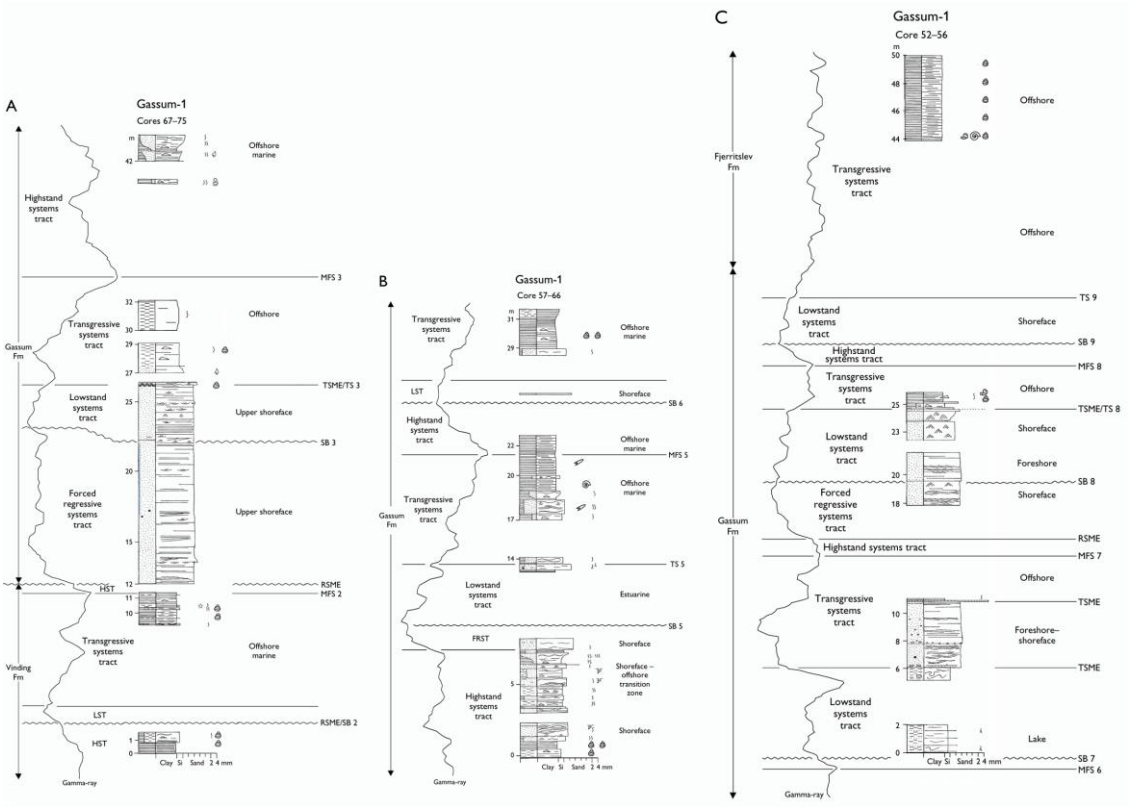


**Figure 7.1.9.** *Core interpretation of the Gassum Formation in the Gassum-1 well shown together with the gamma-ray motif and sequence stratigraphic surfaces (moving stratigraphic upwards from A to C). The location of the boundary to the underlying Vinding Fm and the overlying Fjerritslev Fm is indicated next to the gamma-ray log. From Nielsen (2003). Note that core depths are corrected to log depths by subtracting 20–25 ft (Nielsen 2003).*

### *Reservoir quality (porosity and permeability)*

Characterization of the reservoir quality of the Gassum Formation in the Gassum structure is primarily based on core descriptions and core measurements. In this well only gamma ray (GR) log was recorded within the Gassum Formation, hence the volume of shale ($V_{shale}$), as indicated in Figures 7.1.1 and 7.1.2, is based on this log. The quality of the GR log itself seems to be fair, as there is good agreement between the log derived lithologies and the descriptions of the corresponding cores. The baseline of the GR representing clean sand is relatively high, which is expected in a sandstone containing a high content of feldspar (Fig. 7.1.7). The $V_{shale}$ curve forms the basis for the classification of the rocks into mudstones, siltstones and sandstones. Overall, the Gassum Formation is divided into the Reservoir Zones 1-3 (Figs. 7.1.1, 7.1.2) based on the derived $V_{shale}$, which illustrate relatively thick mudstones separating the sandy zones. Herein 'Net sand' is defined as sandstone intervals characterized by fairly high porosities (>10%) and low shale content (<50%).

In Figures 7.1.1 and 7.1.2, track 9 from the left shows the log derived effective porosity, PHIE. This curve is a linear fitting of the $V_{shale}$ and the porosity from the core measurements, hence it is not derived by proper/standard petrophysical interpretation. It is included in the figures mainly for illustrative purposes and does not contribute to the evaluation of the reservoir quality of this formation.

Reservoir Zone 1 consists of an 18.8 m sand and a net to gross ratio of 1.0. The porosity and permeability characterizing this unit is estimated based on the core measurements as arithmetic mean of the porosities and permeabilities, respectively. Thus, the Reservoir Zone 1 is characterized by average porosity of 29.6% and average permeability of 2637 mD.

Reservoir Zones 2 and 3 are considered together in terms of porosity and permeability, as the numbers of measurements is limited in Zone 2. Reservoir Zone 2 has a gross thickness of 40.9 m and a combined net reservoir sand thickness of 20.9 m, constituting a net to gross ratio of 0.51. Reservoir Zone 3 has a gross thickness of 27.4 m and a combined net reservoir sand thickness of 16.6 m, constituting a net to gross ratio of 0.61. The average porosities of Reservoir Zones 2–3 are calculated to be 27.9%, whereas the average permeability is calculated to be 511 mD.

By comparing the reservoir properties of Reservoir Zone 1 and Reservoir Zones 2–3 there seems to be a marked difference in the porosity-permeability relationship, as the lowermost zone has slightly higher average porosities but significantly higher average permeabilities. In fact, this relationship in the lowermost sand is comparable to the high permeabilities observed in the lowermost sand in the Stenlille-19 well. Therefore, this relation is considered trustworthy.

Furthermore, for comparison the reservoir characteristics of the Hobro-1, Kvols-1 and Voldum-1 are listed for a quick asset. For these wells the reservoir parameters are averaged for the entire net sand within the Gassum Formation in these wells. For the Hobro-1 the average porosity is found to be 20.8%, corresponding to 260 mD; for the Kvols-1 the average porosity is 18.2%, corresponding to 152 mD; and for the Voldum-1 the average porosity is 12.8%, corresponding to average permeability of 32 mD.

### Conclusion on reservoir characterization

Two scenarios predicting the reservoir properties of the Gassum Formation within the Gassum structure are presented based on the Gassum-1 well and the surrounding wells relevant to this study. The first scenario 1 is simply propagating the parameters derived from the Gassum-1 well into the entire structure, while the second scenario 2 is based also on considerations from the surrounding wells. In order to compare the numbers representing the entire Gassum Formation, the average for the Gassum Formation within the Gassum-1 well is presented in the table below (Table 7.1.2).

For scenario 2, a simple average for the four wells is calculated with each well all having a weight of 1. These probably skew the numbers, as the thin sandstones of the Voldum-1 and Kvols-1 are becoming relatively more important in this scenario. This may therefore be considered a low-case scenario of the reservoir characteristics of the Gassum Formation within the Gassum structure.

**Table 7.1.2.** *Summarizing the Scenarios 1 and 2 predicting the reservoir characteristics of the Gassum Formation within the Gassum structure. These scenarios show fair to excellent reservoir qualities and thicknesses quantified by the transmissivity ranging from 21–85 Dm (Darcymeter).*

| | Reservoir (m) | Net to Gross (v/v) | PHIE (%) | PERM (mD) | Transmissivity (Dm) |
|---|---|---|---|---|---|
| **Scenario 1** | 56.7 | 0.46 | 28.5 | 1500 | 85 |
| **Scenario 2** | 43.2 | - | 20.1 | 486 | 21 |
| **Average** | 50.0 | - | 24.3 | 993 | 50 |

## The secondary reservoirs: Frederikshavn and Skagerrak formations

### The Frederikshavn Formation

The Upper Jurassic–Lower Cretaceous Frederikshavn Formation is known from wells drilled in the Danish Basin in northern and central Jutland. The formation is generally 50–150 m thick but can be more than 230 m thick in the Sorgenfrei-Tornquist Zone (Nielsen & Japsen 1991). The formation is dominated by layers of siltstones and fine-grained sandstones alternating with silty claystones (Michelsen 1978; Michelsen & Bertelsen;1979, Michelsen et al. 1981, 2003). The sediments may contain glauconite and marine fossils. Thin layers of limestone occur in the lower and upper part of the formation, and in Northern Jutland there are a few cm-thick coal layers in the upper part of the formation; In Gassum-1, coal fragments are also present. The sediments were supplied to the Danish Basin from the Scandinavian bedrock area. Thus, the grain size and the thickness and proportion of sandstone layers in general increase towards NE. Sand was mainly deposited in deltaic and coastal environments that prograded into the basin during periods of stable or falling sea level and were subsequently flooded during periods of rising sea level, whereby the deposition of sand was replaced by the deposition of silt and clay. The formation typically comprises two to three coarsening-upwards successions from offshore mudstones to shoreface sandstone, best developed in the central and northern part of the Skagerrak-Kattegat Platform (Michelsen 1978, Michelsen & Nielsen 1991). Distally, the formation thins out and becomes finer-grained until it is replaced by the claystone-dominated Vedsted Formation. The presence of sandy layers in the southwestern part of the basin indicates that the Ringkøbing-Fyn High may also have been a sediment source during periods of low sea level.

*The Frederikshavn Formation in the study area*

The Frederikshavn Formation is present in the Gassum-1 well in the depth interval 1078–1179 m MD and is thus c. 101 m thick (Fig. 7.1.1 and 7.1.10). Seismic mapping (incl. thin Børglum Formation) shows significant thickness variations of c. 50–200 m, especially at faults (Chapter 6; Fig. 6.2.3-H). It consists almost entirely of sandstones in the well apart from a. c. 13 m thick siltstone-dominated interval in the lower part of the formation (Fig. 7.1.10). It is thus present in a suitable depth for $CO_2$ storage and furthermore have excellent reservoir properties as outlined below. As mentioned previously, the reason for not considering it as the primary reservoir for storage relies on a larger uncertainty of the seal properties of the overlying Lower Cretaceous mudstone interval in comparison to the Lower Jurassic Fjerritslev Formation which forms the seal for the Gassum Formation. The Frederikshavn Formation shows large lateral variations in lithology between the included wells (Fig. 7.1.10).

Three overall coarsening-upwards successions, reflected by the GR motif, are recognized in the Gassum-1 well. In the sandstone dominated part of the formation, these probably reflect shoreface shallowing-upwards successions, possibly related to delta progradation. Cores of varying quality largely covers the formation in the Gassum-1 well (Figs. 7.1.1 and 7.1.11). The cores may form a good basis for studies of depositional environments, reservoir properties, mineralogy, diagenesis etc.

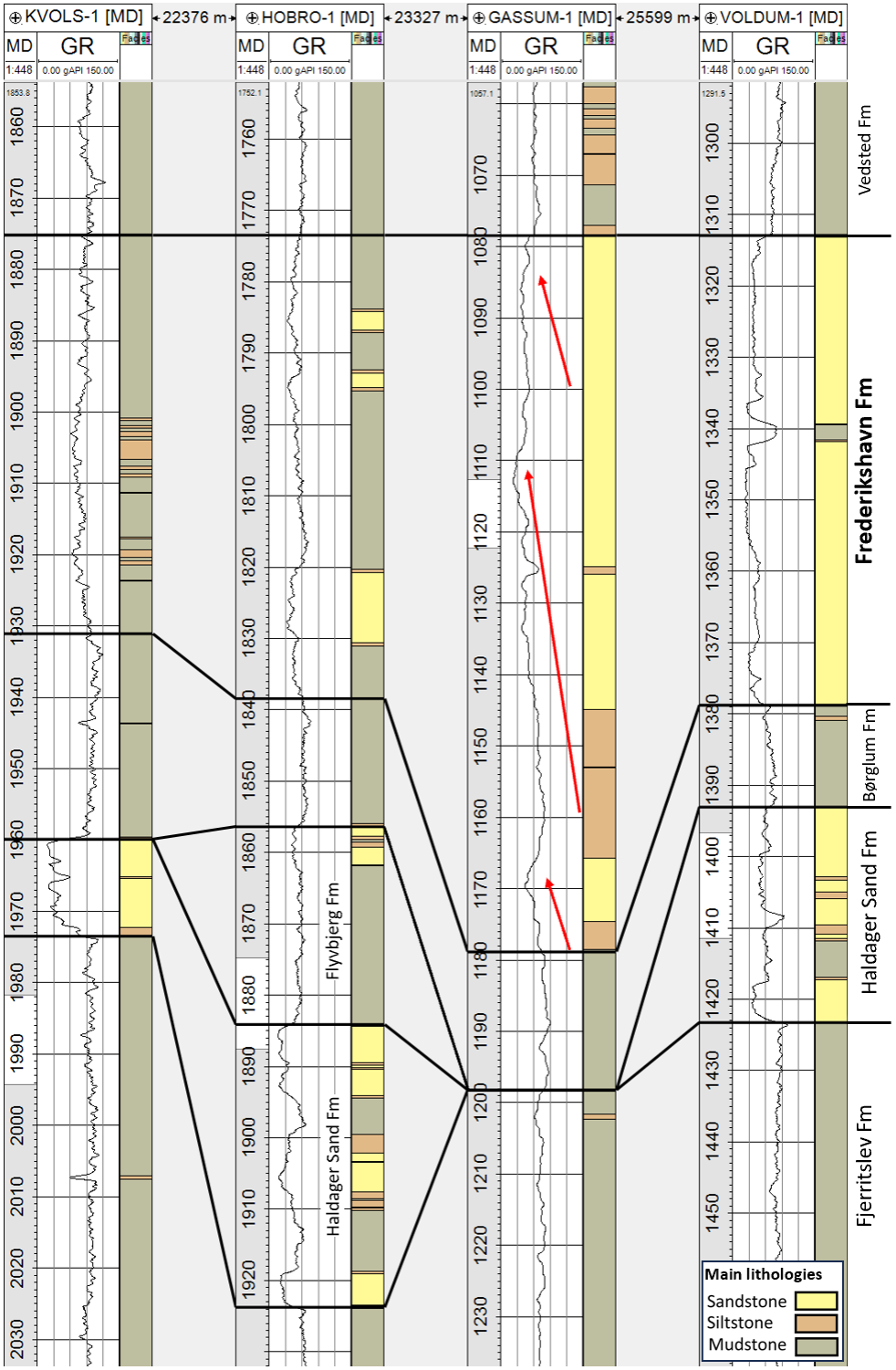


**Figure 7.1.10.** *Correlation panel focusing on the Upper Jurassic–Lower Cretaceous Frederikshavn Fm. In the Gassum-1 and Voldum-1 wells, the formation consists almost entirely of sandstones, locally with coal fragments, whereas mudstone dominate the formation towards west in the Hobro-1 and Kvovls-1 wells. The very different lithological composition of the formation may suggest a lithostratigraphic subdivision of the formation. Two to three overall coarsening-upwards successions are reflected by the GR motif of the wells (in Gassum-1 emphasized with red arrows as an example). In the Gassum-1 well these probably reflect shoreface shallowing-upwards successions, possibly related to delta progradation.*


**Figure 7.1.11.** *Core examples of the Frederikshavn Fm from the Gassum-1 well dominated by very fine-grained sandstones that are greenish grey in colour, probably due to a content of glauconite. In general, the cores are fragmented or even disintegrated, but more coherent (cemented) sections still exist. Given the state of preservation the cores may form a basis for studies of depositional environments, reservoir and seal properties including porosity, permeability, grain size, mineralogy, diagenesis. Core diameter is c. 8.5 cm.*

*Reservoir quality (porosity and permeability)*

The characteristics of the Frederikshavn Formation within the Gassum structure is primarily based on the core descriptions and measurements from the Gassum-1 well, as only a GR log was recorded in the relevant depth interval.

The GR log forms the basis for the derived $V_{shale}$ curve, with forms the basis for the classification of the lithology of the Frederikshavn Formation into mudstone, siltstone and sandstone, respectively. This interval is relatively sand-rich, with Figure 7.1.1 showing well-developed sandstones interbedded with siltstones in some intervals.

The Frederikshavn Formation is 100.0 m thick of which net reservoir sand comprise 74.4 m, making up a net to gross ratio of 0.74. From the conventional core measurements, the average porosity within this formation is calculated to be 28.7% and the average permeability is 830 mD (Table 7.1.3). Thus, it can be deducted that the Frederikshavn forms an excellent secondary reservoir within the Gassum structure.

**Table 7.1.3.** *Summarizing the reservoir characteristics of the Frederikshavn Fm within the Gassum structure, which has excellent reservoir qualities and thicknesses quantified by the transmissivity of 61.8 Dm (Darcymeter).*

| | Reservoir (m) | Net to Gross (v/v) | PHIE (%) | PERM (mD) | Transmissivity (Dm) |
|---|---|---|---|---|---|
| **Gassum-1** | 74.4 | 0.74 | 28.7 | 830 | 61.8 |

**Skagerrak Formation**

The Lower–Upper Triassic Skagerrak Formation was deposited in an arid to semi-arid climate and is present in the northern part of the Danish area and may have thicknesses of up to 5000 m (Bertelsen 1980; Liboriussen et al. 1987). The formation consists of interbedded conglomerates, sandstones, siltstones and claystones. The sediments were deposited in alluvial fans along the Fennoscandian Border Zone and in braided streams and ephemeral lakes in the more distal part of the basin towards the southwest (Pedersen & Andersen 1980; Olsen 1988; Weibel et al. 2017). In places, aeolian deposits have been identified, originating from aeolian reworking of the fluvial deposits (Pedersen & Andersen 1980). Weibel et al. (2020) describes the alluvial fan deposits as consisting of moderately to poorly sorted conglomerates, fine-grained sandstones, or siltstones, whereas the braided stream sandstones are well-sorted and fine- to medium-grained. The sandstones are dominated by subarkoses, lithic subarkoses, arkoses and smaller contents of sublitharenite, feldspatic litharenite and litharenite according to the classification of McBride (1963). Anhydrite, dolomite and limestone are encountered locally.

In the literature, the stratigraphic interval has for some wells in the Danish Basin been referred to as the Lower Triassic Bunter Sandstone Formation. This has also been the case for the interval in the Gassum-1 well (e.g., Nielsen & Japsen 1991; Pedersen & Andersen 1980). However, the very thick sandstone succession which characterize the interval in the Gassum-1 well fits well with being the Skagerrak Formation (as also suggested by Weibel et al. 2017) and do not in any way resemble the classic Bunter Sandstone Formation known from the North German Basin. Consequently, the interval is here considered as being the Skagerrak Formation. In general, the Triassic interval below the Gassum Formation has not been in much focus and would benefit from a throughout regional revision based on interpretations and compilation of well data and seismic data.

*Skagerrak Formation in the study area*

The Skagerrak Formation is present in the Gassum-1 well in the depth interval 2747–3441 m MD and is thus 694 m thick (Fig. 7.1.1). Seismic mapping shows significant thicknesses of c. 550–750 m in the structure (Chapter 6; Fig. 6.2.3B). Digital GR and SP logs only cover the formation down to a depth of c. 3068 m MD). Down to 3000 m depth the Skagerrak Formation is dominated almost entirely of clayey immature sandstones (Weibel et al. 2020; Fig. 7.1.1). Core and ditch sample descriptions in the completion report refer the sandstones as being fine and medium grained and clayey (Danish American Prospecting Co 1951).

*Reservoir quality (porosity and permeability)*

The characteristics of the Skagerrak Formation within the Gassum structure is heavily based on the core descriptions and measurements from the Gassum-1 well, as only a GR and resistivity logs were recorded in the formation.

The GR log forms the basis for the derived $V_{shale}$ curve, which forms the basis for the classification of the lithology of the Skagerrak Formation as a sandstone in its entirety. This is further supported by the cores and cuttings descriptions from the well (Danish American Prospecting Co 1951), although the comments on the plugs for the laboratory measurements indicate clayey intervals towards the base of the formation.

The Skagerrak Formation is 693.7 m thick of which logs cover the uppermost 400 m. As no logs are available for the lower approximately 300 m, the classification of the rock is based on the descriptions found in the Final Well Report, where it is stated that the entire section consists of sandstones (Danish American Prospecting Co 1951). Therefore, this lithofacies is extended throughout this formation.

Conventional core analysis forms the basis for the evaluation of the reservoir properties (e.g., porosity and permeability), and these measurements extend further down into the well than the logs.

Based on the log derived $V_{shale}$ curve and the core description, the entire Skagerrak Formation is considered to be net reservoir sand with an average porosity of 15.4% (it should be noted that the lowermost measurement at 3418 m MD reports a porosity value of 3% and this is the only data point below 3130 m MD). The corresponding average permeability is calculated to be 123 mD, which leads to a transmissivity of 85 Dm (Table 7.1.4). Therefore, the Skagerrak Formation within the Gassum structure is considered an excellent secondary reservoir.

As no of the other wells within the study area reach the Skagerrak Formation, the reservoir properties derived from the Løve-1 well are listed for comparison (Table 7.1.4). This well is located almost 100 km to the south of the Gassum-1 well and the interval is reported as the Bunter Sandstone Formation. However, it is questionable if this is correct since the interval consists of a very thick sandstone succession resembling the Skagerrak Formation further to the north and being very much different from the classic Bunter Sandstone Formation in the North German Basin. Thus, the interval lacks the characteristic depositional cycles of the Bunter Sandstone Formation consisting of ephemeral fluvial and aeolian sandstone that grade upwards into thick successions of lacustrine/playa mudstone. Consequently, it is here tentatively referred to as the 'Skagerrak equivalent'. It is 151 m thick in the Løve-1 well where the present-day depth of its top is 1800 m MD. The average log derived PHIE is 23% with a corresponding permeability of 378 mD. This also results in an excellent reservoir transmissivity of 57 Dm (Table 7.1.4).

**Table 7.1.4.** *Summarizing the reservoir characteristics of the Skagerrak Fm within the Gassum structure. The formation has excellent reservoir qualities and thicknesses quantified by the transmissivity of 85 Dm (Darcymeter). For comparison, the 'Skagerrak equivalent' in the Løve-1 well is included as no other wells within the study area reach the Skagerrak Formation.*

| | Reservoir (m) | Net to Gross (v/v) | PHIE (%) | PERM (mD) | Transmissivity (Dm) |
|---|---|---|---|---|---|
| **Gassum-1** | 693.7 | 1.0 | 15.4 | 123 | 85 |
| **Løve-1** | 151.0 | 0.59 | 23.0 | 378 | 57 |

### Risks associated with formation water composition

Understanding the significance of salt content in the context of $CO_2$ storage is important for several reasons:

- Corrosion and material selection: High salt concentrations can accelerate corrosion in the materials used for storage wells and associated infrastructure. This can lead to increased maintenance costs and potential safety risks. An accurate assessment

of salt content is crucial for selecting the right materials and designing effective corrosion protection systems.

- Scaling and operational efficiency: Salts, especially when present in high concentrations, can precipitate and form scales inside the storage reservoir and in the equipment. Scaling can reduce the efficiency of $CO_2$ injection and retrieval processes, potentially leading to operational challenges and increased costs.
- $CO_2$ solubility and storage capacity: The solubility of $CO_2$ in formation water is affected by the salinity of the water. Higher salt content typically reduces the solubility of $CO_2$, which could impact the overall storage capacity of the reservoir. Understanding the salt content helps in accurately estimating how much $CO_2$ can be stored.
- Geochemical reactions and long-term stability: Salt content can influence the geochemical reactions between $CO_2$, formation water, and reservoir rocks. These reactions are crucial for the long-term stability of stored $CO_2$. Predicting and monitoring these reactions require a thorough understanding of the formation water chemistry, including its salt content.

*Assessing the formation water chemistry in the Gassum structure*

*Background and Challenges in the Gassum Area:* In the Gassum well, a brine sample was retrieved during drilling due to uncontrolled well flow, as reported in the Final Well Report (Danish American Prospecting Co 1951, p. 324). The samples contained 180,770.0 mg/l $Cl^-$ (287,986.0 mg/l Total Dissolved Solids). Owing to the conditions under which the sample was collected, the exact depth remains uncertain but is believed to represent 'from sands logged at and below 8816 feet (2687 m, Danish American Prospecting Co 1951). Laier (2008) included this sample in his compilation, assigning it a depth of approximately 2625 m within the Ørslev Formation. We have retained this estimate while noting that the actual depth could be somewhat deeper (Table 7.1. 5).

In the vicinity of the Gassum structure, there are no additional direct measurements of formation brine chemistry, leading to uncertainties in pre-drilling evaluations. However, the composition of formation water in onshore Denmark is relatively well documented in the Danish Basin. Here, it is recognized to vary both geographically and with burial depth, as highlighted in studies by Laier (2002, 2008) and Holmslykke et al. (2019).

*Methodology for Estimating Salinity in Gassum structure*: For the assessment of formation water chemistry within the Gassum structure reservoirs, we have leveraged the established relationship between geological depth and salinity derived from the Danish Basin (Figure 7.1.12). Utilizing this methodology, we estimate that at the depth of the Frederikshavn Formation in Gassum, situated approximately at 1100 m, the formation water exhibits a chloride concentration around 98,000 mg/l $Cl^-$ (equivalent to 162,000 mg/l Total Dissolved Solids (TDS)). Within the primary reservoir of the Gassum Formation, located at roughly 1500 m, the estimated salinity reaches approximately 112,000 mg/l $Cl^-$ (185,000 mg/l TDS). Meanwhile, at the depth of the Skagerrak sandstone reservoir, around 2800 m, salinity is estimated to be approximately 201,000 mg/l $Cl^-$ (333,000 mg/l TDS), indicating that it is nearing saturation with respect to halite (cf. Holmslykke et al. 2019 for comparative calculations in the Tønder area). Further geochemical modelling will be presented elsewhere (Schovsbo et al. in preparation).

**Table 7.1.5.** *Measured and estimated salinities ($Cl^-$ and TDS) in the Gassum structure. From Schovsbo et al. (in preparation).*

| Formation | Depth (m) | Estimated Cl (mg/l) | Estimated TDS (mg/l) | Measured Cl (mg/l) | Measured TDS (mg/l) |
|---|---|---|---|---|---|
| Frederikshavn | 1100 | 97,906 | 162,132 | | |
| Gassum | 1500 | 111,691 | 184,960 | | |
| Ørslev | 2625* | | | 180,770 | 287,986 |
| Skagerrak | 2800 | 200,887 | 333,668 | | |
| * depth uncertain | | | | | |

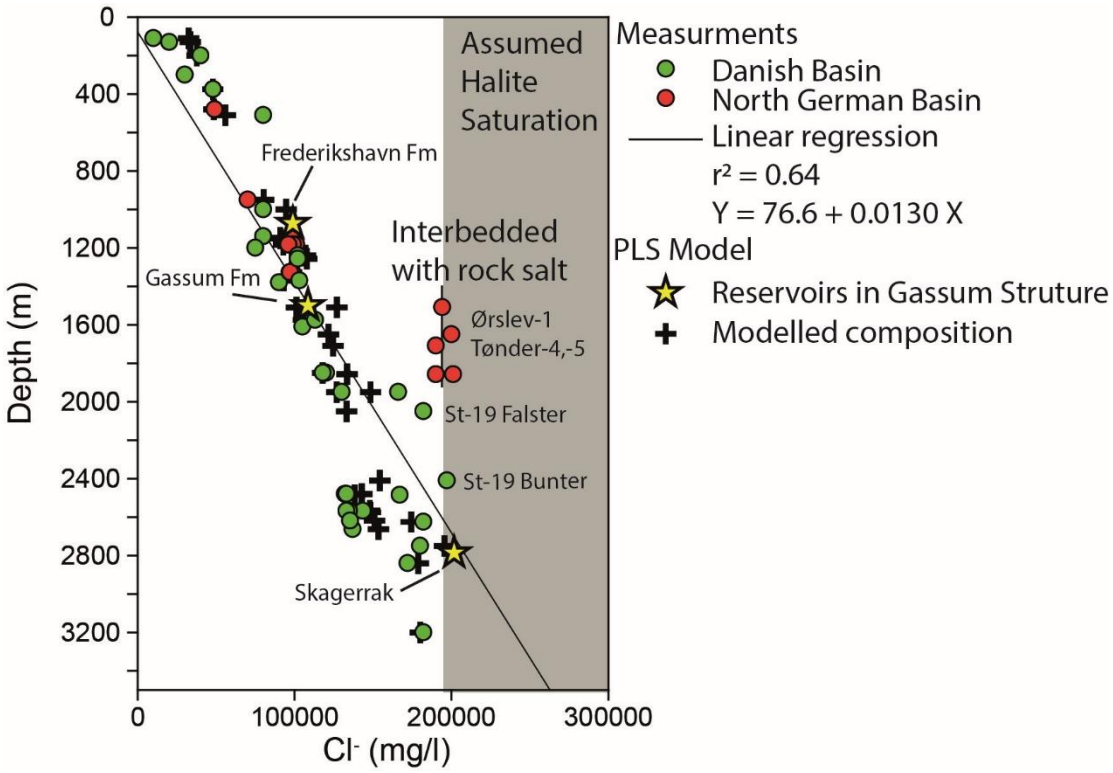


**Figure 7.1.12.** *Salinity with depth in Eastern Denmark and the Øresund Area. This figure is derived from the data compilation by Laier (2008), incorporating minor updates based on recent findings in Holmslykke et al. (2019) and the Final Well Report (Gulf Denmark 1968) from the Ørslev-1 well. Modelled salinity (PLS model) is based on a numerical analysis (Schovsbo et al. in preparation). Field of halite (NaCl) supersaturation (grey) assumes stoichiometric concentration of $Na^+$ and is loosely based on Holmslykke et al. (2019). No account for temperature and pressure effect has been made but will be made in later refinements of the model.*

## 7.2 Seals – Summary of geology and parameters

The contents of this section include the Fjerritslev Formation seal to the primary Gassum Formation reservoir, the Vedsted Formation, Rødby Formation and lower part of Chalk Group seal units to the secondary Frederikshavn Formation reservoir and finally the Ørslev Formation, Falster Formation and Tønder Formation (in part) seals to the secondary Skagerrak Formation reservoir Fig 7.2.1.

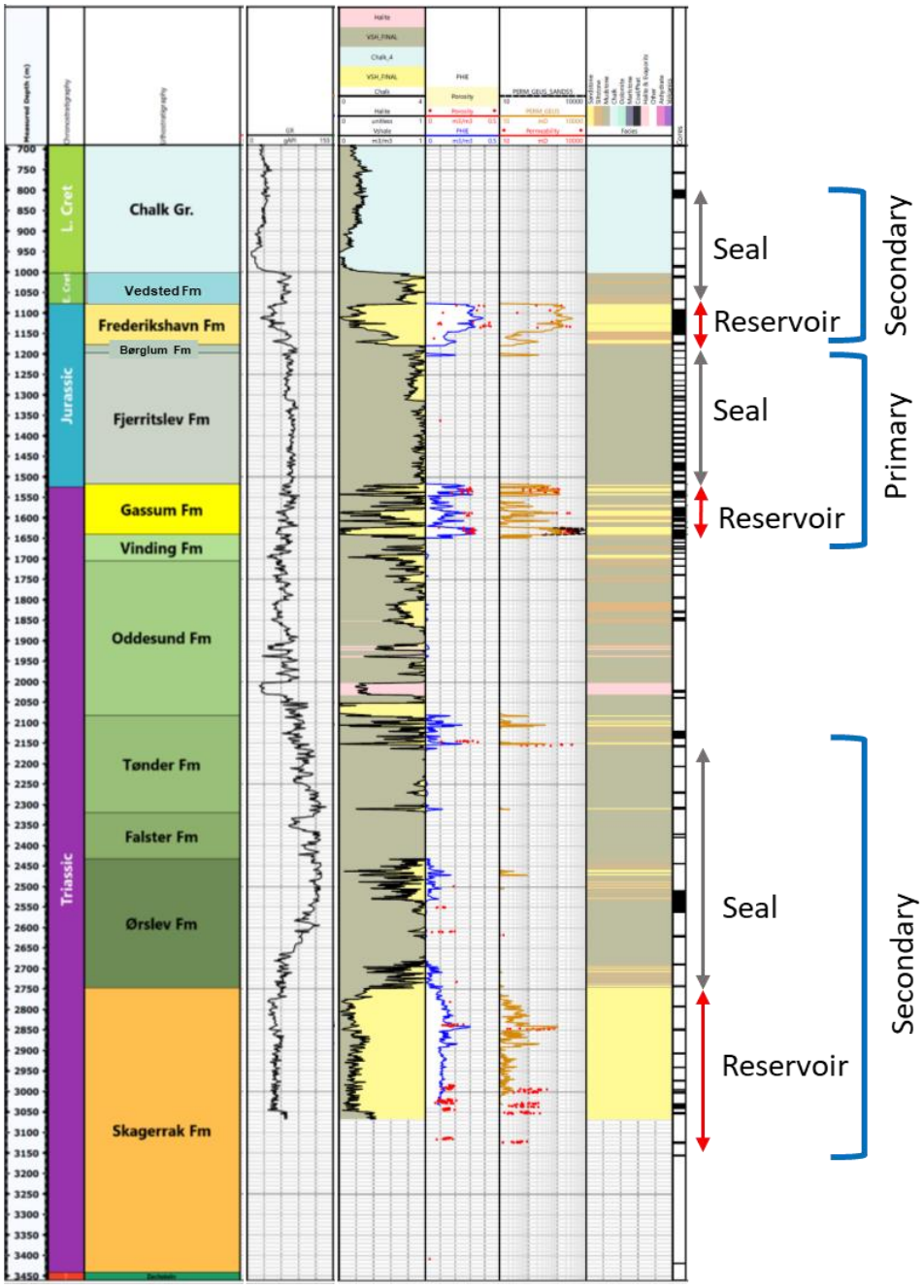


**Figure 7.2.1.** *Petrophysical logs from Gassum-1 well showing the primary reservoir–seal pair of the Gassum sandstones and the overlying Fjerritslev mudstones, succeeded by the secondary reservoir–seal pair of the Frederikshavn Fm/Vedsted Fm and the overlying Chalk Group. The secondary reservoir of the Triassic Skagerrak Fm with overlying sealing units of the Ørslev Fm, Falster Fm and Tønder Fm (in part) are also shown.*

### The primary seal of the Gassum Formation: The Fjerritslev Formation

The Lower Jurassic Fjerritslev Formation is known from more than 60 deep wells in the Danish onshore and nearshore areas. The lithostratigraphy and positions of the wells drilled before 1990 were compiled by Nielsen & Japsen (1991). The Gassum-1 well penetrates the mapped Gassum structure, and in a periphery of 30–40 km of the structure are the Kvols-1, -2A, Hobro-1 and Voldum-1 wells that are also included in the evaluation of the seal (Fig. 7.2.2), as are the detailed knowledge of the seal from the Stenlille area on Zealand hosting a gas storage facility.

The thickness of the Fjerritslev Formation is 318.5 m in the Gassum-1 well with the base situated at 1517.9 m (all depths refer to measured depth below rotary table situated 4.6 m above terrain). The seismic data show an uneven, thick formation from c. 300–350 m at the top with a suggested marked thickness increase towards the north. Abundant mapped faults occur in the top part of the Gassum structure (see Chapter 6; Fig. 6.2.3G). However, part of the significant thicknesses towards north may also be caused by wedges towards the structure of Middle–Late Jurassic formations (see discussion in Chapter 6; Fig. 6.2.5). The well data presented in Table 7.2.1 suggest a marked thickness increase to the west in Kvols-1 (450.5 m) and to the WNW in Hobro-1 (453 m).

The Gassum-1 well provides a number of short cores of the Fjerritslev Formation (Cores 32–52) but these are in general in poor condition today due to long-term storage and intensive sampling (Fig. 7.2.3). Data from the Vedsted-1 well in northern Jutland are also included regarding assessment of seal capacity.

The Fjerritslev Formation comprises a succession of marine claystones and mudstones, interbedded with subordinate thin sandstone beds. It is present in the Danish Basin, north of the Ringkøbing-Fyn High , and in the North German Basin south of the Ringkøbing-Fyn High but absent on the high itself. In the central and western part of the Danish Basin, the fluvial to shallow marine Gassum Formation is of Rhaetian (latest Triassic) age and is overlain by the Fjerritslev Formation of Early Jurassic Hettangian–Early Toarcian age (Fig. 7.1.3). In the area of the Gassum structure, the formation extends up into the earliest Jurassic. Compared to the Stenlille area, the Fjerritslev Formation is more fine-grained and contains less siltstone and sandstone layers in the Gassum structure. This suggests that the formation represents a more distal depositional setting in the Gassum area (although the drowning of the Gassum Formation took place later than in Stenlille – at TS 9 contra TS 7 in Stenlille).

The Fjerritslev Formation is unconformably overlain by Upper Jurassic (Oxfordian–Kimmeridgian) mudstones, c. 20 m thick, of the Børglum Formation that can be regarded as a secondary seal to the Gassum Formation sandstone reservoir. The Middle Jurassic and lower part of the Upper Jurassic are thus missing in the Gassum-1 well (Dybkjær 1988, 1991; Fig. 3.6, Appendix B). This hiatus expands markedly southwards along the Ringkøbing-Fyn High , were Lower Cretaceous unconformably overlies Lower Triassic sediments. Towards the north in the Sorgenfrei Tornquist Zone, Middle to Upper Jurassic strata are present in a graben structure represented by the marginal marine and terrestrial Haldager Sand Formation and Flyvbjerg Formation (Chapter 3, Michelsen 1989a, Michelsen et al. 2003, Nielsen 2003). These formations are also documented in nearby wells (Fig. 7.1.10) and it may be speculated that these formations extend laterally southwards into the northern part of the Gassum structure e.g. north of the main fault (see Chapter 6). The seismic interpretation shows that the structural evolution of the Gassum structure mainly formed due to growth of a salt pillow at the base of the structure (Chapter 6). Pulses of halokinesis affected

accumulation during the Triassic–Cenozoic and especially during deposition of the Fjerritslev Formation and onwards in the Gassum area.

*Lithological subdivision*

The Fjerritslev Formation was defined by Larsen (1966) and revised by Michelsen (1978, 1989a; Michelsen et al. 2003). The formation is subdivided into five informal members F-Ia, F-Ib, F-II, F-III, and F-IV using the Hyllebjerg-1 in northern Jutland as reference section (Michelsen 1989a). A detailed correlation between wells located centrally in the Danish Basin shows that characteristic log-patterns can be traced across long distances suggesting that the formation comprises several laterally continuous depositional units (Michelsen 1989b). The biostratigraphy of the Fjerritslev Formation in Gassum-1 shows that the formation spans the Lower Jurassic Hettangian–lower part of Toarcian based on dating by palynostratigrapy (Dybkjær 1991 and GEUS in house data). The high-resolution biostratigraphy combined with petrophysical logs patterns enables a sequence stratigraphic subdivision of the formation. The Fjerritslev Formation in the Gassum-1 well is thus represented by sequences 9 to 15 (sensu Nielsen 2003) and the informal lithostratigraphic members F-I to F-III (Appendix B). Semi regionally the same base of the Fjerritslev Formation (corresponding approximately to the transgressive surface TS 9) is recorded in Hyllebjerg-1, Kvols-1 and Hobro-1 but the stratigraphical range is expanded in some of these wells to also include the upper member F-IV and thus well into the Toarcian (Appendix B).

A sequence stratigraphic division of the Gassum and Fjerritslev formations was presented by Nielsen (2003), and the base of Fjerritslev Formation is defined at TS 7 in the central part of the Danish Basin and at the slightly younger TS 9 in the Gassum area. Only the F-Ia, F-Ib, F-II, F-III members are present in the Gassum-1 well; the boundaries between the members corresponds to sequence stratigraphic surfaces of either transgressive surfaces, recognized by prominent increases in the GR log, or sequence boundaries (Fig. 7.2.2). The sequence stratigraphic breakdown is based on updated GEUS inhouse data in the region that builds on the sequence stratigraphic framework in Nielsen (2003).

The core material represents different intervals of the Fjerritslev Formation in the Gassum-1 well (Fig. 7.2.1, Appendix A). The cores have been described and studied with regards to the bivalve composition by Pedersen (1986) and organic content (Petersen et al. 2008). The formation is characterized by mudstones and silt-streaked mudstones with subordinate layers of mottled sandy siltstones in the lower part. All facies are bioturbated and the bivalve content suggest that the mudstones were deposition in normal marine outer shelf environment (Pedersen 1986).

*The F-Ia member*

The member is 87.4 m thick in Gassum-1, and it is bounded by the sequence stratigraphic surfaces TS 9 and TS 11. It is represented by the cores 47–52 that comprise mainly very dark grey planar laminated mudstone with few thin fine sandstone laminae and is interpreted as deposited in offshore environments (Pedersen 1986). The GR log readings are relatively uniform medium–high values with subtle low GR readings e.g. associated with sequence boundaries SB 10 and SB 11 and TS 10 that may indicate the presence of thin sandstone or siltstone beds, however this has not been resolved in the petrophysical log interpretation (Fig. 7.2.2). The cored section with SB 11 shows a thin unit of sandy mudstones (Fig. 7.2.3A).

The thickness range of the member is 54.3–87.4 m in the reference wells (Fig. 7.2.2, Table 7.2.1).

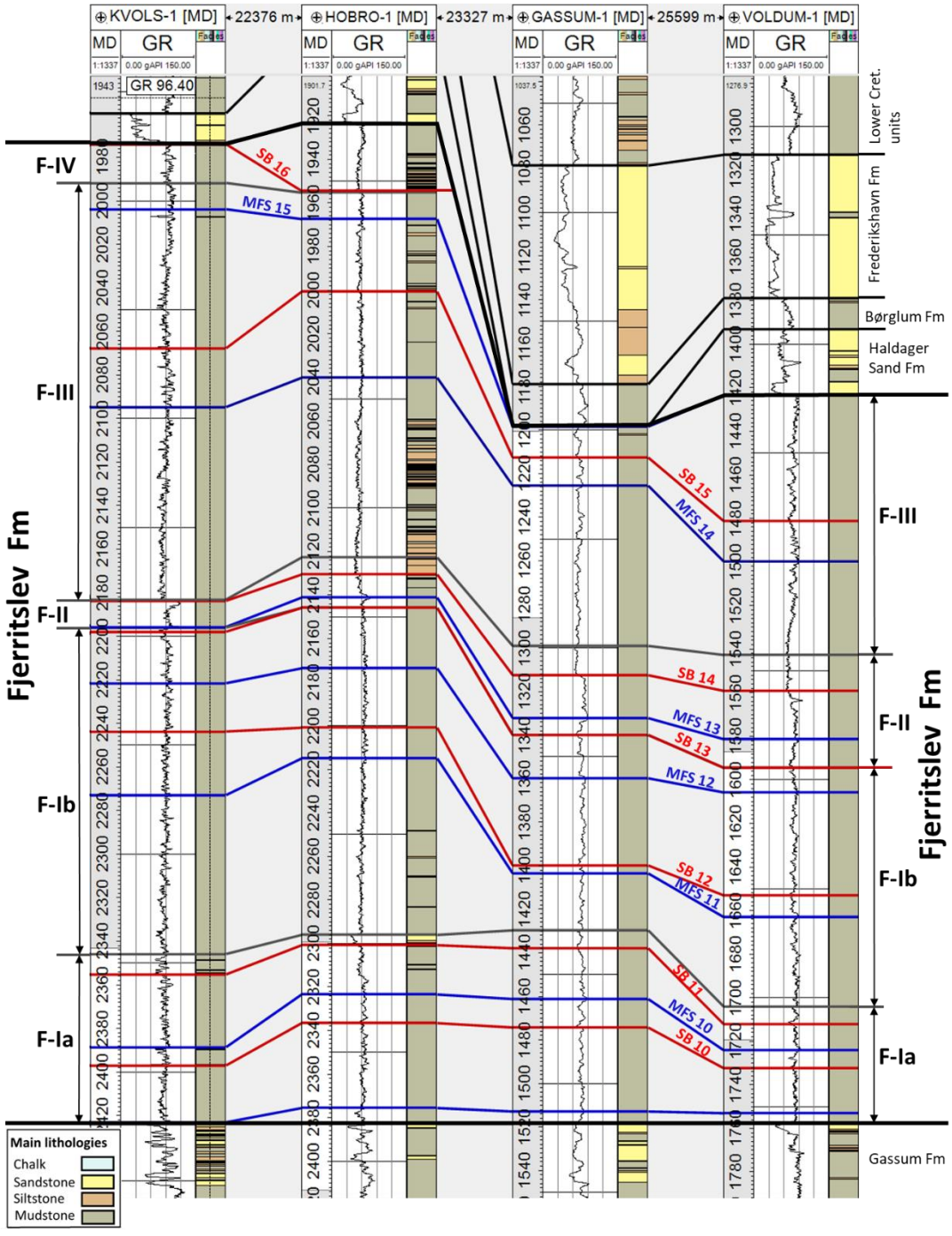


**Figure 7.2.2.** *Correlation panel focusing on the Fjerritslev Fm seal in the nearest wells to the Gassum structure. Placement of sequence stratigraphic surfaces and interpretation of depositional environments is tentative and would benefit from supplementary palynological data. The transgressive surface TS 9 represents the base of the Fjerritslev Fm in the wells and is used as datum line. Locations of wells relative to the Gassum structure are shown in Figs. 3.1 and 7.1.3.*

**Table 7.2.1.** *Thicknesses of the members of the Fjerritslev Fm in the nearest wells to the Gassum structure in the Danish Basin. *The lower boundary of the F-IV member is positioned between MFS 15 and SB 16 according to Nielsen 2003. In none of the included wells is the whole member preserved (see biostratigraphic charts in Appendix B). Hy-1, Hyllebjerg-1; Kv-1, Kvols-1; Hb-1, Hobro-1; Ga-1, Gassum-1; Vo-1, Voldum-1; Rø-1, Rønde-1; Hr-1, Horsens-1. The biostratigraphy conducted in this study is modified from Dybkjær (1991). Sequence stratigraphy and thicknesses of members partly modified after Nielsen (2003).*

| Fjerritslev Fm | | | | | | | | | | | Age |
|---|---|---|---|---|---|---|---|---|---|---|---|
| Location/wells | | | | Hy-1 | Kv-1 | Hb-1 | Ga-1 | Vo-1 | Rø-1 | Hr-1 | |
| Measured Depth (m) to | | Top Fjerritslev Fm | | 1922 | 1973.5 | 1923.7 | 1198.5 | 1423 | 2138 | 1294.4 | Toarcian |
| | | Base Fjerritslev Fm | | 2582.6 | 2424 | 2376.7 | 1517 | 1758.4 | 2613 | 1533.8 | L. Rhaetian–E. Sinemurian |
| | | Thickness (m) | | 660.6 | 450.5 | 453 | 318.5 | 335.4 | 475 | 239.4 | |
| | | Sequence stratigraphy | | Thickness (m) | | | | | | | |
| | | Lower boundary | Upper boundary | | | | | | | | |
| Lithostratigraphy | F-IV mb* | SB 16 | SB 19 | 55 | 18.5 | 31.3 | None | None | 38 | None | Middle Toarcian–E. Aalenian |
| | F-III mb | TS 14 | SB 16* | 228 | 191 | 167.6 | 100.6 | 119.6 | 145 | | Early–Middle Toarcian |
| | F-II mb | SB 13 | TS 14 | 86.6 | 13 | 23.2 | 40.8 | 51.8 | 73 | 21.9 | Pliensbachian |
| | F-Ib mb | TS 11 | SB 13 | 210.3 | 149.9 | 150.1 | 89.7 | 109.7 | 141 | 136,4 | Sinemurian–E. Pliensbachian |
| | F-Ia mb | TS 7 / TS 9 | TS 11 | 80.7 | 78.1 | 80.8 | 87.4 | 54.3 | 64 | 83 | Rhaetian–Hettangian |

*The F-Ib member*

The member is 89.7 m thick in Gassum-1, and it is bounded by the sequence stratigraphic surfaces TS 11 and SB 13. It is represented by the cores 41–46 that like the cores of the F-Ia member also comprise mainly very dark grey mudstones with few thin fine sandstone laminae that are interpreted as deposited in an offshore environment (Pedersen 1986). The GR log readings are relatively uniform medium–high values with few subtle low GR readings e.g. associated with the sequence boundary SB 12 that may indicate the presence of thin sandstones or siltstones, however this has not been observed in the cored sections. Based on the well log correlation panel, the thickness range of the member is 89.7– 210.3 m (Fig. 7.2.2, Table 7.2.1).


**Figure 7.2.3.** *Core photos of the Fjerritslev Fm, Gassum-1 well. (A) F-Ia mb, Hettangian–Sinemurian transition. The SB 11 is present in sandy grey mudstones in the lower part of the core and is overlain by very dark grey mudstones. Core 47, 4702–4722' (c.1433–1439 m). (B) F-III mb, Pliensbachian. Grey bioturbated silty mudstones, sequence 14. Core 33, 4016–4021' (c.1224–1226 m). (C) F-III mb, Toarcian. Grey bioturbated silty mudstones above SB 15. Core 32, 3967–3972' (c.1209–1211 m). (D) Børglum Fm, Oxfordian–Kimmeridgian. Greenish grey and reddish mudstones indicating diagenetic overprinting due to subaerial weathering. Core 31, 3903–3914', (c.1190–1193 m). Note the general poor core conditions, core diameter 8.5 cm. Core depths may differ from log depths, see Nielsen (2003, Fig. 13).*

*The F-II member*

The member is 40.8 m thick in Gassum-1, and it is bounded by the sequence stratigraphic surfaces SB 13 and TS 14. It is represented by the cores 38–40 that comprise very dark grey mudstones commonly laminated with few thin fine sandstone laminae. It is interpreted to represent deposition in an oxygen deficient offshore environment (Pedersen 1986). The GR log readings show a relatively low amplitude peak at SB 13 indicating minor increase in fine sand and silt constituents. An interval with prominent high GR readings is present from MFS 13 to SB 14. The interval correlates with a relatively high organic content as measured on the ditch cuttings samples (Fig. 7.2.5). The high organic content in the unit is recognized regionally, especially in the northern part of Jutland (Nielsen 2003). The member shows a thickness of 13–86.6 m in the reference wells (Table 7.2.1). In northern Jutland, the F-II

member is characterized by influx of sand and silt, which resulted in deposition of a heterolithic mudstone and sandstone unit that is recognized in the Hobro-1 well and wells situated further north towards the basin margin. But this is not the case in the Gassum area, where the member is characterized by mudstones.

*The F-III member*

The member is 100.6 m thick in Gassum-1, and it is bounded by the sequence stratigraphic surface TS 14 at the base and at the top it is unconformably overlain by the Upper Jurassic Børglum Formation. The youngest sequence stratigraphic surface of the Fjerritslev Formation that is recognized in Gassum-1 is TS 15. The F-III member is represented by the cores 32–37 that comprise dark grey mudstones with few thin fine sandstone laminae. It is interpreted to reflect deposition in an oxygen deficient offshore environment as also indicated by a lack of benthic fauna (Pedersen 1986). Towards the north, in Hobro-1, the lower part of the member is characterized by an increase of thin siltstone and sandstone beds. The GR log readings show a minor low amplitude peak at SB 13 indicating a moderate increase in fine sand and silt, but otherwise the unit has relatively uniform medium to high GR readings with an upward slightly increasing trend. Based on the reference wells the member is 167.6–228 m thick when overlain by the F-IV member. In general, the thickness decreases southwards, and the member is not present in the Horsens-1 well.

*The F-IV member*

The F-IV member is not present in Gassum-1, but it is recorded towards the northwest and east with thicknesses of 18.5–55 m (Table 7.2.1). Palynomorphs from the F-IV member indicate that deposition of marine mud continued into the Toarcian (Dybkjær 1991). The unconformity on top of the Fjerritslev Formation in the Gassum structure may have been caused partly by uplift and erosion due to growth of the Gassum salt pillow, and partly by regional mid Jurassic uplift as recognized for e.g. the salt pillow structures of Stenlille and Havnsø (Gregersen et al. 2023). The mid Jurassic uplift and erosion with expanded hiatus along the Ringkøbing-Fyn High is well documented by Nielsen & Japsen (1991) and Nielsen (2003) (Fig. 3.6).

*Bulk mineralogy*

The bulk mineralogy of the Fjerritslev Formation mudstones has not been studied in detail from the Gassum-1 cores. Data from 10 cutting samples in the relative nearby Kvols-1 and Kvols-2A, show that quartz is the dominant mineral in all samples with little or minor amounts of kaolinite and illite or mica and calcite (Vosgerau et al. 2016). Pyrite occurs in small or trace amounts. Feldspars, siderite and ankerite may occur in trace amounts. Calcite, siderite or pyrite are present in some samples, mainly in the mudstones. Mbia et al. (2014) presented petrophysical and mineralogical data from the Vedsted-1 and Stenlille-2 wells. The total clay content is less than 50 (wt%) and dominated by illite.

*Clay minerals*

The clay fraction of the Fjerritslev Formation mudstones in Kvols-1 and Kvols-2A generally ranges between 42 and 46 (wt%) and accordingly the silt–very fine sand fraction ranges between 54–58 (wt%) (Vosgerau et al. 2016). A single outlier analysis shows a clay content of 26%. The clay mineral assemblages record kaolinite with 35–39 (wt%), vermiculite and mixed layer minerals with 45–49 (wt%) and illte, mica with 10–14 (wt%).

*Burial and exhumation*

Vitrinite reflectance (VR) values increase with increasing temperature and are thus a proxy for maximum burial depth in undisturbed sedimentary successions. The process is irreversible, and the VR values therefore always record the maximum temperature the organic matter has experienced. Petersen et al. (2008) measured 560 vitrinite reflectance values in samples from 26 wells in the Norwegian–Danish Basin and showed that 25 of these had too high VR values compared to present-day depth due to a significant post Early Cretaceous uplift in most of the basin. The Gassum-1 well shows VR values from 0.49–0.52% in the F-Ia and F-III members of the Fjerritslev Formation in the depth interval from 1231–1480 m corresponding to a net-exhumation magnitude of 579 m based on chalk sonic velocity data (Japsen et al. 2007). This suggests a corrected maximum burial depth of c. 2570 m of the Fjerritslev Formation. This burial depth may be considered when the capacity and quality of the Fjerritslev seal is evaluated.

*Characterization of the Fjerritslev Formation seal in Gassum-1*

Schovsbo and Petersen (2024) have reported new data from the Gassum-1 well relevant for seal evaluation. The relevant parts of their report are presented here to complement the description of the sealing section in the Gassum structure. Element concentrations using Handheld XRF (HH-XRF) were determined from 30 cuttings samples, and 8 cuttings were imaged from this well, covering the range between 1193–1661 m, which encompasses the Fjerritslev, Gassum and Vinding formations.

The cuttings from the Fjerritslev Formation display a high degree of colour variability, including reddish, yellow, white, and different shades of grey and greenish (Fig. 7.2.4)**.** This range is somewhat broader than what is typically expected for the Fjerritslev Formation and may indicate that the cuttings samples could have been mixed by cavings or that other processes were involved, leading to a preferential concentration of hardened and/or cemented parts of the formation.

The natural radioactive elements in the Gassum-1 well cuttings are generally determined to be below the level of detection from the HH-XRF determination, resulting in a calculated spectral gamma-ray (SGR) from HH-XRF determination that is very low compared to the recorded gamma-ray (GR) log in the well (Figure 7.2.5). The SGR_max, where the maximum API value is estimated, is much higher but lacks the GR motif shown by the GR log measured in the borehole. From below 1450 m, the alignment between the GR log curve and the SGR_max appears to be reasonably good. However, it seems that no section in the well have a good match between cuttings chemistry and the in-situ radioactivity. The overall impression is thus that the lithologies of the cuttings is biased compared to the subsurface, being less radiogenic in the main part of the Fjerritslev and more radiogenic and clay-rich in the Gassum Formation than expected based on the GR log. Unfortunately, for this well, the

GR log was the only measurement made, thus no further information is available for comparison. It should also be noted that the GR log in the well is of general poor quality.

The Al and Si/Al curves more closely resemble the GR log curve, although the choice of display scales significantly influences the visual impression of the 'correlation' (Figure 7.2.5). Thus, it seems reasonable to utilize this curve and the key elements normalized to Al, i.e., Si/Al and K/Al, to evaluate the properties.

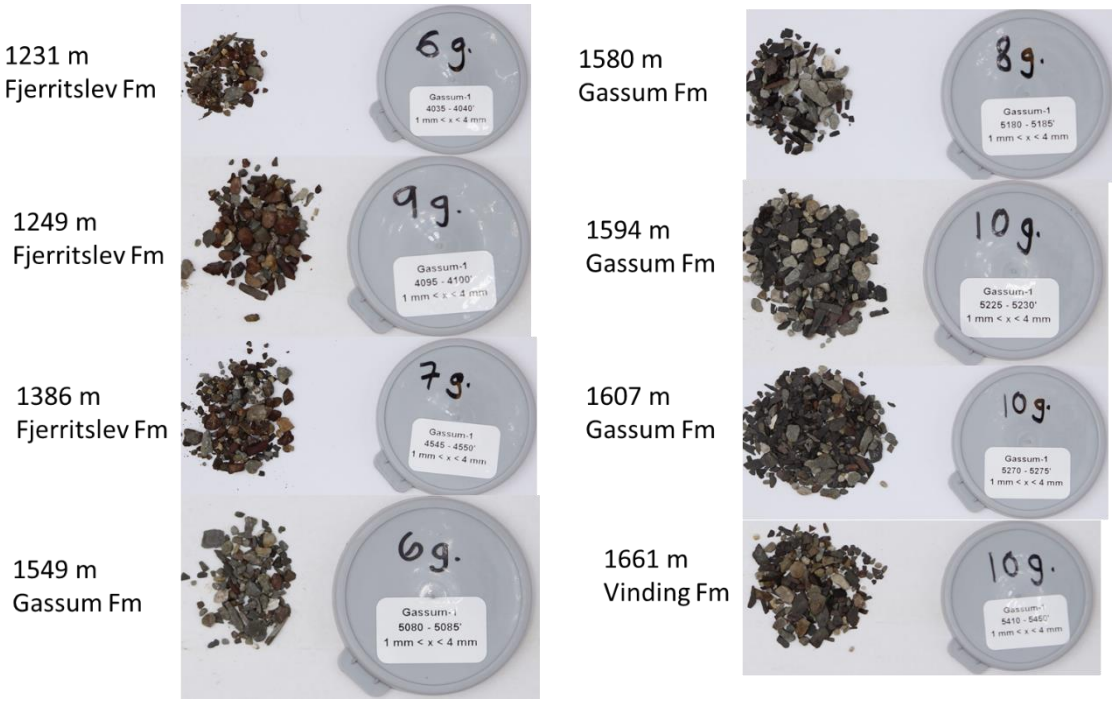


**Figure 7.2.4.** *Cuttings samples pictures from the Gassum-1 well. Grey lids shown to the right have a diameter of 45 mm.*

The K/Al ratio in the Gassum and Fjerritslev formations is approximately 0.3 to 0.4, similar to what is measured in other sections of the Fjerritslev Formation, such as Vedsted-1, J-1X, and Fjerritslev-2 (c.f. Schovsbo and Petersen 2024). The Si/Al ratio ranges between 2–5, which is also consistent with other wells penetrating the Fjerritslev Formation, indicating that the Gassum-1 well section through the Fjerritslev is expected to have similar properties as observed in other wells. However, the generally poor quality of the cuttings from Gassum-1 limits the comparisons that can be made. Future studies on this well are recommended to be based on cored sections.

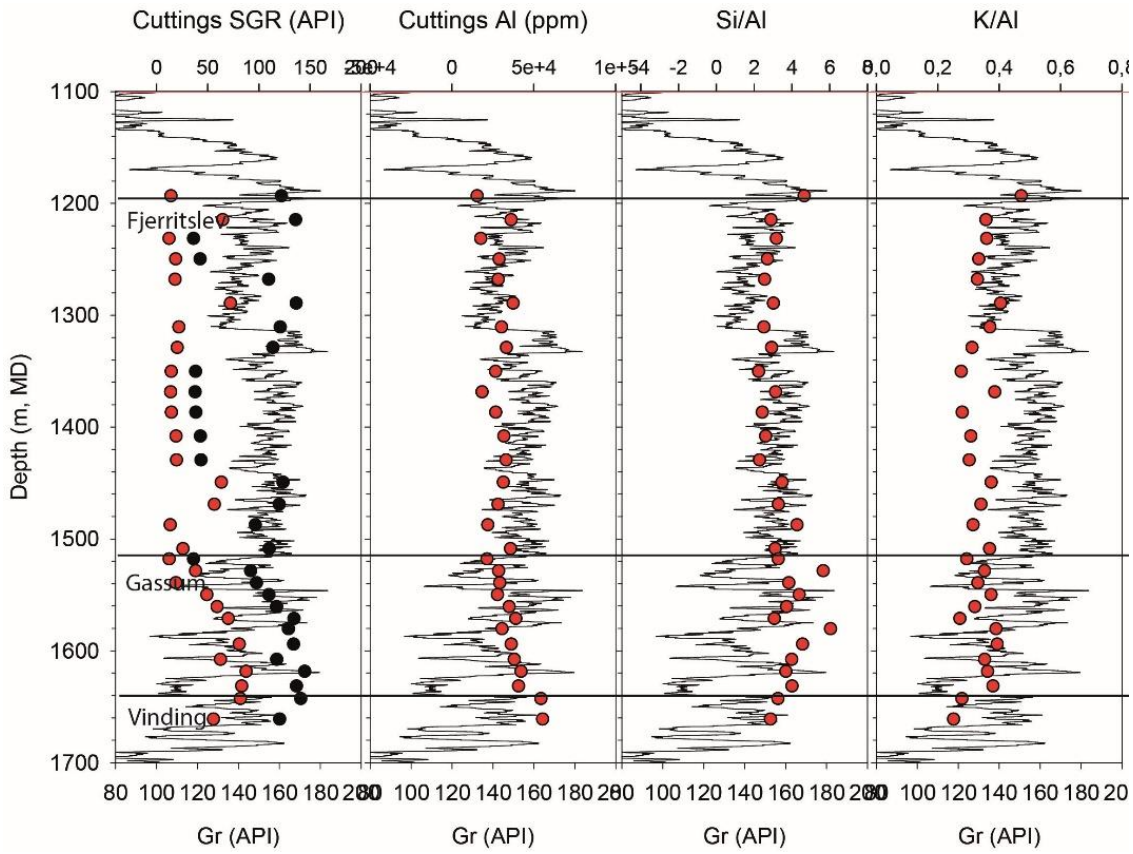


**Figure 7.2.5.** *GR log curve and API values calculated from cuttings samples based on HH XRF data (Red is SGR and black is SGR_maks), Al Si/Al, K/Al ratio from the Gassum-1 well.*

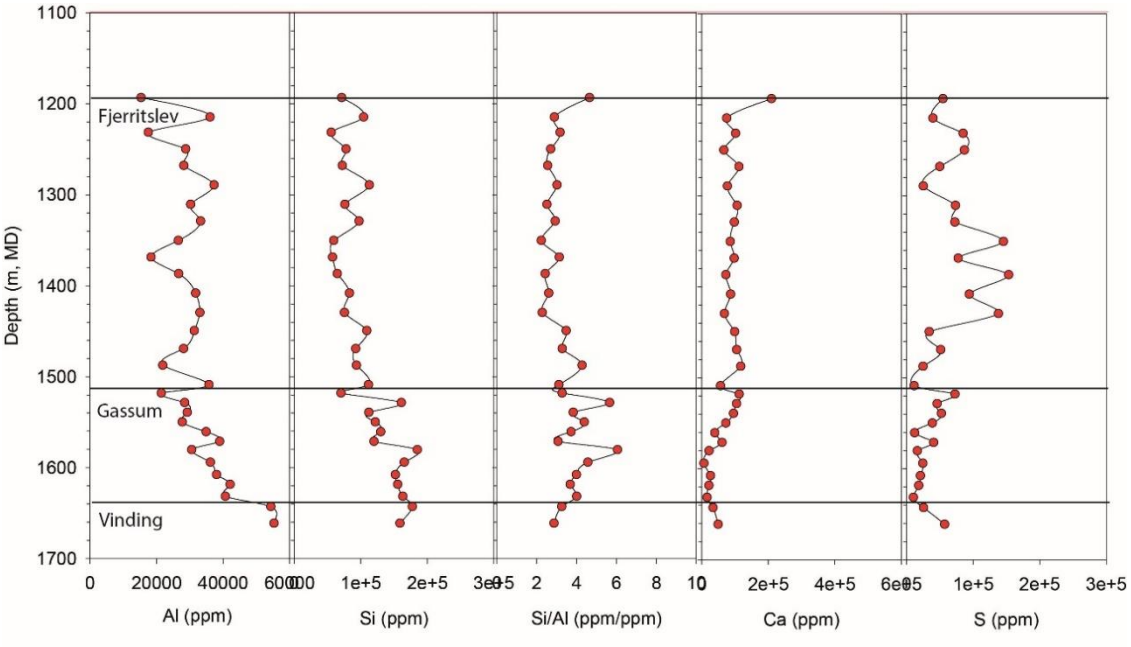


**Figure 7.2.6.** *Elemental logs of Al, Si, the Si/Al ratio, Ca and S from the Gassum-1 well.*

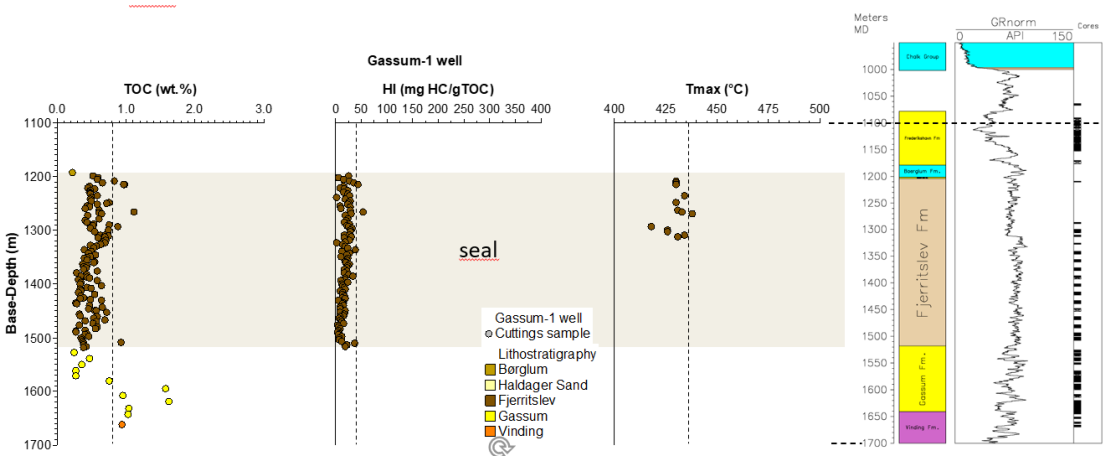


**Figure 7.2.7.** *TOC, HI and Tmax profiles in the Gassum-1 well.*

*Seal capacity of the Fjerritslev Formation*

The technical reports on the seal capacity of the Fjerritslev Formation, as investigated by Springer et al. (2020) and Gregersen et al. (2023), highlights its significant potential for sealing, particularly in the context of $CO_2$ storage. The Fjerritslev Formation, investigated primarily in the Stenlille area, features here a seal succession approximately 250–300 m thick, characterized mainly by mudstones but with interbedded porous, thin sandy and silty layers especially within the F-Ia member but also in the overlying members F-Ib–F-IV. Key findings for the seal include an average porosity of 11%, air-permeability of 160 µD, and liquid permeability reaching 3 nD – comparable to the best-known petroleum caprocks. Additional overburden measurements indicated liquid permeabilities around 200 nD, underscoring the formation's excellent seal quality, which has been validated by over 30 years of natural gas storage in the underlying Gassum Formation.

Capillary entry pressure, a critical factor for assessing seal capacity, was assessed from Mercury Injection Capillary Pressure (MICP) experiments. Despite the challenges in converting results from the mercury/air system to the $CO_2$/brine system, due to differences in contact angle and interfacial tension, standard conversion values suggest capillary entry pressures ranging from 5–10 MPa, with newer samples indicating a lower range of 1–5 MPa. The buoyancy force exerted by the $CO_2$ on the caprock, influenced by the density difference between formation water and injected $CO_2$, dictates the seal capacity for $CO_2$ storage. Estimations show that the caprock capillary system can support $CO_2$ column heights ranging from approximately 290 m to over 1000 m. Although site specific data from the Fjerritslev Formation in the Gassum area are needed, the comparison to Stenlille area suggests its excellence as a primary seal for the Gassum Formation, possessing potential robust sealing capabilities here also.

*Comparison between the Gassum-1 and Vedsted-1 wells*

No HH-XRF data have been collected from the Stenlille wells, from which the good seal properties cited above have been established. However, similar good seal properties have been measured in the Vedsted-1 well (Mbia et al. 2014), as also noted by Springer et al. (2020) in their review. The cuttings chemistry in the Gassum-1 well appears to be similar to

that of the Vedsted-1 well, and it seems reasonable to suggest, as a first approximation, that the Gassum-1 well likely share similar good seal properties as in Vedsted-1 considering their position in the basin with the Gasum-1 being located more centrally at a larger distance to the basin margin.

The clay content in the Vedsted-1 well ranges between 40–45% within the 1350–1745 m interval (7 samples) studied by Mbia et al. (2014). This interval exhibits a Si/Al ratio of 4 and an Al content of about 4000 ppm or slightly higher. Smectite and kaolinite may constitute up to 50% of the clay volume in Vedsted-1, a significant portion of which will go undetected by the GR curve, as these clay types are non-radioactive due to their lack of potassium (K), thorium (Th), and uranium (U) – although smectite might potentially include surface-bound U. A similar K/Al trend, as observed in Vedsted-1, can also be seen in the Gassum-1 well, suggesting that a similar clay mineral assemblage is likely present here.

### Recommendations for further studies on seal capacity

Site-specific studies on the seal capacity are needed for all structures to be matured towards $CO_2$ storage. For the Gassum structure, no site-specific studies exist presently for the sealing units and the need to establish fundamental knowledge of the seal properties is very high. For the Fjerritslev Formation we can draw parallels to the better-known Fjerritslev Formation in the Stenlille area and the Vedsted-1 sample set as a basis for the evaluation, but we cannot safely rely on the representation of these. For the younger secondary sealing units in the Gassum structure no analytical data exist on the seal capacity.

In Figure 7.2.8, a workflow to establish the fundamental seal information is outlined. In this workflow, the studies conducted here, i.e., HH-XRF, cuttings imaging, and TOC and Rock Eval analysis, form only part of the screening data that needs to be gathered. Other important high-volume samples include porosity, surface area determination, mineralogy, and clay type determination combined with grain size analysis. Once established, selection for more costly but crucial analyses such as pore size distribution and capillary entry pressures, as well as petrographic and microfacies descriptions, is advised.

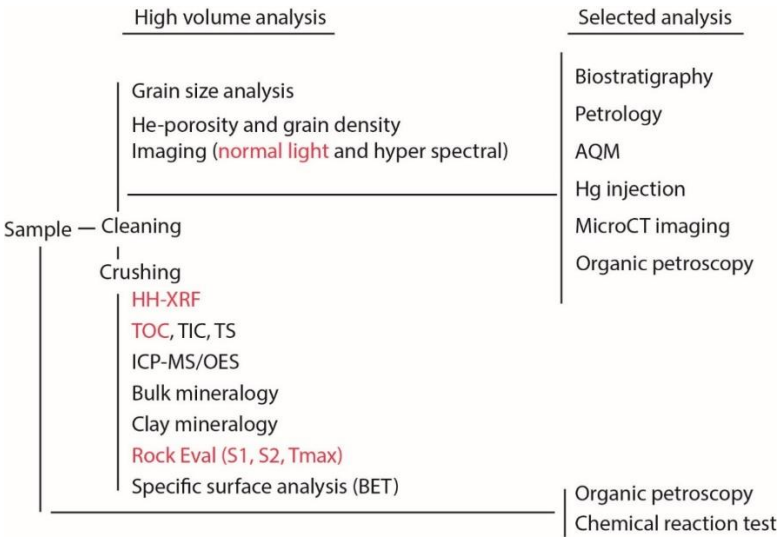


**Figure 7.2.8.** *Workflow for seal and reservoir characterisation. In red are methods applied here. Based on Schovsbo & Petersen (2024).*

### Secondary seals of the Gassum Formation: The Børglum Formation

The Børglum Formation may represent an additional or secondary seal unit to the Gassum Formation. It is 20 m thick in Gassum-1 (1178–1198 m) and is dominated by dark grey, sandy mudstones. The core 31, from 1193–1189 m, is represented by hard, greenish grey claystones with shining, conchoidal fractures. Irregular patches of deep red and purple colours may indicate a subaerial induced weathering horizon (Fig. 7.2.3D; Norwood et al. 1951; Larsen 1966). This fits not well with the typical marine mudstones of the Børglum Formation, as discussed introductory wise in this chapter, and possibly the basal part of the interval shall be assigned to the Middle Jurassic Haldager Sand Formation.

The Børglum Formation is Oxfordian–Kimmeridgian in age revealing an unconformable lower boundary to the Lower Jurassic Fjerritslev Formation in the Gassum-1 well. It is however possible that the potential reservoirs of the Haldager Sand Formation and Flyvbjerg Formation are present in the northern part of the Gassum structure (see Chapter 6), and in this case the Børglum Formation will be a seal to these units (Mathiesen et al. 2022). The Børglum Formation represents a relatively condensed interval in the Gassum area where it shows a minor thickness decrease towards the east (e.g., 13 m in Voldum-1, Fig 7.2.2) and a general thickness increase towards the NW and W (e.g., 29 m in Kvols-1). The formation represents generally offshore muddy depositional environments, and it interdigitates in the upper part with shallow marine sandstones of the Frederikshavn Formation towards the North and Northeast (Michelsen et al. 2003). In Gassum-1, the upper boundary of the Børglum Formation is suggested conformable and overlain by sandstones of the Frederikshavn Formation of Kimmeridgian–Valanginian age (Dybkjær 1991; Appendix B). No data exists on seal performance and integrity of the Børglum Formation onshore Denmark (Mathiesen et al. 2022).

### Seals of the Frederikshavn Formation: The Vedsted Formation, Rødby Formation and lower part of the Chalk Group

Sealing units of the Frederikshavn Formation reservoir (uppermost Jurassic–Lower Cretaceous) in the Gassum area comprise overlying mudstones of the Vedsted Formation and potentially; mudstones of the Rødby Formation and tight carbonates in lower part of the Chalk Group (Fig 7.2.1; Mathiesen et al. 2022). The seismic data between the mapped Top Frederikshavn Formation and base Chalk Group show a general uniform thickness across the Gassum structure and a thickness increase towards the northwest. The marine mudstones of the Vedsted Formation are considered as the main sealing unit with a thickness of 76.5 m recorded on the Gassum-1 well. The Rødby Formation is not recorded in the Gassum-1 well, but it is present in the nearest wells (distance of 30–40 km) to the north and to the west with thicknesses of up to 20 m (Fig. 7.2.9). The Chalk Group is >950 m thick in the area but only the deepest 200 m of the group is considered as part of the potential sealing (i.e. deeper than 800 m). The Chalk Group is overlain by 30 m of Quaternary deposits in Gassum-1. The seal performance to the Frederikshavn Formation reservoir onshore Denmark is essentially unknown (Mathiesen et al. 2022).

*Stratigraphic framework*

The Vedsted Formation in the Danish Basin spans the Valanginian to Albian. The lower boundary of the Vedsted Formation coincides with the transition from marine silty claystones

to less silty claystones in the central part of the Danish Basin (e.g., in Hyllebjerg-1; Michelsen et al. 2003; Larsen 1966). The Rødby Formation, which overlies or in some places are lateral transitional to the upper part of the Vedsted Formation, consists of marine red marlstones and marly chalks. Its base is suggested to be late Aptian or early Albian in age in the Danish Basin based on foraminifers and ammonites (Sorgenfrei and Buch 1964) and its upper boundary with the Late Cretaceous Chalk Group is late Albian to early Cenomanian in age (Lauridsen et al. 2022; Jensen et al. 1986). Mudstones and carbonate beds forming the upper part of the Vedsted Formation and the overlying Rødby Formation were deposited in a mixed siliciclastic-calcareous depositional system indicating lowstands when marly chalk and marl dominated deposition, and highstands when pure chalk was deposited (Ineson 1993; Ineson et al. 1997, 2022). Onset of pelagic carbonate production started in the late Early Cretaceous (Late Albian) and dominated the depositional environment in the Danish Basin from the Early Cenomanian. In the Lavø-1 well, the siliciclastic sedimentation continued into the Early Cenomanian. The Late Cretaceous (Cenomanian)–Danian Chalk Group represents deposition dominated by pelagic chalk. The Cenomanian–Campanian part represents an overall transgression in the region.

The Lower Cretaceous Vedsted Formation varies in thickness from a maximum of 700 m in the Fjerritslev Trough in the northern Danish Basin to around 50 m or less in the eastern and southeastern parts of Denmark (e.g., in the Slagelse-1 and Stenlille-1 wells where less than 23 m and 42 m, respectively, of Lower Cretaceous strata are preserved). A recent core study on parts of the Vedsted Formation in the Vinding-1 well in central western Jutland presents the vertical lithological variation in the formation and a revised biostratigraphic breakdown of the Lower Cretaceous. The study indicates the presence of several unconformities and condensed intervals in the sedimentary record (Lauridsen et al. 2022). The Vinding-1 well is located 85 km to the southwest of the Gassum structure in the southern part of the Danish Basin and the Vedsted Formation is here about 190 m thick. In the Gassum-1 well this discontinuous sedimentation pattern can be seen in the Lower Cretaceous where new nannofossil biostratigraphic data confirm the presence of Early Hauterivian, nannofossil subzone BC8a (core 18) and middle Barremian, Zone BC15 (core 17) deposits. Core 16 is dated as Late Cenomanian (subzones UC2c-3b) and the strata in between cores 16 and 17 may represent the Rødby Formation. However, more biostratigraphic work on cuttings samples is needed to confirm if the Rødby Formation is present. The undated Lower Cretaceous interval in the Gassum-1 well spans less than 20 m, that may indicate the presence of discontinuous or condensed sedimentary units in the upper part of the Lower Cretaceous succession in the Gassum area. Evidence of erosion and condensed sections are most pronounced along the basin margins (e.g., only around 15 m of Lower Cretaceous strata is preserved in the Ullerslev-1 well drilled on the Ringkøbing-Fyn High, RFH). The RFH remained an uplifted landmass from the Middle Jurassic to Early Cretaceous and formed the southern border of the Danish Basin (Michelsen et al. 2003).

The Lower Cretaceous successions in northern Jutland, in the central parts of the Danish Basin (encountered e.g. in the Hyllebjerg-1, Fjerritslev-2, Haldager-1, and Vedsted-1 wells) are all thicker than 400 m and reflect significant accommodation space for deposition. In contrast, the successions in the wells on the Stenlille structure and the Slagelse-1, Horsens-1 and Vinding-1 wells are thinner, reflecting less accommodation space along the basin margin. The seismic mapping of the Gassum area indicates that the composite thickness of the Lower Cretaceous Vedsted Formation (between Top Frederikshavn Formation and Base Chalk) is uneven, thick, between c. 50–150 m (thinnest at the top of the structure Figs. 6.2.3I,

7.1.6) and thus comparable to the thickness on the Stenlille and Havnsø structures (Gregersen et al. 2022, 2023).

The upper boundary of the Lower Cretaceous with the Upper Cretaceous Chalk Group is considered to be transitional, and the lower part of the Chalk Group is characterised by the presence of numerous marl layers in the lower 200–300 m.

*The Vedsted Formation in the Gassum area*

The Vedsted Formation is represented by cores 17 and 18 in the Gassum-1 well and in sidewall cores from the Kvols-1, Hobro-1, Hyllebjerg-1 and Voldum-1 wells (Table 7.2.2). In the Gassum-1 well, the Vedsted Formation has a thickness of 76.5 m. The Vedsted Formation in the other wells varies from 66 to 292 m in thickness (Table 7.2.3, Fig. 7.2.9). In the Hyllebjerg-1 well, the thick Vedsted Formation (292 m) is dated as Valanginian–Albian in age using foraminifera from cuttings and sidewall cores and is described as dark grey to black, brown, and green mudstone with calcareous intervals. The Hyllebjerg-1 well therefore possibly represents a distal depositional environment. Focus here is on core data from the Gassum-1 well. Cores 17 and 18 from the Vedsted Formation are unfortunately very fragmented (Fig. 7.2.10).

The boundary between the Frederikshavn Formation and the Vedsted Formation is based on the marked upwards increase on the gamma ray log indicating a change from sandstone to mudstone. The lower part of the Vedsted Formation, present in core 18, comprises grey to dark grey, medium hard to hard, sandy, and calcareous mudstone with fossil remains of bivalves, gastropods, belemnites and fish scales (Fig. 7.2.10A). It has been dated based on the nannofossils as early Hauterivian (Zone BC8a) confirming a previous dating based on poorly preserved ammonites (Sorgenfrei & Buch 1964). The upper part of the formation is present in core 17 and comprises homogenous, calcareous, dark, pyrite rich, hard mudstone (Fig. 7.2.10B). Fossil remains include ammonites, gastropods, bivalve and fish debris. This upper part was previously dated as Aptian but is revised here to the middle Barremian (Zone BC15) based on nannofossil biostratigraphy. The carbonate content of the Vedsted Formation generally increases upwards.

*The Rødby Formation in the Gassum area*

The Rødby Formation (Late Aptian to Early Cenomanian) is not cored in the Gassum area and therefore is not defined with certainty (Table 7.2.3). However, based on petrophysical logs and vintage biostratigraphy of cutting samples in the completion reports suggest presence of the Rødby Formation in wells west and north of the Gassum structure (Figure 7.2.9, Table 7.2.3). The Rødby Formation is thus between 2 m (Hyllebjerg-1) and 14 m (Kvols-1 well) thick. In the Hyllebjerg-1, Hobro-1 and Kvols-1 wells the formation is described as dark grey, green, red, black calcareous mudstones. In Hyllebjerg-1 occasionally thin beds of sandstone occur.

In the Gassum-1 well, the Rødby Formation is not identified with certainty since vintage biostratigraphy (based on foraminifera) from the Lower–Upper Cretaceous was inconclusive and identified solely based on colour and comparison with the presence of Rødby Formation in the Vinding-1 core. However, revisions of Vinding-1 showed no presence of the Rødby Formation in the interval previously suggested and underlined that the colours of the facies are not useful in identifying the Rødby Formation lithology (Lauridsen et al. 2022). The Rødby

Formation has been characterized as marine red marlstones and marly chalks (Sorgenfrei & Buch 1964), but a revision of the Rødby Formation is highly needed based on revised biostratigraphy and lithology.

The geological completion report from the Gassum-1 well suggests that the upper boundary of Lower Cretaceous is represented by an unconformity while biostratigraphic notes within that report suggest a transitional boundary. In Kvols-1 and Voldum-1 an unconformity at the upper boundary of Lower Cretaceous is also suggested based on both geological observations and biostratigraphy. In other parts of the Danish Basin, the upper boundary of the Rødby Formation is transitional, based on petrophysical log data indicating an upward decrease in the gamma ray signal.

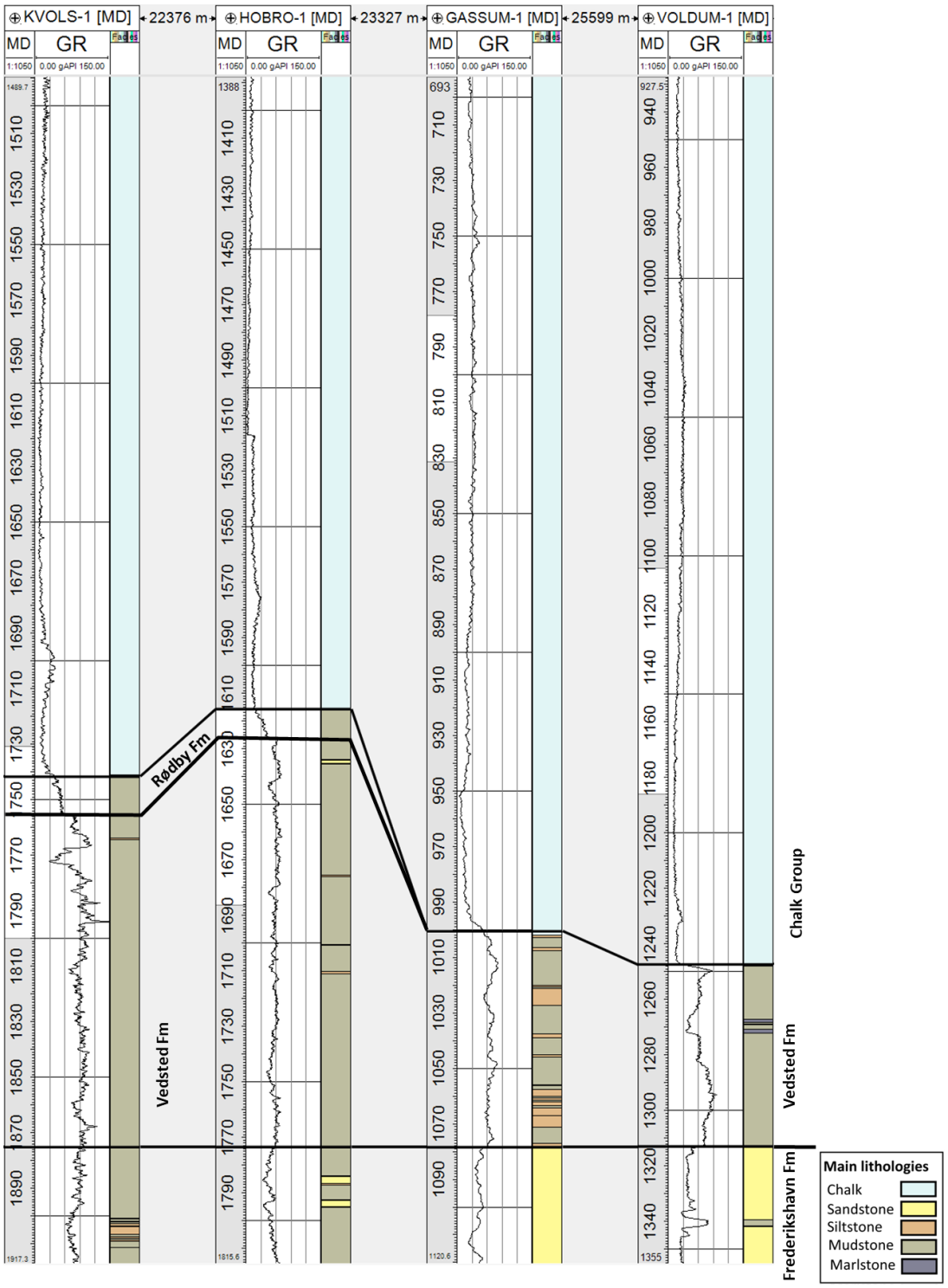


**Figure 7.2.9.** *Correlation panel focusing on the sealing units to the Frederikshavn Fm reservoir in the nearest wells to the Gassum structure; namely the Lower Cretaceous Vedsted Fm and Rødby Fm and lower part of the Upper Cretaceous Chalk Group. Top Frederikshavn Fm is used as baseline. Note the thickness increase of the Vedsted Fm seal towards the west in Hobro-1 and Kvols-1, and the pinching out of the Rødby Fm towards the east in Gassum-1 and Voldum-1. Potential sealing units in the lower part of the Chalk Group is characterised by e.g. subtle increasing GR readings indicating marly units.*

**Table 7.2.2.** *Available sample material from the Lower and Upper Cretaceous in the Gassum area; cores, sidewall cores (SWC) and ditch cuttings samples (grey shade).*

| | **Chalk Group** | | **Rødby Fm** | **Vedsted Fm** |
|---|---|---|---|---|
| | **Upper Cretaceous, Turonian–Maastrichtian** | **Upper Cretaceous, Cenomanian** | **Lower Cretaceous** | |
| **Gassum-1** | Cores 1 to 15 | Core 16 | | Cores 17 and 18 |
| **Kvols-1** | | SWC | | SWC |
| **Hobro-1** | | | | SWC |
| **Hyllebjerg-1** | | SWC | | SWC |
| **Voldum-1** | | | | SWC |


**Figure 7.2.10.** *Core photos of the Vested Fm, Gassum-1 well. (A) Lower Hauterivian, grey–dark grey calcareous mudstones Core 18, 3490–3501' (c. 1064–1067 m). (B) Middle Barremian highly calcareous grey mudstones. Core 17, 3305–3325' (c. 1007–1013 m). Note the general poor core condition, core diameter 8.5 cm.*

*The Chalk Group in the Gassum area*

The Chalk Group in the Gassum area spans the Cenomanian–Danian (Table 7.2.3). The base of the Chalk Group is situated at 1001.9 m in Gassum-1, and the uppermost Maastrichtian–Danian part is missing. In this report only the lower part is described in some detail as most of the Chalk Group is shallower than 800 m. Basic subdivisions of the Chalk Group, where chronostratigraphic subdivision is based on biostratigraphy or final well reports, are shown in stratigraphic summary charts for in selected wells (Appendix B). Schematic logs of cores 11–16 from the Gassum-1 well are presented in Figure 7.2.11, where the revised ages of the lower part of the Chalk Group and main facies are also shown.

**Table 7.2.3.** *Thicknesses and depths of Lower Cretaceous units (Vedsted Fm and Rødby Fm) and the Upper Cretaceous Chalk Group in the nearest wells to the Gassum structure.*

| | | Hyllebjerg | | Kvols-1 | | Hobro-1 | | Gassum-1 | | Voldum-1 | |
|---|---|---|---|---|---|---|---|---|---|---|---|
| | | Depth (m) | **Thickness (m)** | Depth (m) | **Thickness (m)** | Depth (m) | **Thickness (m)** | Depth (m) | **Thickness (m)** | Depth (m) | **Thickness (m)** |
| **Chalk Group** | Top Chalk Group | 26 | **1372** | 253 | **1488** | 73 | **1542.4** | 28.3 | **973.6** | 27 | **1220** |
| | Top Danian | ?26 | | 253 | | 73 | | | | | |
| | Top Cretaceous | ?161.5 | | 537 | | 159 | | 28.3 | | 27 | |
| **Rødby Fm** | Top Rødby Fm | 1398 | **2** | 1741 | **14** | 1615.4 | **4.4** | 1001.9 | **0** | 1247 | **0** |
| **Vedsted Fm** | Top Vedsted Fm | 1400 | **292** | 1755 | **120** | 1619.8 | **153.2** | 1001.9 | **76.5** | 1247 | **66** |
| | Base Vedsted Fm | 1692 | | 1875 | | 1773 | | 1078.4 | | 1313 | |

The lower part of the Chalk Group is Cenomanian in age and locally consists of hard and microcrystalline chalk. This significant hard, lithified chalk likely causes locally increased seismic velocities in the lowermost part of the Chalk Group (Fig. 7.1.6). On the sonic logs from the Hobro-1, Kvols-1 and Hyllebjerg-1 wells, a downwards increase in sonic velocity towards the base of the Chalk indicates this hard, lithified chalk (Appendix A). Sonic logs do not exist for the Gassum-1 and Voldum-1 wells. In the basal part of the Cenomanian of the Hobro-1 well, a glauconitic calcareous silt- to mudstone bed is present. In Kvols-1 white to light grey soft to firm chalk are present in a SWC drilled at the base of the Upper Cretaceous.

Core 16 in Gassum-1 is taken about 10 m above the base of the Chalk Group and it is dated as Late Cenomanian nannofossil subzones UC2c to UC3b. The core was previously dated as Santonian in the completion report (Danish American Prospecting Co 1951). The core consists of greyish, bioturbated marly chalk (facies 1) intercalated in a cyclic manner by thin, dark, marly laminated beds (facies 2) with marly beds appearing for each 30 to 50 cm (Fig. 7.2.11). Bioturbation related to the marl beds is not recorded. Some of the marly chalk beds have a coarse-grained fraction of fossil fragments, predominantly bivalves. Flaser bedding and solution seams reflecting chemical dissolution during burial diagenesis are common. Flint is not present. Core 15 is taken 55 m above the base of the Chalk Group, and it is dated as Late Turonian nannofossil subzone UC8ab. The core comprises clean, soft, white chalk with a few thin, marly, slightly laminated beds (facies 3, Fig. 7.2.11). Core 14 is taken 100 m above the base of the Chalk Group, and it is dated as mid Campanian nannofossil subzones UC14d–15d. The core comprises clean, soft, white chalk with a few thin, marly, slightly laminated beds (facies 3). Cores 13–12 are situated 180 m and 200 m, above the base Chalk Group, respectively, and are dated as mid Campanian subzone UC15d. The cores consist of marly chalk (facies 4), which is also reflected in slightly higher GR values. Core 11 is taken 250 m above the base of the Chalk Group at c. 750 m. It is dated as mid Campanian nannofossil subzones UC15c-d and comprises cyclic marly chalk alternating with thin marl beds

(facies 1). The remaining cores 1–10 from the Chalk Group are situated at shallower depth than 750 m.

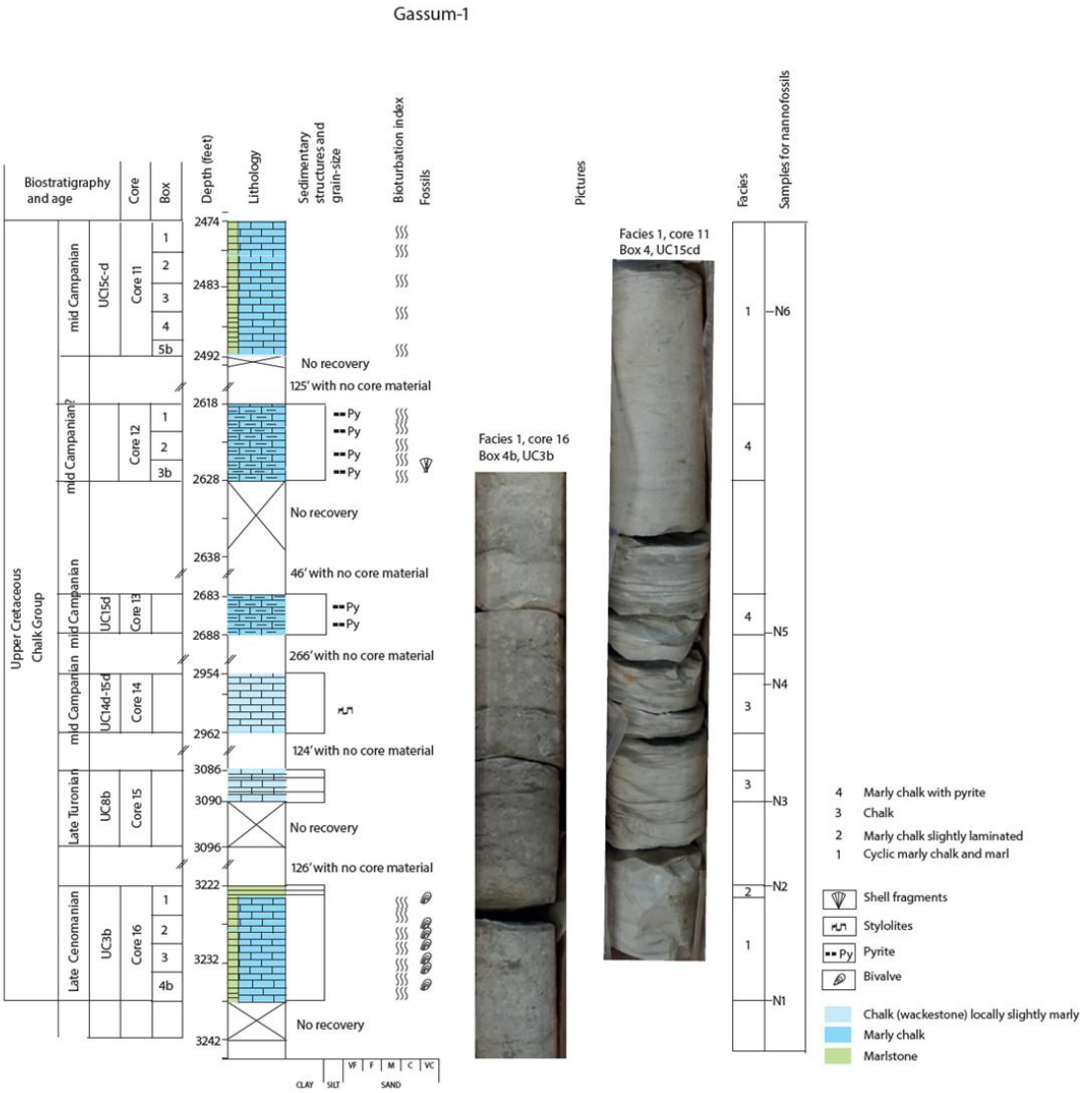


**Figure 7.2.11.** *Upper Cretaceous cores in the lower part of the Chalk Group in the Gassum-1 well, with biostratigraphic ages and main facies.*

*Porosity and permeability data of the lower part of the Chalk Group*

Porous chalk reservoir is tested as $CO_2$ reservoir in its own rights (Yu et al. 2023), in contrast the possibility for low porous chalk to act as seal for $CO_2$ migration of supercritical $CO_2$ from below has been less studied.

There are no porosity and permeability data from the Chalk Group in the Gassum-1 well. However, porosity and permeability data from the Upper Cretaceous of the Stevns-1 and Stenlille-5 wells onshore Denmark and from Danish offshore wells are plotted in Figure 7.2.12. It is evident that the Coniacian chalks in the Stenlille-5 well have the lowest porosity and permeability values (Gregersen et al. 2022). The relatively high porosity and permeability

values from the Upper Campanian to Maastrichtian from the Stevns-1 well can be explained by the relatively shallow burial history of this location, with maximal burial of 450–600 m (Nielsen et al. 2011). Burial depths for the offshore chalks of the Danish Central Graben often exceed 3000 m, but these chalk reservoirs have preserved a relatively high porosity due to retarded compaction caused by regional overpressure of the formations and the presence of oil and gas (e.g., Japsen 1998). The Stenlille data show a normal burial compaction with no overpressure.

The non-reservoir chalks (low porosity and permeability) of the Central Graben have been investigated with respect to understanding their capability as a pressure seal (Mallon & Swarbrick 2002, 2008). Non-reservoir chalks have permeabilities which are similar to those of siliciclastic mudstones. These studies show that both in clean and argillaceous chalks, diagenetic alterations resulted in low permeability. Furthermore, the diversity of rock types that exhibit low permeabilities suggests that seals are pervasive throughout the Chalk Group. Non-reservoir chalks such as those presumably present in the Gassum area can therefore potentially act as significant barriers to fluid flow and as significant pressure seals to formations beneath the Chalk Group.

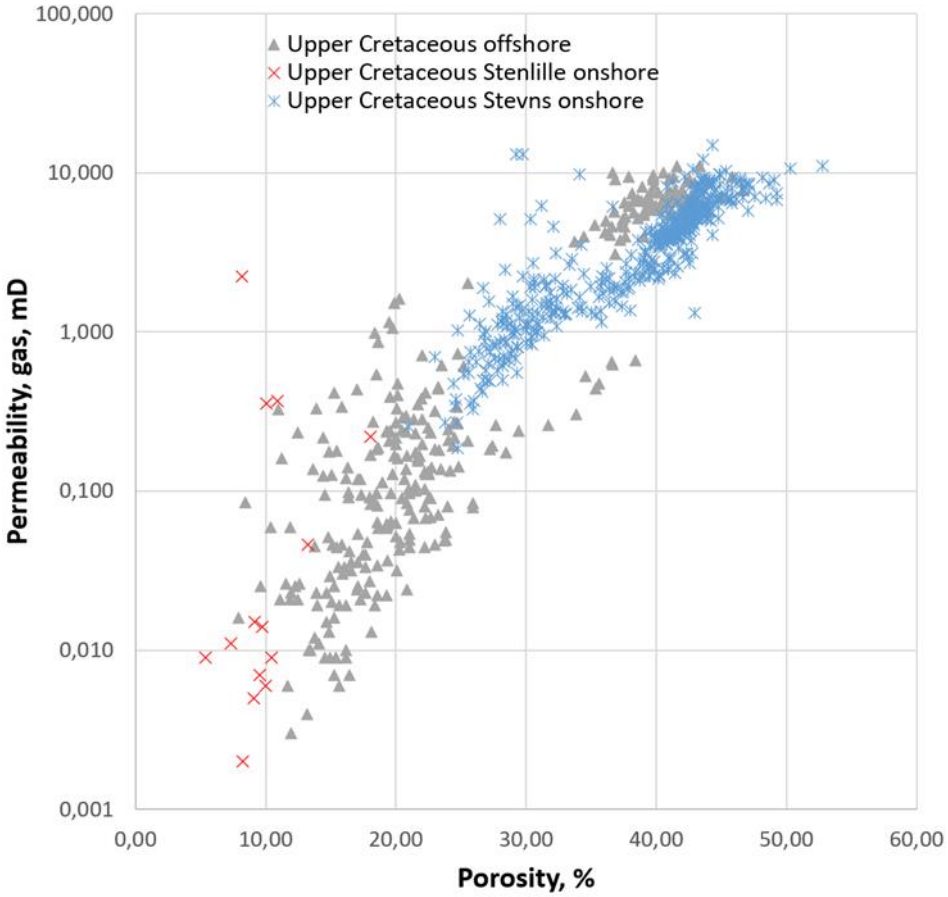


**Figure 7.2.12.** *Porosity and permeability plot of Upper Cretaceous chalks from onshore wells Stenlille-5 core, Stevns-1 core and from offshore wells in the Danish Central Graben (GEUS in-house data).*

*Summary remarks on the seal of the Frederikshavn Formation*

The seals of the Frederikshavn Formation in the Gassum area comprise the overlying Lower Cretaceous Vedsted and Rødby formations and the lower part of the Upper Cretaceous Chalk Group. As these formations have neither been the main target for coring in the Gassum area nor in other areas in the vicinity of the Gassum structure, this report summarizes the present knowledge of these units based on vintage data. The Vedsted Formation is considered as the main sealing unit of Frederikshavn Formation in the Gassum area with a thickness of 76.5 m in the Gassum-1 well.

In the Gassum area the Vedsted Formation varies in thickness from 66–292 m and consists of relatively homogenous mudstones with minor variations in silt content and with upwards increasing carbonate content. The Vedsted Formation possibly contains several unconformities related to erosion and non-deposition, but more biostratigraphic dating is needed to confirm this. E.g. in the Gassum-1 well, Lower Hauterivian to middle Barremian deposits are present, but the presence of Upper Barremian and Lower to middle Aptian strata is not confirmed. The Rødby Formation is not identified in the Gassum-1 well but in the Hobro-1 and Kvols-1 wells it is 4.4 m and 14 m thick, respectively, and described as dark grey, green, red, black calcareous shale- and claystone. It is suggested that the upper boundary of the Lower Cretaceous represents an unconformity in at least the Gassum-1, Kvols-1 and Voldum-1 wells (Appendix B). There exists no analytical seal characterisation data (Mathiesen et al. 2022, Fig. 7.2.8) on the Vedsted Formation and Rødby Formation and their seal performance is therefore essentially unknown.

The Chalk Group in the Gassum area spans the Cenomanian–Danian, the uppermost part of the Maastrichtian–Danian part is however missing in Gassum-1. The Cenomanian part cored in the Gassum-1 well is represented by greyish, completely bioturbated, marly chalk intercalated in a cyclic manner by thin, dark, marly laminated beds. The marly chalk is very hard and is indicated by increasing sonic velocities in other wells closest to the Gassum structure. The cored Turonian part in Gassum-1 comprises clean, soft, white chalk with few thin marly beds and stylolites. The cored mid Campanian part comprises an increasing marly upward succession going from clean chalk via marly chalk to and cyclic marly chalk with thin marl beds.

The porosity and permeability data for the Chalk Group in Denmark are shown in Figure 7.2.12. Porosity and permeability values of the lower part of the Chalk Group are generally very low when compared with other onshore data from the Danish Basin (Stevns-1). The porosity and permeability data from the lower part of the Chalk Group in the Stenlille-5 well reveal an ordinary burial compaction with no overpressure. There are however no data from Gassum-1 cores or from the nearest wells to the Gassum structure.

The properties of the lower few hundred meters of the Chalk Group, in their potential capacity as a secondary seal, can be compared with studies from the Danish Central Graben (Mallon & Swarbrick 2002, 2008; Amour et al. 2022). It is possible that this lower part of the Chalk Group will act as a seal to upwards fluid flow and high-pressure propagation from the underlying formations in the Gassum area. However, this can be further investigated if core material from Gassum-1 and material from new wells are analysed. Sidewall core material from the closest deep wells (e.g., Kvols-1 and Hyllebjerg-1) can also be very useful and relevant to study in more detail regarding the sealing capacity of the lower part of the Chalk Group.

## Seals of the Skagerrak Formation: The Ørslev Formation, Falster Formation and Tønder Formation (in part)

The sealing unit of the secondary Skagerrak Formation reservoir is represented by the Lower to Middle Triassic Ørslev Formation, with a recorded thickness of 315 m in Gassum-1 (measured depths of 2432.3–2747.2 m, Fig. 7.2.1). Seismic mapping shows thicknesses of the Ørslev Formation of c. 300–450 m in the structure (see Chapter 6; Fig. 6.2.3C). The formation is represented by cores 100–111, consisting of brown to dark brown argillaceous sandstones and shales with minor anhydrite and gypsum units representing mainly lacustrine–distal fluvial plain depositional environments. The lithology derived from the petrophysical logs show a lower unit, 65 m thick, of alternating mudstones and siltstones with thin sandstones, a middle mudstone-dominated unit, 150 m thick, and an upper unit, 100 m thick, of mudstones and minor amounts of thin siltstone and sandstone beds. The middle unit may be considered as the main sealing unit of this formation due to the mudstone dominated signature. Only a few other wells reach the Ørslev Formation and Skagerrak Formation in the region, e.g. Rønde-1 to the southeast (40 km) where the Ørslev Formation is 235 m thick and has significantly high amounts of sandstones in the lower part. The Ørslev Formation is only 83 m thick in Nøvling-1 situated 85 km towards the SW and here the formation consists of mudstones with minor amounts of dolomites in the middle part.

The overlying Falster Formation and lower part of the Tønder Formation form a composite mudstone dominated succession, nearly 300 m thick, in Gassum-1 that may serve as an additional seal unit to the Skagerrak Formation reservoir. Selected cored intervals are represented by cores 99–93 (Appendix B).

A number of vintage reservoir property measurements exist from the Ørslev Formation in the Gassum-1 well (Michelsen et al. 1981). These data show a wide range of reservoir properties, but they are not related to detailed geological and petrographic descriptions. Associated analyses of grain sizes by sieving are achieved for 7 samples in the lower part of the Ørslev Formation. These show a grain size range between 0.02 mm and 0.15 mm. Analysis of other 20 samples did not provide any results on average grain size due to fine-grained nature of the mudstones. No data are available regarding bulk mineralogy, clay mineralogy and other specialized analyses relevant for addressing the seal performance of the Ørslev Formation, the Falster Formation and lower part of the Tønder Formation.

# 8. Discussion of storage and potential risks

## 8.1 Volumetrics and Storage Capacity

Primary input for the estimation of potential $CO_2$ storage capacity has been the seismic reinterpretation of primary Gassum reservoir within the current older 2D survey lines combined with extended interpretation across the newly acquired GEUS2023-GASSUM 2D seismic survey (see also Section 4.1). Sandstone reservoirs in the Frederikshavn and Haldager Sand formations may also possess a considerable reservoir potential (see also Section 7.1). But the storage potential of these two units has not been evaluated in this study due to the insufficient logging suite in the Gassum-1 well. The same applies for the Skagerrak Formation. Combined, these units may provide a significant upside to the storage capacity of the Gassum structure. The detailed well analysis and a crucial element of revising the depth conversion impacts the understanding of the reservoirs and their geometry in this well-defined relief structure (see Figure 8.1.1).

The storage capacity estimates are average values for the whole structure. The well derived data in Table 7.1.2, Scenario 1 is the primary input for the storage assessment. The petrophysical and geological understanding of thicknesses and average net to gross reservoir ratio of aquifer across the entire trap (the N/G ratio) in the Gassum-1 and neighboring wells is therefore transformed into structure-specific geological-based average values for the storage capacity estimation simplifying the spatial distribution/variation within the Gross Rock Volume (GRV).

Traditionally the GRV is calculated as a total volume between the top and base reservoir surfaces (see Figure 8.1.1). The so-called Waste Rock Volume (WRV) (James et al. 2013) is subtracted from the total volume to give the resulting GRV. Average reservoir thickness (i.e. net sand thickness) is not just equal to the isochore thickness (or the relief) between top and base surfaces, why the gross thickness is corrected with the N/G ratio to get a more realistic reservoir sand thickness for the GRV. Preferably, the thickness correction could also incorporate potential thin sandstone wedges between top point and the spill point on the flanks of the structure, if the seismic data support this.

For the storage capacity estimation of the Gassum structure, the Gassum Formation have been evaluated as a structural four-way dip closure and is calculated so it can be compared to $CO_2$ capacities of other structures across Denmark (e.g., Gregersen et al. 2023; Hjelm et al. 2022).

The physical properties of the Gassum reservoir units are described in Section 7.1. At a later stage the reservoir unit and identification of possible faulting must be assessed in more detail by dynamic 3D reservoir simulation models to ensure optimal development, injection and filling of the reservoir unit of the structure, and to ensure less uncertainty on storage capacity.

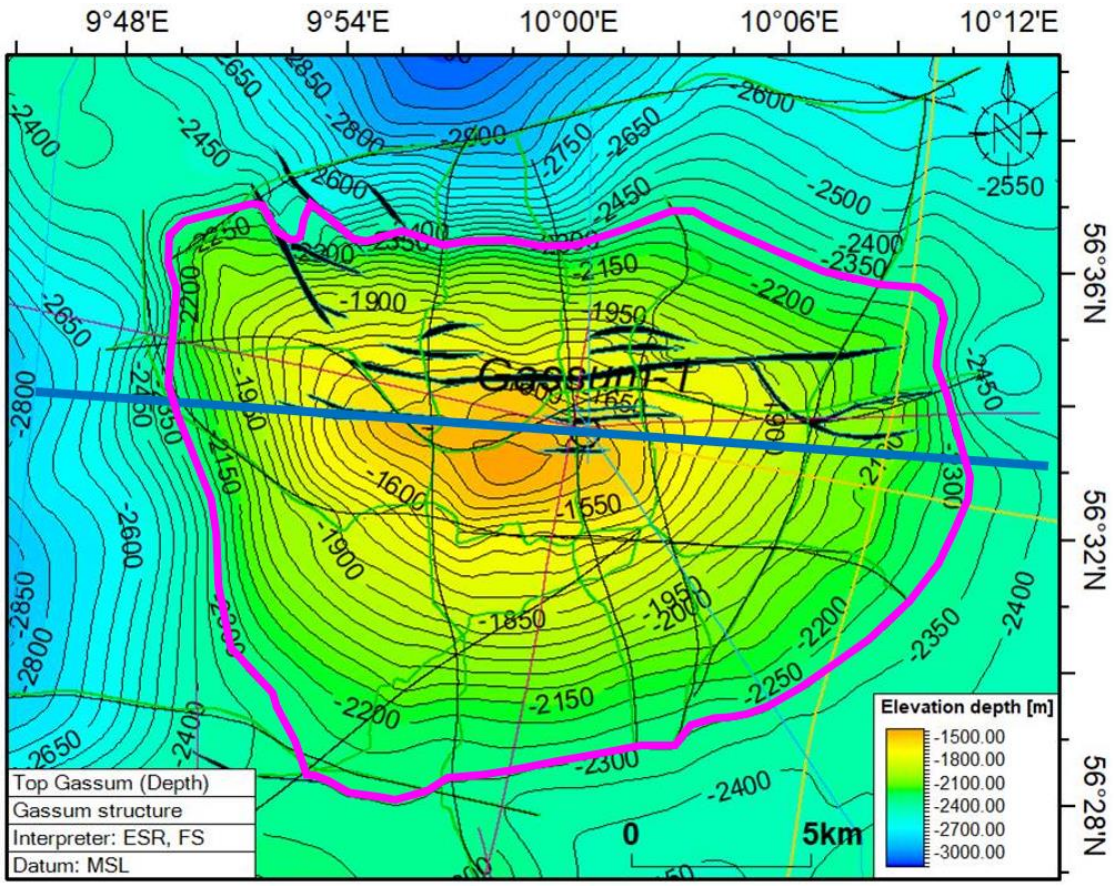


**Figure 8.1.1.** *The Gassum depth structure map in meters (m) (generated in Petrel®, tied to nearest wells and gridded by 250x250 m) provides the primary input to the capacity assessment. The Gassum structure are located south of a W–E orientated fault system. The structural top point is located at c. 1375 m and the deepest closing contour at 2300 m (marked in bold purple), and with an area within the spill point of c. 280 km². See also Chapter 6 for fault analyses and map location. A schematic W–E profile across the structure is shown in Figure 8.1.3 (blue line).*

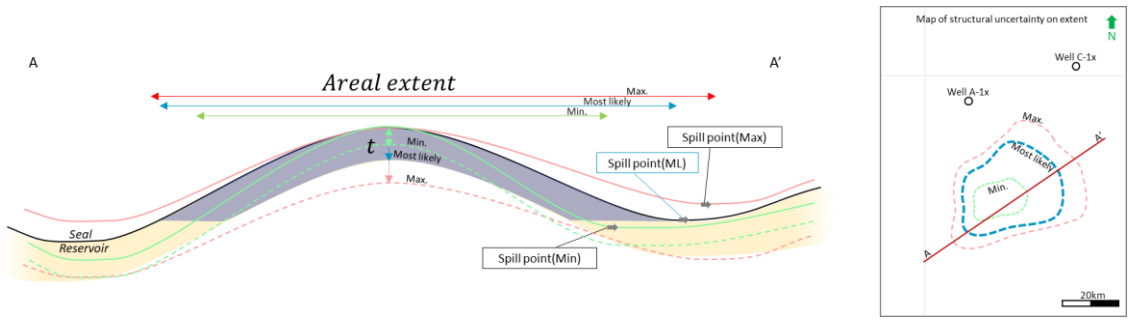


**Figure 8.1.2.** *Conceptual profile (A–A') across a potential structure. The uncertainty in mapping the structure results in the hypothetically min. and max. scenarios looking very different from the most likely mapped scenario. Variance in area and in thickness (t) will affect the Gross Rock Volume (GRV) of the structure. The uncertainty is addressed by applying uncertainty on the resulting GRV.*

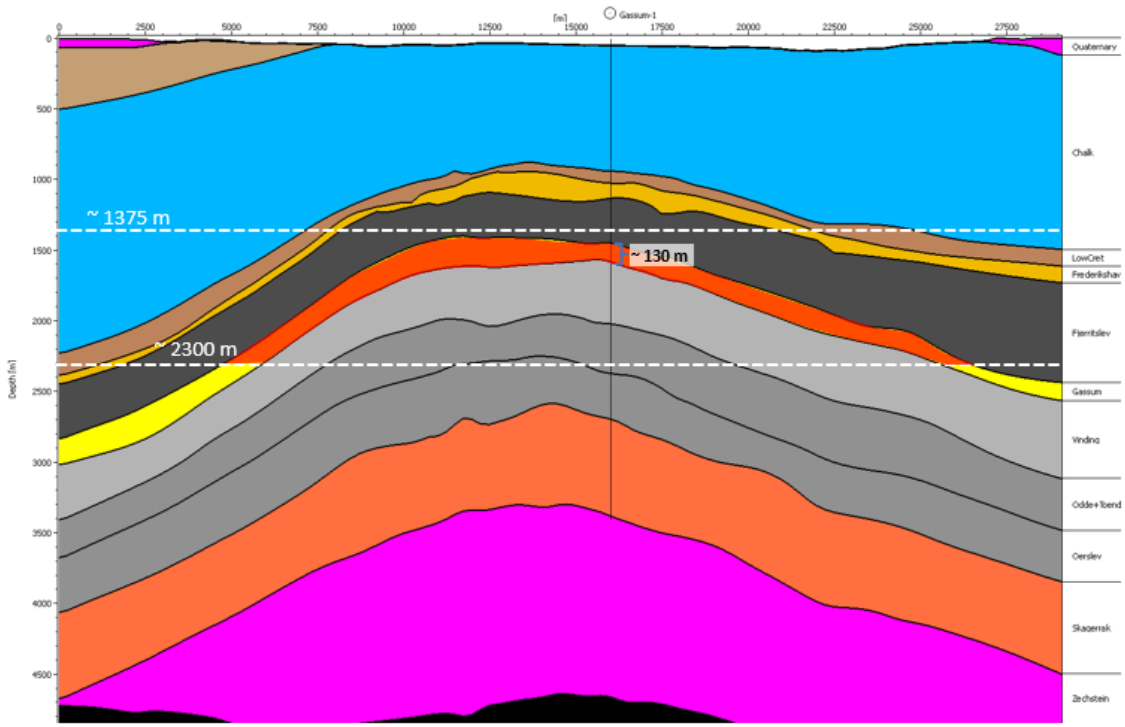


**Figure 8.1.3.** *W–E schematic cross section of the Gassum structure showing the location of the top and spill points for the Gassum Fm at the c. 1375 m and 2300 m contours. The cross section highlights the interval between 1375 m and 2300 m used for a realistic GRV estimation (marked with red polygon above 2300 m). For the Gassum reservoir, the GRV is calculated in Petrel® as the volume between the top Gassum and base Gassum surfaces (i.e. the spill point). Near the top of the Gassum structure the Gassum-1 well has a thickness of 130 m, but the mean thickness within the 2300 contour-area of 180 m has been used storage capacity estimation based on the new interpretation and depth conversion (see Fig. 6.2.3F). Notice that the profile is located south of the fault zone north of the Gassum structure (see Figure 8.1.1.for location of the section and the fault zone). The influence of the faults on the estimated storage capacity in not considered in this study.*

## 8.2 Volumetric input parameters

Evaluation and maturation of a $CO_2$ storage site includes several steps. The maturation phase, carried out by GEUS, includes static calculation of theoretical storage capacity – primary based on Gross Rock Volume (GRV), net/sand thickness, average porosity and density of the $CO_2$ (see also Section 7.1).

The current maturation phase does not provide dynamic capacity estimates of the potential $CO_2$ structures but focus on identifying and assessing extent and quality of reservoir aquifers. Furthermore, no attempts are made to address e.g. seal breach, fault leakage, fault reactivation, solubility of $CO_2$ in water, the effect of high concentration of salt etc.

To do detailed $CO_2$ storage capacity evaluation, it is important to assess aquifer quality and connectivity, i.e. to identify the existence of thick, high permeable sandstone aquifers with high connectivity with no major faults. This will require dynamic reservoir simulation, that may result in different storage capacity than static estimations and will normally be the next step for potential license holders.

*Gross rock volume*

The Gross Rock Volumes (GRV) of the Gassum structure was original based on the Area and Thickness vs. Depth methodology described by e.g. James et al. (2013). The calculated Gross Reservoir Volume (GRV) is in this study estimated from the seismic mapped and depth converted top and base reservoir surfaces, where the base surface is constrained by the spill point surface (Figs. 8.1.2, 8.1.3).

The GRV is calculated in Petrel as the volume between the top Gassum and the base Gassum reservoir surfaces, giving a Gassum Formation thickness of c. 130 m (see Fig. 8.1.3). The expected reservoir sand thickness is multiplied with the net/gross ratio estimated from petrophysical analysis based on the nearest wells (see Section 7.1). Calculating GRV this way provides greater accuracy and flexibility compared to previous used correction factors for geometries with overestimated wedge volumes. This is because it allows for uncertainty ranges on GRV and reservoir sand thickness to be modeled independently. Furthermore, the method allows for a rapid GRV calculation, that can be used in a Monte Carlo simulation, to establish an unbiased estimated range of GRV.

To evaluate the uncertainty on the GRV across the Gassum structure, a minimum and maximum case was also calculated as illustrated in Figure 8.1.2. by assigned a minimum, mode, and maximum uncertainty range, where mode is the data value that occurs most often in the dataset. This variation in GRV was inferred to cover uncertainty in interpretations, seismic well ties, mapping and depth conversion. To reflect this uncertainty, a distribution for the average GRV was constructed by defining the minimum and maximum of the distribution based on surrounding wells and supplied by c. ±10% (Table 8.2.1). It is assumed that the GRV distribution follows a Pert distribution defined by the minimum, mode, and maximum values. The Pert distribution is believed to give suitable representation for naturally occurring events following the subjective input estimates (Clark 1962).

For the reservoir unit, the other input parameters are also given as minimum, mode, and maximum values – Net to Gross ratio, porosity, $CO_2$ reservoir density and the storage efficiency factor are also assumed to follow a Pert distribution.

**Table 8.2.1.** *Assessment of important parameters for the Gassum reservoir in Gassum structure, where only the resulting Gross Rock Volume (GRV) min., mode and max. estimates are used for the capacity estimation in Table 8.2.3. The mean thickness of the Gassum Fm (i.e. the Gross sand thickness) is taken from Section 7.1 and Fig. 6.2.3F*

| **Reservoir** | **Apex (m, TVDSS)** | **Spill point (m, TVDSS)** | **Area ($km^2$)** | **Gross Sand TCK (m)** | | | **GRV ($km^2$)** | | |
|---|---|---|---|---|---|---|---|---|---|
| | | Mode | Mode | Min. | Mode | Max. | Min. | Mode | Max. |
| **Gassum Fm** | 1375 | 2300 | 280 | 144 | 180 | 216 | 45.40 | 50.44 | 55.48 |

*Net to Gross ratio*

The Net to Gross (N/G) ratios estimated from the petrophysical analysis of the Gassum-1 well are evaluated and reasonable average N/G-ratios across the entire structure is defined as the mode of the distribution (see also Section 7.1). Some variance is expected due to lateral variation of the lithologies owing to differences in facies distribution, depositional environment, diagenesis and general poor quality of the Gassum-1 logs. To reflect this uncertainty, a distribution for the average N/G ratio was constructed by defining the minimum and

maximum of the distribution as c. ±20% with minor adjustments. A Pert distribution has been applied.

*Porosity*

The porosity (ϕ) was estimated from petrophysical analysis of the Gassum-1 and surrounding wells as described in Section 7.1. The well-derived estimates are considered as reasonable average porosity across the entire structure (i.e. set as mode). Some variance is expected as lateral and depth variations may occur (see Chapter 7). To reflect this, an average porosity distribution has been constructed defining the minimum and maximum of the distribution as c. ±20% with minor adjustments. A Pert distribution for this element has been applied.

*$CO_2$ density*

The average in-situ density of $CO_2$ was estimated using the 'Calculation of thermodynamic state variables of carbon dioxide' web-tool essentially based on Span and Wagner (1996) [*http://www.peacesoftware.de/einigewerte/co2_e.html*]. The average reservoir pressure was calculated on the assumption that the reservoir is under hydrostatic pressure and a single pressure point midway between apex and maximum spill point was selected representing the entire reservoir.

Temperature for this midway point was calculated assuming a surface temperature of 8°C and a geothermal gradient of 28 °C/km based on the Gassum-1 well, which is slightly higher than the typical onshore gradient of c. 27 °C/km estimated by Fuchs et al. (2020). Assumptions and calculated densities for the individual reservoir units are tabulated in Table 8.2.2. For a quick estimation of the uncertainty on $CO_2$ density, various P-T scenarios were tested and in general terms a –5% (min.) and +10% (max.) variation from the calculated mode was applied for building a Pert distribution. All calculations showed that $CO_2$ would be in supercritical state.

**Table 8.2.2.** *$CO_2$ fluid parameter assumption and estimated values.*

| Reservoir | Apex depth (TVDSS, m) | Spill point depth (TVDSS, m) | Structural relief (m) | Pressure HydroS. (MPa) | GeoThermal grad. (°C/km) | Mid Res. Temp. (°C) | $CO_2$ density (kg/m$^3$) |
|---|---|---|---|---|---|---|---|
| **Gassum Fm** | 1375 | 2300 | 975 | 18.03 | 28 | 59.45 | 694.37 |

## 8.3 Storage efficiency

Storage efficiency is heavily influenced by local geological subsurface factors such as confinement, reservoir performance, compartmentalisation etc. together with injection design and operation (i.e. financial controlled factors) (e.g., Wang et al. 2013). A sufficient analogue storage efficiency database is not available to this study and accurate storage efficiency factor-ranges lacks at this early stage of maturation. This emphasises the need for further investigations of the subsurface and development of scenarios and dynamic reservoir simulation to better understand the potential storage efficiency ranges. In this evaluation, a range from 5% to 20% with a mode of 10% is used as a possible range. The use of a storage efficiency factor value of 10% assumes that the Gassum reservoir in the Gassum structure have good reservoir characteristics based on Gassum-1, Scenario 1, and the uncertainty caused by the identification of a faults on the northern side of the Gassum structure penetrating both the seal and reservoir on the new seismic data which reduces the mode value (Fig. 8.1.1). A Pert distribution for this element has also been applied.

## 8.4 Summary of input factors

In Tables 8.4.1, input parameter distributions are listed (all selected to follow Pert distributions defined by minimum, mode, and maximum). Input parameter distributions for the Gassum reservoir is displayed in Figure 8.4.1.

**Table 8.4.1.** *Input parameters for the Gassum structure* – ***Gassum Fm***

| **Parameter** | **Assumption** | | |
|---|---|---|---|
| | Min. | Mode | Max. |
| **GRV (km$^3$)** | 45.40 | 50.44 | 55.48 |
| **Net/Gross** | 0.37 | 0.46 | 0.55 |
| **Porosity** | 0.23 | 0.285 | 0.34 |
| **Storage eff.** | 0.05 | 0.1 | 0.2 |
| ***In situ* $CO_2$ density (kg/m$^3$)** | 659.65 | 694.37 | 763.81 |

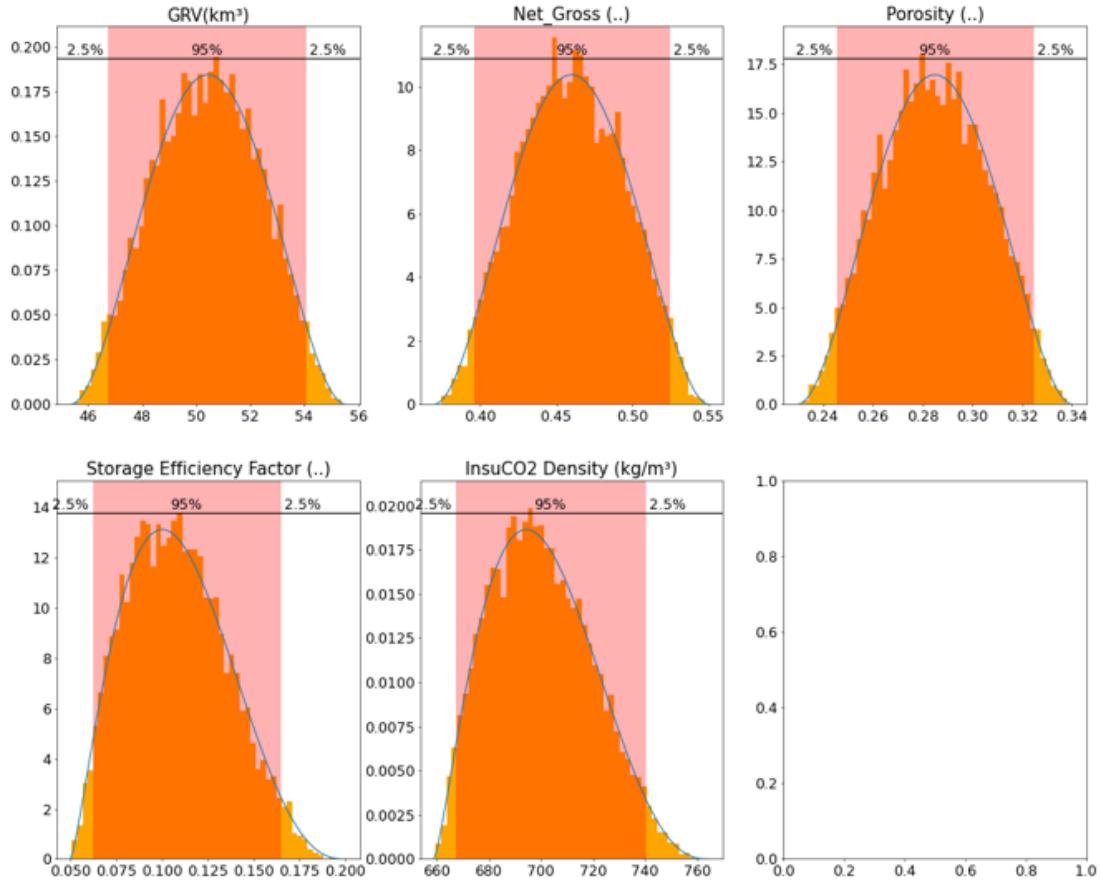


**Figure 8.4.1**. *Example of some of the distribution shapes (Pert distributions) for the five input parameters for the Gassum reservoir. The last input distribution plot is empty and not used.*

## 8.5 Storage capacity results

The modelled volumetrics was made on the assumption of the presence of an efficient reservoir/seal pair capable of retaining $CO_2$ in the reservoir. This basic assumption needs to be tested by new 3D seismic data and further geological investigation. In Tables 8.5.1, the results of the Monte Carlo simulations are tabulated. The tables indicate both the pore volume available within the trap (full potential above structural spill), the effective volume accessible for $CO_2$ storage (applying the Storage efficiency factor to pore volume) and mass of $CO_2$ in mega-tons (MT) that can be stored. The tables present the 90%, 50% and 10% percentiles (P90, P50 and P10) corresponding to the chance for a given storage volume scenario to exceed the given storage capacity value. Mean values of the resultant outcome distribution are also tabulated and is considered the "best" single value representation for the entire distribution.

Without addressing the influence of the faults located north of the top point of the Gassum structure the increase in a mean unrisked static storage capacity of c. 498 Mt $CO_2$ is calculated for the Gassum Formation, Scenario 1 with a range between c. 325 Mt $CO_2$ (P90) and c. 689 Mt $CO_2$ (P10) and a P50 of c. 485 Mt $CO_2$ (Figure 8.5.1). Due to the variability-ranges of the behind-lying factors, the modelled storage capacity has a significant range. As illustrated in Figure 8.5.2, the storage capacity uncertainty is linked with the uncertainty of the storage efficiency factor. In comparison, $CO_2$ density at reservoir conditions, is believed to be of minor concern.

**Table 8.5.1.** *Gassum structure –* ***Gassum Fm*** *storage capacity potential*

| **Results** | **P90** | **P50** | **P10** | **Mean** |
|---|---|---|---|---|
| Buoyant trapping pore volume ($km^3$) | 5.672 | 6.578 | 7.584 | 6.602 |
| Buoyant eff. storage volume ($km^3$) | 0.466 | 0.693 | 0.693 | 0.712 |
| Buoyant storage capacity (Mt $CO_2$) | 325.36 | 485.77 | 688.98 | 498.44 |

Notice that the storage efficiency factor is here assumed to be 10% compared to the previously used 40% (Hjelm et al. 2022), thus reducing the estimated $CO_2$ storage capacity. A storage efficiency of 40% is only valid in a closed confined system with good well control etc., such as the Stenlille area. The efficiency factor is the most widely ranging parameter in the storage calculation in deep saline aquifers. In the literature, the efficiency factor varies between 0.01% and 40%, but the processes underlying its derivation are not always clear, as presented by Ehlig-Economides and Economides (2010). This estimation of $CO_2$ storage capacity must be investigated further by, e.g., reservoir simulation modelling to ensure optimal development and filling of the Gassum structure, and to minimise uncertainty.

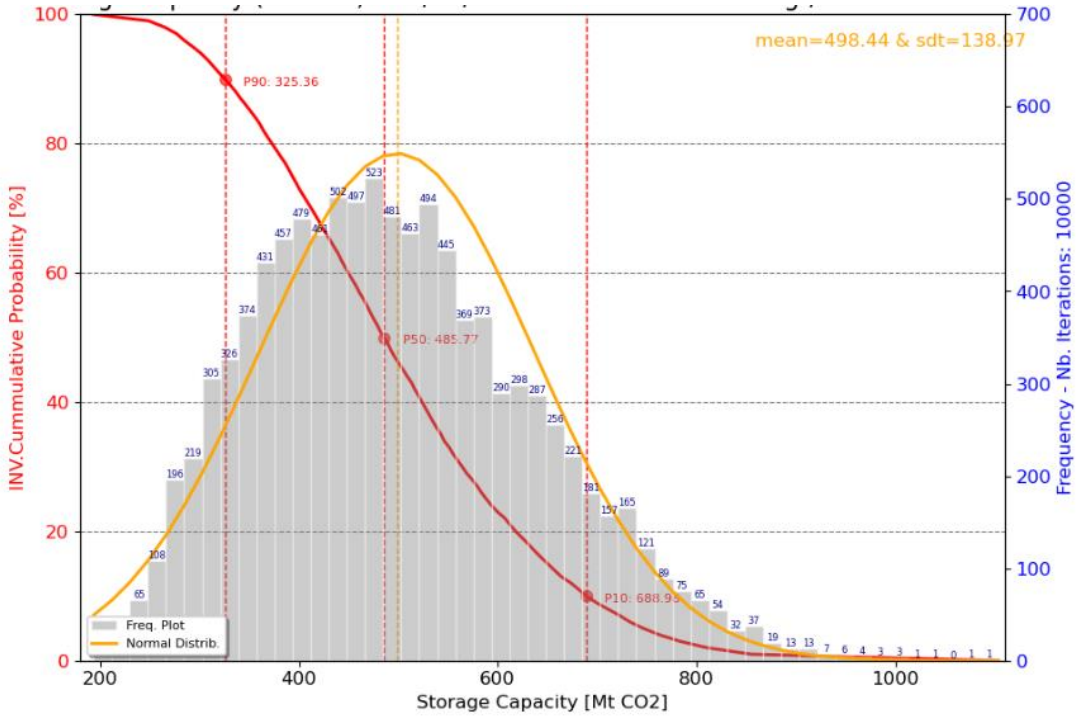


**Figure 8.5.1.** *Modelled statistical distribution of the combined storage capacity potential for the Gassum reservoir in the Gassum structure.*

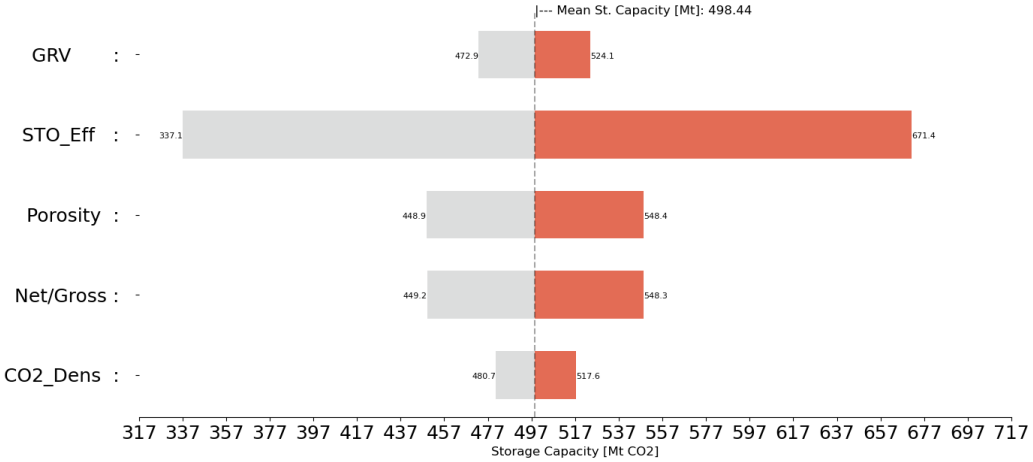


**Figure 8.5.2.** *Sensitivity or Tornado plot to how the various input parameters affect the estimate mean of storage capacity (c. 498 Mt $CO_2$) of the Gassum reservoir. The horizontal bars for each parameter indicate change in storage capacity given that only that parameter is changed leaving all other constant (end levels being P90 and P10, respectively, in the parameter input range). The colours show the symmetric representation of the parameters on both sides of the mean storage capacity.*

## 8.6 Potential risks

The present report provides an updated geological mapping describing reservoir-seal couples, the extent, thickness, closure, reservoir quality and volume of the primary reservoir formation, as well as larger faults, but does not comprise a dedicated study of risks or risk assessment of the structure for potential storage of $CO_2$. Thus, the report provides a geological characterization and maturation of these identified elements and points out geological related potential risks, that are recommended to be included for further evaluation and maturation of the Gassum structure.

Not all geological risks can be identified at this early stage due to lack of dense seismic coverage and well information, while other risks identified at this stage will be mitigated by collection of new geophysical and geological data and further investigations. The risks described below are not considered a full list, but rather emphasizes important points that needs further attention in future studies and data collections.

### Faults

Leakage along existing faults and compartmentalization of the reservoir due to faults in of the Gassum-Fjerritslev formations reservoir-seal pair is considered the primary risks at the current level of understanding. Especially the major east-west trending fault zone that extends for c. 15 km near the top of the structure constitute an element that warrants further investigations. The faults extend from the Ørslev Formation to the upper part of the Chalk Group. The main fault movement in the fault zone is interpreted to have taken place during the Late Cretaceous and/or during the Cenozoic, at the same time as major inversion tectonism was taking place in the Sorgenfrei-Tornquist Zone. Besides this large fault zone, smaller north-south trending faults are present in the top Fjerritslev Formation and shallower successions in the southern part of the Gassum structure.

Faults are also present in the Stenlille structure, where the mapped faults are typically minor in both lateral extension (up to few km) and vertical throws (typical up to 10–15 milliseconds) and located kilometres apart (Gregersen et al. 2023). Despite the presence of faults in the Stenlille structure, there are not registered any leakage or natural escape of gas, which has been stored in the Stenlille structure since 1989 (Laier and Øbro 2009). It is not known whether the faults in the Gassum structure could act as migration pathways for $CO_2$, hence, at this point the faults should be considered as a potential risk of vertical leakage from storage in the Gassum Formation, that needs to be addressed when maturing the structure further.

Faults could also be a challenge to lateral migration by causing compartmentalization of the reservoir, such as known from the Gassum Formation in the Stenlille structure. Compartmentalization due to faults may reduce internal reservoir communication, and thus lower the storage efficiency and increase the number of injection wells required to fill the structure.

### Legacy well

The Gassum-1 well, spudded in March 1948 and finalised in 1951, is located near the top of the structure and extends down to the uppermost part of the Zechstein, intersecting the primary reservoir-seal pair of the Gassum-Fjerritslev formations. Abandoned and improperly sealed wells can leak fluids or gas into shallower stratigraphic layers, the groundwater, or the atmosphere. Corrosion, casing failure, inadequate cementing, improper plugging, or

physical damage to the wellbore could all be cause of leakage. The status and integrity of the Gassum-1 well has not been investigated in this report; hence, this needs to be addressed when maturing the structure further.

### Earthquake hazard

Denmark is a low risk area for earthquakes though small earthquakes do occur (Fig. 8.6.1). Earthquake hazard for Denmark can be found in Voss al. (2015), where also lists of felt and damaging earthquakes can be found. The largest earthquakes in or near Denmark have occurred offshore Thy and in Kattegat. Large earthquakes have occurred in Kattegat, with a M 4.7 event in 1985 in the Swedish part of Kattegat (Arvidsson et al. 1991), and another large earthquake in 1759 in northern Kattegat (Wood 1988). The largest instrumentally recorded earthquake offshore Thy occurred in 2010 and had a M 4.3 (Fig. 8.6.2). The depths of the earthquakes are very uncertain, but they are located within Earth's crust.

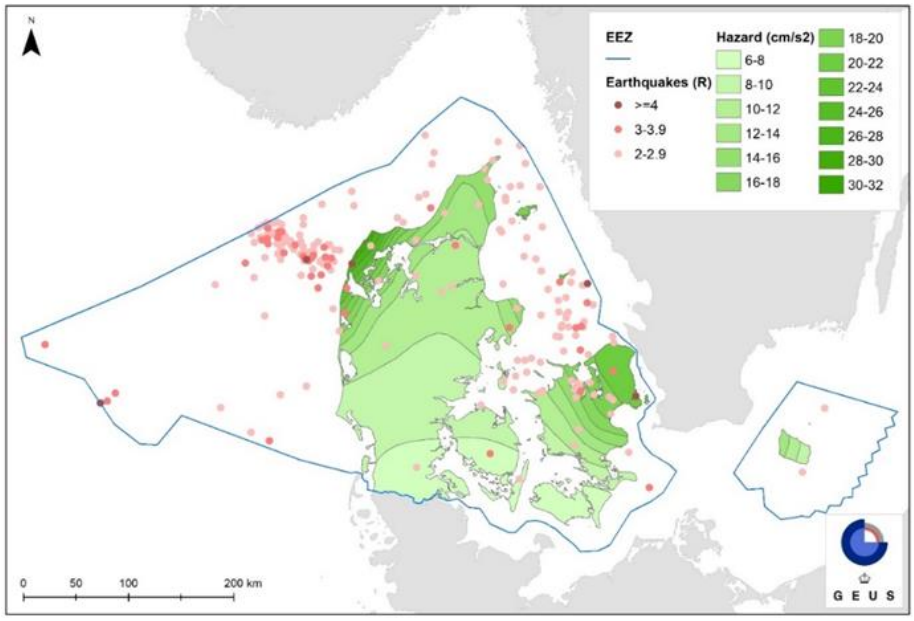


**Figure 8.6.1.** *The coloured contours are redrawn onshore from Voss et al. (2015) and show the estimated hazards given by the peak ground accelerations [cm/s$^2$] for a return period of 475 years. This corresponds to a 90% non-exceedance probability in 50 years. Given values are only valid onshore Denmark. The contours are based on a validated catalogue of earthquakes over Magnitude 3 from 1960 to 2013. As the attenuation of earthquakes (ground motion prediction) has not been determined specifically for Denmark, the global reference model by Spudich et al. (1997) that describes attenuation from normal faults in hard-rock conditions was used.*

A monitoring study was carried out around Gas Storage Denmark gas storage facility close to Stenlille. Six seismic stations were in operation for almost three years during 2018–2021, i.e. during a period with seasonal injection and withdrawal of natural gas, but 30 years after the start of the gas storage operation. The detection limit within the storage area was calculated to be at least ML 0.0. No local events were detected within the survey period (Dahl-Jensen et al. 2021). Based on the permanent seismic network, only few, small earthquakes have been recorded near the Gassum structure and the seismic hazard of the area is low (Fig. 8.6.2).

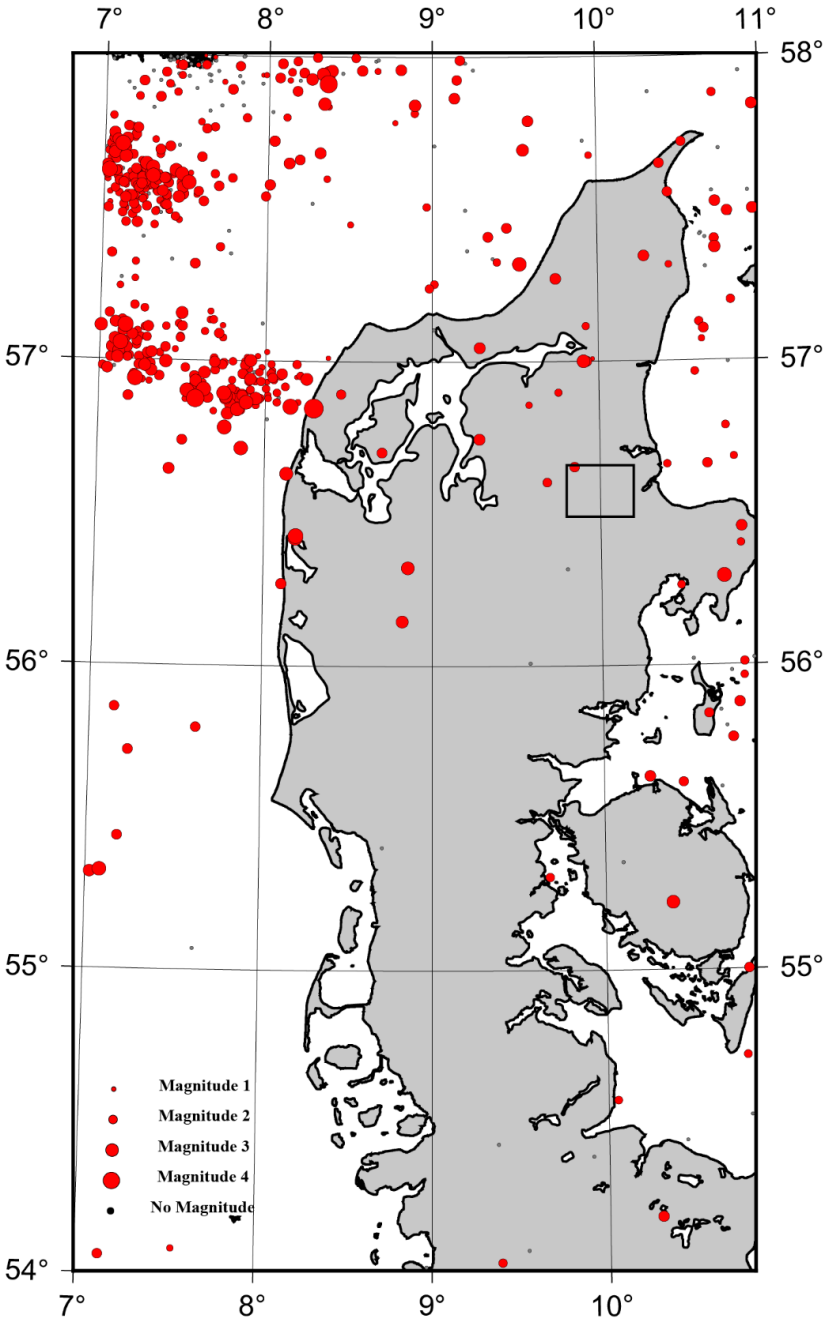


**Figure 8.6.2.** *All known earthquakes until the end of 2022, located since 1930 within the shown area. The magnitude (shown by the size of the red dots) varies from ML 4.0 and down. All known and assumed explosions have been removed, but some may remain, mainly offshore. The Gassum study area of this report is marked with a black rectangle. The earthquake shown at the edge of the rectangle was a M2.3 earthquake in 2007. Based on the permanent seismic network, only few, small earthquakes have been recorded near the Gassum structure.*

# 9. Conclusions

This study shows that the Gassum structure forms a well-defined structural anticlinal dome, with a four-way dip closure, cored by a Zechstein salt pillow that is overlain by a thick Triassic−Lower Jurassic succession and younger strata. For this project, new seismic 2D lines with a total length of c. 221 km were acquired during February to May 2023 to improve the seismic data coverage of the structure.

The primary reservoir in the Gassum structure is considered to be sandstones of the Upper Triassic–lowermost Jurassic Gassum Formation, with a thick mudstone succession of the Lower Jurassic Fjerritslev Formation as the primary seal. Both formations are well-known from nearby wells including the Gassum-1 well near the centre of the Gassum structure. In addition, excellent secondary sandstone reservoirs may be present in the structure: The deeper situated Triassic Skagerrak Formation with mudstones of the Ørslev–Falster–Tønder formations as a seal, and the shallower Upper Jurassic–Lower Cretaceous Frederikshavn Formation with the Lower Cretaceous claystone-dominated Vedsted Formation as a seal. Both the Gassum and Frederikshavn formations have large closure areas and likely good reservoir properties. As discussed in this report, the Middle Jurassic Haldager Sand and lower Upper Jurassic Flyvbjerg formations possibly form additional reservoirs in parts of the structure with the Upper Jurassic Børglum Formation as a seal.

Characterization of the reservoir quality of the Gassum Formation in the Gassum structure is primarily based on core descriptions and core measurements. Overall, the Gassum Formation is divided into three reservoir zones separated by relatively thick mudstones. In the Gassum-1 well, the Reservoir Zone 1 in the lower part of the Gassum Formation consists of 18.8 m sandstones and a net to gross ratio of 1.0 with an average porosity of 29.6% and average permeability of 2637 mD. The shallower Reservoir Zones 2 and 3 have a net reservoir sandstone thickness of 20.9 m and 16.6 m, respectively, with calculated average porosity of 27.9% and permeability of 511 mD. Within the primary reservoir of the Gassum Formation, located at roughly 1500 m, the estimated salinity reaches approximately 112,000 mg/l $Cl^-$. Meanwhile, at the depth of the Skagerrak sandstone reservoir, located around 2800 m, salinity is estimated to be approximately 201,000 mg/l $Cl^-$, indicating that it is approaching saturation with respect to halite.

The mudstone dominated Fjerritslev Formation is known to have good seal properties. The thickness of the Fjerritslev Formation in the Gassum-1 well is 318.5 m. The seismic data shows an uneven thickness of the Fjerritslev Formation from c. 300–350 m at the top with a suggested marked thickness increase towards the north. The marine claystones and mudstones of the formation forms an effectively seal for the seasonal storage of natural gas in the Gassum Formation in the Stenlille structure. Compared to the Stenlille area, the Fjerritslev Formation is more fine-grained and contains less siltstone and sandstone layers in the Gassum structure.

Faults are interpreted and described from the 2D seismic data with focus on their occurrence in the Gassum and Fjerritslev formations. A major fault zone is present north of the top of the structure (Fig. 1.4) where it can be followed for c. 15 km. Individual faults can be identified at multiple seismic profiles and cause offsets in top Gassum Formation as well as the seal (Fjerritslev Formation) and shallower successions of up to 40–60 milliseconds, corresponding to c. 100 m offset. As faults may act as migration pathways or result in mechanical

weakening of the seal or compartmentalization of the reservoir, it is recommended to investigate this further by additional data acquisition and analyses.

The areal extent of the Gassum reservoir in the Gassum structure is estimated to be c. 280 $km^2$, and is thus slightly larger than indicated in the previous regional study (233 $km^2$ in Hjelm et al. 2022), which was based on vintage seismic and velocity data. Also, the structural relief is larger than previously estimated (925 m compared to 725 m in Hjelm et al. 2022), due to a better constrained depth conversion based on data from the new seismic survey. Without addressing the influence of the faults located north of the top point of the Gassum structure, the increase in the rock volume of the structure, together with an assumed storage efficiency factor of 10% compared to the previously assumed 40%, the estimated storage capacity of 586 Mt $CO_2$ in Hjelm et al. (2022) is updated to a unrisked mean of 498 Mt $CO_2$ or between c. 325–689 Mt $CO_2$. The estimations are based on a static assessment of the storage capacity and must be investigated further by more site-specific assessments and reservoir simulation modelling.

# 10. Recommendations for further work

The new data of the GEUS2023-GASSUM 2D seismic survey together with the existing data provided a comprehensive database for the present updated mapping and analyses of the size, spill-point, volume, details of reservoir- and seal successions, and faults of the Gassum structure, included in this initial maturation. However, it is recommended, that a further maturation of the structure should include new seismic acquisition, a drilling program, and a risk assessment with seal integrity study, including analysis of leakage risk at faults and the legacy well.

A 3D seismic acquisition over the potential injection and storage sites is recommended, for more detailed interpretation prior to $CO_2$ injection. Acquisition of 3D seismic data over the structure can add important new data towards mitigating the fault related risks, develop scenarios to evaluate optimal well design, as well as provide data for modelling studies of $CO_2$ migration.

During a potential future $CO_2$ injection phase, repeated seismic surveys in the same area can contribute to monitor the extent of the $CO_2$ migration, together with other monitoring techniques (e.g., sampling in monitoring wells, seismometers, and other instrumentation). Such data will also enable a more precise definition of trap closures and reservoir outline, which again will feed into a refined storage volume calculation.

The study documents the existence of a major fault zone near the top of the Gassum structure. Faults can lead to compartmentalization of the reservoir and weaken the seal, which may pose significant risks to $CO_2$ storage projects. The risk of leakage, fault reactivation and compartmentalization should be addressed in geomechanical and reservoir modelling studies.

The existing Gassum-1 well was drilled in the period between 1948 and 1951. While several cores were cut during drilling contributing to the geological understanding, the electrical logging program run at the time of drilling reflects the technical capability at that time. The quality and extend of the logging suite impact the accuracy to which reservoir and seal properties can be evaluated. The area under structural closure at top Frederikshavn Formation level is compatible with that at Top Gassum level. The Frederikshavn Formation may possess a considerable reservoir potential level. But the storage potential of this unit has not been evaluated in this study due to the insufficient logging suite available. The same applies for the Skagerrak Formation. Combined, these units may provide a significant upside to the storage capacity of the Gassum structure, which should be evaluated once new wells with modern electrical log suites and coring programs has been carried out. In addition, reservoir sandstones of the Haldager Sand and Flyvbjerg formations are probably present in parts of the Gassum structure and if so, then provide a further upside of the storage capacity. Biostratigraphic analysis of samples from the interval referred to the Upper Jurassic Børglum Formation in the Gassum-1 well may contribute to elucidate if part of this interval in fact shall be referred to the Haldager Sand Formation and/or the Flyvbjerg Formation. Should that be the case, this Middle–lowermost Upper Jurassic interval should then be mapped out on the seismic data.

Site-specific studies on the seal capacity are needed for all structures to be matured towards $CO_2$ storage. For the Gassum structure, no site-specific studies exist for the sealing units and the need to establish fundamental knowledge of the seal properties is very high. For the

Fjerritslev Formation we can draw parallels to the better-known Fjerritslev Formation in the Stenlille area and the Vedsted-1 sample set as a basis for the evaluation, but we cannot safely rely on its representation. For the younger secondary sealing units in the Gassum structure no analytical data exist on the seal capacity.

The geometry of the structure on the mapped surface of the Top Gassum Formation and the relief from the deepest closure (spill-point) to the top structure is sensitive to mapping and depth conversion constraints despite the much-improved database. Thus, it is recommended to still improve the database and conduct a careful mapping and time-to-depth models.

A key element for the quantification of the storage potential of the structure is the understanding of the storage efficiency. The storage efficiency factor is mostly dependent on reservoir architecture and performance and thus potential heterogeneity, permeability, and compartmentalization, but also by economic aspects such as well density, well layout and injection design. Better understanding of the reservoir and dynamic simulation of reservoir flow could constrain storage efficiency better and thus narrow the estimated final capacity range.

# 11. Acknowledgements – The new seismic data

GEUS appreciates the excellent collaboration with Professor Alireza Malehmir and his researcher team from Uppsala University, including Michael Westgate, Emmanouil Konstantinidis, Kristina Kucinskaite, Samuel Zappalá, Grzegorz Paletko, Tatiana Pertuz, Myrto Papadopoulou, Lea Gyger, and Jolanta Putnaite on the planning, acquisition and completion of the GEUS2023-GASSUM seismic survey.

We also acknowledge the work by Geopartner Geofizyka on the operation of the seismic sources and the great field assistance from all the students from the University of Copenhagen. Furthermore, the good cooperation with COWI on permits, logistics and communication with local citizens during the acquisition is highly appreciated.

The good cooperation with the geophysics company Realtimeseismic during reprocessing of the 2D survey is also appreciated.

# References


Abramovitz, T., Vosgerau, H., Gregersen, U., Smit, F.W.H., Bjerager, M., Jusri, T.A., Mathiesen, A., Mørk, F., Schovsbo, N.H., Petersen, H.I., Nielsen, L.H., Laghari, S., Rasmussen, L.M. and Keiding, M. 2024. CCS2022-2024 WP1: The Rødby structure. Seismic data and interpretation to mature potential geological storage of $CO_2$. Danmarks og Grønlands Geologiske Undersøgelse Rapport 2024/18. https://doi.org/10.22008/gpub/34739

Amour, F., Hajiabadi, M.R., Hosseinzadehsadati, S. and Nick, H.M. 2022. Impacts of $CO_2$ injection on the compaction behaviour of chalk reservoirs. Proceedings of the 16th Greenhouse Gas Control Technologies Conference (GHGT-16). 9 pp. https://dx.doi.org/10.2139/ssrn.4286144

Anthonsen, K.L., Aagaard, P., Bergmo, P.E.S., Gislason, S.R., Lothe, A.E., Mortensen, G.M. and Snæbjörnsdóttir, S.Ó. 2014. Characterisation and selection of the most prospective $CO_2$ storage sites in the Nordic region. Energy Procedia 63, 4884–4896. https://doi.org/10.1016/j.egypro.2014.11.519

Arvidsson, R., Gregersen, S., Kulhánek, O. and Wahlström, R. 1991. Recent Kattegat earthquakes – evidence of active intraplate tectonics in southern Scandinavia. Physics of the Earth and Planetary Interiors 67 (3–4), 275–287. https://doi.org/10.1016/0031-9201(91)90024-C

Beckel, R.A. and Juhlin, C. 2019. The cross-dip correction as a tool to improve imaging of crooked-line seismic data: a case study from the post-glacial Burtrask fault, Sweden. Solid Earth 10 (2), 581–598. https://doi.org/10.5194/se-10-581-2019

Bertelsen, F. 1978. The Upper Triassic – Lower Jurassic Vinding and Gassum Formations of the Norwegian–Danish Basin. Danmarks Geologiske Undersøgelse Serie B 3, 26 pp. https://geusjournals.org/index.php/serieb/issue/view/927

Bertelsen, F. 1980. Lithostratigraphy and depositional history of the Danish Triassic. Danmarks Geologiske Undersøgelse Serie B 4, 59 pp. https://geusjournals.org/index.php/serieb/issue/view/928

Catuneanu, O. 2019. Model-independent sequence stratigraphy. Earth-Science Reviews 188, 312–388. https://doi.org/10.1016/j.earscirev.2018.09.017

Chadwick, R.A., Zweigel, P., Gregersen, U., Kirby, G.A., Holloway, S. and Johannesen, P.N. 2004. Geological reservoir characterization of a $CO_2$ storage site: The Utsira Sand, Sleipner, northern North Sea. Energy 29 (9−10), 1371–1381. https://doi.org/10.1016/j.energy.2004.03.071

Clark, C.E. 1962. The PERT model for the distribution of an activity Time. Operations Research 10 (3), 405–406. https://doi.org/10.1287/opre.10.3.405

Clausen, O.R., Nielsen, S.B., Egholm, D.L. and Gołędowski, B. 2012. Cenozoic structures in the eastern North Sea Basin – A case for salt tectonics. Tectonophysics 514–517, 156–167. https://doi.org/10.1016/j.tecto.2011.10.017

Dahl-Jensen, T., Jakobsen, R., Bech, T.B., Nielsen, C.M., Albers, C.N., Voss, P.H. and Larsen, T.B. 2021. Monitoring for seismological and geochemical groundwater effects of high-volume pumping of natural gas at the Stenlille underground gas storage facility, Denmark. GEUS Bulletin 47, 5552. https://doi.org/10.34194/geusb.v47.5552

Danish American Prospecting Co 1951. Gassum-1, Completion report (Compiled March 1993).

Dybkjær, K. 1988. Palynological zonation and stratigraphy of the Jurassic section in the Gassum No. 1-borehole, Denmark. Danmarks Geologiske Undersøgelse Serie A 21, 73 pp. https://geusjournals.org/index.php/seriea/article/view/7040

Dybkjær, K. 1991. Palynological zonation and palynofacies investigation of the Fjerritslev Formation (Lower Jurassic – basal Middle Jurassic) in the Danish Subbasin. Danmarks Geologiske Undersøgelse Serie A 30, 150 pp. https://doi.org/10.34194/seriea.v30.7050

Fam, H.J.A., Naghizadeh, M., Smith, R., Yilmaz, Ö., Cheraghi, S. and Rubingh, K. 2023. High-resolution 2.5D multifocusing imaging of a crooked seismic profile in a crystalline rock environment: Results from the Larder Lake area, Ontario, Canada. Geophysical Prospecting 71 (7), 1152–1180. http://dx.doi.org/10.1111/1365-2478.13285

Fuchs, S., Balling, N. and Mathiesen, A. 2020. Deep basin temperature and heat-flow field in Denmark – New insights from borehole analysis and 3D geothermal modelling. Geothermics, 83, 101722. http://doi.org/10.1016/j.geothermics.2019.101722

Ehlig-Economides, C. and Economides, M.J. 2010. Sequestering carbon dioxide in a closed underground volume. Journal of Petroleum Science and Engineering 70 (1–2), 123–130. https://doi.org/10.1016/j.petrol.2009.11.002

Goodman, A., Hakala, A., Bromhal, G., Deel, D., Rodosta, T., Frailey, S., Small, M., Allen, D., Romanov, V., Fazio, J., Huerta, N., McIntyre, D., Kutchko, B. and Guthrie, G. 2011. U.S. DOE methodology for the development of geologic storage potential for carbon dioxide at the national and regional scale, International Journal of Greenhouse Gas Control 5 (4), 952–965. https://doi.org/10.1016/j.ijggc.2011.03.010

Gorecki, C.D., Holubnyak, Y.I., Ayash, S.C., Bremer, J.M., Sorensen, J.A., Steadman, E.N. and Harju, J.A. 2009. A new classification system for evaluating $CO_2$ storage resource/capacity estimates. SPE International Conference on $CO_2$ Capture, Storage, and Utilization, San Diego, California, USA. https://doi.org/10.2118/126421-MS

Global CCS Institute 2022. Gobal status of CCS 2022. URL: https://status22.globalccsinstitute.com

Gregersen, U., Hjelm, L., Vosgerau, H., Smit, F.W.H., Nielsen, C.M., Rasmussen, R., Bredesen, K., Lorentzen, M., Mørk, F., Lauridsen, B.W., Pedersen, G.K., Nielsen, L.H., Mathiesen, A., Laghari, S., Kristensen, L., Sheldon, E., Dahl-Jensen, T., Dybkjær, K., Hidalgo, C.A. and Rasmussen, L.M. 2023. CCS2022-2024 WP1: The Stenlille structure – Seismic data and interpretation to mature potential geological storage of $CO_2$. Danmarks og Grønlands Geologiske Undersøgelse Rapport 2022/26. 164 pp. https://doi.org/10.22008/gpub/34661

Gregersen, U., Vosgerau, H., Smit, F.W.H., Lauridsen, B.W., Mathiesen, A., Mørk, F., Nielsen, L.H., Rasmussen, R., Funck, T., Dybkjær, K., Sheldon, E., Pedersen, G.K., Nielsen, C.M., Bredesen, K., Laghari, S., Olsen, M.L. and Rasmussen, L.M. 2023. CCS2022-2024 WP1: The Havnsø structure. Seismic data and interpretation to mature potential geological storage of $CO_2$. Danmarks og Grønlands Geologiske Undersøgelse Rapport 2023/38. 200 pp. https://doi.org/10.22008/gpub/34705

Gulf Denmark 1968. Ørslev-1, Completion report.

Hamberg, L. and Nielsen, L.H. 2000. Shingled, sharp-based shoreface sandstones: depositional response to stepwise forced regression in a shallow basin, Upper Triassic Gassum

Formation, Denmark. In: Hunt, D. and Gawthorpe, R.L. (eds): Sedimentary Responses to Forced Regressions. Geological Society, London, Special Publications 172, 69–89. https://doi.org/10.1144/GSL.SP.2000.172.01.04

Hansen, J.P.V. and Rasmussen, E.S. 2008. Structural, sedimentologic, and sea-level controls on sand distribution in a steep-clinoform asymmetric wave-dominated delta: Miocene Billund sand, eastern Danish North Sea and Jylland. Journal of Sedimentary Research 78 (2), 130–146. https://doi.org/10.2110/jsr.2008.010

Hjelm L., Anthonsen K.L., Dideriksen K., Nielsen C.M., Nielsen L.H. and Mathiesen A. 2022. Capture, Storage and Use of $CO_2$ (CCUS). Evaluation of the $CO_2$ storage potential in Denmark. Vol.1: Report & Vol 2: Appendix A and B [Published as two separate volumes both with Series number 2020/46]. Danmarks og Grønlands Geologiske Undersøgelse Rapport 2020/46, 141 pp. https://doi.org/10.22008/gpub/34543

Holmslykke, H.D., Schovsbo, N.H., Kristensen, L., Weibel, R. and Nielsen, L.H. 2019. Characterising brines in deep Mesozoic sandstone reservoirs, Denmark. GEUS Bulletin 43. https://doi.org/10.34194/GEUSB-201943-01-04

IPCC (Intergovernmental Panel on Climate Change) 2022. Climate Change 2022: Mitigation of Climate Change. Working Group III contribution to the Sixth Assessment Report of the Intergovernmental Panel on Climate Change. UN, New York. 2913 pp.

Ineson, J.R. 1993. The Lower Cretaceous chalk play in the Danish Central Trough. Geological Society, London, Petroleum Geology Conference Series 4, 175–183. https://doi.org/10.1144/00401

Ineson, J.R., Jutson, D.J. and Schiøler, P. 1997. Mid-Cretaceous sequence stratigraphy in the Danish Central Trough. Danmarks og Grønlands Geologiske Undersøgelse Rapport 1997/109, 60 pp. https://doi.org/10.22008/gpub/14675

Ineson, J.R., Petersen, H.I., Andersen, C., Bjerager, M., Jakobsen, F.C., Kristensen, L., Mørk, F. and Sheldon, E. 2022. Early Cretaceous stratigraphic and basinal evolution of the Danish Central Graben: a review. Bulletin of the Geological Society of Denmark 71, 75–98. https://doi.org/10.37570/bgsd-2022-71-05

James, B., Grundy, A.T. and Sykes, M.A. 2013. The Depth-Area-Thickness (DAT) method for calculating gross rock volume: a better way to model hydrocarbon contact uncertainty. AAPG International Conference & Exhibition, Cartagena, Colombia.

Japsen, P. 1998. Regional velocity–depth anomalies, North Sea chalk: a record of overpressure and Neogene uplift and erosion. AAPG Bulletin 82, 2031–2074.

Japsen, P. and Bidstrup, T. 1999. Quantification of late Cenozoic erosion in Denmark based on sonic data and basin modelling. Bulletin of the Geological Society of Denmark 46, 79–99. https://doi.org/10.37570/bgsd-1999-46-08

Japsen, P., Green, P.F., Nielsen, L.H., Rasmussen, E.S. and Bidstrup, T. 2007. Mesozoic–Cenozoic exhumation events in the eastern North Sea Basin: a multi-disciplinary study based on palaeothermal, palaeoburial, stratigraphic and seismic data. Basin Research 19 (4), 451–490. https://doi.org/10.1111/j.1365-2117.2007.00329.x

Jensen, E.F. 2023. Towards inferring elastic moduli for argillaceous sandstones: clay content estimation in drill core utilizing hyperspectral imaging. Master thesis. University of Copenhagen. https://pub.geus.dk/files/40976670/EFJ_THESIS.pdf

Jensen, T.F, Holm, L., Frandsen, N. and Michelsen, O. 1986. Jurassic-Lower Cretaceous Lithostratigraphic Nomenclature for the Danish Central Trough. Danmarks Geologiske Undersøgelse Serie A 12, 65 pp. https://doi.org/10.34194/seriea.v12.7031

Konstantinidis, E., Malehmir, A., Westgate, M., Kucinskaite, K., Gregersen, U., Keiding, M. 2023. Velocity model building and seismic imaging of the Gassum structure for potential $CO_2$ storage in Denmark. 4th EAGE Global Energy Transition Conference & Exhibition (GET 2023), 5 pp. https://doi.org/10.3997/2214-4609.202321050

Laier, T. 2002. Vurdering af udfældningsrisici ved geotermisk produktion fra Margretheholmboringen MAH-1A. Beregning af mætningsindeks for mineraler i saltvand fra Danmarks dybere undergrund. Danmarks og Grønlands Geologiske Undersøgelse Rapport 2002/95, 48 pp. https://data.geus.dk/pure-pdf/18501_GEUS_R_2002_95_opt.pdf

Laier, T. 2008. Chemistry of Danish saline formation waters relevant for core fluid experiments: fluid chemistry data for lab experiments related to $CO_2$ storage in deep aquifers. Danmarks og Grønlands Geologiske Undersøgelse Rapport 2008/48. 10 pp. https://data.geus.dk/pure-pdf/27171_GEUS-R_2008_48_opt.pdf

Laier, T. and Øbro, H. 2009. Environmental and safety monitoring of the natural gas underground storage at Stenlille, Denmark. Geological Society, London, Special Publications 313, 81–92. https://doi.org/10.1144/SP313.6

Larner, K.L., Gibson, B.R., Chambers, R. and Wiggins, R.A. 1979. Simultaneous estimation of residual static and cross-dip corrections. Geophysics 44 (7), 1175–1192. https://doi.org/10.1190/1.1441001

Larsen, G. 1966. Rhaetic–Jurassic– Lower Cretaceous sediments un the Danish Embayment (A heavy-mineral study). Danmarks Geologiske Undersøgelse II. Række 91, 127 pp. https://doi.org/10.34194/raekke2.v91.6882

Larsen, M., Bidstrup, T. and Dalhoff F. 2003. Mapping of deep saline aquifers in Denmark with potential for future $CO_2$ storage. Danmarks og Grønlands Geologiske Undersøgelse Rapport 2003/39, 83 pp. https://doi.org/10.22008/gpub/19006

Lauridsen, B.W., Lode, S., Sheldon, E., Frykman, P., Anderskouv, K. and Ineson, J. 2022. Lower Cretaceous (Hauterivian–Aptian) pelagic carbonates in the Danish Basin: new data from the Vinding-1 well, central Jylland, Danmark. Bulletin of the Geological Society of Denmark 71, 7–29. https://doi.org/10.37570/bgsd-2022-71-02

Liboriussen, J., Ashton, P. and Tygesen, T. 1987. The tectonic evolution of the Fennoscandian Border Zone in Denmark. Techtonophysics 137, 21–29. https://doi.org/10.1016/0040-1951(87)90310-6

Lindström, S., Pedersen, G.K., Vosgerau, H., Hovikoski, J., Dybkjær, K. and Nielsen, L.H. 2023. Palynology of the Triassic–Jurassic transition of the Danish Basin (Denmark): a palynostratigraphic zonation of the Gassum–lower Fjerritslev formations. Palynology 47 (4), 1–34. https://doi.org/10.1080/01916122.2023.2241068

Malehmir, A. and Westgate, M., 2023. GEUS2023-GASSUM seismic survey – Acquisition, processing and results. Final report. Uppsala University, Sweden. 26 pp.

Mallon, A.J. and Swarbrick, R.E. 2002. A compaction trend for non-reservoir North Sea Chalk. Marine and Petroleum Geology 19 (5), 527–539. https://doi.org/10.1016/S0264-8172(02)00027-2

Mallon, A.J. and Swarbrick, R.E. 2008. Diagenetic characteristics of low permeability, non-reservoir chalk from the Central North Sea, Marine and Petroleum Geology 25 (10), 1097–1108. https://doi.org/10.1016/j.marpetgeo.2007.12.001

Mancuso, C. and Naghizadeh, M. 2021. Generalized cross dip moveout correction of crooked 2D seismic surveys. Geophysics 86 (4), 1–61. https://doi.org/10.1190/geo2020-0278.1

Mathiesen, A., Dam, G., Fyhn, M.B.W., Kristensen, L., Mørk, F., Petersen, H.I. and Schovsbo, N.H. 2022. Foreløbig evaluering af $CO_2$ lagringspotentiale af de saline akviferer i Nordsøen. Danmarks og Grønlands Geologiske Undersøgelse Rapport 2022/15, 151 pp. https://doi.org/10.22008/gpub/34650

Mbia, E.N., Fabricius, I.L., Krogsbøll, A., Frykman, P. and Dalhoff, F. 2014: Permeability, compressibility and porosity of Jurassic shale from the Norwegian-Danish Basin. Petroleum Geoscience 20, 257–281. https://doi.org/10.1144/petgeo2013-035

McBride, E.F. 1963. A classification of common sandstones. Journal of Sedimentary Research 33, 664–669.

Michelsen, O. 1975. Lower Jurassic biostratigraphy and ostracods of the Danish Embayment. Danmarks Geologiske Undersøgelse II. Række 104, 1–287. https://doi.org/10.34194/raekke2.v104.6895

Michelsen, O. 1978. Stratigraphy and distribution of Jurassic deposits of the Norwegian–Danish Basin. Danmarks Geologiske Undersøgelse Serie B 2, 28 pp. https://doi.org/10.34194/serieb.v2.7057

Michelsen, O. 1989a. Revision of the Jurassic lithostratigraphy of the Danish Subbasin. Danmarks Geologiske Undersøgelse Serie A 24, 22 pp. https://doi.org/10.34194/seriea.v24.7044

Michelsen, O. 1989b. Log-sequence analysis and environmental aspects of the Lower Jurassic Fjerritslev Formation in the Danish Subbasin. Danmarks Geologiske Undersøgelse Serie A 25, 23 pp. https://doi.org/10.34194/seriea.v25.7045

Michelsen, O. and Bertelsen, F. 1979. Geotermiske reservoirformationer i den danske lagserie. Danmarks Geologiske Undersøgelse, Årbog 1978, 151–163. https://data.geus.dk/pure-pdf/1979_Michelsen_Geotermiske_reservoirformationer.pdf

Michelsen O. and Nielsen, L.H. 1991. Well records on the Phanerozoic stratigraphy in the Fennoscandian Border Zone, Denmark: Hans-1, Sæby-1, and Terne-1 wells. Danmarks Geologiske Undersøgelse Serie A 29. 37 pp. https://doi.org/10.34194/seriea.v29.7049

Michelsen, O. and Nielsen, L.H. 1993. Structural development of the Fennoscandian Border Zone, offshore Denmark. Marine and Petroleum Geology 10 (2), 124–134. https://doi.org/10.1016/0264-8172(93)90017-M

Michelsen, O., Saxov, S. Leth, J.A., Andersen, C., Balling, N., Breiner, N., Holm, L., Jensen, K., Kristensen, J.I., Laier, T., Nygaard, E., Olsen, J.C., Poulsen, K.D., Priisholm, S., Raade, T.B., Sørensen, T.R. and Würtz, J. 1981. Kortlægning af potentielle geotermiske reservoirer i Danmark. Danmarks Geologiske Undersøgelse Serie B 5, 96 pp.

Michelsen, O., Nielsen, L.H., Johannessen, P.N., Andsbjerg, J. and Surlyk, F. 2003. Jurassic lithostratigraphy and stratigraphic development onshore and offshore Denmark. In: Ineson, J.R. and Surlyk, F. (eds): The Jurassic of Denmark and Greenland. GEUS Bulletin 1, 145–216. https://doi.org/10.34194/geusb.v1.4651

Mogensen, T.E. and Korstgård, J. 1993. Structural development and trap formation along the Børglum Fault, Tornquist Zone, Denmark, and a comparison with the Painted Canyon Fault, San Andreas Zone, USA. In: Spencer A.M. (Ed.), Generation, Accumulation and Production of Europe's Hydrocarbons 3, 89–97, Springer Verlag, Berlin. https://doi.org/10.1007/978-3-642-77859-9_8

Nedimović, M.R. and West, G.F. 2003. Crooked-line 2D seismic reflection imaging in crystalline terrains: Part 1, data processing. Geophysics 68 (1), 274–285. https://doi.org/10.1190/1.1543213

Nielsen, L.H. 2003. Late Triassic – Jurassic development of the Danish Basin and the Fennoscandian Border Zone, southern Scandinavia. In: Ineson, J.R. and Surlyk, F. (eds): The Jurassic of Denmark and Greenland. GEUS Bulletin 1, 459–526. https://doi.org/10.34194/geusb.v1.4681

Nielsen, L.H. and Japsen, P. 1991. Deep wells in Denmark 1935–1990. Lithostratigraphic subdivision. Danmarks Geologiske Undersøgelse, Danmarks Geologiske Undersøgelse Serie A 31, 179 pp. https://doi.org/10.34194/seriea.v31.7051

Nielsen, L., Boldreel, L.O., Hansen, T.M, Lykke-Andersen, H., Stemmerik, L., Surlyk, F. and Thybo, H. 2011. Integrated seismic analysis of the Chalk Group in eastern Denmark – Implications for estimates of maximum palaeo-burial in southwest Scandinavia. Tectonophysics 511 (1–2), 14–26. https://doi.org/10.1016/j.tecto.2011.08.010

Norwood, J.A., Norvang, A. and von Elm, C. 1951. Final Report on Gassum No. 1. Danmarks Geologiske Undersøgelse (unpublished report). 134 pp.

Olivarius, M., Heredia, B.D., Malkki, S.N., Thomsen, T.B. and Vosgerau, H. 2020. Capture, Storage and Use of $CO_2$ (CCUS): Provenance of the of Gassum Formation: Implications for reservoir distribution and mineralogy (Part of Work package 6 in the CCUS project). Danmarks og Grønlands Geologiske Undersøgelse Rapport 2020/38, 35 pp. https://doi.org/10.22008/gpub/34535

Olivarius, M., Vosgerau, H., Nielsen, L.H., Weibel, R., Malkki, S.N., Heredia, B.D. and Thomsen, T.B. 2022. Maturity Matters in Provenance Analysis: Mineralogical differences explained by sediment transport from Fennoscandian and Variscian sources. Geosciences 2022, 12, 308, 24 pp. https://doi.org/10.3390/geosciences12080308

Olsen, H. 1988. Sandy braid plan deposits from the Triassic Skagerrak Formation in the Thisted-2 well, Denmark. Geological Survey of Denmark Serie B 11, 26 pp.

Palmer, D. 1980. The generalized reciprocal method of seismic refraction interpretation. Society of Exploration Geophysicists. https://doi.org/10.1190/1.9781560802426

Payton, C.E. 1977. Seismic Stratigraphy – applications to hydrocarbon exploration. AAPG Memoir 26, 516 pp. https://doi.org/10.1306/M26490

Pedersen, G.K. 1986. Changes in the bivalve assemblage of an early Jurassic mudstone sequence (the Fjerritslev Formation in the Gassum 1 Well, Denmark). Palaeogeography, Palaeoclimatology, Palaeoecology 53 (2–4), 139–168. https://doi.org/10.1016/0031-0182(86)90042-8

Pedersen, G.K. and Andersen, P.R. 1980. Depositional environments, diagenetic history and source areas of some Bunter Sandstones in northern Jutland. Danmarks Geologiske Undersøgelse, Årbog 1979, 69–93. https://data.geus.dk/pure-pdf/1980_Pedersen_Depositional_environments.pdf

Petersen, H. I., Nielsen, L. H., Bojesen-Koefoed, J. A., Mathiesen, A., Kristensen, L. and Dalhoff, F. 2008. Evaluation of the quality, thermal maturity and distribution of potential source rocks in the Danish part of the Norwegian–Danish Basin. GEUS Bulletin 16, 66 pp. https://doi.org/10.34194/geusb.v16.4989

Poulsen, N.E. 1996. Dinoflagellate cysts from marine Jurassic deposits of Denmark and Poland. American Association of Stratigraphic Palynologists contribution series 31, 227 pp.

Poulsen, N.E. and Riding, J.B. 2003. The Jurassic dinoflagellate cyst zonation of Subboreal Northwest Europe. GEUS Bulletin 1, 115–144. https://doi.org/10.34194/geusb.v1.4650

Rasmussen, E.S. 2004. The interplay between true eustatic sea-level changes, tectonics and climatic changes: what is the dominating factor in sequence formation of the Upper Oligocene – Miocene succession in the eastern North Sea Basin, Denmark. Global and Planetary Changes 41 (1), 15–30. https://doi.org/10.1016/j.gloplacha.2003.08.004

Rasmussen, E.S. 2009. Neogene inversion of the Central Graben and Ringkøbing-Fyn High, Denmark. Tectonophysics 465 (1–4), 84–97. https://doi.org/10.1016/j.tecto.2008.10.025

Rasmussen, E.S. and Dybkjær, K. 2005. Sequence stratigraphy of the Upper Oligocene-Lower Miocene of eastern Jylland, Denmark: role of structural relief and variable sediment supply in controlling sequence development. Sedimentology 52 (1), 25–63. https://doi.org/10.1111/j.1365-3091.2004.00681.x

Rasmussen, E.S. and Nielsen, A.T. 2020. Danmarks Geologi – En kort introduktion. Junior Geologerne. https://junior-geologerne.dk/wp-content/uploads/2020/06/Junior-Geologerne_Danmarks_geologi.pdf

Realtimeseismic 2024. GEUS2023-GASSUM-RE2023 – Reprocessing of the GEUS2023-GASSUM 2D Seismic Survey for the Geological Survey of Denmark and Greenland. 68 pp.

Schmelzbach, C., Juhlin, C., Carbonell, R. and Simancas, J.F. 2007. Prestack and poststack migration of crooked-line seismic reflection data: a case study from the South Portuguese Zone fold belt, southwestern Iberia. Geophysics 72 (2), B9–B18. https://doi.org/10.1190/1.2407267

Schonewille, M., Klaedtke, A., Vigner, A., Brittan, J. and Martin, T. 2009. Seismic data regularization with the anti-alias anti-leakage Fourier transform. First Break 27 (9). https://doi.org/10.3997/1365-2397.27.1304.32570

Schovsbo, N.H. and Petersen, H.I. 2024. Analysis of the applicability of cuttings samples to test seal integrity, examples from the Triassic to Jurassic interval in 8 wells in Eastern Denmark. Danmarks og Grønlands Geologiske Undersøgelse Rapport 2024/10, 67 pp. https://doi.org/10.22008/gpub/34731

Schovsbo, N., Holmslykke, H., Mathiesen, A. and Møller Nielsen, C. in prep. Assessment of brine salinity in selected $CO_2$ storage sites, Eastern Denmark.

Sirocko, F., Reicherter, K., Lehné, R., Hübscher, C., Winsemann, J. and Stackebrandt, W. 2008. Glaciation, salt and the present landscape. In: Littke, R., et al. (Eds.), Dynamics of Complex Intracontinental Basins: the Central European Basin System, 233–245. Springer Verlag, Heidelberg. https://link.springer.com/chapter/10.1007/978-3-540-85085-4_4

Sorgenfrei, T. and Buch, A. 1964. Deep Tests in Denmark 1935–1959. Danmarks Geologiske Undersøgelse III. Række 36, 146 pp. https://doi.org/10.34194/raekke3.v36.6941

Span, R. and Wagner, W. 1996. A new equation of state for carbon dioxide covering the fluid region from the triple-point temperature to 1100K at pressures up to 800 MPa. Journal of Physical and Chemical Reference Data 25 (6), 1509–1596.

Springer, N., Didriksen, K., Holmslykke, H.D., Kjøller, C., Olivarius, M. and Schovsbo, N. 2020. Capture, Storage and Use of $CO_2$ (CCUS): Seal capacity and geochemical modelling (Part of work package 5 in the CCUS project). Danmarks og Grønlands Geologiske Undersøgelse Rapport 2020/30, 42 pp. https://doi.org/10.22008/gpub/34527

Spudich, P., Fletcher, J.B., Hellweg, M., Boatwright, J., Sullivan, C., Joyner, W.B., Hanks, T.C., Boore, D.M., McGarr, A., Baker, L.M. and Lindh, A.G. 1997. SEA96 – A New Predictive Relation for Earthquake Ground Motions in Extensional Tectonic Regimes. Seismological Research Letters 68 (1), 190–198. https://doi.org/10.1785/gssrl.68.1.190

Vejbæk O.V. 1997. Dybe strukturer i danske sedimentære bassiner. Geologisk Tidsskrift 1997 (4), 1–31. https://2dgf.dk/xpdf/gt1997-4-1-31.pdf

Vejbæk, O.V. and Britze, P. 1994. Geological map of Denmark 1:750.000. Top pre-Zechstein. Danmarks Geologiske Undersøgelse Map series 45, 9 pp.

Vejbæk, O.V., Bidstrup, T., Britze, P., Erlstrøm, M., Rasmussen, E.S. and Sivhed, U. 2007. Chalk depth structure maps, Central to Eastern North Sea, Denmark. In: Review of Survey activity 2006 (Ed. M. Sønderholm and A.K. Higgins), GEUS Bulletin 13, 9–12. https://doi.org/10.34194/geusb.v13.4962

Vood, R.M 1988. The Scandinavian earthquakes of 22 December 1759 and 31 August 1819. Disasters 12 (3), 223–236. https://doi.org/10.1111/j.1467-7717.1988.tb00672.x

Voss; P., Dahl-Jensen, T. and Larsen, T.B. 2015. Earthquake hazard in Denmark. Danmarks og Grønlands Geologiske Undersøgelse Rapport 2015/24, 54 pp. https://doi.org/10.22008/gpub/30674

Vosgerau, H., Gregersen, U., Hjuler, M.L., Holmslykke, H.D., Kristensen, L., Lindström, S., Mathiesen, A., Nielsen, C.M., Olivarius, M., Pedersen, G.K. and Nielsen, L.H. 2016. Reservoir prognosis of the Gassum Formation and the Karlebo Member within two areas of interest in northern Copenhagen. The EUDP project “Geothermal pilot well, phase 1b”. Danmarks og Grønlands Geologiske Undersøgelse Rapport 2016/56, 138 pp + app 1–5. https://doi.org/10.22008/gpub/32477

Vosgerau, H., Gregersen, U. and Laghari, S. 2020. Capture, Storage and Use of $CO_2$ (CCUS): Seismic interpretation of existing 3D seismic data around the Stenlille structure within the framework of sequence stratigraphy and with focus on the Gassum Formation (Part of Work package 6 in the CCUS project). Danmarks og Grønlands Geologiske Undersøgelse Rapport 2020/34, 53 pp. https://doi.org/10.22008/gpub/34531

Wang, Y., Zhangb, K. and Wua, N. 2013. Numerical investigation of the storage efficiency factor for $CO_2$ geological sequestration in saline formations. Energy Procedia 37, 5267–5274. https://doi.org/10.1016/j.egypro.2013.06.443

Weibel, R., Olivarius, M., Kjøller, C., Kristensen, L., Hjuler, M.L., Friis, H., Pedersen, P.K., Boyce, A., Andersen, M.S., Kamla, E., Boldreel, L.O., Mathiesen, A. and Nielsen, L.H. 2017. The influence of climate on early and burial diagenesis in Triassic and Jurassic sand stones from the Norwegian–Danish Basin. The Depositional Record 3 (1), 60–91. https://doi.org/10.1002/dep2.27

Weibel, R., Olivarius, M., Vosgerau, H., Mathiesen, A., Kristensen, L., Nielsen, C.M. and Nielsen, L.H. 2020. Overview of potential geothermal reservoirs in Denmark. Netherlands Journal of Geosciences 99, 14 pp. https://doi.org/10.1017/njg.2020.5

Westgate, M., Malehmir, A., Konstantinidis, E., Kucinskaite, K., Hjelm, L., Gregersen, U., Keiding, M. & Bjerager, M. 2023. Seismic imaging of the Gassum formation in Denmark for $CO_2$ storage potential using a dual-recording method. 29th European Meeting of Environmental and Engineering Geophysics, Near Surface Geoscience Conference and Exhibition 2023 (NSG 2023), 101–105.

Westgate, M., Malehmir, A., Kucinskaite, K., Konstantinidis, E., Gregersen, U., Keiding, M., Bjerager, M. 2024. High-resolution, large-scale seismic imaging of halokinetic-induced structures for geological carbon storage: results from East Jutland, Denmark. 30th European Meeting of Environmental and Engineering Geophysics (NSG 2024), 5 pp.

Westgate, M., Kucinskaite, K., Konstantinidis, E., Malehmir, A., Papadopoulou, M., Gregersen, U., Keiding, M., Bjerager, M. (submitted). Seismic Imaging of Halokinetic Sequences and Structures with High-Resolution, Dual-Element Acquisition and Processing: Applications to the Gassum Structure in Eastern Jutland, Denmark.

Wu, J. 1996. Potential pitfalls of crooked-line seismic reflection surveys. Geophysics 61 (1), 277–281. https://doi.org/10.1190/1.1443949

Yilmaz, Ö. 2001. Seismic Data Analysis: Processing, Inversion, and Interpretation of Seismic Data. Society of Exploration Geophysicists. 2065 pp.

Yu, T., Gholami, R., Raza, A., Vorland K.A.N. and Mamoud M. 2023. $CO_2$ storage in chalks: What are we afraid of? International Journal of Greenhouse Gas Control 123, 103832. https://doi.org/10.1016/j.ijggc.2023.103832

Zhang, J. and Toksöz, M.N. 1998. Nonlinear refraction traveltime tomography. Geophysics 63 (5), 1726–1737. https://doi.org/10.1190/1.1444468

Zhu, X., Sixta, D.P. and Angstman, B.G. 1992. Tomostatics: turning-ray tomography + static corrections. The Leading Edge 11 (12), 15–23. https://doi.org/10.1190/1.1436864

# Appendix A – Well-log interpretations

(Gassum-1 and the nearest wells)

Links to well-log interpretations

- Gassum-1
- Hobro-1
- Kvols-1
- Voldum-1

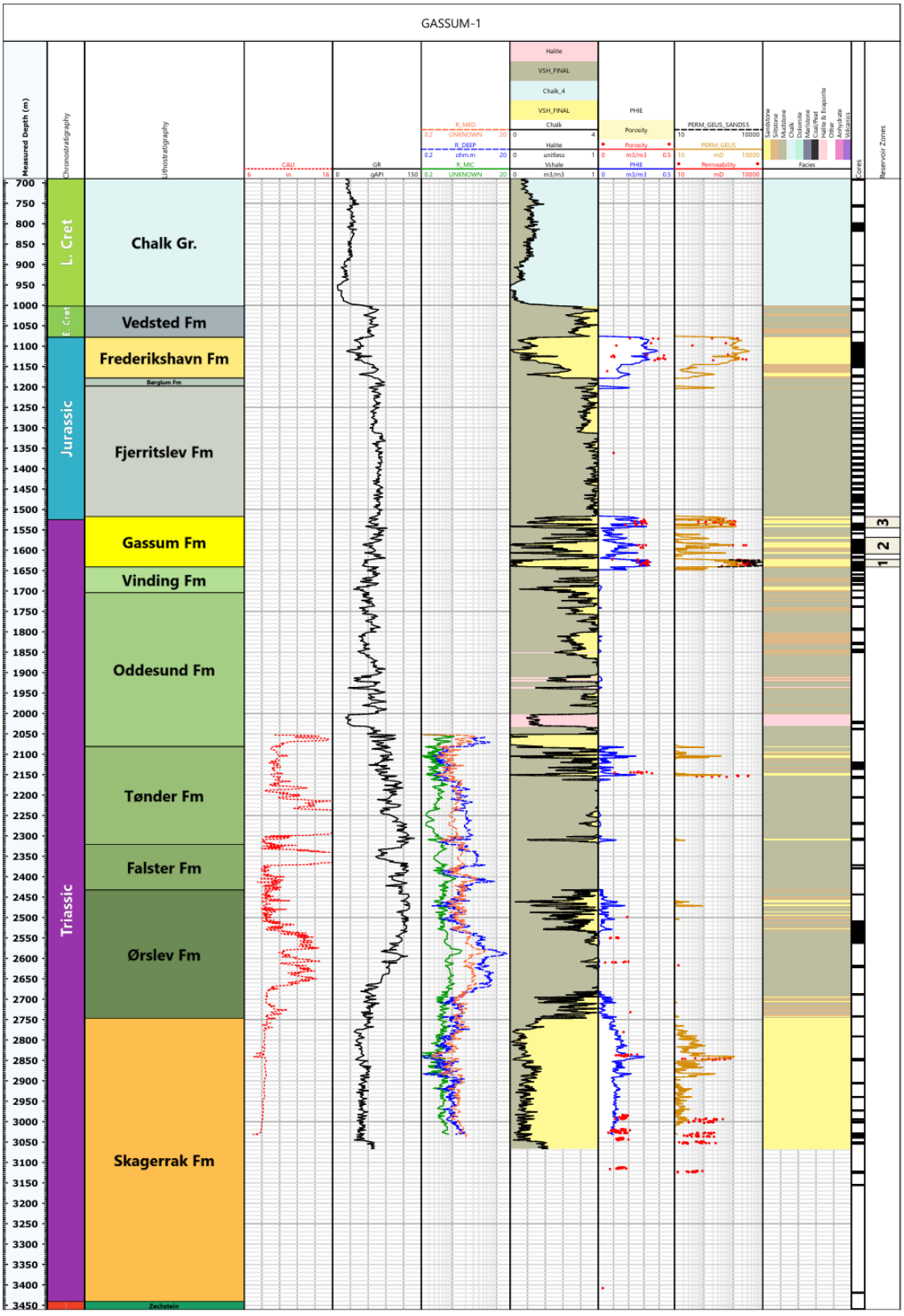
GASSUM-1
Measured Depth (m)
Chronostratigraphy
Lithostratigraphy
L. Cret
E. Cret
Jurassic
Triassic
Chalk Gr.
Vedsted Fm
Frederikshavn Fm
Berglum Fm
Fjerritslev Fm
Gassum Fm
Vinding Fm
Oddesund Fm
Tønder Fm
Falster Fm
Ørslev Fm
Skagerrak Fm
Zechstein
CALI
GR
R_MED
R_DEEP
R_MIC
Halite
VSH_FINAL
Chalk_4
Chalk
Vshale
PHIE
Porosity
PERM_GEUS_SANDS
PERM_GEUS
Permeability
Facies
Cores
Reservoir Zones
1
2
3

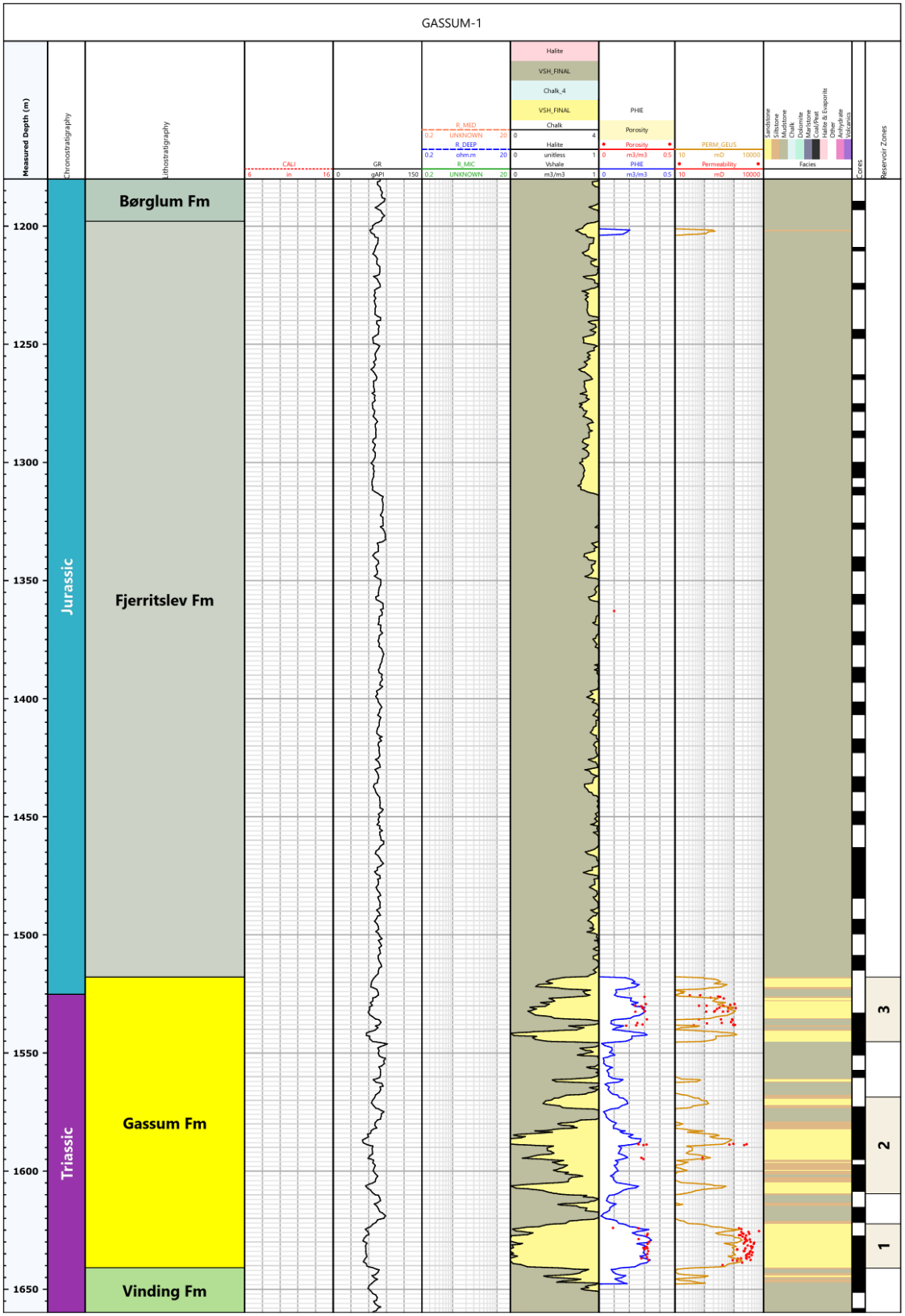
GASSUM-1
Measured Depth (m)
Chronostratigraphy
Lithostratigraphy
CALI
GR
R_MED
R_DEEP
R_MIC
Halite
VSH_FINAL
Chalk_4
VSH_FINAL
Chalk
Halite
Vshale
PHIE
Porosity
PHIE
PERM_GEUS
Permeability
Facies
Cores
Reservoir Zones
Jurassic
Triassic
Børglum Fm
Fjerritslev Fm
Gassum Fm
Vinding Fm
1200
1250
1300
1350
1400
1450
1500
1550
1600
1650
3
2
1

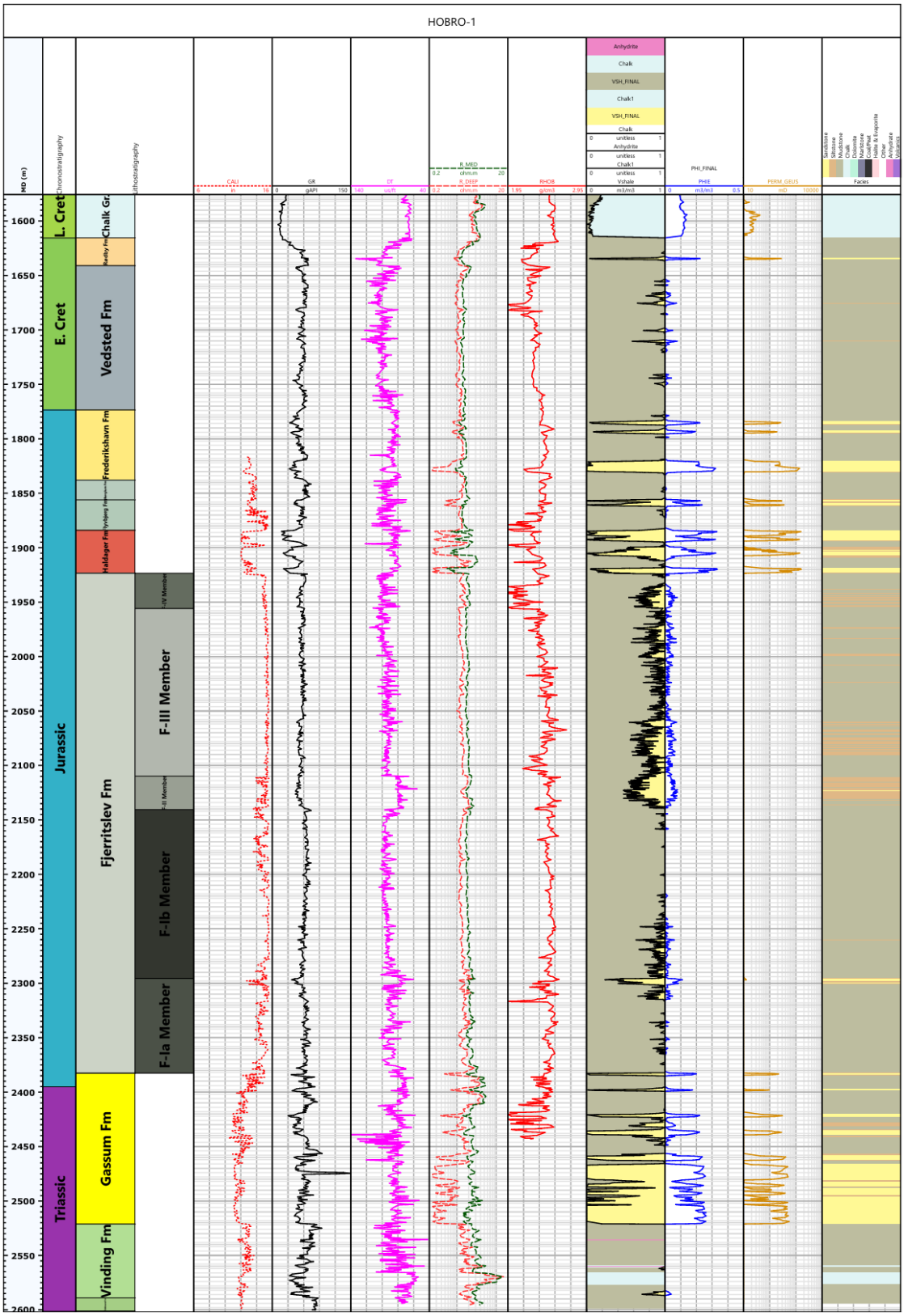
HOBRO-1
MD (m)
Chronostratigraphy
Lithostratigraphy
L. Cret
E. Cret
Jurassic
Triassic
Chalk Gr.
Vedsted Fm
Frederikshavn Fm
Haldager Fm
Fjerritslev Fm
F-IV Member
F-III Member
F-II Member
F-Ib Member
F-Ia Member
Gassum Fm
Vinding Fm
CALI
GR
DT
R_MED
R_DEEP
RHOB
PHI_FINAL
PHIE
PERM_GEUS
Anhydrite
Chalk
VSH_FINAL
Chalk1
Facies

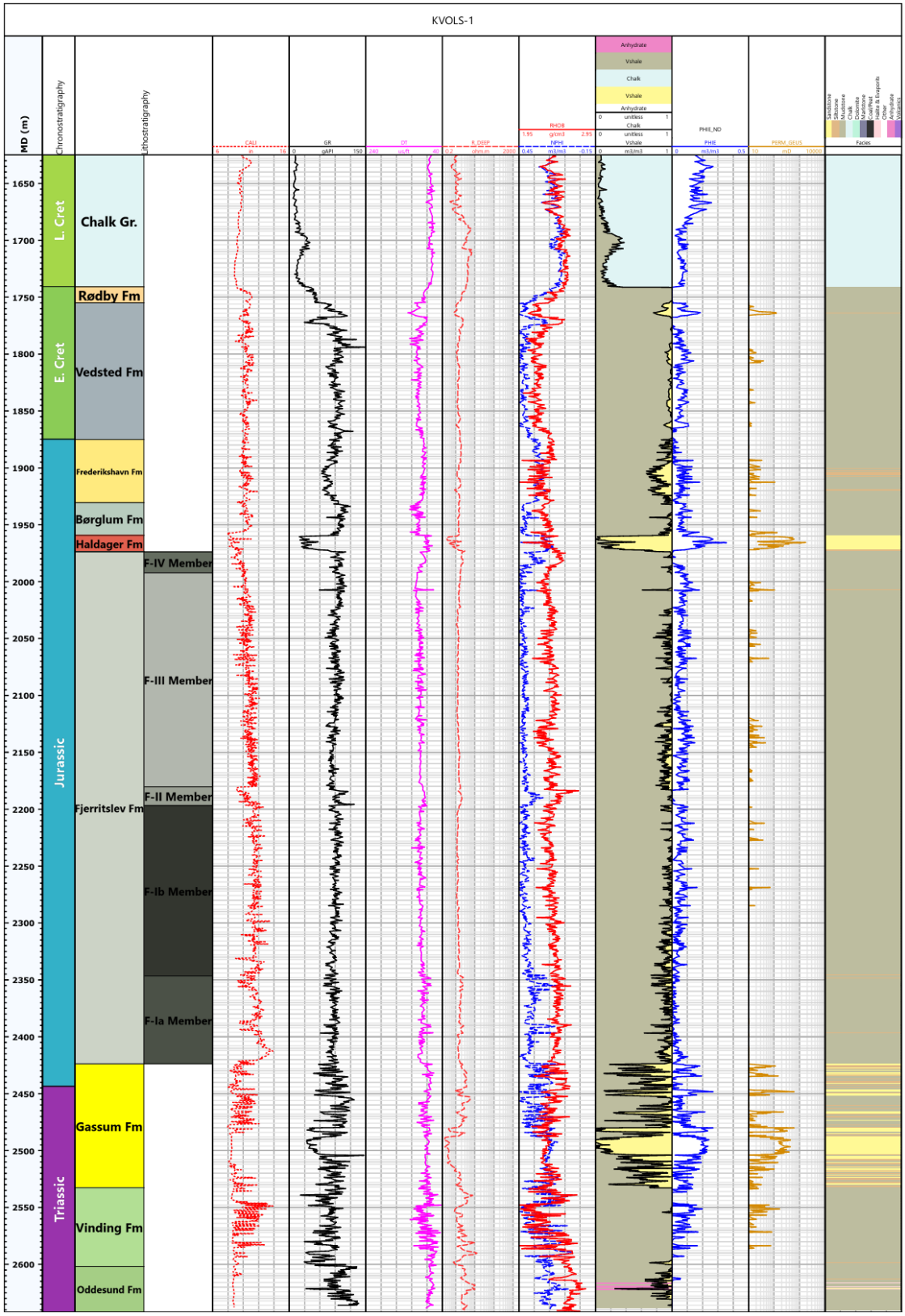
KVOLS-1
MD (m)
Chronostratigraphy
Lithostratigraphy
L. Cret
E. Cret
Jurassic
Triassic
Chalk Gr.
Rødby Fm
Vedsted Fm
Frederikshavn Fm
Børglum Fm
Haldager Fm
Fjerritslev Fm
F-IV Member
F-III Member
F-II Member
F-Ib Member
F-Ia Member
Gassum Fm
Vinding Fm
Oddesund Fm
CALI
GR
DT
R_DEEP
RHOB
NPHI
PHIE_ND
PHIE
PERM_GEUS
Facies
Anhydrate
Vshale
Chalk
Vshale
Anhydrate
Vshale
Sandstone
Siltstone
Limestone
Chalk
Dolomite
Dolerite
Coal/Mud
Halite & Evaporite
Tuffite
Anhydrate
Volcanics

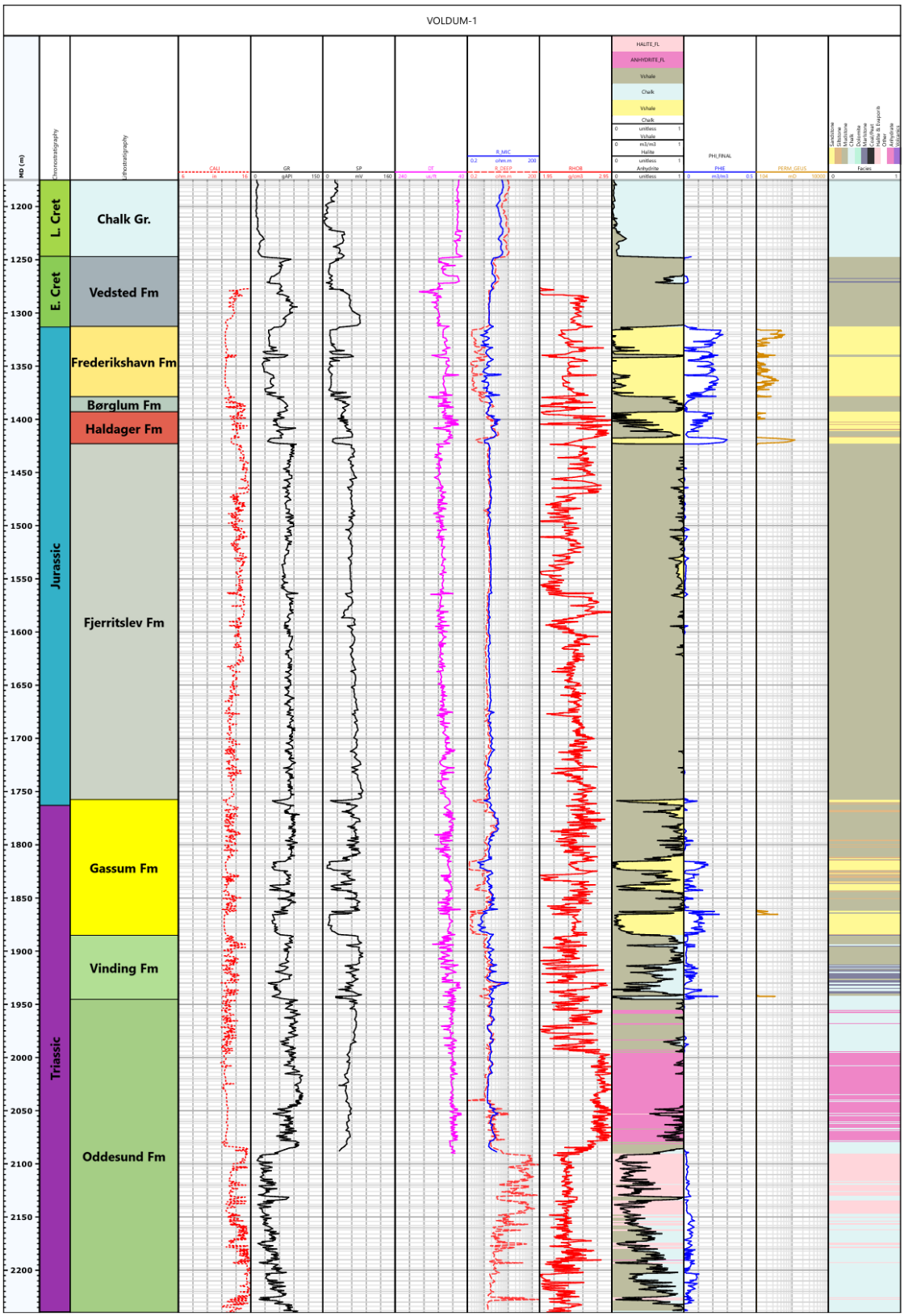
VOLDUM-1
MD (m)
Chronostratigraphy
Lithostratigraphy
L. Cret
E. Cret
Jurassic
Triassic
Chalk Gr.
Vedsted Fm
Frederikshavn Fm
Børglum Fm
Haldager Fm
Fjerritslev Fm
Gassum Fm
Vinding Fm
Oddesund Fm
CALI
GR
SP
DT
R_MIC
R_DEEP
RHOB
HALITE_FL
ANHYDRITE_FL
PHI_FINAL
PHIE
PERM_GEUS
Facies

# Appendix B – Biostratigraphy (see Chapter 7)

(Gassum-1 and the nearest wells)

Links to stratigraphic summary charts

- Gassum-1
- Hobro-1
- Hyllebjerg-1
- Kvols-1
- Voldum-1

**Introduction**

The Gassum-1 well penetrates the Gassum structure. In this well a series of cores were taken from the Upper Cretaceous to the TD in Permian deposits and several biostratigraphic studies have been performed on the core material. The biostratigraphic framework for the Gassum structure is therefore mainly based on these data but is supported by data from four offset wells located relatively near the structure, including Hobro-1, Hyllebjerg-1, Kvols-1 and Voldum-1. The present summary of the biostratigraphy in these 5 wells is mainly focused on the time interval represented by the Gassum and Fjerritslev formations.

The biostratigraphy has been used to guide the sequence stratigraphic framework for each well and for the correlations between the wells.

For each well a link is given to two different digital stratigraphic summary charts as these contain too many details to be seen in a printed version. One chart focuses on the Gassum- and Fjerritslev formations and combines the chronostratigraphy, lithostratigraphy, biostratigraphy and sequence stratigraphy and further include the bio-events and biozonations for the succession representing these two formations and their lower and upper boundaries. Another chart shows the overall stratigraphy for the full well, combining the chronostratigraphy, lithostratigraphy and sequence stratigraphy.

Provenance data (Olivarius et al. 2022) are included in the summary charts from those wells from which such analysis have been made.

**Zonations**

The zonations used include the ostracod zonation of Michelsen (1975a), the dinocyst zonation of Poulsen & Riding (2003) and a combination of the spore-pollen zonations of Lund (1977), Dybkjær (1991), Koppelhus & Nielsen (1994) and Lindström et al. (2023).

### Biostratigraphic summary for each of the key-wells

The biostratigraphy summarised here for each well is based on data from reports and publications combined with new data from some of the wells.

### Gassum-1

The succession in the Gassum-1 well referred to the Gassum- and Fjerritslev formations is represented by a close series of cores and the biostratigraphic data from this interval are based on these cores. The data comprise analysis of spores, pollen, dinoflagellate cysts (Nielsen 1983; Dybkjær 1988, 1991; Poulsen 1996) and ostracods (Michelsen 1975a).

The biostratigraphic data strongly support the lithostratigraphic subdivision for the Gassum-1 well presented in Nielsen & Japsen (1991), indicating the presence of a 123 m thick Gassum Formation overlain by a 320 m thick Fjerritslev Formation. The boundary between the Gassum and Fjerritslev formations is located in the lower Hettangian. The upper part of the Fjerritslev Formation (uppermost part of F-III Member and F-IV Member) is missing. The Fjerritslev Formation is unconformably overlain by Upper Jurassic deposits referred to the Børglum and Frederikshavn formations.

### Hobro-1

A series of sidewall-cores through the interval from the lower Frederikshavn Formation down to the lower part of the Gassum Formation were analysed for their content of spores, pollen and dinoflagellate cysts by Bertelsen (FB) (Lyngsie et al. 1974).

Michelsen (OM) (in Lyngsie et al. 1974) studied ostrocods from a very dense series of ditch cuttings samples from the Haldager Sand Formation down to the basal part of the Gassum Formation (Lyngsie et al. 1974). The samples in the Haldager Sand Formation and the upper part of the Fjerritslev Formation were barren of ostracods. Except for one species recorded in the lowermost part of the formation, all the ostracods recorded from the Gassum Formation were interpreted as being caved from younger parts of the succession.

The results of these analysis strongly support the lithostratigraphic subdivision of the succession referred to the Gassum and Fjerritslev formations. The boundary between the Gassum and Fjerritslev formations is located in the lower Hettangian. The upper part of the F-IV Member of the Fjerritslev Formation is missing, and the formation is unconformably overlain by the Middle Jurassic Haldager Sand Formation.

### Hyllebjerg-1

Palynological analysis have been made by Robertson Research (1983), Koppelhus (in Nielsen 1995) and Poulsen (1996). The analyses were made mainly on ditch cuttings samples but also on a few sidewall core samples. In spite of these three reports, the stratigraphically useful palynoevents within the succession referred to the Gassum and Fjerritslev formations are rather sparse.

Michelsen (1989) presented the results of a very detailed study of the ostracods within the Jurassic succession in the Hyllebjerg-1 well. This study resulted in a subdivision of the Fjerritslev Formation strongly supporting the lithostratigraphic subdivision presented here.

The boundary between the Gassum and Fjerritslev formations is located in the Hettangian. The upper part of the F-IV Member of the Fjerritslev Formation is missing, and the formation is unconformably overlain by the Middle Jurassic Haldager Sand Formation.

**Kvols-1**

Based on a mixture of ditch cuttings samples and sidewall core samples a series of palynoevents was presented by Robertson Research (1976, 1983) from the Lower Cretaceous down to the base of the well.

Ostracod data exists only from the upper part of the Fjerritslev Formation (Michelsen 1989).

The results of these analysis strongly support the lithostratigraphic subdivision of the succession referred to the Gassum and Fjerritslev formations. The boundary between the Gassum and Fjerritslev formations is located in the Hettangian. The upper part of the F-IV Member of the Fjerritslev Formation is missing, and the formation is unconformably overlain by the Middle Jurassic Haldager Sand Formation.

The biostratigraphy in the Kvols-1 wells indicates a different correlation of sequence stratigraphic surfaces with e.g. the Gassum-1 well at several stratigraphic levels within the Fjerritslev Formation than the correlations presented in the present study, which mainly is based on log correlations and sequence stratigraphy. A new, more detailed, biostratigraphic study in the Kvols-1 well is therefore suggested.

**Voldum-1**

A few sidewall core samples have been analysed palynologically by Bertelsen (1974). Only one sample represent the Gassum Formation, three the Fjerritslev Formation while six samples represents the overlying Middle Jurassic – Lower Cretaceous units. All these samples were also examined for the present study by Karen Dybkjær in order to try to identify additional stratigraphically important taxa.

Michelsen (1975b) analysed ostracods in a series of ditch cuttings samples covering the Vinding, Gassum and Fjerritslev formations. The resulting data are rather sparse as several of the samples were either barren or characterised by caved material. However, three ostracod zones were identified.

The results of these analysis generally support the lithostratigraphic subdivision of the succession referred to the Gassum and Fjerritslev formations. The upper boundary of the Gassum Formation is dated as early Hettangian. The upper part of the F-III Member and the F-IV Member of the Fjerritslev Formation is missing, and the formation is unconformably overlain by the Middle Jurassic Haldager Sand Formation.

**References**

Dybkjær, K. 1988. Palynological zonation and stratigraphy of the Jurassic section in the Gassum No.1-borehole, Denmark. DGU Serie A 21, 72 pp.

Dybkjær, K. 1991: Palynological zonation and palynofacies investigation of the Fjerritslev Formation (Lower Jurassic – basal Middle Jurassic) in the Danish Subbasin. Danmarks Geologiske Undersøgelse Serie A 30, 1–150.

Dybkjær, K. 1998. Datering og palynofacies-analyse af 6 udvalgte prøver fra Stenlille-boringerne. Danmarks og Grønlands Geologiske Undersøgelse Rapport 1998/75.

Gassum-1, Completion report (1951). Compilated March 1993.

Ineson, J.R. 1993. The Lower Cretaceous chalk play in the Danish Central Trough. Geological Society, London, Petroleum Geology Conference Series 4, 175–183.

Ineson, J.R., Jutson, D.J. and Schiøler, P. 1997. Mid-Cretaceous sequence stratigraphy in the Danish Central Trough. Danmarks og Grønlands Geologiske Undersøgelser Rapport 1997/109, 60 pp.

Japsen, P. 1998. Regional velocity–depth anomalies, North Sea chalk: a record of overpressure and Neogene uplift and erosion. AAPG Bull. 82, 2031–2074.

Jensen, T.F, Holm, L., Frandsen, N. and Michelsen, O. 1986. Jurassic-Lower Cretaceous Lithostratigraphic Nomenclature for the Danish Central Trough. Danmarks Geologiske Undersøgelse Serie A 12, 65 pp. https://doi.org/10.34194/seriea.v12.7031

Koppelhus, E.B. and Nielsen, L.H. 1994. Palynostratigraphy and palaeoenvironments of the Lower to Middle Jurassic Bagå Formation of Bornholm, Denmark. Palynology 18 (1), 139–194.

Larsen, G. 1966. Rhaetic–Jurassic– Lower Cretaceous sediments in the Danish Embayment (A heavy-mineral study). Geological Survey of Denmark, II Series, No. 91, 127 pp. plus plates. https://doi.org/10.34194/raekke2.v91.6882

Lauridsen, B.W., Lode, S., Sheldon, E., Frykman, P., Anderskouv, K. and Ineson, J. 2022. Lower Cretaceous (Hauterivian–Aptian) pelagic carbonates in the Danish Basin: new data from the Vinding-1 well, central Jylland, Danmark. Bulletin of the Geological Society of Denmark 71, 7–29. https://doi.org/10.37570/bgsd-2022-71-02

Lindström, S., Pedersen, G.K., Vosgerau, H., Hovikoski, J., Dybkjær, K. and Nielsen, L.H., 2023. Palynology of the Triassic–Jurassic transition of the Danish Basin (Denmark): a palyno-stratigraphic zonation of the Gassum – lower Fjerritslev formations. Palynology, https://doi.org/10.1080/01916122.2023.2241068

Lyngsie, F., Dinesen, A., Bang, I., Buch, A., Christensen, O.B., Bertelsen, F. and Michelsen, O. 1974. Hobro-1. The lithostratigraphical and biostratigraphical zonation – based upon well-site observations, studies of the logs run by “Dresser atlas” and micropaleontology. DGU report. 3 pp. and 7 enclosures.

Mallon, A.J. and Swarbrick, R.E. 2002. A compaction trend for non-reservoir North Sea Chalk, Marine and Petroleum Geology 19, 10, 527–539.

Mallon, A.J. and Swarbrick, R.E. 2008. Diagenetic characteristics of low permeability, non-reservoir chalk from the Central North Sea, Marine and Petroleum Geology 25, 10, 1097–1108. https://doi.org/10.1016/j.marpetgeo.2007.12.001

Michelsen, O., 1975a. Lower Jurassic ostracods of the Danish Embayment. Danmarks Geologiske Undersøgelse, II Række, nr. 104. 287 pp.

Michelsen, O., 1975b. Foreløbig stratigrafisk inddeling baseret på ostracoder. Unpublished DGU report. 3 pp and 1 enclosure.

Michelsen, O. 1989. Revision of the Jurassic lithostratigraphy of the Danish Subbasin. DGU Serie A 24, 21 pp.

Michelsen, O., Nielsen, L.H., Johannessen, P.N., Andsbjerg, J. and Surlyk, F. 2003. Jurassic lithostratigraphy and stratigraphic development onshore and offshore Denmark. In: Ineson, J.R. and Surlyk, F. (eds): The Jurassic of Denmark and Greenland. Geological Survey of Denmark and Greenland Bulletin 1, 145–216. https://doi.org/10.34194/geusb.v1.4651

Nielsen, L.H. and Japsen, P. 1991. Deep wells in Denmark 1935-1990. Lithostratigraphic subdivision. Danmarks Geologiske Undersøgelse, DGU Serie A, No. 31, 177 pp.

Nielsen, L.H., 2003. Late Triassic – Jurassic development of the Danish Basin and the Fennoscandian Border Zone, southern Scandinavia. Geological Survey of Denmark and Greenland Bulletin 1, 459–526.

Nielsen, L., Boldreel, L.O., Hansen, T.M, Lykke-Andersen, H., Stemmerik, L., Surlyk, F. and Thybo, H. 2011. Integrated seismic analysis of the Chalk Group in eastern Denmark – Implications for estimates of maximum palaeo-burial in southwest Scandinavia. Tectonophysics 511, 14–26. doi:10.1016/j.tecto.2011.08.010

Nielsen, M.V. 1983. Palynologisk undersøgelse af Øvre Trias i Gassum-1 boringen, Volume 1+2. Master thesis, University of Aarhus.

Olivarius, M., Vosgerau, H., Nielsen, L.H., Weibel, R., Malkki, S.N., Heredia, B.D. and Thomsen, T.B. 2022. Maturity matters in provenance analysis: Mineralogical differences explained by sediment transport from Fennoscandian and Variscan sources. Geosciences 12, 308, 24 pp.

Poulsen, N.E., 1996. Dinoflagellate cysts from marine Jurassic deposits of Denmark and Poland. AASP contribution series 31, 227 pp.

Poulsen, N.E., Riding, J.B. 2003. The Jurassic dinoflagellate cyst zonation of Subboreal Northwest Europe. Geological Survey of Denmark and Greenland Bulletin 1, 115–144.

Sorgenfrei, T. and Buch, A. 1964. Deep Tests in Denmark 1935–1959. Danmarks Geologiske Undersøgelse, Række III, Nr. 36, 146 pp. https://doi.org/10.34194/raekke3.v36.6941